The Preparation and Electrical Properties of Semiconducting III - V Alloys

by

William M. Coderre

Submitted in partial fulfillment
of the requirements for the degree
of Doctor of Philosophy

Department of Physics,
Faculty of Pure and Applied Science,
University of Ottawa,
Ottawa, Canada.

1969

Statement of Originality

So far as the author is aware the following aspects of the present work are original:

1. Preparation of alloy material of a relatively high degree of homogeneity over the full alloy composition range for the system $InAs_xSb_{1-x}$.

2. Measurement of the Hall Effect and resistivity at high temperatures of samples of the alloy system $InAs_xSb_{1-x}$.

3. The interpretation of the experimental results of electrical measurements on the alloy systems $Ga_xIn_{1-x}Sb$, $Ga_xIn_{1-x}As$, and $InAs_xSb_{1-x}$ considering such effects as non-parabolicity, electron degeneracy, and the presence of two valence band and up to three conduction band contributions.

4. The determination by electrical means of the intrinsic energy gaps as functions of temperature and alloy composition for the entire alloy range of the systems, $Ga_xIn_{1-x}Sb$, $Ga_xIn_{1-x}As$, and $InAs_xSb_{1-x}$.

5. The determination by electrical means of the energy separation of the various conduction bands in those alloys where the higher bands make a significant contribution to conduction processes.

Work on the preparation of the alloy systems $Ga_xIn_{1-x}As$ and $Ga_xIn_{1-x}Sb$ by the step freeze method was performed in collaboration with other workers in these laboratories.

Work on the electrical measurements of the alloy system $InAs_xSb_{1-x}$ was performed concurrently with, but independent from, the present work by Kudman and Ekstrom (68K2) and by Sirota and Bolvanovich (67S2)(67S3).

Abstract

Homogeneous polycrystalline alloy material has been prepared for the alloy systems $Ga_xIn_{1-x}Sb$, $Ga_xIn_{1-x}As$, and $InAs_xSb_{1-x}$, using various growth techniques. The Hall effect and the resistivity were measured at all temperatures from 300°K to 1000°K where possible, on samples from each of these systems.

Using both a two band analysis, and a multiband analysis including such factors as band non-parabolicity and electron degeneracy, the intrinsic energy gap was determined for each system as functions of temperature and composition. Information concerning the carrier mobilities, and the positions of significant subsidiary conduction bands was also obtained.

Acknowledgement

I would like to thank Drs. J. M. Robson and J. C. Woolley, who were the chairmen of the Physics Department during my tenure at the University of Ottawa, for providing me with the opportunity to use the facilities of the University of Ottawa laboratories.

I would especially like to thank my supervisor, Dr. Woolley for the never-ending patience and encouragement which accompanied his advice throughout the progress of this work.

I have benefited from my association with the other professors of the Physics Department, most notably, Dr. Y. P. Varshni, and with my fellow students who were most generous with their time and suggestions.

Many thanks to Miss Loretta Sawyer, who typed this thesis, and most of all I acknowledge the immeasurable debt I owe my wife, Jacqueline, without whose encouragement and support my work would have been much more difficult.

Finally, the financial support of the Province of Ontario is gratefully acknowledged.

Table of Contents

List of Figures

List of Tables

CHAPTER I

INTRODUCTION

1.1 Motivation For The Present Work

In 1960 Woolley and Gillett (60W8) published the results of an investigation of the electrical properties of alloys of the system $Ga_x In_{1-x} Sb$. They find agreement with published values of the optical energy gap in the region $0.0 < x < 0.65$ but report anomalous variation in the energy gap as a function of alloy composition in the region $0.65 < x < 1.0$. Various postulates were presented to explain this anomaly (65W2). It became apparent that these alloys exhibit multiband conduction processes in the GaSb rich region.

The present work was begun with the intention of further investigating the electrical properties of this system with special emphasis on the contribution of electrons in the higher conduction bands. This work has involved preparation of homogeneous material at all alloy compositions, as well as measurement of the Hall coefficient and the resistivity as functions of temperature and composition for these alloys. A multiband analysis of the electrical measurements was applied in order to derive

information about the various energy band minima and the properties of electrons in these minima.

The variation of the three lowest conduction band minima with composition has been determined for the entire alloy system. The composition variation of the (000) minimum and its temperature dependence have been found to agree with the optically determined values (59W7). The variations of the ⟨111⟩ and ⟨100⟩ minima with their temperature dependences have also been determined but with decreasing certainty as the composition varies from GaSb to InSb and the contribution to conduction processes of these bands diminishes. A computer analysis enables the variation of the Fermi level, the effective masses, and the carrier concentrations of any sample to be determined as functions of temperature.

The room temperature electron mobility has been found to vary almost linearly with composition for specimens having similar carrier concentrations.

In 1964 Woolley and Warner (64W2) reported from optical measurements that the energy gap of the alloy system $InAs_x Sb_{1-x}$ exhibits a pronounced minimum in its variation with composition. The present work was instigated to verify the presence of this minimum by measurement of electrical properties. The energy gap minimum has

been found in the present work as well and both qualitative and quantitative agreement with the optical results has been observed (68C1).

In order to study this alloy system it was first required to produce homogeneous material at all compositions. This was accomplished by means of a horizontal Brigdman type crystal growth technique and also by zone recrystallization. High temperature Hall and resistivity measurements were again carried out and the data obtained were analysed using a non-parabolic (000) band minimum and Fermi statistics. These considerations were found necessary since these materials have very small energy gaps in the middle composition range.

The electron mobility was found to vary linearly with composition at all temperatures and to have an empirical temperature dependence of the form $\mu_e = \mu_o e^{-T/T_\theta}$.

In 1959 Abrahams et al (59A1) determined the optical energy gap of the system $Ga_x In_{1-x} As$ as a function of alloy composition, but with inhomogeneous material. Woolley, Gillett and Evans (61W7) reported a more linear optical energy gap variation using more homogeneous material. Hockings et al (66H1) also gave the optical energy gap as a function of composition but reported lower values than Woolley et al in the middle composition regions. In 1968,

Woolley, Thomas and Thompson (68W1) confirmed the earlier results of Woolley et al (1961) with better material and with a more sophisticated analysis taking into account Burstein shift.

No electrical determination of the energy gap has yet been reported. In the present work this was done for the entire composition range by means of high temperature Hall effect measurements. The energy gaps so determined agree with those of Woolley et al (68W1). Electron mobility was also determined as a function of both temperature and composition and was found to exhibit a linear composition dependence and the same form of temperature dependence as did that of the $InAs_xSb_{1-x}$ alloys. Good homogeneous material has been prepared for this work by means of the horizontal Bridgman method.

In the analysis of the Hall data the position of the ⟨100⟩ conduction band minima was determined for GaAs rich alloys. Agreement has been found with the work of Ehrenreich (60E3) which reports that in GaAs these minima are 0.36 eV above the (000) minimum at $0^{o}K$. The temperature dependence of the (000) minimum has been determined using the formulation of Varshni (67V1),

$$E_g = E_o + \frac{\beta T^2}{\alpha + T} \quad .$$

Preliminary measurements of alloys of the $GaAs_x Sb_{1-x}$ system in the present work indicate that there is a pronounced minimum in the energy gap variation with composition. Some homogeneous alloys have been prepared but as yet no one has obtained homogeneous solid bulk samples over the entire composition range.

It must be pointed out that the author is a member of a group of several students working on allied projects under Dr. J. C. Woolley. Since all members of this group are involved in the various phenomena associated with III - V alloys, it is necessarily true that all of the work reported here must acknowledge a debt to each of these workers. In particular, the work of preparation of alloys bears the mark of many hands. Alloys of $Ga_x In_{1-x} Sb$ have been prepared by vanTongerloo and Aubin for their specific purposes (69A2) as have alloys of $Ga_x In_{1-x} As$ by Thompson (68W1). For these two systems, the present work required material with smaller impurity concentrations and hence the measurements reported here were performed on samples prepared by the author, with very few exceptions.

The work on the preparation of alloys of $InAs_x Sb_{1-x}$ was performed exclusively by the author and has already been reported (68C1). All material produced in the group is available for general investigation and so other workers have used these alloys for their own purposes (viz. vanTongerloo

(68V1), Aubin (68A1) and Vishnubhatla (68V2)). The preliminary work on the preparation of alloys of $GaAs_x Sb_{1-x}$ was carried out by the author in collaboration with Thomas.

Wherever there is an overlap between the present work and that of another member of the group, or when the present work has drawn on the results of another, references will be explicitly given. However, none of the work presented in this thesis was performed in isolation and the many non-specific contributions of the author's co-workers are gratefully acknowledged.

1.2 Historical Background

This thesis is concerned with the preparation of alloys of certain III - V semiconducting compounds and the measurement of their energy gaps and the mobility of their conduction electrons as functions of alloy composition. In order to have a grasp of how this work fits into the mosaic of semiconductor physics, a brief background covering the fundamentals of the field will be presented.

During the past quarter century the industrial world has shown increasing interest in the applications of semiconductors and impressive advances are being built upon the base of the new materials whose semiconducting properties are continuously being investigated. Most early research had been concentrated on the elemental semiconductors, silicon and germanium, but since 1952 the amount of work on other materials has increased greatly with a corresponding broadening of the availability of the parameters which are of interest. It was reasoned that those compounds which were iso-electronic with the elemental semiconductors might also share their properties (52W1) and this led to the investigation of the III - V compounds. InSb was the first of these to be extensively studied; also of interest was GaAs since it is the structural and electronic analog of germanium.

As the list of III - V semiconductors grew, paced by the demand for varying optical and electrical parameters, the obviously advantageous possibility of alloying known semiconductors was considered. This way, instead of discrete values of such parameters as energy gap or effective mass, there could be available completely continuous ranges. Among the possible alloys of the common III - V compounds direct energy gaps of all values from 0.10 to ~2.1 eV can be obtained at room temperature. The first semiconducting alloy system studied (1939) was that of $Ge_x Si_{1-x}$, using samples produced by annealing of powders. In the mid 1950's work was begun on the mixed III - V crystal systems by such workers as Goryunova, Ivanov-Omskii and Woolley.

1.3 Crystal Structure Of III - V Semiconductors

Most of the common III - V compounds have the zincblende crystal structure. This would be equivalent to the diamond lattice if the two constituent atoms were identical. It is a face-centered cubic lattice with the atoms of group III situated on one face-centered sub-lattice and the group V atoms situated on a similar sub-lattice interpenetrated with the first at one quarter the distance along its body diagonal. Each atom is then at the center of a tetrahedron with four opposite atoms at the vertices.

Alloying two III - V compounds involves the substitution of atoms of one or both groups with other atoms of the corresponding group. For example, indium atoms can replace some of the gallium in GaSb to form the alloy $Ga_xIn_{1-x}Sb$. In this case the expression (1 - x) indicates the mole fraction of indium atoms that are present in the alloy crystal. If the substitution is completely random, the alloy is said to be disordered.

III - V alloys have been prepared by several workers since 1955. A brief summary of their work is given on table 1.3.1 indicating the method used and the alloy produced. The second chapter of this thesis will discuss the work of alloy preparation up to the present day. This will be presented as a useful review of the state of the art for the

TABLE 1.3.1

METHODS OF ALLOY PREPARATION

ALLOY	Z - R	G - F	H - B	S - L	V - T	CZ	MISC.
$Al_xGa_{1-x}As$					66B5		67R1 61S20
$Al_xGa_{1-x}Sb$	60M3 58B6						
$Al_xIn_{1-x}Sb$	62A7						60B2
GaP_xAs_{1-x}			59B10		66T1	68W3	62S12
$(GaAs_x(InP)_{1-x}$	63S9						
$GaAs_xSb_{1-x}$					64P3		67S1 65S1
$Ga_xIn_{1-x}As$	59A1	61W7	63M5	66H1	67C1		68J2
$Ga_xIn_{1-x}Sb$	59I2	59W7	69V1	67K1		62T5	64M1
$InAs_xSb_{1-x}$	64W1	64W1	68C1	68K2	64P4	66B2	66B1
$InBi_xSb_{1-x}$						66J1	

Z - R Zone Recrystallization
G - F Gradient Freezing
H - B Horizontal Bridgman
S - L Step Levelling
V - T Vapour Transport
CZ Czochralski Pulling
MISC. Miscellaneous Method

interested reader. The present work on preparation of III - V alloys will be presented in the third chapter.

1.4 Band Structure

Assuming the crystal potential to be constant, Sommerfeld (28S1) was able to show that free electrons in a solid can be represented as plane waves of the form,

$$\psi_{\hbar} = Ae^{i\hbar.r} \quad .$$

These waves are functions of the wave vector $\hbar$, where each value of $\hbar$ represents a possible electronic state. The energy dependence of the states on $\hbar$ was found to be parabolic and of the form,

$$E = \frac{\hbar\hbar^2}{2m} \quad .$$

Bloch (28B1) modified this analysis by replacing the constant crystal field with a potential having the periodicity of the crystal lattice. He then found that the electron wave was altered by the addition of a periodic function $U_{\hbar}(r)$. Hence,

$$\psi_{\hbar} = U_{\hbar}(r)\ e^{i\hbar.r}$$

where $U_{\hbar}(r) = U_{\hbar}(r + \ell)$, where ℓ is a lattice vector, having components which are integral combinations of the lattice spacing. The result of the analysis based on the model of a periodic crystal potential shows that there exist for the electrons, bands of allowed and forbidden energy. The values and limits of these bands are determined by the

particular crystal structure and the atoms which make up the crystal. The energy bands are functions of the electronic wave vector $\hbar$. When the allowed electron energy is plotted in $\hbar$ space, energy discontinuities are found at certain $\hbar$ values. The locus of the position of the first such discontinuity is defined as the first Brillouin zone boundary. Every wave vector in $\hbar$ space is equivalent to a wave vector within the first Brillouin zone differing only by vectors of the reciprocal lattice. All energy states can thus be shown in a "reduced zone scheme" including only the non-equivalent points of $\hbar$ space, i.e. those within the first Brillouin zone. The amplification of these basic notions has been thoroughly carried out by Brillouin (30B1) and Wilson (31W1,2) and the details of their development can be found in any number of standard texts, (Dekker 57D4, Kittel (64K6), Ziman (64Z1)).

In order to show the dependence of the available energy states of electrons in a crystal lattice on the wave vector, diagrams selecting specific $\hbar$ directions are normally used. Since most transport properties in semiconductors involve the electrons in the lowest conduction band minima, it is convenient to show the energy variation in those $\hbar$ directions where such minima occur. In the case of zincblende materials the most important minima are thought to be at $\hbar = 0$, i.e. the (000) point, at the

Brillouin zone boundary in the ⟨111⟩ directions and at a point along the ⟨100⟩ directions.

Hence, a typical band picture will show the variation of the band edges along the ⟨111⟩ and ⟨100⟩ directions proceeding from the (000) point as far as the first Brillouin zone boundary. (see fig. 1.4.1)

Much work has been done in the calculations of these band structure diagrams by quasi-empirical analysis over the past several years. By continual reference to experimentally determined parameters a fairly complete quantitative band picture has been built up for the group IV semiconductors and for some of the common III - V's as well.

FIGURE 1.4.1

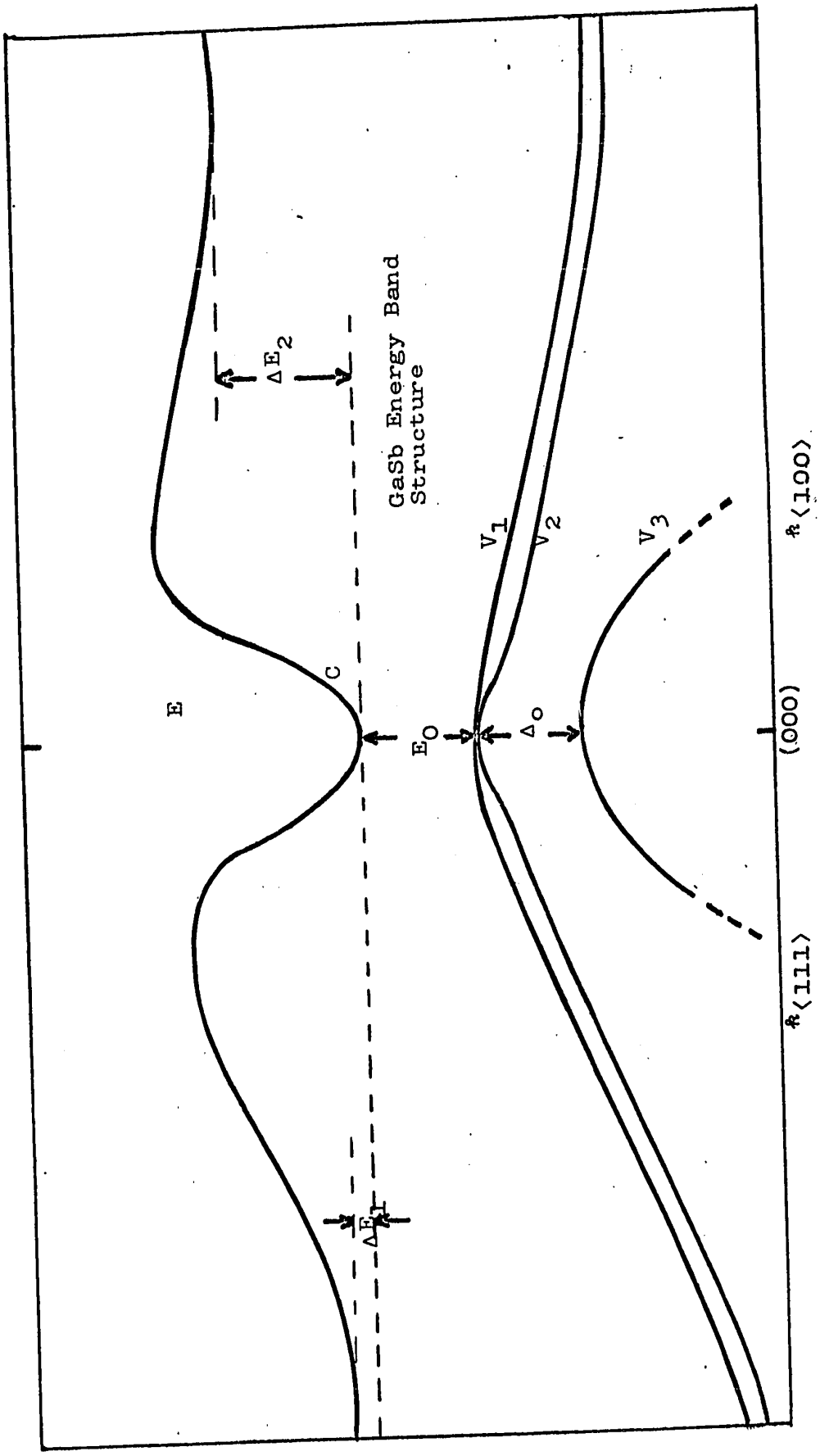
GaSb Energy Band Structure
E
C
E_O
ΔE_2
ΔE_1
Δ_o
V_1
V_2
V_3
(000)
k⟨100⟩
k⟨111⟩

1.5 Virtual Crystal Model

In the case of disordered alloys, the assumption of band theory that there is a regular periodic potential field in the crystal is no longer strictly valid. The potential remains periodic, since the atoms remain on the same lattice sites, but since the atoms on these lattice sites are randomly different, the magnitude of the field contribution from each atom is randomly altered.

In any system featuring this kind of disorder, a model may be proposed which represents the crystal potential as being composed of two parts, one periodic, and one aperiodic. Nordheim (31N1) has proposed that a disordered alloy can be considered as a "virtual crystal" having a regular periodic potential which is the average potential over all possible random configurations of atoms; with a superimposed aperiodic term which corresponds to the difference between the real crystal potential and that of the virtual crystal. Since then Muto (38M1) and Parmenter (55P2,3,5) have shown that if the aperiodic term is small, perturbation theory can be used to show its effect on various properties of the alloy. If the alloy can be formed this is evidente that the perturbation factor is not prohibitively disruptive. Analysis along these lines has indicated that second order perturbations will cause a

finite shift of the band edges, coupled with a smearing of these edges. This effect modifies the band picture but does not invalidate it.

The virtual crystal model predicts a linear composition dependence for various parameters while second order perturbation terms indicate that there will be a deviation from linearity which is some function of the form $x(1 - x)$. Observation of the composition dependence of various parameters such as band edges, effective masses, etc. has been one of the main objectives of the semiconductor group at the University of Ottawa Physics Laboratories.

CHAPTER II

ALLOYS OF THE III - V COMPOUNDS

2.1 Introduction

This chapter contains a discussion of the phenomenon of alloying with respect to III - V compounds. A brief description of the work needed to determine the range of solid solution of an alloy will be presented. The recent work on preparation of III - V alloys will be reviewed as well. This review will include a discussion of the methods used and the materials obtained by various workers. The early work on the preparation of III - V alloys has already been summarized thoroughly in reviews by Woolley (62W7) and by Madelung (64M4). Since these references are readily available, the material covered therein will be considered only briefly, with a heavier emphasis placed on more recent results. This review, while not exhaustive, is intended to be representative with respect to the various techniques applied to alloy preparation and to the resultant materials.

In order that the reader may conveniently refer to Madelung's text, the reference notation used in this thesis has been made compatible with his. Where a reference is common, the same notation is used; where it is new, a

number not previously used by Madelung has been assigned.

2.2 Group IV Alloys

The first semiconducting alloys produced were those of silicon and germanium. As early as 1939 Stöhr and Klemm (39S1) showed that by annealling powders a complete range of solid solution could be obtained. It wasn't until 1954 however that Johnson and Christian (54J1) produced solid alloys upon which they performed infrared absorption measurements. Since that time these alloys have been thoroughly studied using many different techniques and phenomena. Optical absorption measurements were made by Braunstein et al (58B7). Hall effect (60B12, 64D2), magnetoresistance and conductivity (55G4), thermal conductivity (64D2, 58S7), cyclotron resonance (55D2, 6501) and reflectivity (61T1, 2) measurements as functions of temperature and alloy composition have been carried out. The effect of pressure on the energy gap was studied by Paul (58P5) and recently electroreflectance measurements were carried out by Cardona.

Other mixed crystals of group IV elements form only over a limited composition range. Germanium and gray tin are mutually soluble only within a few percent of either element, and silicon and carbon form only the single compound, silicon carbide. This immiscibility is primarily due to the differing atomic sizes of the atoms, among other influences which will not be discussed here.

2.3 III - V Alloys

2.3.1 Binary Equilibrium Diagrams

When two or more crystalline materials are heated to a sufficiently high temperature at normal pressures, the usual result is a homogeneous liquid alloy. If this liquid is cooled it will solidify but not necessarily retain its homogeneity. Provided sufficient time is allowed, each alloy will come to an equilibrium condition depending on the temperature and the pressure. It is possible to show diagrammatically the extent of the various phases present in an alloy system as functions of temperature, composition and pressure. Since the vapour pressures involved in the present work as in most metallurgical work are usually small and since the materials are not subjected to high pressures, this factor will be neglected. Diagrams showing the equilibrium states of alloys as functions of composition and temperature alone are usually employed.

Such diagrams delineate the extent of regions of single phase homogeneity and those of mixed phases. In a binary alloy there can never be more than two phases in equilibrium.

In the present work the alloys of interest are not binary but ternary. Since however, the three elements involved in each case combine stochiometrically to form

2.3 III - V Alloys

2.3.1 Binary Equilibrium Diagrams

When two or more crystalline materials are heated to a sufficiently high temperature at normal pressures, the usual result is a homogeneous liquid alloy. If this liquid is cooled it will solidify but not necessarily retain its homogeneity. Provided sufficient time is allowed, each alloy will come to an equilibrium condition depending on the temperature and the pressure. It is possible to show diagrammatically the extent of the various phases present in an alloy system as functions of temperature, composition and pressure. Since the vapour pressures involved in the present work as in most metallurgical work are usually small and since the materials are not subjected to high pressures, this factor will be neglected. Diagrams showing the equilibrium states of alloys as functions of composition and temperature alone are usually employed.

Such diagrams delineate the extent of regions of single phase homogeneity and those of mixed phases. In a binary alloy there can never be more than two phases in equilibrium.

In the present work the alloys of interest are not binary but ternary. Since however, the three elements involved in each case combine stochiometrically to form

compounds which then act as the two constituents of a binary-like alloy, pseudo-binary equilibrium diagrams can be used. (see figure 2.3.1)

In order to proceed systematically in the investigation of such alloys it is first necessary to determine the range of composition over which single phase alloys exist for a given temperature, and as well to ensure that the alloy system is in fact pseudo-binary.

Constituents of a given mole percentage are melted together in an evacuated capsule and are thoroughly mixed, then quenched. The quenching ensures relatively intimate proximity of the resulting phases in the material. The sample is then powdered to further guarantee thorough mixing and the powder is again encapsulated in vacuum. By annealling for several weeks, and sometimes longer, at a constant known temperature, the sample is gradually brought to an equilibrium condition by the process of atomic diffusion. After annealling, part of the sample is powdered and X-rayed to determine its homogeneity. Normally the X-ray photographs would show diffuse diffraction patterns, indicating a spread in composition within the alloy. With further annealling however, these blurs merge into one or two sets of sharp lines each set corresponding to an equilibrium phase. Repeated steps of annealling and X-raying are taken until the equilibrium condition is reached. This procedure is followed for

FIGURE 2.3.1

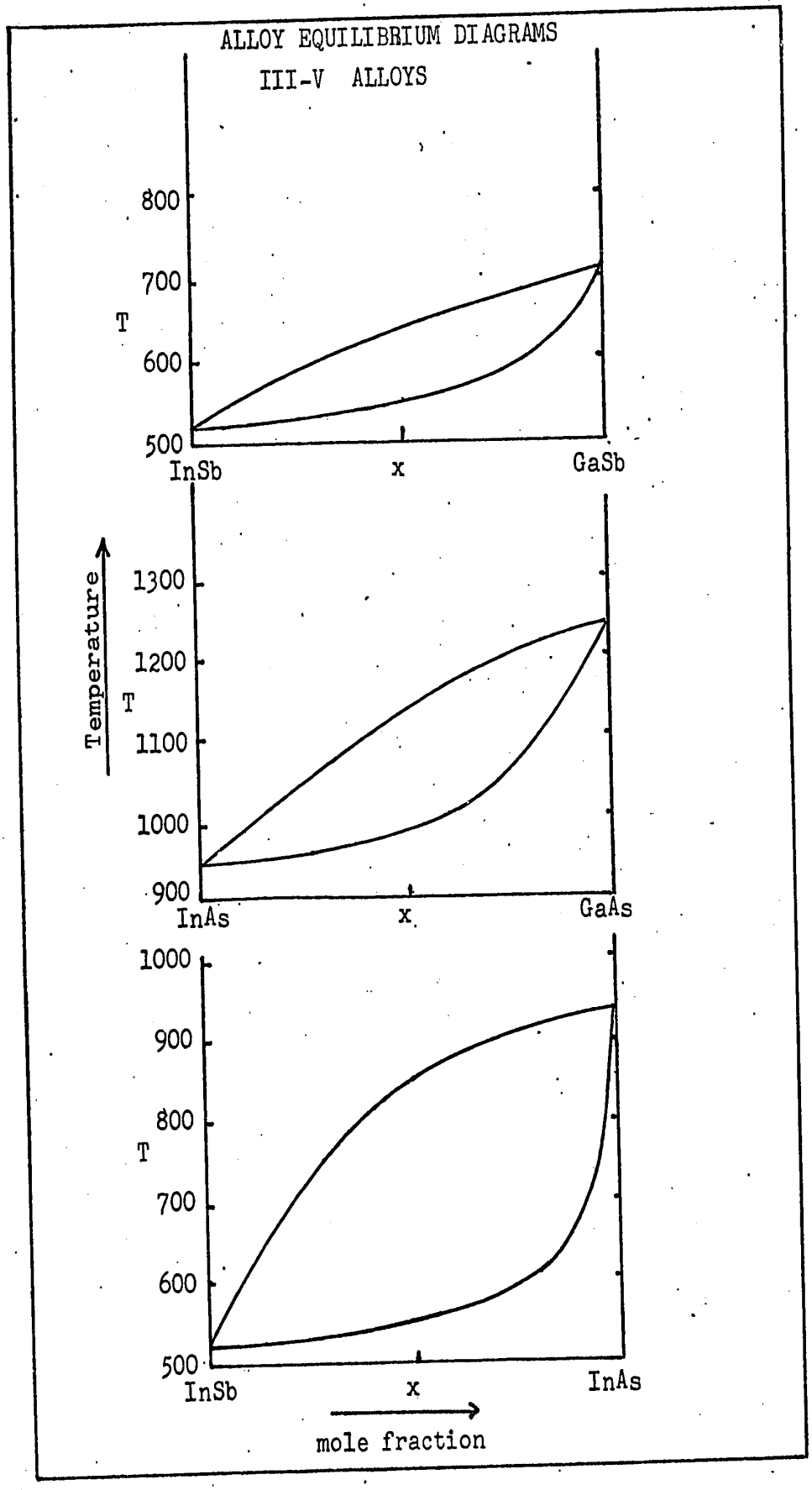
ALLOY EQUILIBRIUM DIAGRAMS
III-V ALLOYS
800
700
T
600
500
InSb
x
GaSb
Temperature
1300
1200
T
1100
1000
900
InAs
x
GaAs
1000
900
800
T
700
600
500
InSb
x
InAs
mole fraction

several different annealling temperatures and compositions until the regions of single phase homogeneity are defined.

In order to show that an alloy is pseudo-binary, alloys of different composition are annealled to equilibrium at the same temperature in a two phase region. When these samples are quenched, freezing in the equilibrium phases, these phases must have the same compositions in the different samples. If these compositions differ from sample to sample then the alloy system is not pseudo-binary since only two particular phase compositions can co-exist at equilibrium at a given temperature in a binary alloy. If the alloy system is completely miscible and if it is pseudo-binary, a graph showing a smooth continuous variation of lattice parameter with composition can be obtained from X-ray photography. With such a graph, the composition of any unknown sample in the alloy system can be determined. (see figure 2.3.2).

Another method for determining the equilibrium diagram of an alloy has been reported by Woolley (58W9, 59W8). In this case note is taken of the lattice parameter of the phases frozen in when a specimen of known mean composition is quenched after being annealled to equilibrium in the two phase solid-liquid region. From the lattice parameters, the compositions of the two phases in equilibrium at that temperature can be obtained. This is a useful method since it

FIGURE 2.3.2

LATTICE PARAMETER versus ALLOY COMPOSITION

$In\ As_x\ Sb_{1-x}$

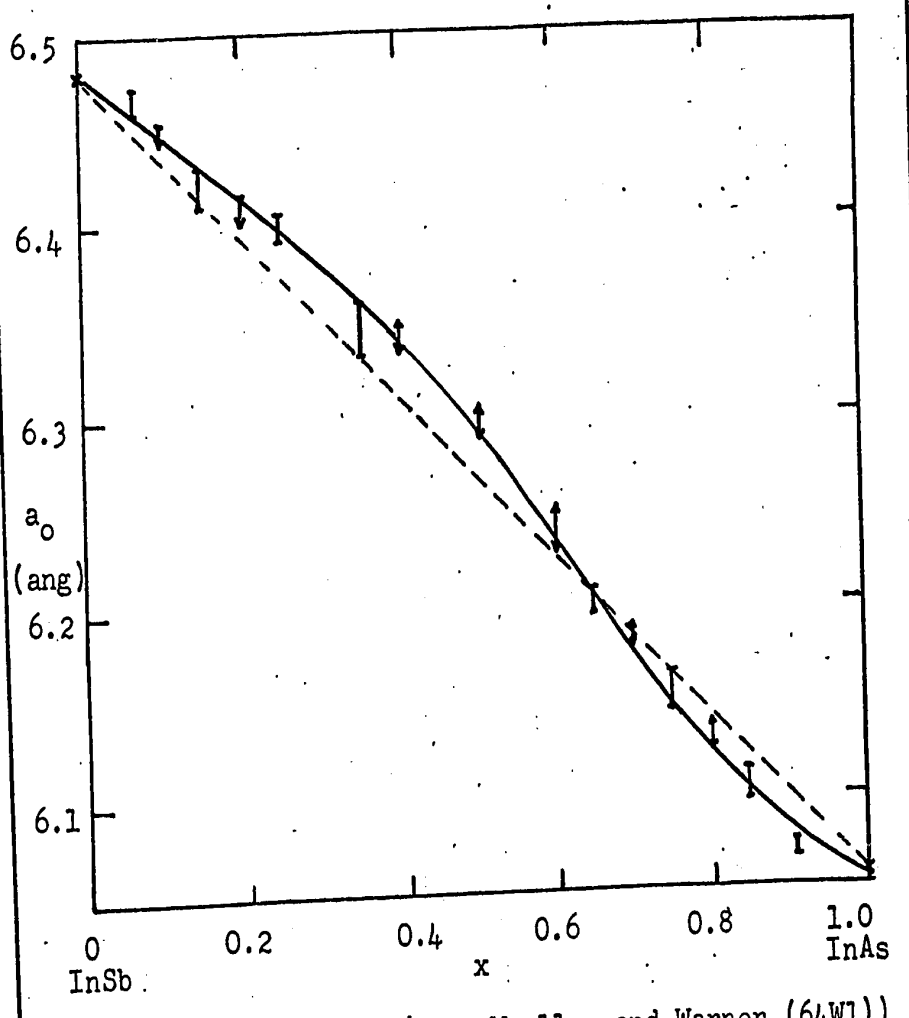

(from Woolley and Warner (64W1))

does not involve the melting of single phase samples for determination of the solidus temperature, as does the heating curve method; but it can only be applied in materials with very slow diffusion rates.

The interested reader is referred to Hume-Rothery et al. (52H1) for further discussion of methods for the determination of equilibrium diagrams.

A discussion of the experimental work resulting in the determination of the equilibrium diagrams of the III - V alloys of interest can be found in Woolley (62W7).

2.3.2 Solid Solubility of III - V Compounds

If two materials are to undergo complete solid solution it is important that the lattice spacing of the constituent compounds be similar, so that there will not be excessive strain in the alloy (see table 2.3.1). Of all the III - V alloy systems known to have a complete range of solid solutions, the percentage change in the lattice parameter with alloying is less than 8%, with the one exception of the GaP-InAs system (10.6% change). Conversely, of the systems known to have a limited miscibility range only GaSb-InP and GaSb-InAs involve a lattice parameter change of less than 8%.

It has been observed by Müller and Richards (64M5) that a miscibility gap will exist in a III - V alloy system

Table 2.3.1

LATTICE CONSTANT OF III - V COMPOUNDS

III - V COMPOUNDS	LATTICE CONSTANT
AlP	5.46 angstroms
AlAs	5.63
AlSb	6.135
GaP	5.45
GaAs	5.653
GaSb	6.095
InP	5.869
InAs	6.058
InSb	6.479

Table 2.3.2

ATOMIC RADII OF III - V ELEMENTS

ELEMENT	ATOMIC RADIUS
Al	1.25 angstroms
Ga	1.26
In	1.42
P	1.10
As	1.18
Sb	1.40

when the atomic radius difference between the atoms undergoing substitution exceeds a critical value of 17%. This critical value is slightly higher when there is substitution of atoms of only one group and is somewhat lower when the atoms of both groups are being replaced. The radius mismatch for phosphorous and arsenic is only 7%, and that for gallium and indium is 12% (see table 2.3.2), hence there is complete miscibility in all alloys involving the compounds GaP, GaAs, InP and InAs (see figure 2.3.3a). The atomic radius difference between phosphorous and antimony is relatively large, i.e. 24%, and hence alloys involving substitution of these atoms show wide miscibility gaps (see figure 2.3.3c). The substitution of arsenic and antimony (atomic radius mismatch of 17%) forms alloys with a complete range of solid solutions when the group III atom is unchanged but when there is substitution of these atoms as well, there is a wide miscibility gap (see figure 2.3.3b).

Since aluminum and gallium have almost identical atomic radii, the conclusions drawn concerning alloy of gallium compounds should apply as well to alloys with aluminum. There is however, limited experimental work on the aluminum alloys.

The critical radius mismatch value of 17% is notably close to the similar critical value of 15% for the atomic radius difference for miscibility in metals.

FIGURE 2.3.3

EXTENT OF SOLID SOLUBILITY IN SOME III-V COMPOUNDS

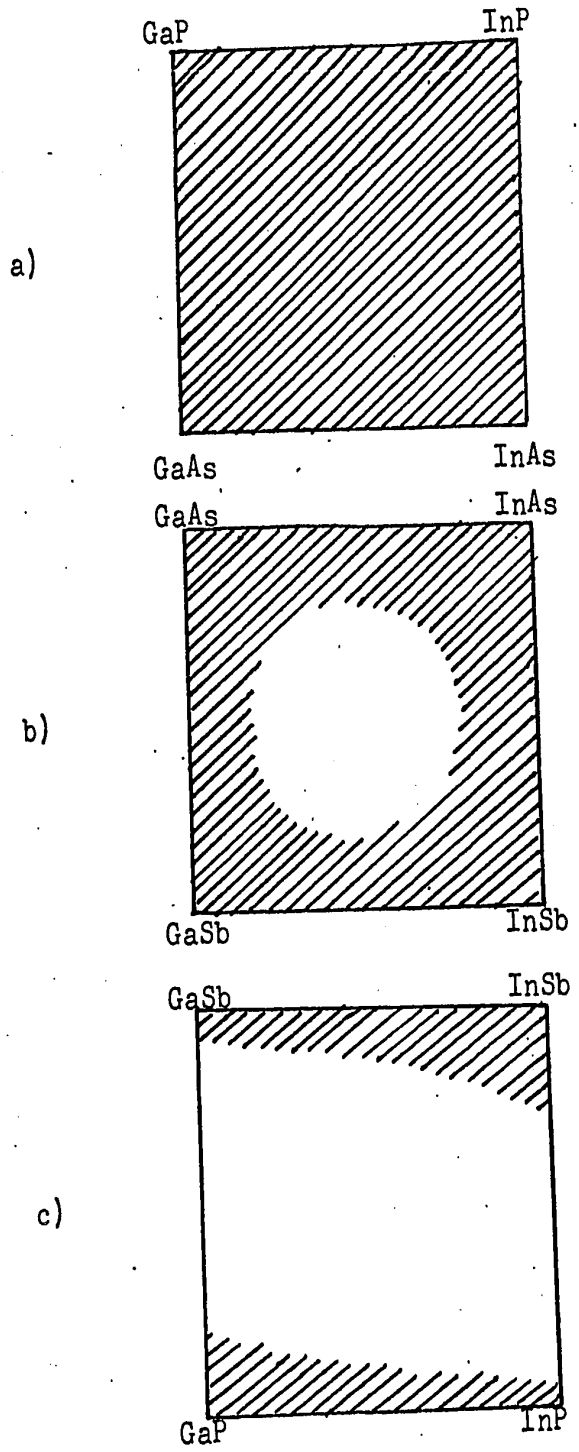

(from Müller and Richards (64M1))

In alloys of III - V compounds as compared with group IV alloys there is an added factor influencing the range of solid solubility. This is the ionicity of the bonding in the compounds concerned. In III - V compounds the valence electrons tend to be polarized in the direction of the strongly positively charged core of the group V atoms. The degree of this polarization varies from compound to compound, and if two compounds with very dissimilar polarizations are alloyed there will be strain within the lattice due to this dissimilarity. Folberth (58F4) has arranged the common III - V compounds with respect to their polarization: AlSb, (GaSb, GaP, GaAs), InSb, (InP, InAs). He has concluded from this that the systems $InAs_x P_{1-x}$ and $Al_x Ga_{1-x} Sb$ will have less internal strain than the systems $InP_x Sb_{1-x}$ and $InAs_x Sb_{1-x}$ and that because of this there would be more probability of finding complete solid solution in the former. Müller observes however, that the atomic radius difference is far more important than the ionicity in influencing miscibility in III - V alloys.

2.4 Preparation of Alloy Material: Review

It has been found that although single phase alloys can be obtained by annealling of powders, when solid material is required, the time needed to anneal a specimen to equilibrium is prohibitive. In order to produce solid single phase samples upon which electrical experiments may be performed, more sophisticated techniques must be employed. In the present work a wide range of composition was needed and as well each specimen had to have sufficiently large dimensions that a parallelepiped of ~1 x 1.5 x 10 mm could be cut from it for the measurement of the Hall effect. This requirement precluded the use of such methods as vapour transport or epitaxial growth without proceeding to an impractical level of complication. Hence in the survey of alloy production which is presented in the following sections, those methods will be emphasized which might produce alloy material of practical form for the present work.

2.4.1 Production of $Ga_x In_{1-x} Sb$ Alloys

These alloys are not easily prepared in solid form. In 1955 and again in 1957 (55K4, 57K6) it was reported that there was a wide miscibility gap in this system. The first alloys were prepared by Goryunova and Federova (55G2), but reliable growth procedures awaited the work of Woolley et al

(56W6, 58W9, 59W7) and Ivanov-Omskii and Kolomiets (59I2). The composition spread in a given sample as reported by Woolley was between 1.5 mol % and 3.0 mol %, but the Russian workers gave no quantitative indication of the degree of homogeneity attained in their crystals. Woolley et al produced alloys in the form of graded polycrystalline ingots by gradient freezing, using different mean starting compositions. Ivanov-Omskii and Kolomiets used a very slow zone levelling technique to produce polycrystalline alloy ingots.(see also 61W7, 62I1). The degree of homogeneity obtained by either group was not sufficient to allow unambiguous determination of the electrical parameters over the entire alloy range.

Later work in this system has been reported by Trumbore et al (62T5) who produced homogeneous materials of a wide range of compositions using the Czochralski technique. Single crystals were obtained from melts containing as much as 60 mol % InSb. Alloys rich in GaSb were very homogeneous as determined by X-ray powder patterns, while material rich in InSb was less homogeneous having composition spreads of from 3 to 4 mol %.

From their results the authors were able to confirm the binary phase diagram as determined by Woolley and Smith (58W9). As the authors point out this method offers not only the feature of single crystal production, but also the

fact that the total growth time is in the order of hours instead of days or even weeks. Necessarily several different crystals must be pulled in order to study the properties of the complete alloy range.

More recently Kudman et al (67K1) have reported production of polycrystalline alloys by step levelling, a method first reported by Dismukes and Ekstrom (65D1). In this method two different charges, having compositions known to be in equilibrium at a given temperature are chill-cast. The compositions required were determined from the phase diagrams of Trumbore et al. At the equilibrium temperature one charge is molten while the other, adjacent material remains solid. The ingot is caused to pass through a steep temperature step as in a horizontal Bridgman furnace. When the leading edge of the liquid zone is cooled it freezes out material of the same composition as the solid charge thus upsetting the equilibrium between itself and the solid phase. At the interface between the zones material is dissolved in order to re-establish equilibrium. The rate of growth used in this work was 0.6 cm per day which is comparable to the rate for the step freeze method employed in the present work.

This seems to be a promising method but the composition spread of the resulting alloy material is not discussed apart from mention that the back scattered X-ray diffraction lines were used as a criterion for homogeneity. Again it is

required to produce several different ingots in order to obtain samples covering the entire alloy range.

Preparation of polycrystalline ingots of these alloys has been undertaken in the present work. The method used was that of step freezing and consistently homogeneous material has been produced over a wide composition range. The report of this work follows in the next chapter.

2.4.2 Production of $Ga_x In_{1-x} As$ Alloys

This alloy system has a complete range of solid solutions and can be formed from the melt by methods similar to those used in the preceding section (57W3, 58W9, 59W9, 63V4). The presence of the volatile arsenic constituent creates added difficulties however as does the high melting point of GaAs.

Preparation of bulk material was first reported by Woolley et al (61W7) using the gradient freeze method, and by Abrahams et al (59A1) by gradient freezing as well and by zone levelling. The composition spread reported by Woolley was less than 5 mol % for most of the specimens. Abrahams et al attained a similar degree of homogeneity with slow zone levelling but because of high growth rates homogeneous material was not produced with the gradient freeze method.

Melngailus et al (63M5) have fabricated diode masers from $Ga_x In_{1-x} As$ produced by the horizontal Bridgman

technique with a freezing rate of 1 cm. per day but they report neither the composition range nor the homogeneity of the alloys obtained.

Hockings et al (66H1) report production of ingots of this alloy system by means of the step levelling technique. Growth rates of 2 cm. per day and 1 cm. per day were employed for preparation of alloys near x = 0.7 or 0.3 and x = 0.5 respectively. Polycrystalline samples were obtained which were homogeneous within one mol % over an ingot 15 cm. in length. Various ingots were doped with either selenium or zinc to make the alloys n- or p-type.

Jensen, Stein and Mooney (68J2) have very recently described a method for production of these alloys from non-stochiometric, indium rich melts. They employ a vertical Bridgman furnace with a freezing rate of ~ 3 mm. per day. The resulting polycrystalline material ranged from x = .91 to x = .77 in 15 mm. of an ingot.

Many workers have employed the method of vapour transport for production of $Ga_xIn_{1-x}As$ alloys. Among the more successful work in this direction is found that of the following workers: Pizzarello (62P11), Sirrine (64S8), Minden (65M1), Conrad et al (66C1, 67C1), Cardona (67C2). Both open and closed tube methods have been used. Alloys were obtained in the form of single crystals up to one cm.

in length, usually upon substrates of GaAs.

In the present work these alloys have been prepared in the form of polycrystalline ingots with a gradual variation of composition with length by means of the step freeze method. A thorough discussion of the method and the materials produced will be presented in Chapter III.

2.4.3. Production of $InAs_x Sb_{1-x}$ Alloys

This alloy system has proven extremely difficult to prepare over the complete alloy range. The form of the equilibrium diagram as determined by Shih and Peretti (53S1) and Woolley and Smith (58W9) shows that there exists a full miscibility range, but the extreme separation of liquidus and solidus indicates that there is a high degree of strain in these alloys. The first solid samples of $InAs_x Sb_{1-x}$ were prepared by Woolley and Warner (64W1) who grew polycrystalline ingots by using gradient freeze and zone levelling techniques. Material of good homogeneity, i.e. a composition spread of $\sim \pm 1$ mol %, was obtained in the ranges $0 < x < .15$ and $.85 < x < 1.0$ by the gradient freeze method. Slow zone levelling, using a relatively wide zone (5 cm.), extended the range of homogeneous alloy material to 25 mol % InAs at the InSb rich end and yielded a few fairly homogeneous samples at about 60 mol %, but a wide

range of the middle composition was not attained.

Thin films were deposited by evaporation by Potter and Kretschmar (64P4) using a four-temperature method. Samples at all compositions have been produced by this method in the form of single crystal platelets.

More recently, Bolvanovich (66B1) has reported that polycrystalline alloys of this system can be produced by annealling samples of appropriate mean composition at temperatures as close as possible to the solidus. The samples were solid, having been quenched from the molten state. Annealling times as short as one hundred hours were claimed sufficient to achieve homogeneity. Sometimes ultrasonic agitation was employed to assist the diffusion process, but this was not a requisite condition. Within a quenched sample at a temperature close to the solidus there exists a liquid phase. The presence of this phase would increase the diffusion rates and thus allow equilibrium to be reached more quickly. X-ray results from this work indicate that a composition spread of about 3 to 5 mol % was present in each alloy sample.

Goryunova and Tahktareva (61G23) had tried similar methods but reported that homogeneity could not be achieved. Basov et al (66B2) obtained single crystals of this system by the Czochralski pulling technique but report production of alloys only within 2 mol % of InAs.

Kudman and Ekstrom (68K2) have produced $InAs_x Sb_{1-x}$ alloys using the step levelling technique which was described previously. The growth rate used for this method was ~ 0.2 cm./day. The resulting samples were homogeneous enough to allow resolution of the Cu Kα doublet in the back reflection lines of Debye Scherrer X-ray photographs. These lines, however were not sharp indicating a spread in composition perhaps as great as 3 mol %. Nothing more detailed regarding the homogeneity of their material was reported by these workers, but the results of their electrical measurements show that the alloy material is not very homogeneous in the middle composition regions.

In the present work good homogeneous polycrystalline ingots of $InAs_x Sb_{1-x}$ have been prepared which have allowed bulk samples to be obtained at all compositions. A modified zone levelling method and the step freeze method were employed in this work. Complete details and a discussion of this preparation and of the resulting material will follow in the next Chapter.

2.4.4. Production of $GaAs_x Sb_{1-x}$ Alloys

Solid bulk samples of this alloy system have never been prepared over the entire composition range. The liquidus-solidus separation is extremely wide, demonstrating the high

degree of strain with alloys of intermediate composition (58W9, 62W7). Preparation of solid samples of these alloys has all of the difficulties of the preceding system with the additional problems of high melting points and high vapour pressure.

Potter and Stierwalt (64P3) reported success in growing epitaxial layers of $GaAs_x Sb_{1-x}$ on suitable substrates with good homogeneity for the complete composition range. Layers were deposited by vacuum evaporation of the metallic constituents onto alumina, quartz or glass. The composition was determined by X-ray analysis and assuming Vegard's law.

Using long term annealling on powders, Straumanis and Kim (65S1) have produced alloys of this system which were then used to determine the variation of the lattice parameter with composition. They concluded that while GaSb could dissolve GaAs readily, the reverse procedure was quite slow. It was also shown that within experimental error, Vegard's law was obeyed in the range $0 < x < 0.45$, the range over which homogeneous material had been obtained.

Sahm and Pruss (67S1) tried the technique of pressure sintering of powders and achieved partial success with their best results at the GaSb rich end of the com-

position range. The biggest problem was apparently loss of gallium leaving the alloy with an excess of antimony. The resulting material was within 5 mol % of the initial mean charges and had a 10 mol % composition spread in each sample.

Attempts to grow solid bulk ingots of this system have been made in the present work in collaboration with Thomas, and indications are that slow zone recrystallization maybe a useful process. Further discussion of this work will be found in the next chapter.

2.4.5. Other III - V Ternary Alloys

Among the first of the III - V alloy system to be produced were those of $GaAs_{1-x}P_x$ and $InAs_{1-x}P_x$. Preparation was found to be no more involved than for the constituent compounds. The existence of a complete range of solid solutions for both systems was demonstrated as early as 1955 by Folberth (55F2). Stone (62S12) showed that graded $GaAs_{1-x}P_x$ layers could be formed in GaAs wafers by diffusion of phosphorus at 8 atmospheres and 800 - 900°C into GaAs. Vapour transport methods have been applied with much success in this same system by such workers as Alexander (64A2), Rubenstein (65R1) and Tietjen and Amick (66T1). The crystals of Rubenstin and Tietjen were of

excellent homogeneity. Many other workers have prepared $GaAs_{1-x}P_x$ alloys by vapour transport with fairly consistant homogeneity (62P11, 64F2, 64F5, 64H7, 65G2, 67I1). The $InAs_{1-x}P_x$ system was prepared by Bower et al (59B10) in the $0 < x < .4$ range, using a two zone vertical Bridgman furnace. But in all but the $x = .1$ specimens the high angle doublets in the X-ray photographs were split indicating the presence of two phases. This was probably due to the high (2.5 cm./hr.) growth rate.

More recently alloys of this system have been prepared from non-stochiometric solutions by Czochralski crystal pulling by Winkler et al (68W3). This work is as yet unpublished and hence no firm statements concerning homogeneity or composition range are available.

The alloys systems $Al_xGa_{1-x}Sb$ and $Al_xIn_{1-x}Sb$ were found to be difficult to anneal to homogeneity (Koster and Ulrich (58K4), Woolley and Smith (58W9)). Baranov and Goryunova (60B2) showed that the entire $Al_xIn_{1-x}Sb$ system could be prepared by annealling at temperatures closer to the solidus. These same workers reported that zone melting did not produce homogeneous alloys because of the loss of the volatile antimony component, but Ageev et al (62A7) reported that zone melting could be used with fair success and the resulting material was used in a study of the Nernst-Ettingshausen Effect.

$Al_x Ga_{1-x} Sb$ alloys were produced by zone melting by Burdiyan et al (58B6, 58G10, 59B15) where the best results were obtained by a slow zone sweep after a thorough homogenization by several rapid zone passes. The homogeneity of the resulting polycrystalline ingots was excellent being less than one mol % over most of the alloy range.

Miller et al (60M3) have produced polycrystalline ingots of the same material by zone levelling with roughly equivalent results.

The alloys of $Ga_x Al_{1-x} As$ have been prepared by Stambaugh et al (61S20) by a method of solute buildup. In this technique a mixture of molten gallium and aluminum is held in an open boat in a temperature gradient of 5 to $10^{\circ}C/cm.$ at a mean temperature of $1200^{\circ}C$. A second furnace zone at a lower temperature contains a reservoir of arsenic. Both the boat and the arsenic are contained in an evaculated chamber of which no part is cooler than the arsenic reservoir. The vapour pressure of the arsenic is allowed to increase by gradual heating until sufficient arsenic is dissolved by the Al-Ga liquid to cause saturation and solidification at the cooler end of the boat. A further increase in the arsenic pressure causes the gradual solidification along the length of the melt with a variation in the alloy produced from AlAs rich to GaAs rich material. Single phase

samples ranging from x = 0.0052 to x = 0.50 have been obtained from starting materials of varying Al-Ga composition. This method could prove quite adaptable to other alloy systems with volative constituents such as $Ga_xIn_{1-x}P$ or perhaps $GaAs_xSb_{1-x}$ and $Al_xIn_{1-x}As$.

Rupprecht et al (67R1) have grown crystals of $Al_xGa_{1-x}As$ by liquid epitaxy using a method similar to that used by Nelson (63N9) for GaAs. The alloy is deposited on a GaAs substrate from a supercooled solution rich in Ga and Al. The excess material is etched away leaving the alloy material exposed on the substrate.

Black and Ku (66B5) report $Ga_{1-x}Al_xAs$ alloys for injection electroluminescence work, having obtained their material by vapour transport, but they have a drastic composition variation in each specimen of ~ 30 mol % through a 10 mil layer. Solid alloy ingots were produced by these same workers using normal freezing techniques. They obtained alloys of all compositions greater than 50 mol % AlAs with homogeneity of approximately ± 1 mol %.

Of the remaining possible ternary systems, no complete solution has been reported for the following:
$Al_xGa_{1-x}P$, $Al_xIn_{1-x}P$, $InSb_{1-x}P_x$, $GaSb_{1-x}P_x$, AlP_xAs_{1-x}, $AlAs_xSb_{1-x}$ and AlP_xSb_{1-x}.

$InSb_{1-x}Bi_x$ alloys have been prepared by Jean-Louis

and Bernard (66J1) who grew crystal with up to 5 mol % of InBi in a Czochralski crystal pulling apparatus. They found that the lattice parameter is unchanged with alloying. The composition was then determined by microprobe analysis and the homogeneity inferred from the continuous variation of the energy gap with composition.

$In_{1-x}Tl_xSb$ mixed crystals were reported as immiscible by Kradinova (65K1). In the present work it was determined that there was no observable lattice parameter variation when InBi or $Tl_{.5} - Sb_{.5}$ was added to InSb in a Bridgman type furnace. Further investigation of these systems will be carried out in the near future to determine the full extent of alloying and its effects on the electrical properties of InSb.

2.4.6 Quaternary III - V Alloys

Sirota and Makovetskaya (63S9) have reported the preparation of $(GaAs)_x(InP)_{1-x}$ alloys by dissolving the two volatile group V components into a melt of gallium and indium and then by passing a hot zone over the resulting ingot. Alloys were prepared at intervals of 10 mol % but the lattice parameter variation with composition as determined by X-ray diffraction exhibited a pronounced minimum at ~ 40 mol % GaAs. The existence of such a minimum is not compatible with the work of Müller and Richards

(64M5) who show that there is a linear variation of lattice constant with x in this alloy system. No discussion is offered on the homogeneity of the resulting material nor is the composition determined by any method other than by recording the proportion of the initial constituents.

It seems probable that the process of zone levelling of the ingots produced caused the disproportionalization of the alloy to a GaP - InAs alignment. Müller and Richards report a similar tendency for the $(GaAs)_x$ - $(InSb)_{1-x}$ system and suggest that the alloys prefer an arrangement where the tetrahedral bonding is between atoms of similar atomic radius. A shift to a GaP rich phase in the $(GaAs)_x$ - $(InP)_{1-x}$ alloys would explain the decrease in lattice parameter since the atomic spacing in GaP is less than in either GaAs or InP.

Some attempts were made in the present work to prepare ingots of the alloy system $(GaAs)_x$ $(InSb)_{1-x}$ by the step freeze method. However, this system was proven not to be pseudo-binary and not to have a complete range of solid solutions.

According to Müller and Richards the only quaternary alloy systems which have a complete range of miscibility are $(GaP)_x$ $(InAs)_{1-x}$ and $(GaAs)_x$ $(InP)_{1-x}$; all others have limited solid solubility of between 10 and 20 mol % at

either end of the composition range. The ternary alloys $InP_x Sb_{1-x}$ and $GaP_x Sb_{1-x}$ will also have limited miscibility due to the large atomic radius difference of antimony and phosphorous.

Much work remains to be done on production of good homogeneous alloys, not only in order to supply better material for such applications as light detection, filtering and emission, or microwave generation etc., but to allow better determination of band structure parameters to give us a more basic understanding of the nature of semiconductors.

In many of the III - V alloy systems where complete miscibility is known to exist, production of homogeneous material at all compositions has yet to be accomplished. In those alloys where solid samples have been produced for all compositions, single crystals are still rare. Much remains to be done in the field of alloy preparation. In the following chapter the present work in this line will be presented with a discussion of both the methods used and the materials obtained.

CHAPTER III

PREPARATION OF III - V ALLOYS

3.1 Methods of Growth

Three different techniques have been applied in the present work to produce homogeneous alloy material. Samples covering the full composition range have been produced for the three alloy systems, $Ga_x In_{1-x} Sb$, $Ga_x In_{1-x} As$ and $InAs_x Sb_{1-x}$. All methods tried were basically directional solidification from the melt. Differing freezing interface conditions and solidification rates were used in attempts to improve the homogeneity and microstructure. The first method of growth used was gradient freezing. This was superceded by the more successful step freezing or horizontal Bridgman technique. Some alloys of $InAs_x Sb_{1-x}$ and of $GaAs_x Sb_{1-x}$ were also prepared using the method of zone re-crystallization.

3.1.1 Gradient Freeze Method

In this technique a suitable mixture of the constituent compounds is sealed in an evacuated quartz capsule. The compounds are used as source material rather than the elements involved since they are readily available and

since stochiometry is assured in this way for each ingot grown. As well, the problems associated with the use of volatile materials such as arsenic are avoided.

The capsule is heated to a temperature high enough to melt both constituents, and thorough mixing is assured by agitation. After carefully quenching the molten charge and allowing space for the expansion of the ingot on solidification, an ingot is obtained which is quite inhomogeneous but which has a given mean composition throughout. This ingot, still in its capsule, is then placed in a furnace with a linear temperature gradient of approximately $5^{o}C/cm.$, with the cooler end of the ingot above the melting point of either constituent compound.

The temperature is slowly lowered causing the ingot to solidify gradually from one end. This method has in its favour the fact the ingot is mechanically undisturbed throughout the period of growth, but there are many drawbacks as well.

The greatest problem is that of constitutional supercooling (64C2) which results in inhomogeneous solidification at the freezing interface. Figures 3.1.1, and 3.1.2 show an idealized system undergoing gradient freezing. The first material to freeze is rich in the higher melting point compound (A), leaving the molten part of the ingot enriched

GRADIENT FREEZE METHOD

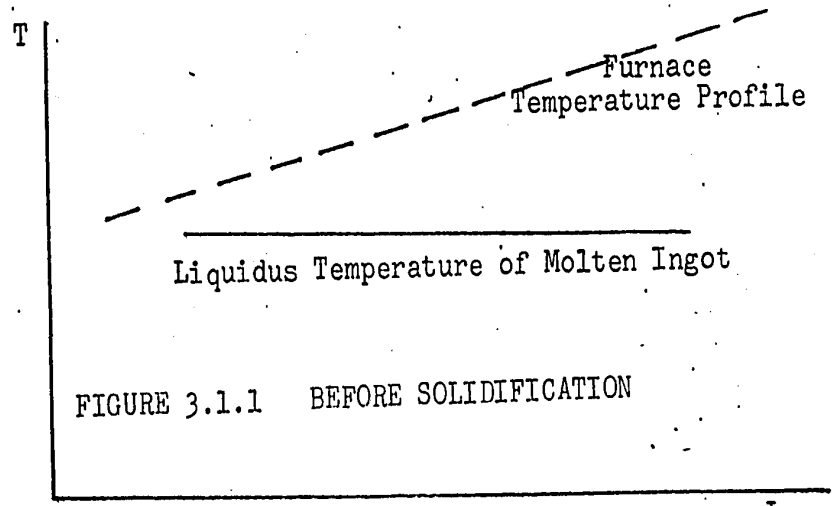

FIGURE 3.1.1 BEFORE SOLIDIFICATION

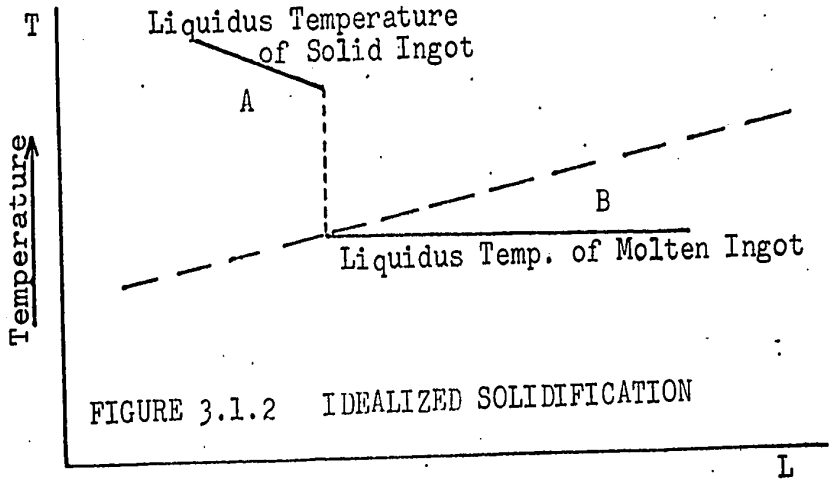

FIGURE 3.1.2 IDEALIZED SOLIDIFICATION

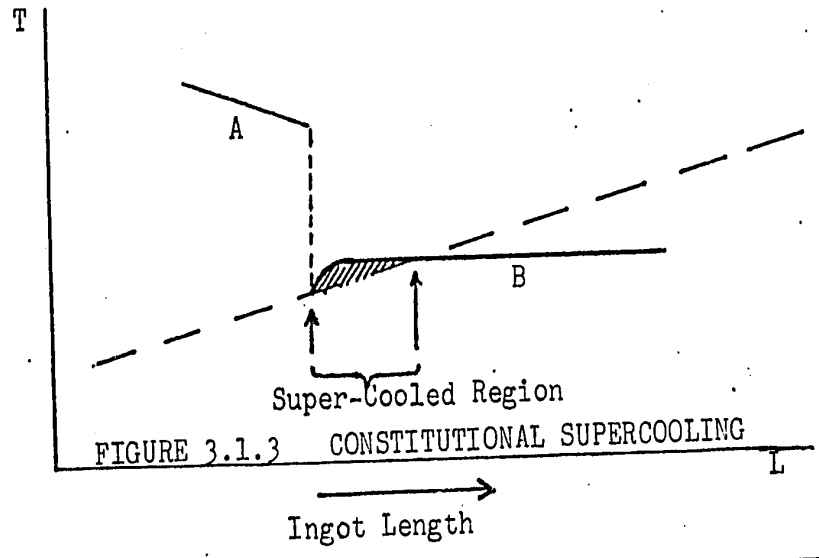

FIGURE 3.1.3 CONSTITUTIONAL SUPERCOOLING

in a lower melting point phase (B). At the interface there is a depletion of A causing a localized drop in the liquidus temperature. This depleted area is replenished with material from the rest of the molten ingot by a process of diffusion. Thus in the idealized case the molten ingot is brought back to a uniform equilibrium. In a real system, however, the rate of diffusion is such that the localized depletion region can never be eliminated. Obviously diffusion cannot begin until a composition gradient has been established. Thus the situation depicted in figure 3.1.3 can arise. In this diagram the furnace gradient is small enough that there is a region of supercooled material immediately in advance of the freezing interface. This situation is quite prevalent in III - V alloys since the diffusion rate in the materials is quite low.

In materials with very high melting points such as GaAs, the starting condition that the entire ingot is above the GaAs melting point means that the temperature gradient cannot be very steep without exceeding the limiting temperature for the quartz capsules which soften at $\sim 1300^{o}C$. This is a great problem where the arsenic vapour pressure is greater than atmospheric, as a weakened ampoule can easily explode.

3.1.2 Step Freeze Method

Consideration of the above drawbacks has led to a study of crystal solidification by the step freeze or horizontal Bridgman method. This technique features two furnaces, each with a flat temperature profile where one furnace is hotter than the melting point of either compound and the other furnace is cooler than either melting point. The temperature gradient between these two zones is made as steep as possible (as indicated in figure 3.1.4). The capsule containing the inhomogeneous ingot is slowly pulled through the temperature step, causing the ingot to solidify gradually from one end.

There are several advantages to be found in the use of this method. First, the solid-liquid interface is fixed by the position of the thermal step and thus the rate of solidification can be controlled by the motion of the ingot and is almost independent of the composition of the molten phase. The steep temperature gradient eliminates the danger of constitutional supercooling. The flat profile of the high temperature zone means that excessively high temperatures above the melting points can be avoided, and since the gradient position is fixed, the temperature of the two zones need not be controlled to the same stability as in gradient freezing. The lower temperature zone can be at room temperature unless one of the constituents is highly

FIGURE 3.1.4

STEP FREEZE METHOD

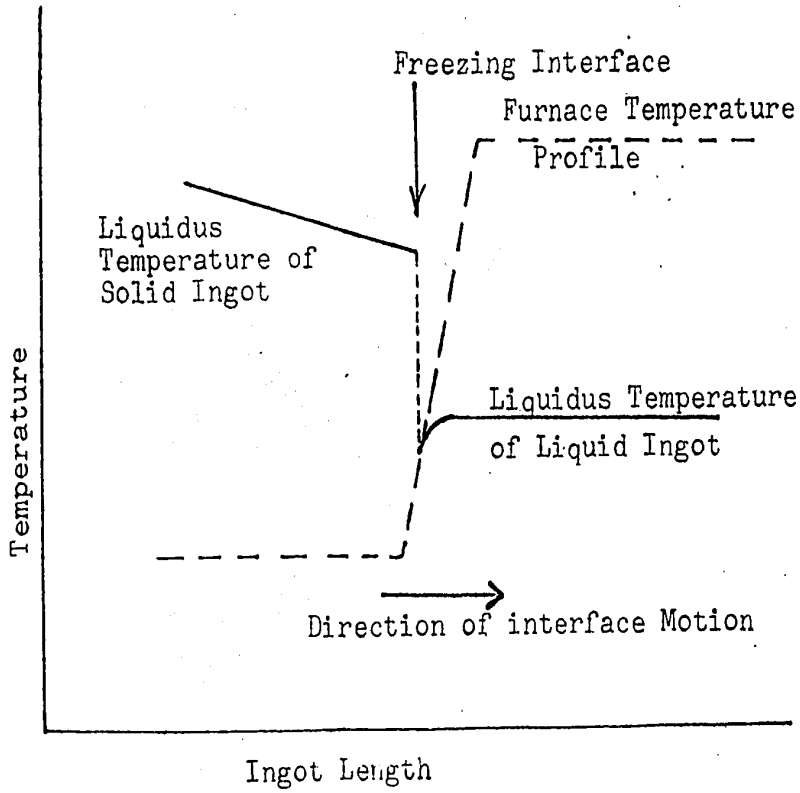

volatile as is the case with arsenides. In these cases a background temperature is required to prevent loss of the volatile component by condensation at the cooler end of the capsule.

3.1.3 Zone Recrystallization

Both of the preceding methods result in ingots which have a variable composition along the length of the ingot, and hence graded parameters. This is a desirable feature in the present work, since many samples of different compositions, which are needed for various experiments, are made available in a single ingot.

If, however, the composition change is too rapid, although the material may be homogeneous throughout, it is impossible to cut bulk specimens thin enough to have a low composition spread. When the equilibrium diagram shows an extreme separation of the liquidus and solidus curves, as is the case in the systems $InAs_x Sb_{1-x}$ and $GaAs_x Sb_{1-x}$, ingots grown by the above methods exhibit a rapid variation of composition with ingot length for the middle of the alloy range (see figure 3.3.6). In these cases, to obtain specimens with a small composition spread, it is necessary to try a form of zone recrystallization.

In zone recrystallization a small region of a flat-profiled furnace is raised in temperature above the melting

point of the alloy, creating a molten zone in a solid ingot. This zone is then caused to traverse the length of the ingot once or several times either by moving the ingot through the zone or by moving the zone over the ingot. At the leading edge of the molten zone, material is dissolved and melted, and at the trailing edge, solidification takes place. The alloy composition within the zone will quickly come to a phase which is in equilibrium with the solid of the mean ingot composition. As material is solidified at the freezing interface, equilibrium in the zone is maintained by dissolution of solid material of the same composition at the melting interface. Thus after a short length of ingot growth in which the zone equilibrium is established, the ingot is "zone levelled" i.e. brought to one composition value along its length (see figure 3.1.5).

It was thought that with a zone width greater than that used in normal zone levelling (i.e. 1/10 of the ingot length), perhaps a compromise between zone levelling and step freezing could be obtained. If the zone width were set at one-third of the ingot length the zone equilibrium would not be quickly established and so a varying composition would result over approximately the first one-third of the ingot. When the zone equilibrium was established there would be another third of the ingot "levelled", then as the leading edge of the molten zone reached the end of the charge,

FIGURE 3.1.5

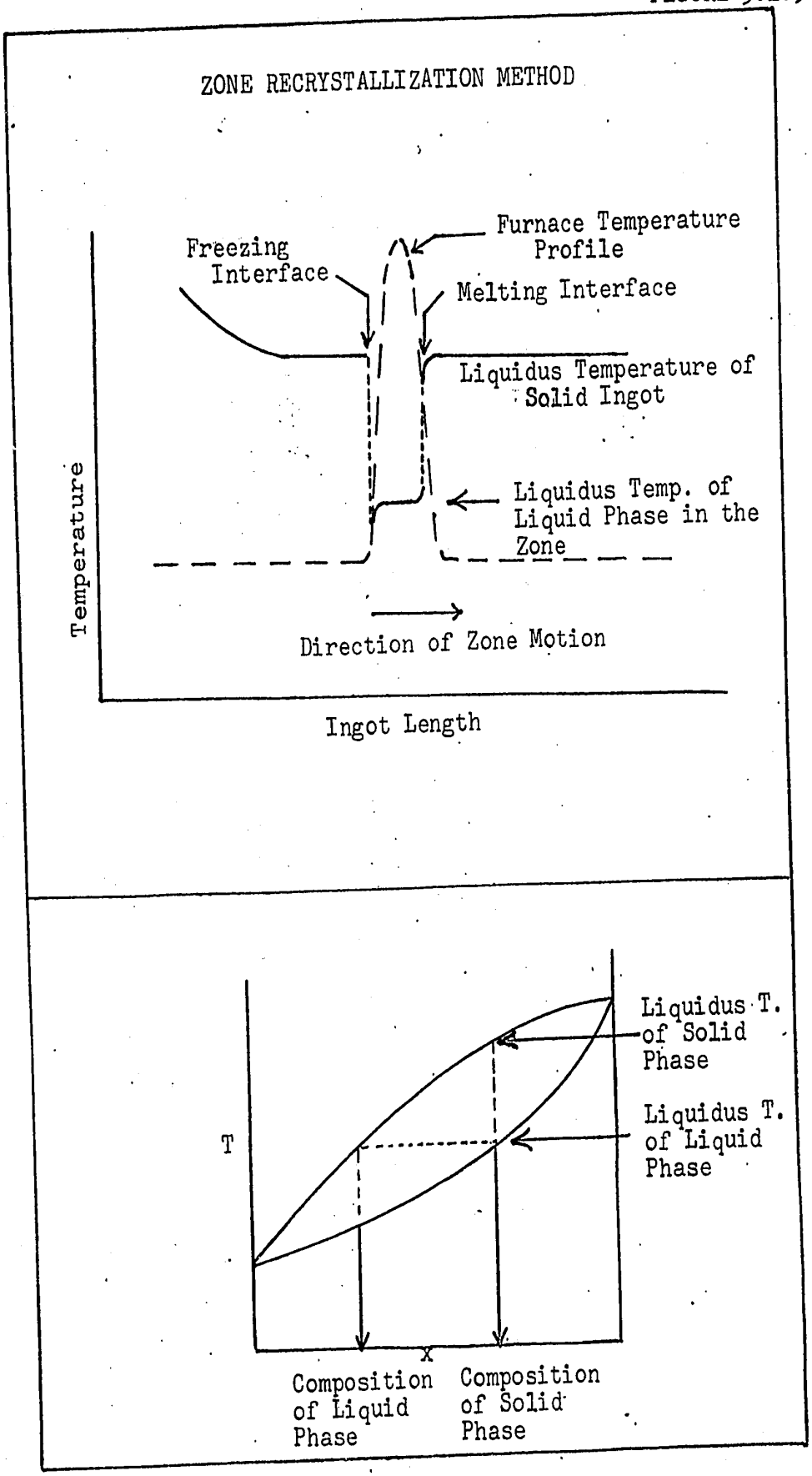
ZONE RECRYSTALLIZATION METHOD
Freezing Interface
Furnace Temperature Profile
Melting Interface
Liquidus Temperature of Solid Ingot
Liquidus Temp. of Liquid Phase in the Zone
Temperature
Direction of Zone Motion
Ingot Length
T
Liquidus T. of Solid Phase
Liquidus T. of Liquid Phase
X
Composition of Liquid Phase
Composition of Solid Phase

the composition in the liquid phase would gradually become enriched in the lower melting point compound.

In practice this procedure has proved difficult to realize. The biggest problem is in controlling the width of the zone while the melting point of the material undergoes drastic variation. The zone is necessarily wider at lower temperatures and is further widened by thermal conduction along the ingot. Some promising results have been obtained using this wide-zone recrystallization technique but much work remains to be done to improve the apparatus.

3.1.4 Other Possible Methods of Alloy Preparation

There remain some potentially very useful techniques which could be employed in production of bulk samples of alloys, but have not yet been used in the present work. The most promising of these are the methods of step levelling as developed by Dismukes (65D1) and applied by Kudman et al (67K1, 68K2), and the method of solute buildup as reported by Stambaugh et al. (61S20) and Sirota et al (63S9). These methods were described in Chapter II. Alloy growth by Czochralski pulling is rapidly gaining ground as a successful method as well, (see sections 2.4.1 and 2.4.3).

3.2 Furnace Design

3.2.1 Gradient Freeze Furnaces

Gradient freeze furnaces have been constructed in basically the same way as reported by Woolley and Smith (58W9) and used by Woolley et al. for the production of ingots of $Ga_xIn_{1-x}Sb$, $Ga_xIn_{1-x}As$ (58W9) and $InAs_xSb_{1-x}$ (64W1). Typical furnaces as shown in figure 3.2.1 were composed of two foot lengths of refractory tubing, either "mullite" or alumina, with inner diameters of 1 or 1½ inches. About these tubes in coil fashion was wound approximately 50 feet of 0.43 Ω per foot Kanthal resistance wire, which results in a furnace resistance of about 20 ohms. The pattern of coil winding needed to achieve a desired thermal profile was evolved by a procedure of trial and correction. The resistance wire coil was fixed in place with an 1/8 inch thick coating of "Kyanex" refractory cement which also served to distribute the heating of the coil more evenly along the furnace tube. The tube was mounted centrally along the main axis of a rectangular box with sheet aluminum walls and square "transite" end plates. The dimensions of the box were 10 x 10 x 24 inches in a general case and the space within was filled with mica insulating material. A Pt-Pt/13% Rh thermocouple was cemented to the furnace tube externally, near the center of its length. This was used to

FIGURE 3.2.1

GRADIENT FREEZE FURNACE

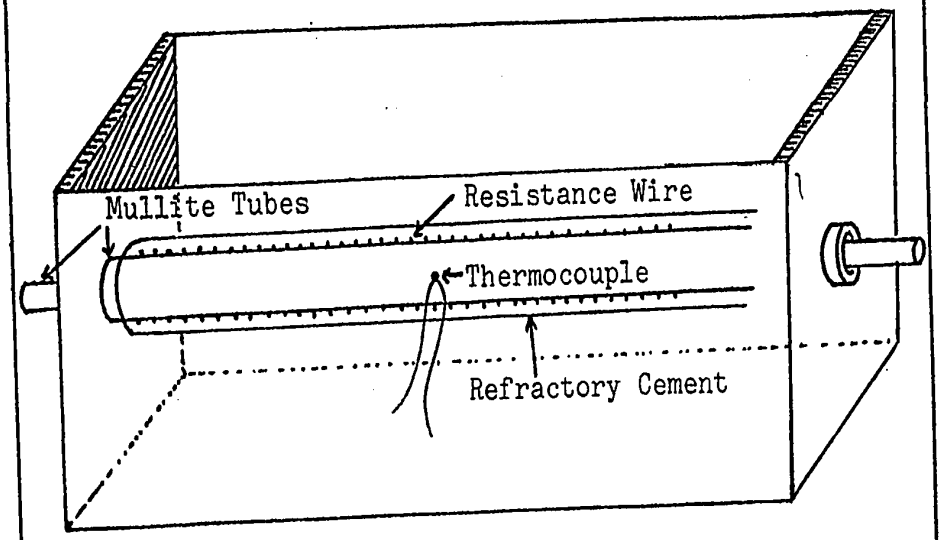

FIGURE 3.2.2

TEMPERATURE PROFILE OF G.F. FURNACE

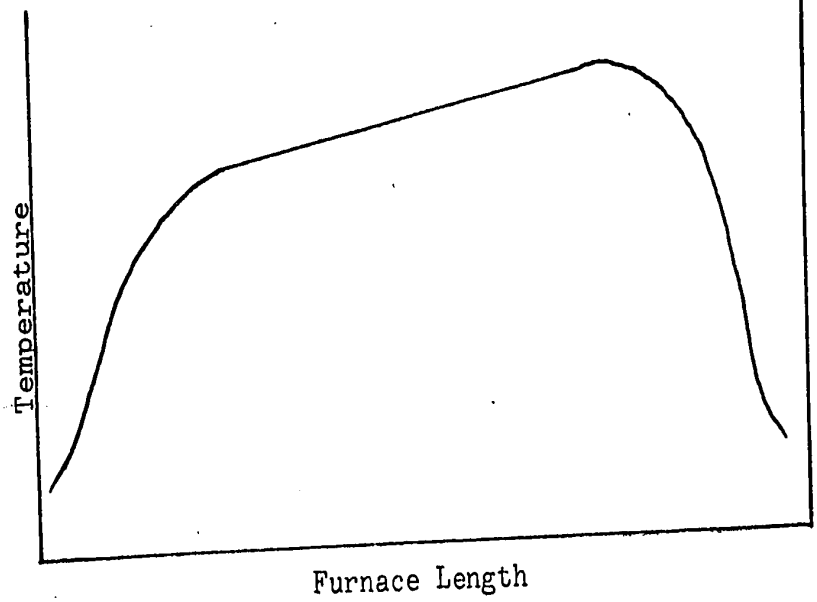

monitor the furnace temperature for the controlling apparatus.

Temperature was maintained to within one degree C. by an "Ether Transitrol" proportional controller which employs a saturable reactor. The temperature was lowered 5-10°C/day by changing the set point on the controller with a motor and "Meccano" gear assembly. The motor ("Barber Colman") had a full load torque of 100 lb-in. and a speed under load of 0.3 rpm. The gear ratio was of the order of 1:5000. When running under normal condition a gradient freeze furnace would draw about five hundred watts. (i.e. 100 Volts; 5 Amperes) Growth times were normally two or three months for ingots 15-20 cm. long. Figure 3.2.2 shows a typical directional freeze furnace temperature profile.

3.2.2 Step Freeze Furnace

Step freeze furnaces were constructed along the same lines as the directional freeze furnaces. The main difference was the pattern for the resistance wire coil windings. In these furnaces a flat temperature profile was desired instead of a gradient. The step freeze furnace was composed of two similar tubular furnaces placed end to end as shown in figure 3.2.3. They were enclosed in an aluminum sheet metal box and were separated by a one inch air gap. At either side of the gap were placed water-cooled copper baffles which served

FIGURE 3.2.3

STEP FREEZE FURNACE

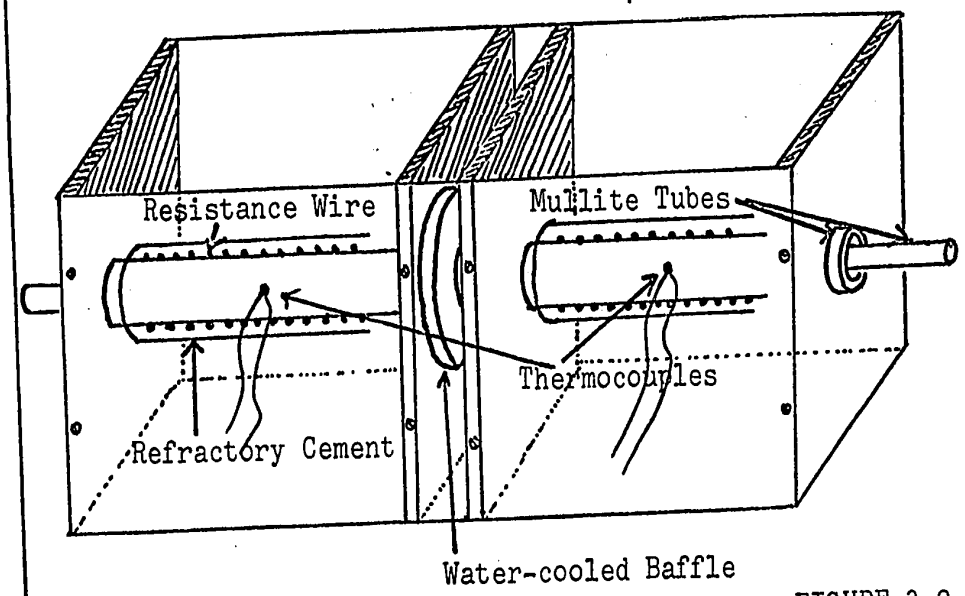

FIGURE 3.2.4

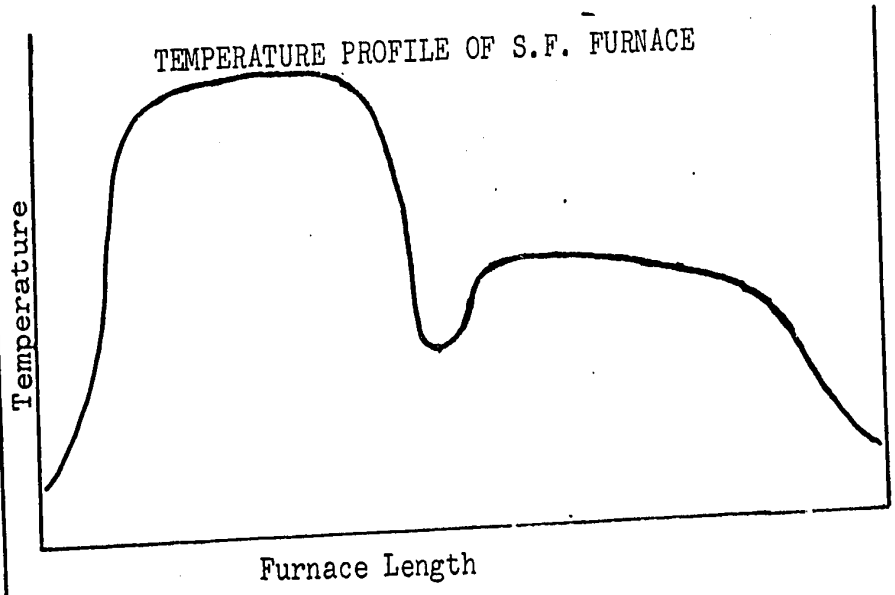

to insulate the two temperature zones from each other in order to ensure a steep temperature gradient. Both furnaces were monitored by Pt-Pt 13% Rh thermocouples cemented to each furnace externally. Each zone was controlled with a Phillips off-on controller which maintained the temperature to within 2 degrees of a set point. This degree of stability was sufficient since neither zone was near to the melting point of any alloy composition. When, however, the temperature of the hot zone approached 1200°C, which is close to the failure point of the Kanthal resistance wire, it was found that use of a proportional control resulted in longer furnace life.

The capsule containing the ingot was placed in a "mullite" carrying tube which was mounted on small wheeled dollies on tracks at either end of the furnace. A "Meccano" worm and gear assembly slowed the drive of a Barber Colman motor from 0.3 rpm to a rate which moved the capsule through the step of the furnace from 0.5 to 2 cm/day depending on the material being grown. Growth times from two weeks to two months were employed for various ingots 15 to 20 cm. in length. Figure 3.2.4 shows a typical step freeze furnace temperature profile.

3.2.3 Zone Recrystallization Furnace

The zone furnace (figure 3.2.5) was made up of two flat-

FIGURE 3.2.5

ZONE RECRYSTALLIZATION FURNACE

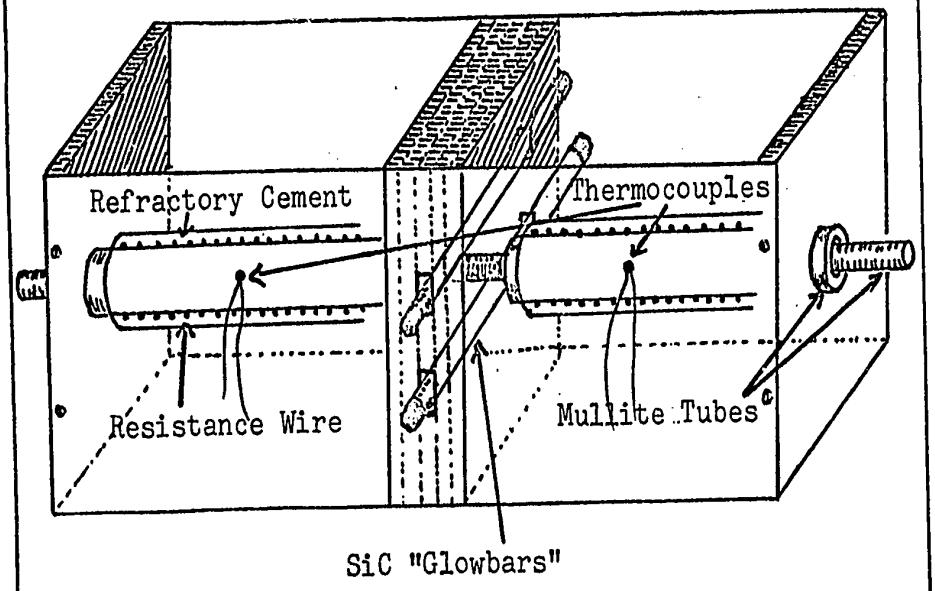

FIGURE 3.2.6

TEMPERATURE PROFILE OF Z.R. FURNACE

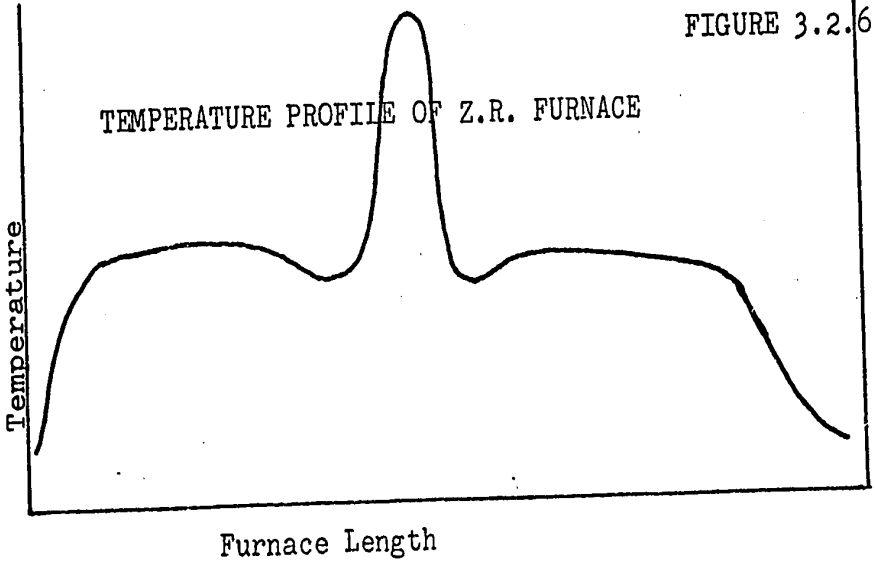

profile furnaces positioned in the same way as for the step freeze furnace but separated by a 5 cm. wide hot zone. At either side of the hot zone there were water-cooled copper baffles to keep the zone width narrow. The zone was heated by two silicon-carbide "Norton" glowbars which were mounted horizontally, at right angles to the furnace axis, one above and one below the ingot. The walls of the hot chamber were composed entirely of "transite" boards coated with liquid porcelain.

Power to the glowbars was supplied through a step-down transformer so that a maximum power of 40 Amperes at 50 Volts was available. The hot zone temperature was monitered by a Platinum-Platinum 13% Rhodium thermocouple feeding the controlling voltage to a proportional, saturable reactor ("Ether-Transitrol") controller which held the zone temperature steady to within $5^{o}C$ at $1000^{o}C$. The lack of better stability is due to the time lag in the heating of the thermocouple in the air of the hot zone. Under normal running conditions the glowbars, which were connected in parallel, draw about 1400 watts. The background furnaces were regulated by Phillips off-on controller within $2\text{-}3^{o}C$ of the set point. A narrower zone could probably be achieved using a radio-frequency induction heater if the condition of long duration continuous running could be met, and this alternative will be looked into in the near future.

The entire furnace assembly was mounted on a cart which was driven up a ten percent grade on tracks. The drive mechanism was a 0.3 rpm (Barber Colman) motor, geared down using a "Meccano" worm and gear assembly to move the furnace at a rate of 0.5 cm/day. This rate could be adjusted to 1.0 or 0.7 cm/day by means of a "Sturmey Archer" bicycle gear arrangement. At 0.5 cm/day the time involved in moving the ingot from one background furnace, through the zone completely, then into the other background was about 90 days for a typical ingot of 15 centimeters.

The ingot and furnace were inclined at a ten percent grade to prevent build up of the crystal at the end last to freeze. These materials tend to expand on freezing and the slope of the ingot kept the cross-section of the ingot relatively uniform. Figure 3.2.6 shows the temperature profile of the zone furnace used to prepare alloys of $InAs_x Sb_{1-x}$.

3.3 Alloy Material Obtained

3.3.1 $Ga_x In_{1-x} Sb$ Alloys

For the $Ga_x In_{1-x} Sb$ alloys the constituents were appropriate weights of pure InSb and GaSb. The Indium antimonide was obtained in the form of polycrystalline ingots from Cominco. The GaSb was prepared in this laboratory from equal atomic weights of 5-9's gallium (Merck) and antimony (Cominco) mixed and melted together in an evacuated quartz capsule then quenched in air. The GaSb was found to be p-type with about 3×10^{17} cm^{-3} acceptors while the InSb had approximately 10^{16} cm^{-3} donors. The acceptors in GaSb are thought to be antimony vacancies which are due to an intrinsic nonstochiometry in the compound (65B2). These acceptors are partially compensated by donors as an ingot of the alloy is grown and perhaps are less prevalent as the ingot becomes enriched in InSb.

Many homogeneous samples of $Ga_x In_{1-x} Sb$ alloys have been prepared in the present work by the gradient freeze technique. The mean composition of the starting material has been varied from $x = 0.7$ to $x = 0.3$ in order to produce alloys of all compositions. Alloy compositions in the range $0.95 > x > 0.0$ have been made available by this method. Figure 3.3.1 shows the variation of alloy composition with ingot length for three gradient frozen ingots. Where a bar

ALLOY COMPOSITION versus INGOT LENGTH FIGURE 3.3.1

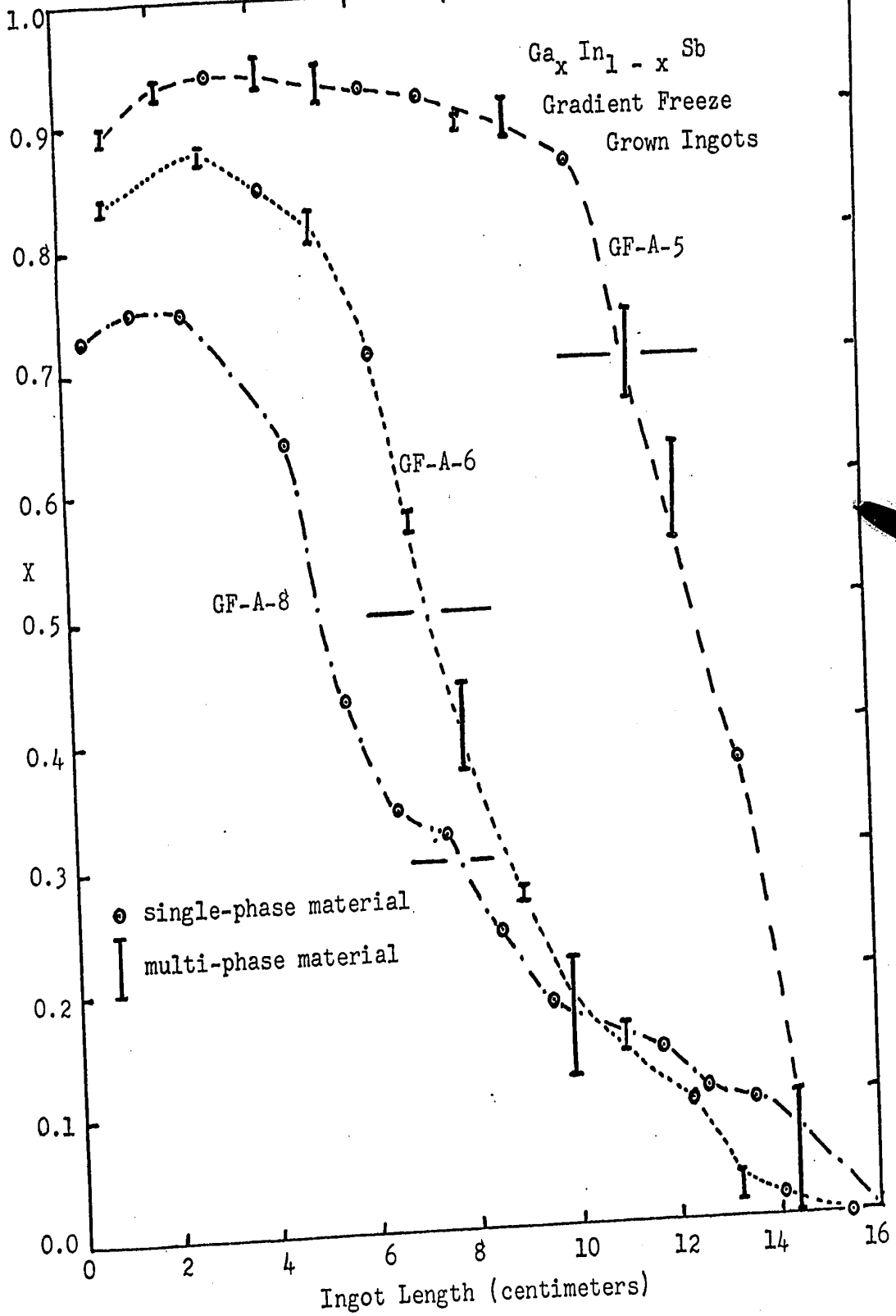

(I) is shown, the ends of the bar indicate the composition of the two phases present in an inhomogeneous sample. The horizontal line on each curve indicates the mean composition of the starting material. An almost complete range of alloys can be obtained by this method but with relatively poor homogeneity in most cases. Structurally the crystals are sound, that is they can be cut, ground and polished without cracking or disintegrating and they contain no voids or cracks. Samples at the InSb rich end of an ingot tend to be more brittle than those rich in GaSb.

All ingots directionally frozen were polycrystalline with crystallite sizes of a few cubic millimeters. The size of crystallites tended to increase along the ingot towards the InSb rich end.

For undoped ingots the carrier concentrations ranged from approximately 10^{17} acceptors cm^{-3} at the GaSb rich end to about 10^{17} donors cm^{-3} at the InSb rich end. Samples from the center of the ingots were more or less compensated and had residual carrier densities as low as $\sim 10^{15}$ cm^{-3} in some cases. More detailed descriptions of the individual samples will be found in chapter VI.

Since the major problem with respect to good homogeneity was felt to be constitutional supercooling, the step freeze method was tried in order to eliminate this condition. The rate of growth for the first trials was set

at 0.5 cm/day but, with increasingly encouraging results, this rate was increased to 1.5 cm/day. This meant that the time of growth for a typical 15 cm. ingot was reduced from 50 to 15 days. In this work ingots were prepared without intentionally adding impurities. Figure 3.3.2. gives the composition as a function of ingot length for three step frozen ingots. The horizontal line indicates the mean starting composition of each ingot. It can be seen that the variation of composition is more regular than with the gradient freeze method, and the homogeneity in all ingots is quite improved. The composition spread in each sample on this figure is within one mol.% of the indicated value and the open circles have diameters appropriate to the positional and compositional uncertainty. Good homogeneous, polycrystalline material at all alloy compositions can be produced using this method of growth.

Structurally the step freeze grown material is free from cracks or voids and is mechanically sound. The InSb rich alloys tend to be more brittle than those rich in GaSb but not so brittle as in the preceding case. Crystallite sizes in a typical ingot range from $\sim 1 \times 1 \times 5$ mm^3 to $\sim 1 \times 3 \times 10$ mm^3. Carrier concentrations were consistantly below 5×10^{16} cm^{-3} when the material was not deliberately doped, and all ingots exhibit a progressive change from p-type to n-type conduction with ingot length. Some

ALLOY COMPOSITION versus INGOT LENGTH FIGURE 3.3.2

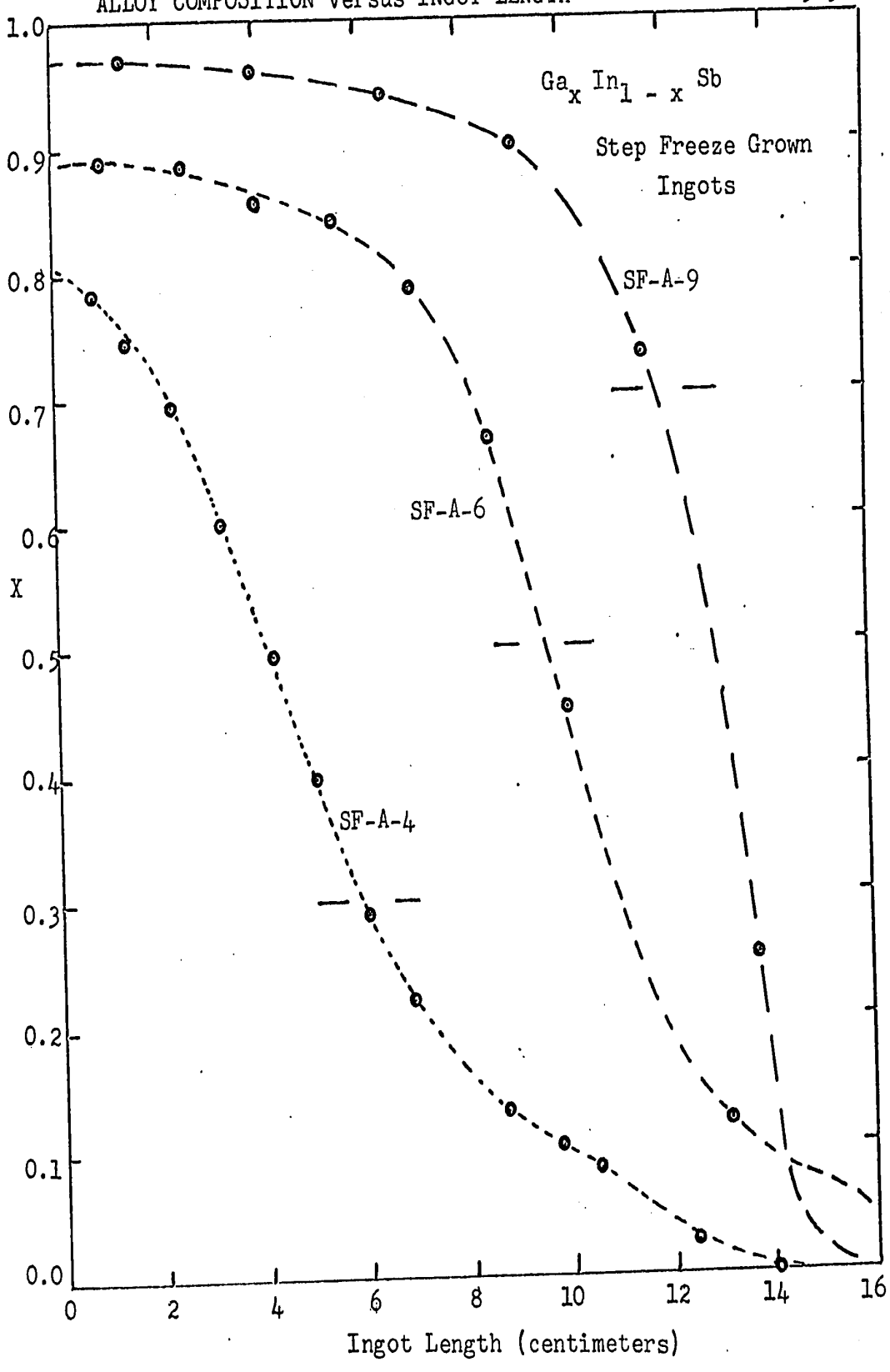

compensated samples from the middle of an ingot had measured residual carrier concentrations of less than 5×10^{14} cm^{-3}.

Cross-sectional slices of about one millimeter thickness were used for composition and homogeneity determination. A small part of such a slice was ground to a fine powder for use in a Debye Scherrer X-ray camera. The position and spacing of the diffraction lines enable the lattice parameter, and hence the composition of a sample to be obtained while their sharpness or multiplicity indicate the homogeneity. The procedure for determining the lattice spacing from X-ray photographs is quite standard and the interested reader is referred to Kittel (56K7), Dekker (57D4) or more specifically Henry et al. (51H1). Figure 3.3.3 shows some of the X-ray films for some step freeze grown samples of $Ga_x In_{1-x} Sb$.

When the lattice parameter has been determined for a sample, in order to obtain the composition, reference must be made to the work of Woolley and Smith (58W9) who have reported the variation of the lattice parameter with composition for this alloy system. Absolute values for the composition are limited by the experimental error in this work which is ± 1 percent.

3.3.2 $Ga_x In_{1-x} As$

Ingots for this mixed crystal system were prepared from

DEBYE SCHERRER X-RAY PHOTOGRAPHS FIGURE 3.3.3

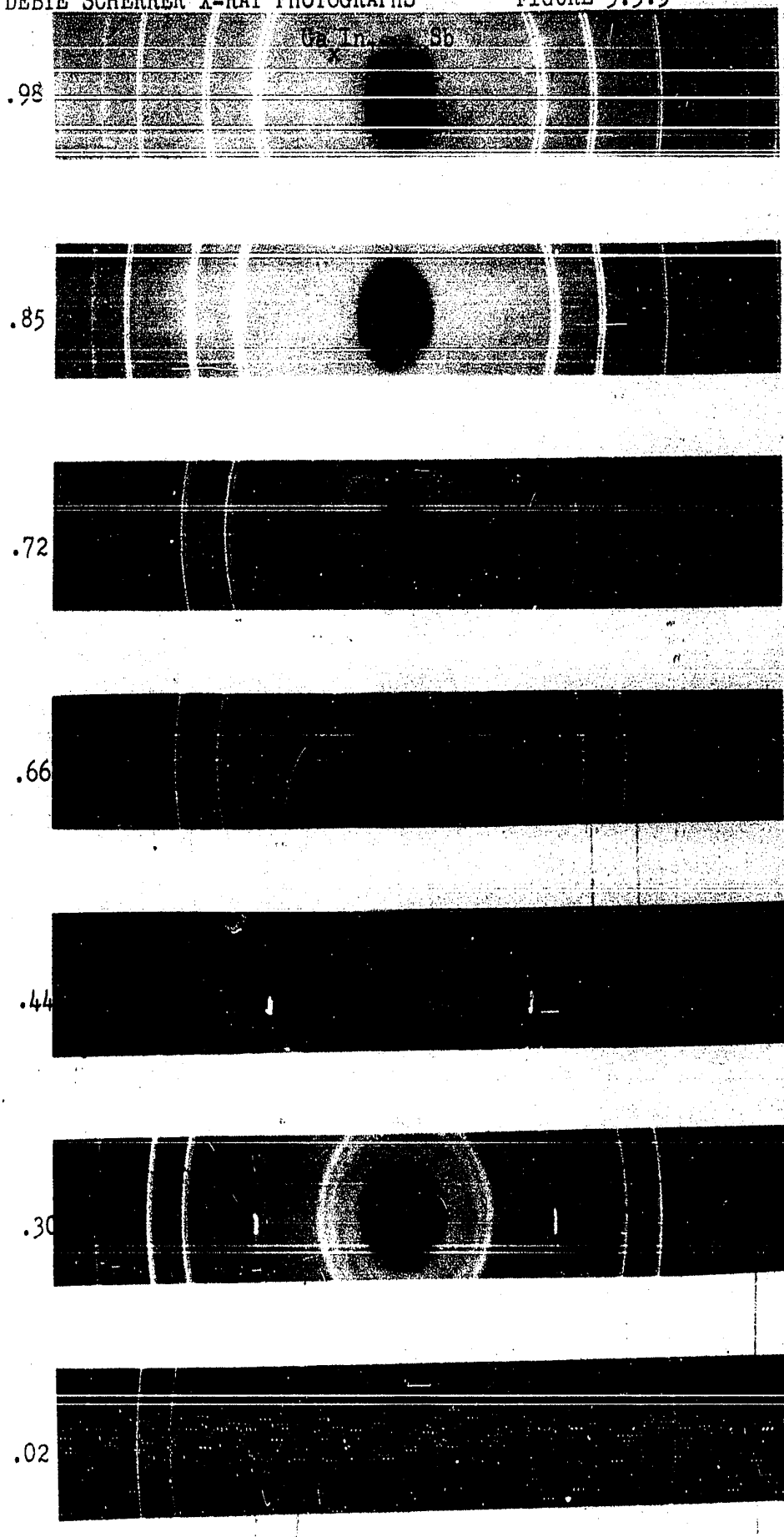

DEBYE SCHERRER X-RAY PHOTOGRAPHS FIGURE 3.3.3

$Ga_xIn_{1-x}Sb$

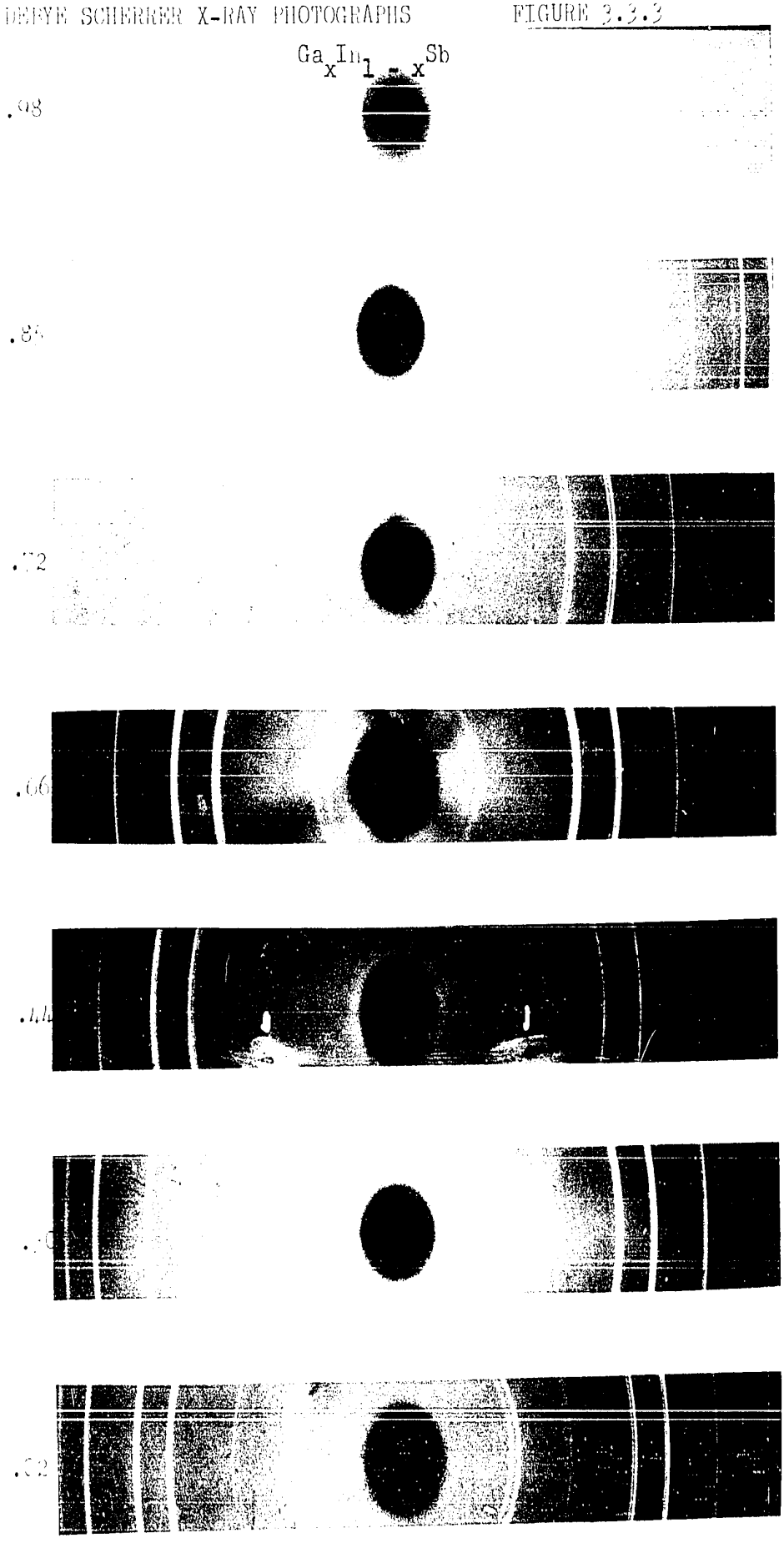

pure InAs obtained from Cominco and from GaAs obtained from Consolidated Electrodynamics Inc. The material was in the form of slabs and pieces from polycrystalline ingots and had approximately 10^{16} donors cm^{-3}. The compounds were melted together in evacuated quartz capsules and thoroughly mixed to form solid inhomogeneous ingots.

The first growth technique tried in this laboratory for this alloy system was gradient freezing. Two ingots were produced in this manner by Thompson (67T1) who reported that constitutional supercooling results in multiphase material throughout most of a typical ingot. This is because of the very slight temperature gradient needed to avoid overheating the furnace and the capsule. Thompson applied the step freeze method to one ingot with a mean charge of $x = 0.3$ and obtained the range of compositions from $0.03 < x < 0.82$ with good homogeneity. In order to compensate for the loss of arsenic by evaporation, a 10% excess of pure metallic arsenic was sealed in the capsule of a fifty gram ingot. The resulting material was n-type and had carrier concentrations ranging from 1.3×10^{18} cm^{-3} for $x = 0.82$ and $x = 0.52$, rising to 1.9×10^{18} cm^{-3} for $x = 0.29$ and to 2.2×10^{18} cm^{-3} for $x = 0.13$. A second ingot with a mean composition of $x = 0.55$ was grown by the same method and yielded good homogeneous specimens in the ranges $0.45 < x < 0.92$ with donor concentrations from 1 to 4×10^{17} cm^{-3}.

In the present work, near-intrinsic material of all compositions was desired and so ingots of this system were prepared by the step freeze method omitting the excess arsenic added by Thompson. Two ingots with mean compositions of $x = 0.3$ and one with a mean composition of $x = 0.7$ were grown in this manner.

The hot zone of the two-zone furnace was set at 1200°C and the background temperature was set at 600°C. This latter temperature is cool enough to allow the ingot to solidify at all compositions but high enough to prevent condensation of arsenic and to maintain the arsenic vapour pressure over the ingot. Growth rates were approximately one cm/day for ingots which were 12 to 15 centimeters in length.

Figure 3.3.4 shows the composition as a function of length for one of the ingots with a mean composition of $x = 0.3$ and for the ingot with $x = 0.7$. It can be seen that alloy samples ranging in composition from $x = 0.92$ to $x = 0.0$ can be obtained from these two ingots. The variation of composition is gradual enough that the composition spread in a given 1 mm. thick slice is one mol. percent or less. Powder X-ray photographs show sharp resolution even at the high angle diffraction lines and the $K\alpha_1 - K\alpha_2$ doublet is clearly resolved, (see figure 3.3.5). All ingots prepared were n-type with extrinsic carrier concentrations ranging from $\sim 5.0 \times 10^{16}$ cm^{-3} at $x = 0.66$ to 1.4×10^{17} cm^{-3} at

ALLOY COMPOSITION versus INGOT LENGTH FIGURE 3.3.4

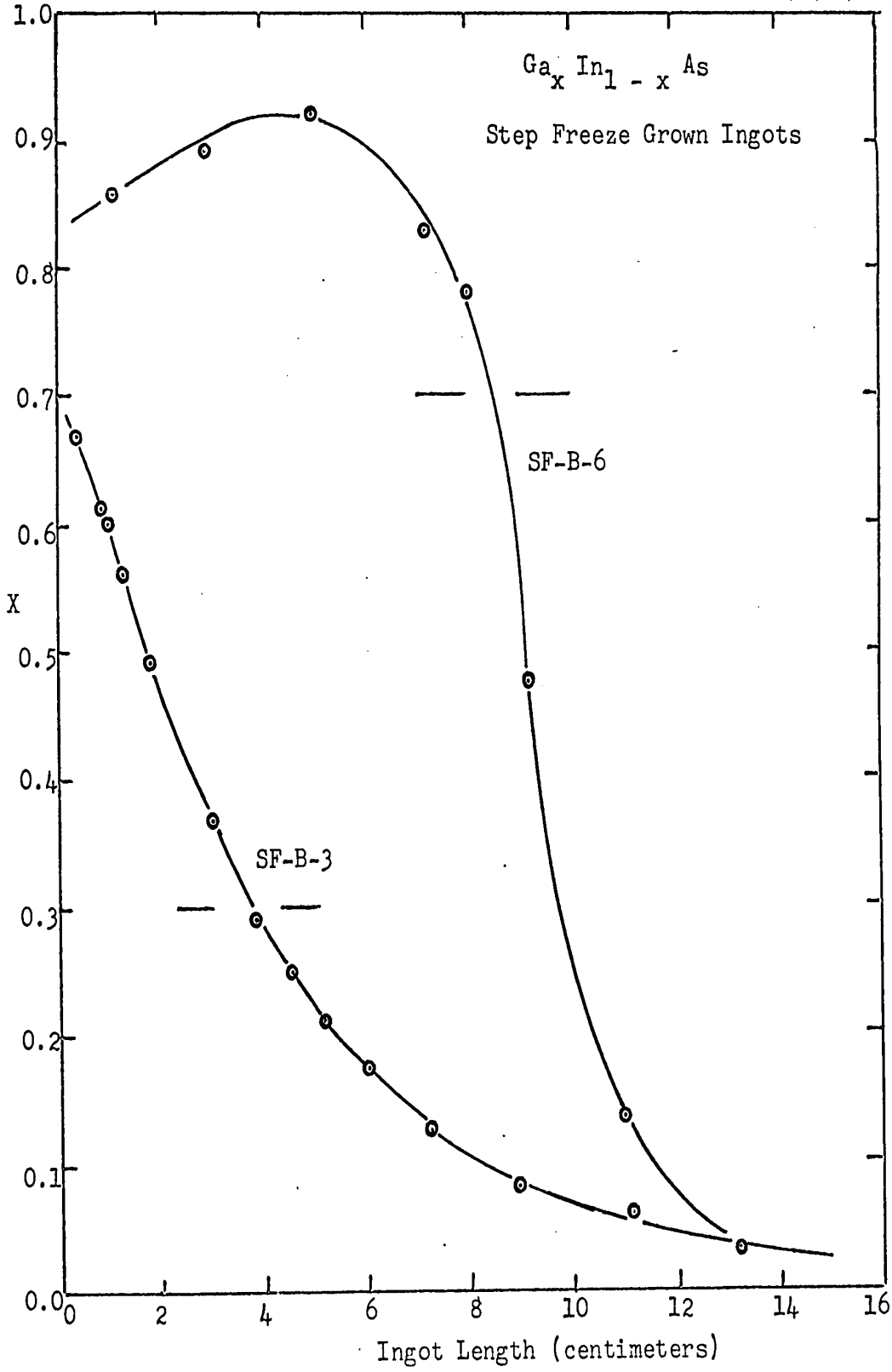

DEBYE SCHERRER X-RAY PHOTOGRAPHS FIGURE 3.3.5

$Ga_xIn_{1-x}As$

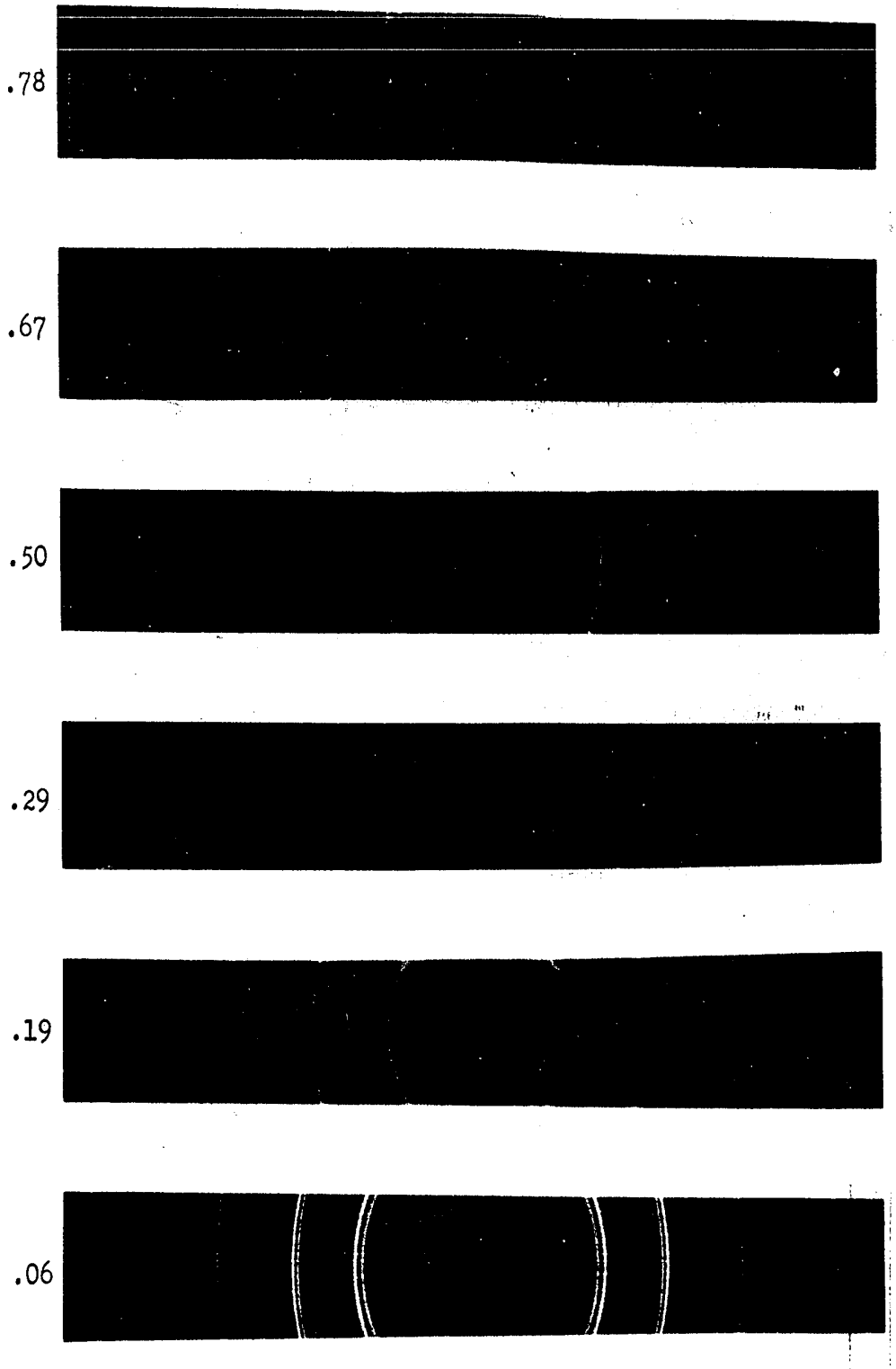

DEBYE SCHERRER X-RAY PHOTOGRAPHS FIGURE 3.3.5

$Ga_xIn_{1-x}As$

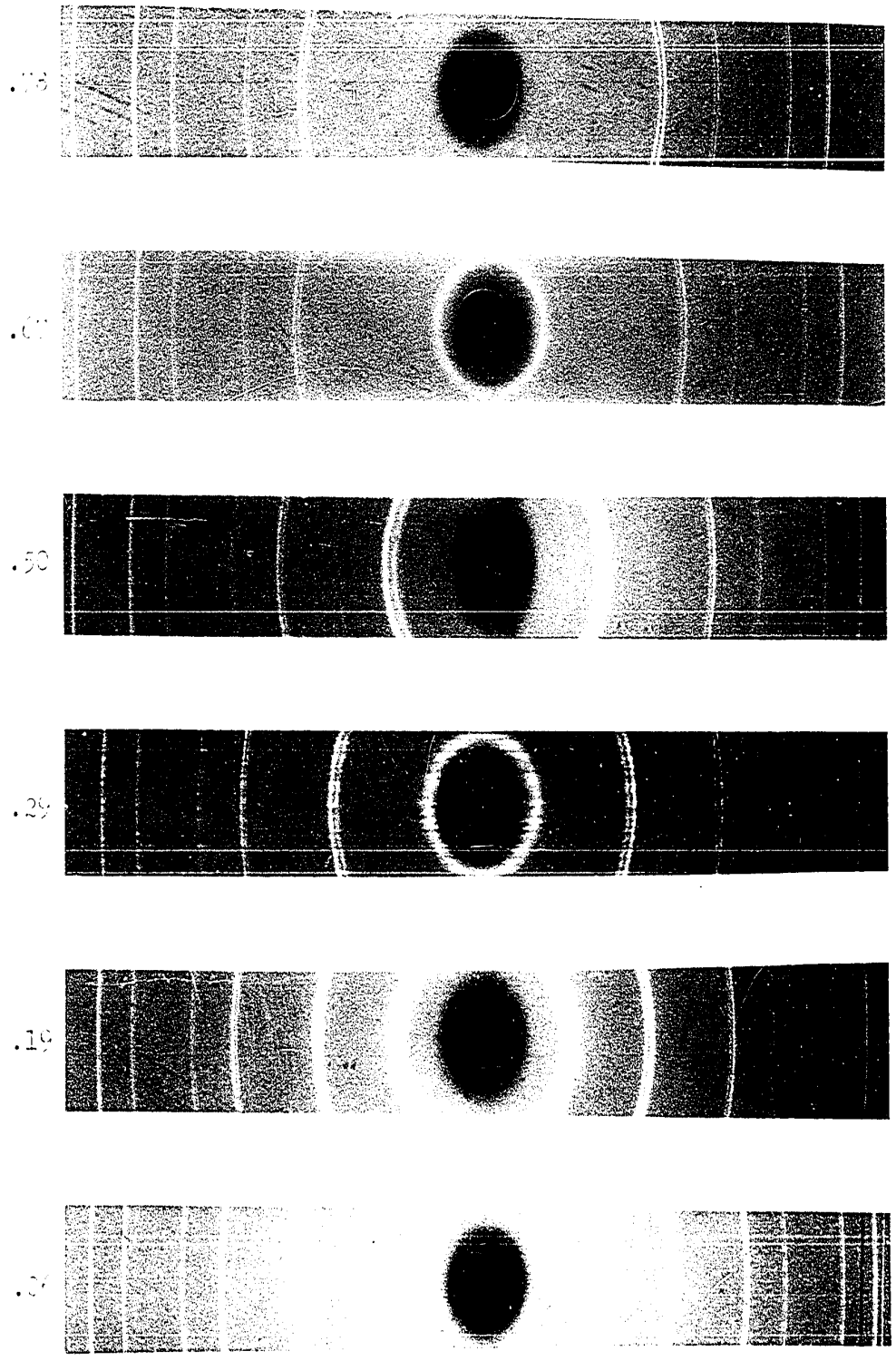

$x = 0.05$ in ingot SF.B.3 and from $\sim 10^{17}$ cm^{-3} at $x = 0.92$, and 1.33×10^{17} cm^{-3} at $x = 0.83$ to 2.5×10^{18} cm^{-3} at $x = 0.13$ for ingot SF.B.6. The ingots were polycrystalline in all cases with crystallite size ranging from one mm^3 at the GaAs rich ends to a condition of only two or three crystallites in a cross-section at the InAs rich ends. Ingots were elliptical in cross-section and had lengths of 12 to 15 cm. Structurally these alloys were sound, containing no internal voids or cracks, although the undersurface of the ingots had frozen-in bubbles of arsenic vapour. All alloys samples were easily cut and ground or polished, with none of the tendency to fracture found in the InSb rich alloys.

3.3.3 $InAs_x Sb_{1-x}$

This difficult alloy system was first prepared in the form of solid ingots by Woolley and Warner (64W1) using a zone levelling apparatus. In the present work, it was thought that this method of growth could be improved upon by a more precise control of the temperature of the hot zone. The imposition of this control, however, did not significantly improve the results. The great problem with this method is the widening of the molten zone by heat conduction along the ingot.

Ingots of this system were prepared from pure polycrystalline InAs and InSb obtained from Cominco in the form

of zone refined ingots or Czochralaki pulled slabs. The impurity concentration of the constituents was approximately 1 ppm as the donor concentration had been determined to be $\sim 10^{16}$ cm^{-3}. The compounds were melted together in an evacuated quartz capsule and thoroughly mixed at 1000°C., then cooled.

The multiphase ingot formed was then placed in a zone recrystallization apparatus for one zone sweep. Figure 3.3.6A shows the composition as a function of ingot length for the first attempt at zone recrystallization of this ingot. The rather unusual form of the curve can be explained only by deductive assumptions. The capsule containing the ingot was held at an approximately ten degree angle during growth, with the low end the first to freeze. Apparently the charge was a few centimeters away from the low end of the capsule when placed in the furnace. When the first part of the ingot melted in the zone, it flowed down to the low end, separating itself from the rest of the charge which had remained solid. This molten part then began to solidify in the manner of a step freeze technique, rapidly freezing out InAs rich alloy and becoming enriched in InSb. As this last part began to freeze out at ~ 3.5 cm. the InAs concentration was restored by the addition of more material from the original charge, now molten, flowing down to the low end of the capsule. This process must have been gradual as the

ALLOY COMPOSITION versus INGOT LENGTH FIGURE 3.3.6

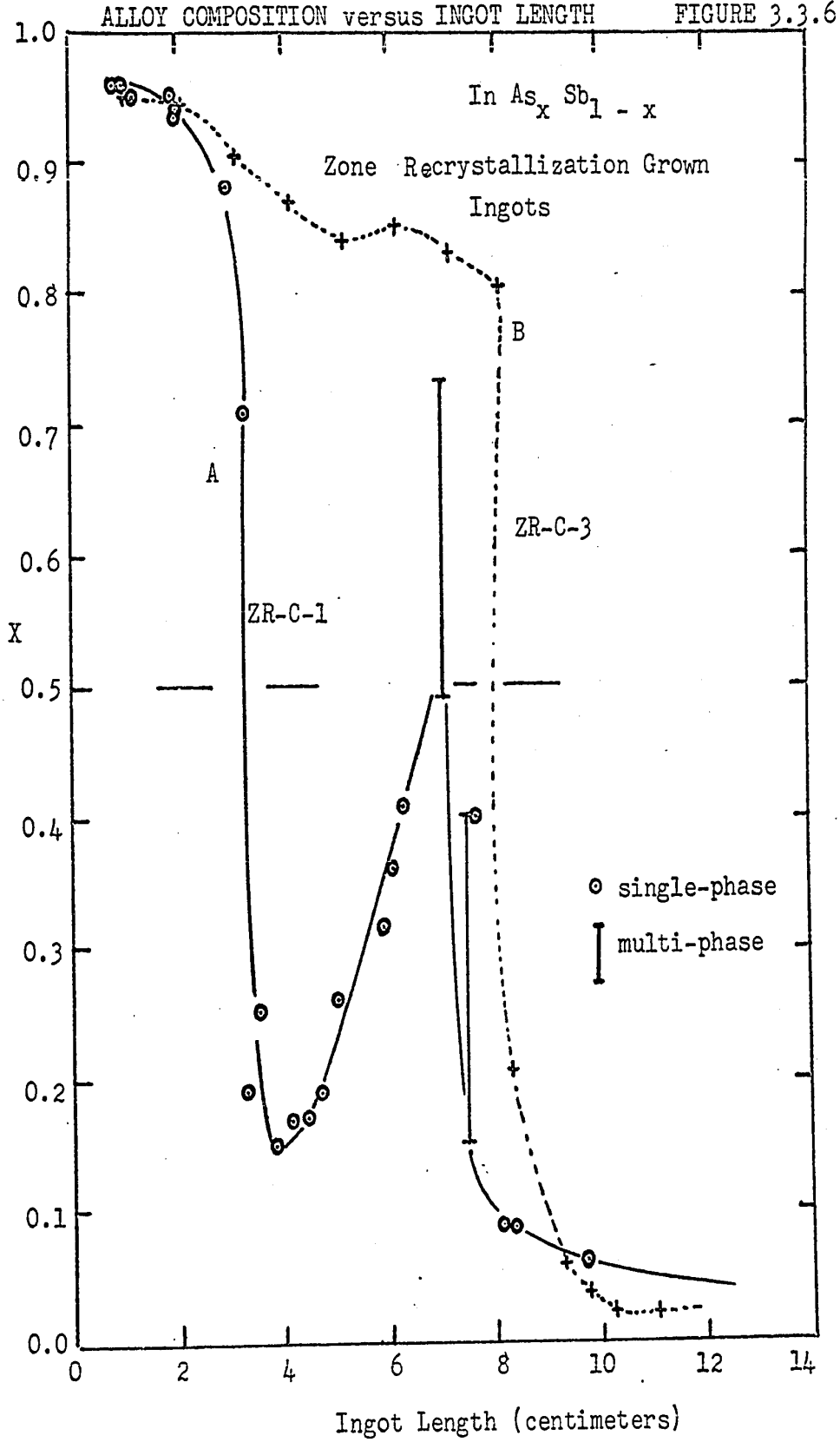

resulting solid shows a gradual enrichment of InAs with length between 3.5 and 6.5 cm. At the 6.5 cm. mark the remainder of the original charge became molten and flowed down the slope to join the lower material abruptly, causing a multiphase region in the ingot from 7 to 7.5 cm. after which the ingot became enriched in the InSb which remained. Because of this serendipidous chain of events, homogeneous material has been obtained for all compositions except $0.7 > x > 0.42$, whereas Woolley and Warner had reported a gap in available compositions which extended from $x = 0.75$ to $x = 0.15$.

Zone recrystallization with a continuous ingot yielded compositions within 20 mol percent of either compound with a rapid change of composition between these compositions (see figure 3.3.6B). Structurally these alloys were sound, except for the samples of very high InSb content which tended to be extremely brittle. Crystallite sizes were quite small ($1 \times 1.5 \times 2$ mm^3) at the InSb rich end of an ingot, but rather large ($2 \times 2 \times 8$ mm^3) at the first frozen InAs rich end. Carrier concentrations of this n-type material were found to be generally low but with a rapid variation along the length of ingot A. (At 2 cm: $\sim 10^{17}$ cm^{-3}; at 4.5 cm: $\sim 10^{14}$ cm^{-3}; at 8 cm: $\sim 10^{16}$ cm^{-3}).

Since horizontal Bridgman growth was proving successful in the $Ga_x In_{1-x} Sb$ and $Ga_x In_{1-s} As$ systems it was felt that it might also work with these alloys. A capsule

containing an ingot with an x = 0.3 mean composition was placed in the hot zone of a two-zone furnace at 1000°C. The cooler zone was set at 500°C. The ingot was moved through the step at a rate of 0.5 cm/day. An ingot which was homogeneous along its entire length was produced, with a smooth, continuously varying composition from x = 0.9 to x = 0.0, although the variation in composition with ingot length was quite rapid in the range $0.4 > x > 0.6$

Cross-sectional slices were powdered and X-ray photographs (figure 3.3.8) were taken to determine the lattice parameter and composition (a_o vs mol % from Woolley and Warner (64W1)) and homogeneity. Figure 3.3.7 shows the variation of composition with ingot length for a typical step freeze ingot. In all cases the composition spread of the specimens obtained was within 3 mol %, and except for the range $0.4 < x < 0.6$, the homogeneity was considerably better than this.

Crystalline sizes in ingots produced by the step freeze method were quite large, starting at approximately 2 x 2 x 8 mm^3 at the InAs end and increasing in size to 4 x 5 x 10 mm^3 at the end last to freeze. In fact, at the InSb end there are only three crystallites presented in a cross-section. In future, samples of this system will be prepared by either narrow zone levelling, or perhaps, solute buildup of the arsenic vapour over a melt of InSb and Indium.

ALLOY COMPOSITION versus INGOT LENGTH FIGURE 3.3.7

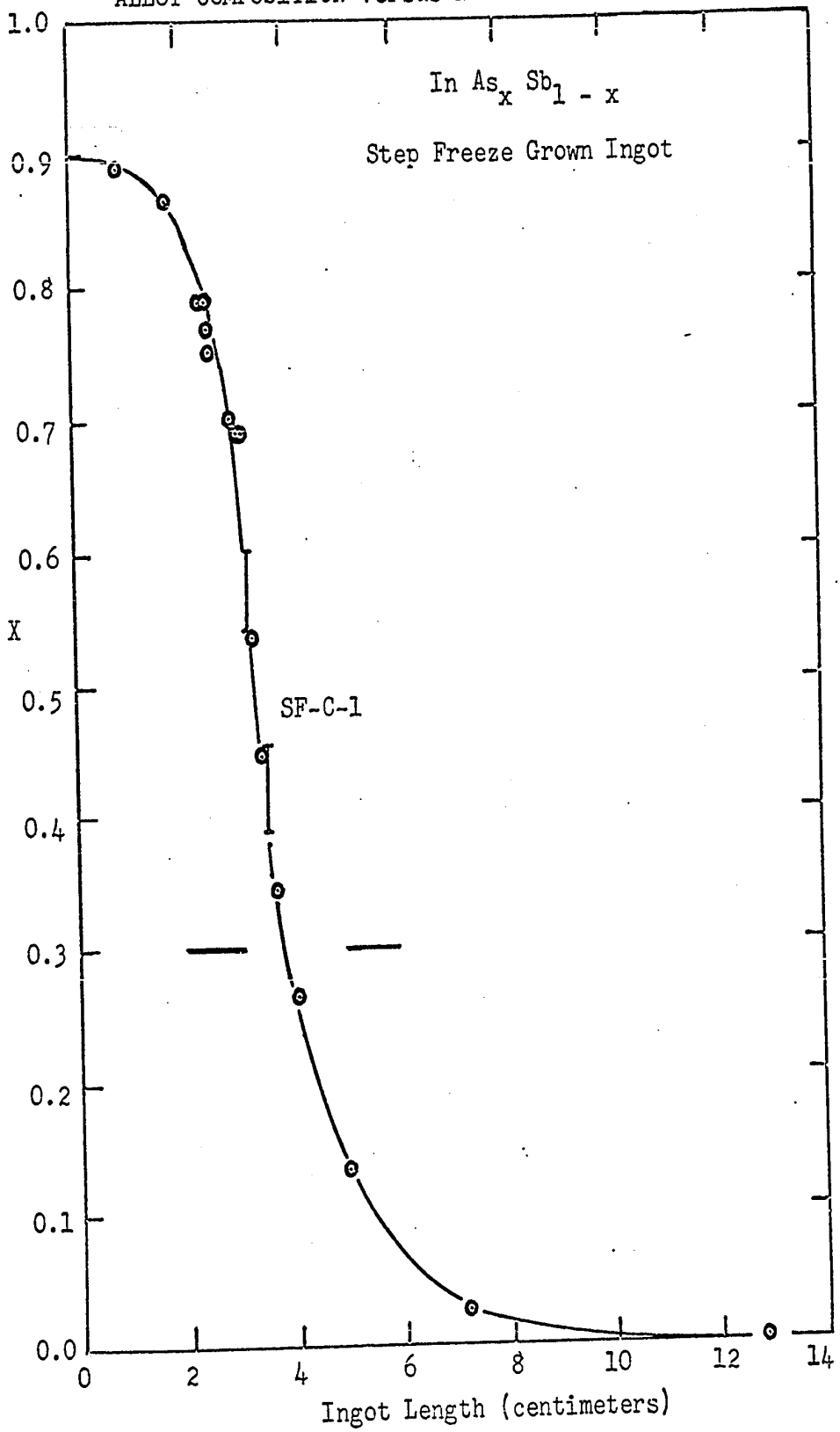

DEBYE SCHERRER X-RAY PHOTOGRAPHS FIGURE 3.3.8

$InAs_xSb_{1-x}$

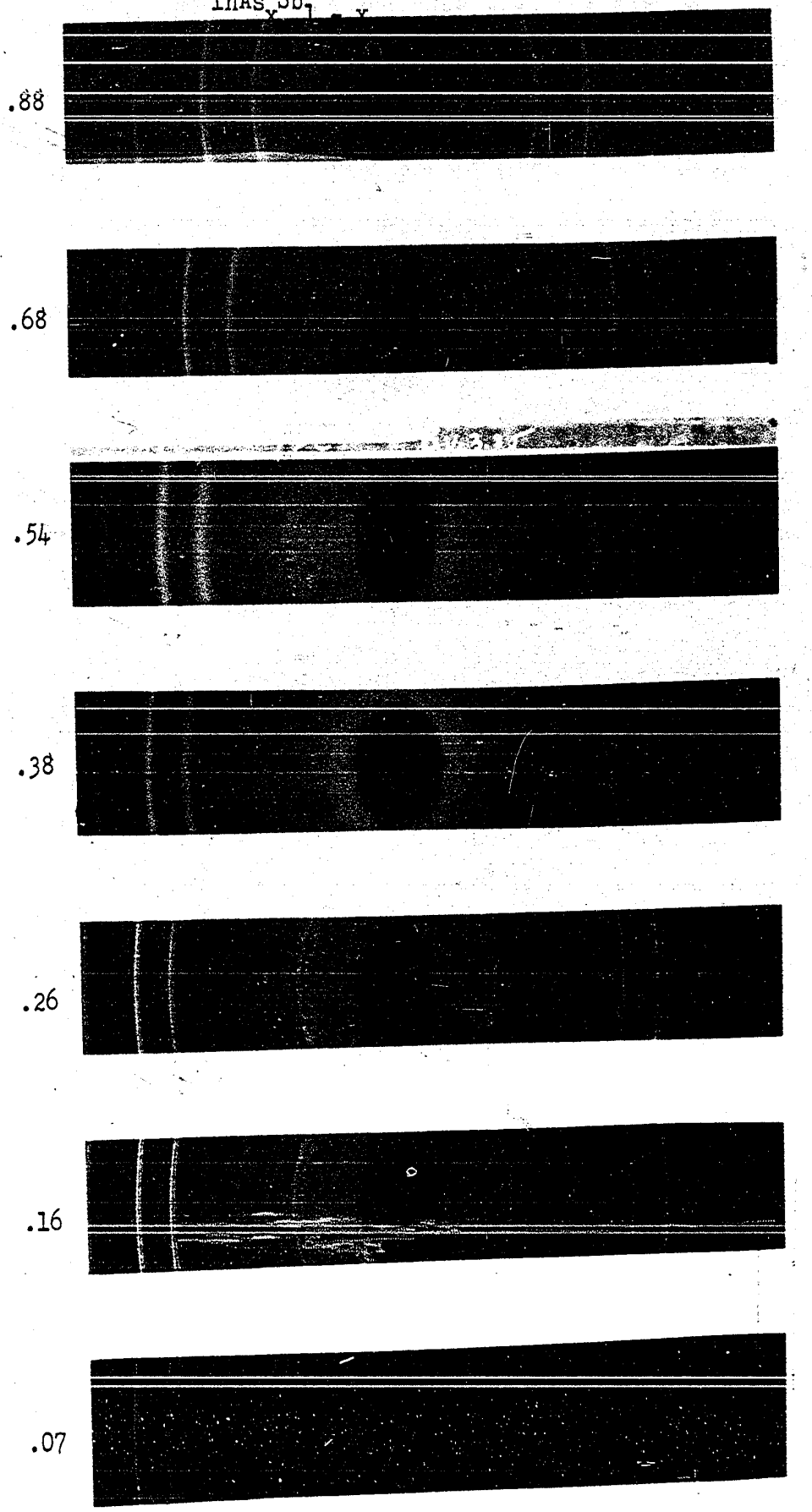

DEBYE SCHERRER X-RAY PHOTOGRAPHS FIGURE 3.3.8

$InAs_xSb_{1-x}$

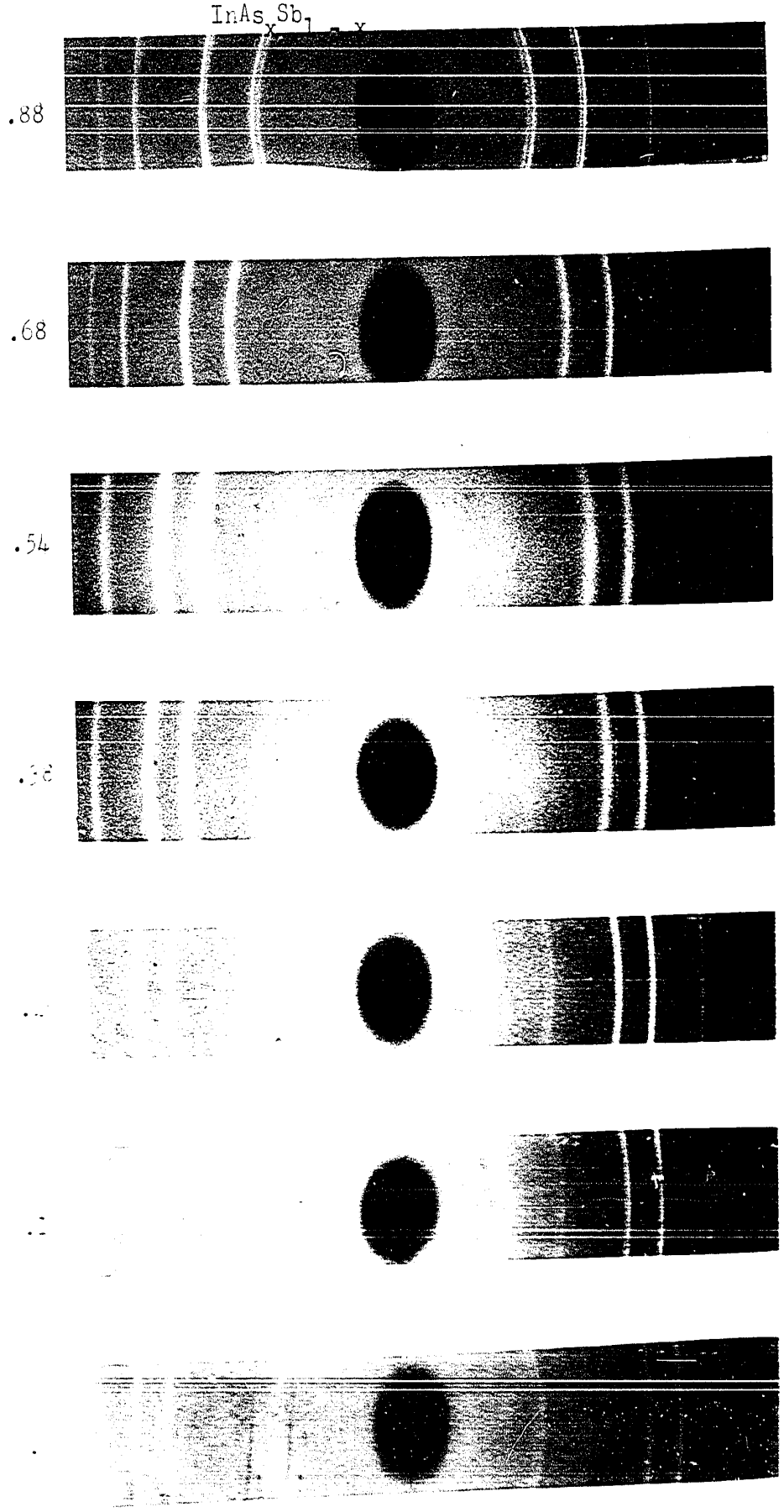

3.3.4 $Ga\ As_x\ Sb_{1-x}$

Ingots of this alloy system have been produced by the same methods as the above system in collaboration with Thomas. The zone-recrystallization apparatus was used with a zone temperature of 1100°C and backgrounds of 650°C. The sweep rate was 0.5 cm/day. In this system zone levelling should prove more feasible since the melting points involved are higher and the zone width at these temperatures narrower. The arsenic vapour pressure for GaAs at high temperature approaches atmospheric pressure and care must be taken to ensure that no part of the quartz capsule containing the ingot is cool enough to allow condensation of the arsenic on its walls and thus have it lost to the alloy. The ingot which had been prepared by this method showed indications that zone levelling was indeed taking place, but much of the material was inhomogeneous. Figure 3.3.9 shows the composition variation with length of the zone recrystallized ingot with a mean composition of $x = 0.3$. The inhomogeneity of each cross-sectional slice which was X-rayed is indicated by the length of the bar on the figure. Vegard's law was assumed valid in determining the compositions. It is felt that this method can be applied to produce homogeneous material of this system in the near future.

ALLOY COMPOSITION versus INGOT LENGTH FIGURE 3.3.9

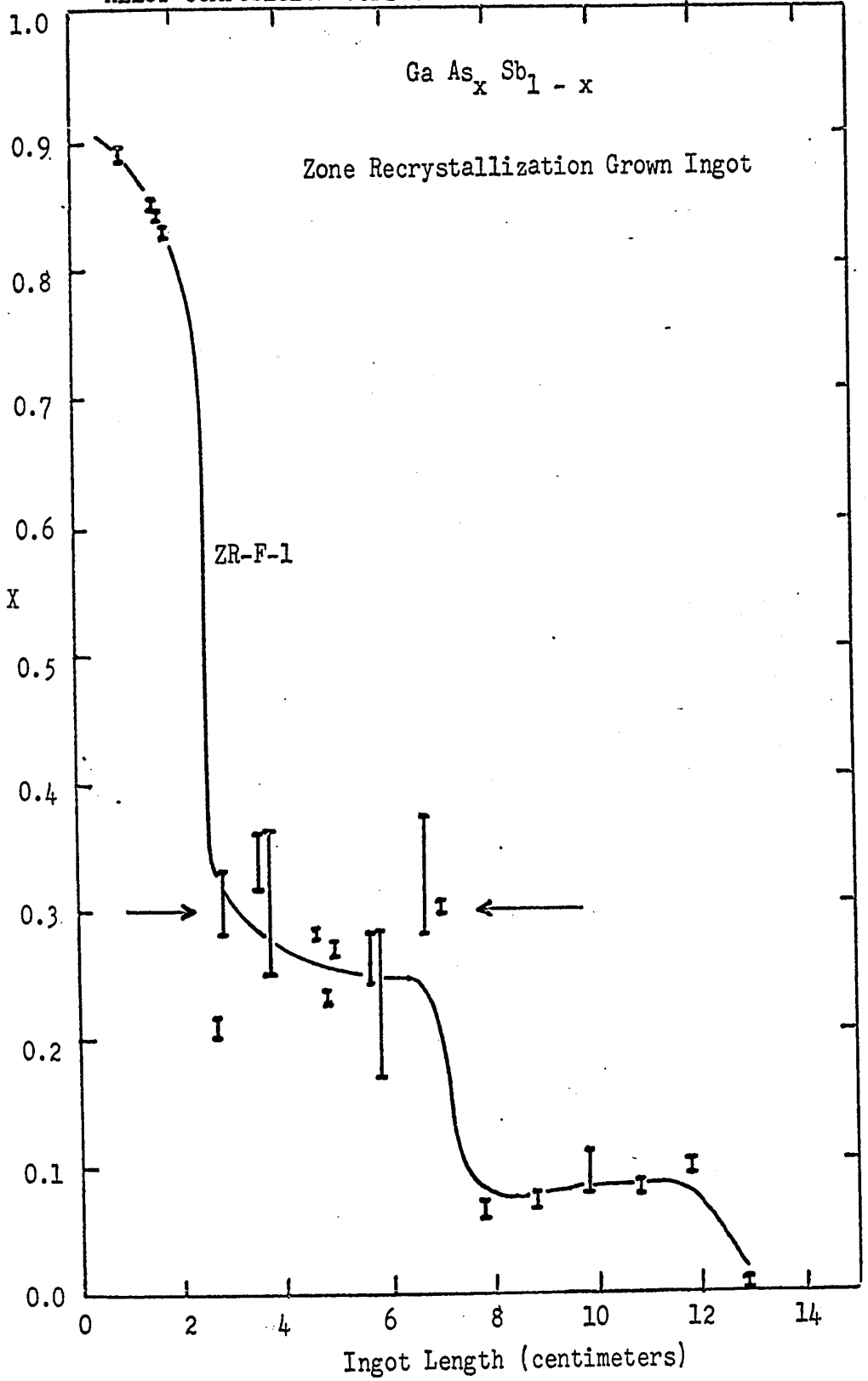

Crystal growth by step freezing was also tried for these alloys but preliminary results indicate that compositions can be obtained only within 5-10 mol % of either compound by this method. The GaAs material used for these investigations was in the form of pure polycrystalline ingots obtained from Cominco, while the GaSb was fabricated from stochiometric amounts of Gallium metal from Merck and Antimony pellets from Cominco, both of which were reported as 99.999% pure.

3.3.5 $(GaAs)_x (InSb)_{1-x}$

Ingots of these quaternary alloys have been produced using a step freeze furnace. Under the assumption that this system was pseudobinary, as indicated by Müller and Richards, (64M5) a series of ingots of $(GaAs)_x (InSb)_{1-x}$ alloys were grown. The composition variation along the length of each ingot was determined by the X-ray powder method assuming Vegard's Law (see figure 3.3.10). In no case was any alloy obtained in the range $0.85 > x > 0.19$. This is in apparent agreement with Müller and Richards who show that there is a miscibility gap over the composition range $0.85 > x > 0.15$. These workers however, were preparing solid samples directly from the vapour phase at substrate temperatures of ~500°C. Under these conditions, the alloy formed has no deviation from the direct tie line from GaAs to InSb. When these alloys

ALLOY COMPOSITION versus INGOT LENGTH FIGURE 3.3.10

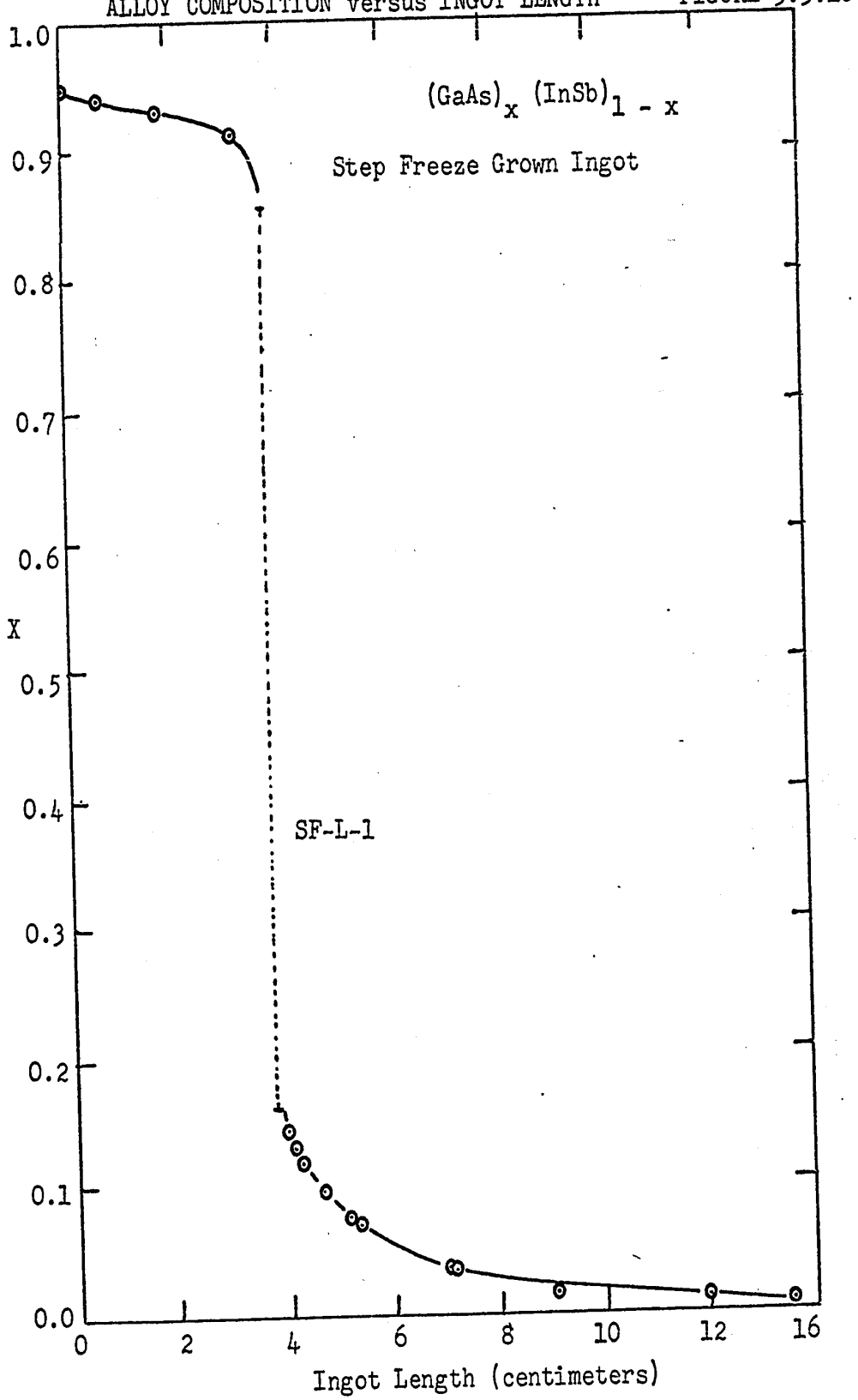

are solidified from the melt this is not necessarily the case.

Mass spectrographic analysis of samples of these alloys was carried out at Bell and Howell Labs in Pasadena, California. The results of this analysis indicate that the alloy which had formed was not along the direct tie line. Hence any X-ray determination of composition can apply to any of a family of quaternary alloys with the same lattice parameter. The values of composition shown in figure 3.3.10 are thus in error.

Since alloy material can be found only at either end of the composition range it may be concluded that the system has a peritectic equilibrium diagram form along the unknown tie lines involved.

3.3.6 Other Alloy Systems

Attempts were made to determine whether or not solid solutions of InBi and InSb could be formed. A small capsule containing 10 mol % InBi was frozen over a period of ~10 hours using a vertical Bridgman procedure. X-ray photographs of the resulting ingot showed only the InSb diffraction pattern and some faint InBi lines. It was concluded that either InBi did not dissolve into InSb in the present conditions, or if there was dissolution, the lattice spacing was unaffected by alloying. This latter assumption has been proven to be the

case by Jean-Louis and Bernard (68J1). These workers have determined that solutions up to 4 mol % InBi can be formed and that the fundamental energy gap is quite dependent on alloying.

No lattice parameter change was noted when an ingot of InSb with 10 mol % of a stochiometric mixture of thallium and antimony was produced. Again either no alloying has taken place or no lattice parameter change is associated with alloying. Since the work of Jean-Louis and Bernard mentioned above has come to light, the system $(In_{1-x}Tl_x)Sb$ is being looked into in more detail and further results are to be expected in the near future.

3.4 Conclusions

In the two preceding chapters it has been attempted to show the state of the art of preparation of III - V alloys. It has been pointed out in section 2.4 that there are several workers in this field employing different techniques with varying degrees of success. There has also been a report of the present work on preparation of alloy material. Although the alloys produced were not single crystals, they did encompass a wide composition range and were quite homogeneous. Results of electrical measurements, to be discussed in subsequent chapters, have shown that these alloys were of a very high quality when compared to bulk samples produced by other workers. Samples from the alloy material prepared in the presented work have been used in a wide variety of experimental programs. These include investigations of Hall effect, conductivity, optical absorption, reflectivity, thermo-electric power, Faraday rotation, magneto-resistance, electro-reflectance, thermo-reflectance and magneto-thermo-electric power. Each of these experiments has extended the understanding of band structure and transport properties in III - V alloys, none of which would be possible without adequate alloy material.

CHAPTER IV

INTRODUCTION TO THE ELECTRICAL PROPERTIES OF III - V ALLOYS

4.1 Introduction

Most of the experimental work on the various properties of semiconducting material can be divided into the two broad categories of optical and electrical phenomena. Within these groupings are the various subdivisions related to piezo, thermal and magnetic effects, while such phenomena as photo-conductivity and field induced light emission overlap both fields.

In the semiconductor group of the University of Ottawa, experiments are being conducted on both optical and electrical phenomena. Measurements of both the absorption and the reflectivity have been made on III - V compounds and alloys. Electro and thermo- and wavelength modulated- reflectance studies have also been carried out as well as measurements of the free carrier Faraday rotation in these materials.

Under the general heading of electrical properties, studies have been made on such effects as magnetoresistance, conductivity, thermoelectric power, the Hall Effect and the longitudinal Nernst effect (magneto-thermoelectric power).

At the present time apparatus is being assembled to measure the Hall effect and the conductivity of alloys as functions of very high hydrostatic pressures.

Various graduate students of the group have been assigned different experimental techniques so that the materials of interest are simultaneously subjected to a wide variety of studies. In this way the maximum advantage will come from the interactions and correlations of these investigations to each of the experimentalists, and the aims of the group as a whole are best served.

In the present work the experimental phenomena studied were the the conductivity and the Hall effect as functions of temperature. These effects are related to the thermal equilibrium distributions of charge carriers in the various energy bands and upon the conditions governing the motion of the carriers in these bands. By studying the Hall effect and the conductivity, it's possible to determine the concentrations of carriers in each band, and to measure the corresponding mobilities.

From a careful analysis of the experimental data, it has been possible to determine the values of the energy band separations in certain III - V alloys as functions of both temperature and composition. In some cases this information corroborates data obtained from optical experimentation.

In the following section a brief review of the experimental work which has been carried out on some of the III - V alloy systems will be presented. The primary emphasis of this review will be on those alloys which were the subject of the present work. In later sections the various band and carrier density relations required for the interpretation of electrical experiments will be presented. The development of parabolic band equations and of the Kane modifications, to allow for non-parabolicity of bands will be dwelt on in some detail.

The necessary calculation for the evaluation of the Hall coefficient in multiband material will be presented in section 4.4. The roles of such factors as electron degeneracy and high electron mobility are carefully considered with respect to their influences on the Hall coefficient.

Finally, in a brief section, the methods for obtaining experimental values of the Hall constant and the conductivity are presented.

4.2 Review of Electrical Investigations of III - V Alloys.

The work which has been published on the electrical properties of III - V alloys has been severely limited by the scarcity of suitable alloy material. Unlike optical studies, which lend themselves well to material in the form of evaporated thin films or epitaxial layers, electrical phenomena of interest are associated with bulk properties and require solid samples of good homogeneity. Until the work described in Chapter III such material was either unavailable or at best, limited in quantity for most III - V alloys.

The following sections are presented as a brief review of the published work on the electrical properties of III - V alloys. Special attention will be paid to those studies which concern the alloys measured in the present work.

4.2.1 Electrical Studies of $Ga_xIn_{1-x}Sb$ Alloys

The earliest reported work on the electrical properties of these alloys was that of Blakemore (57B2) who measured the Hall coefficient and the conductivity of what was supposed to be an equimolar sample of GaSb-InSb. The material had been prepared by horizontal zone levelling, but later work has shown that this method will not produce homogeneous material except with very slow freezing rates. The results given differ greatly from those of latter work (59I2, 59I3, 60I1, 61I3),

and can be assumed to be in error because of inhomogeneity.

The first systematic, electrical investigations of these alloys over the full composition range were carried out by Woolley and Gillett (60W8), and by Ivanov-Omskii and Kolomiets (60I1, 62I1).

The former workers derived from Hall data a roughly linear composition variation of the energy gap extrapolated to $0^{o}K$ up to alloy composition of 65 mol % GaSb. Above this composition, they report an anomalous division of the energy gap into low and high temperature values neither of which corresponds to the optical values (59W7, 59I1, 61W8). This anomaly was later shown to result from the increasing contributions of subsidiary conduction band minima and not to be a phase change in the crystal (65W2, 66W1).

In the same work Woolley and Gillett report a variation of the electron mobility with composition which is non-linear their values having been derived indirectly from measurements on p-type material. The analysis assumed carriers were found in two bands only, one conduction and one valence, employing Boltzmann statistics, parabolic bands, and spherical constant energy surfaces.

Ivanov-Omskii and Kolomiets carried out electrical measurements on n-type material leading to the determination of electron mobility over the complete alloy range. In

contrast to the results of Woolley and Gillett, the mobility was shown to vary linearly with composition for samples of equivalent impurity concentration. Both groups of workers agree that the hole mobility has a constant value of approximately 700 cm^2/V-sec for the entire alloy range. In both studies the degeneracy of the two highest valence band maxima was ignored.

From Hall effect and resistivity measurements, Kudman and Seidel (67K1) have derived values of the electron and hole mobilities as functions of composition which agree qualitatively with earlier results but tend to be smaller in magnitude, presumably because of the very high level of impurity density (i.e. 3×10^{17} - 6×10^{19} carriers/cm^3), in their samples.

These same workers (67K2) have analyzed the variation of the Hall coefficient as a function of temperature in terms of two conduction bands. The method of analysis has been described previously by Aukerman and Willardson (60A15) for GaAs. Values of ΔE_{lo}, the energy band separation of the ⟨111⟩ and (000) minima at 0^oK were calculated for a few heavily doped alloy specimens. Since there was no consideration of the effects of degeneracy in the analysis, the results must be held suspect as this factor can be significant in heavily doped material.

Their results indicate a linear composition dependence for the position of the ⟨111⟩ minima above the valence band. The temperature dependence of the conduction band separation was determined to be positive in GaSb, while in the alloys it was found to have a negative sign.

Pistoulets et al. (68P1) have studied the conduction band of GaSb rich alloys ($1.0 < x < 0.96$) by means of the de Haas - Shubnikov effect, magnetoresistance and the Hall effect all measured at $4.2^{o}K$. Their materials were highly degenerate single crystals having been heavily doped with tellurium. They report ΔE_{lo} values which indicate that the position of the ⟨111⟩ minima rises rapidly in energy as InSb is added. They also report a rapid decrease in the density of states effective electron mass with alloying.

Averous et al. (68A2) have prepared single crystals in the extreme GaSb rich composition range. From Hall and resistivity measurements, they deduce values for the Hall mobility in the order of $1 - 3 \times 10^{3}$ $cm^{2}/V\text{-sec}$ for sample with donor densities of $2.4 - 9.7 \times 10^{17}$ cm^{-3}. The temperature dependence of the measured Hall constant has indicated that there was a significant occupation of the subsidiary conduction band states but no quantitative conclusions were drawn concerning these higher minima.

In none of the published work on these alloys has a systematic analysis been applied which considers such important

factors as the degeneracy of the valence band maxima at $k = 0$, the nonparabolicity of the light hole valence band and of the (000) conduction band, the contributions of two sets of higher conduction band minima at elevated temperatures as well as the possibility of electron degeneracy or quasi-degeneracy in the conduction band in heavily doped n-type material. Because of these factors most of the investigations of electrical properties in these alloys have led to doubtful conclusions. Beyond the problems inherent in the analysis, most workers in this field have been handicapped by the lack of homogeneous alloy material upon which to work.

All of these above factors have been considered in the present work and are presented and discussed in Chapter VI.

4.2.2 Electrical Studies of $Ga_xIn_{1-x}As$ Alloys

Woolley et. al. (61W7) have measured the Hall constant and the conductivity of several of these alloys as functions of temperature over the range 90 to 400°K. The Hall effect measurements indicated that the alloys of the range $0.0 < x < 0.7$ exhibited n-type behaviour whereas higher alloy compositions did not yield detectable Hall voltages. All samples were found to have mixed conduction as exhibited by an increase in the Hall constant with increasing temperature. This rise was much more pronounced in GaAs rich alloys where

subsidiary ⟨100⟩ band minima have been reported to be a few tenths of an electron-Volt above the (000) minimum.

Abrahams et al. (59A1, 60A2) report a Hall mobility which decreases rapidly with increasing GaAs content but their measurements were performed on inhomogeneous material and inhomogeneity tends to lower the magnitude of the mobility (65T1).

Room temperature Hall measurements have been carried out on $Ga_xIn_{1-x}As$ alloys by Hocking et al. (66H1) as well as measurements of resistivity as a function of temperature. Their samples were of a limited composition range being mainly concentrated at $x \simeq .32$ and $x \simeq .68$. N-type alloys with donor concentrations ranging from 2×10^{17} to 1.5×10^{19} cm^{-3} were determined to have mobilities in the range $2 - 7 \times 10^3$ $cm^2/V\text{-sec}$. The hole mobility of very heavily doped ($N_A \sim 10^{19} cm^{-3}$) p-type alloys was found to be approximately 80 $cm^2/V\text{-sec}$ at all compositions.

No systematic study of the energy gap by electrical means has been reported for these alloys although all of the above workers have published values of the optical energy gaps. In a very recent report Babaev et al. (69B1) have given values for E_{oo}, the energy gap extrapolated to 0^oK, from Hall effect measurements for alloys of compositions $x = 0.2$ and $x = 0.25$. These values were $E_{oo} = 0.49$ and $E_{oo} = 0.55$ respectively.

The material measured had relatively high impurity concentrations ($\sim 10^{18} cm^{-3}$) and hence the mobility values determined were quite low (4000 $cm^2/V \cdot sec$). A systematic study of the electrical properties of these alloys has been carried out in the present work. As a result of this work values for the energy gap and the mobility as functions of temperature and alloy composition have been obtained. As well the position of the subsidiary ⟨100⟩ conduction band minima has been calculated for GaAs rich alloys. In this analysis as in the previously mentioned case, conditions of non-parabolicity and possible degeneracy were taken into consideration although these effects were found to be relatively unimportant in these alloys.

4.2.3 Electrical Studies of $InAs_xSb_{1-x}$ Alloys

Measurement of the electrical properties of this alloy system had to await the preparation of adequately homogeneous material. The first results to be published were those of Sirota and Bolvanovich (67S2, 3) whose material was of questionable homogeneity. They have reported an electron mobility variation with alloy composition which exhibits a maximum at approximately $x = 0.3$, a rapid fall to a limiting value at $x = 0.5$ then a constant value in the range $0.5 < x < 1.0$. The hole mobility was found to have a similar composition

dependence. This complex variation is undoubtedly primarily the result of variable homogeneity in their samples which were prepared by annealling. The temperature dependence of the measured mobility was found to obey a power law where the power involved remained approximately -3/2 for all samples.

From high temperature Hall effect and conductivity measurements, these same workers obtained values for the energy gap extrapolated to $0^{o}K$ using a two band analysis assuming Boltzmann statistics. They report a pronounced minimum in the energy gap value at a composition of $x \simeq .4$ where the value is as low as 0.13 eV. Because of inhomogeneity of varying degrees there is considerable scatter in their results. The observation of an energy gap minimum is in qualitative agreement with the optical energy gap observed by Woolley and Warner (64W2). The magnitude of this drop as observed by the Russians was much greater than that indicated by the optical studies however.

Kudman and Ekstrom have performed a similar analysis on $InAs_xSb_{1-x}$ alloys (68K2) from which they report a minimum in the absolute zero extrapolated energy gap at $x \simeq 0.10$. Effects of degeneracy were minimized by lending more weight to the measurements below $500^{o}K$. The variation of the energy gap with composition was found to be roughly linear

in the middle alloy range with a rapid decrease at either end from the value for the constituent III - V compounds.

In neither of the above analyses was the problem of band nonparabolicity taken into account, although it has been shown that this effect can be very important in material with such narrow energy gap (57K2)(63C3). In earlier published work (68C1) the author has reported the variation of the energy gap extrapolated to $0^{o}K$ and the electron mobility as functions of alloy composition in $InAs_xSb_{1-x}$ alloys. The mobility was shown to vary linearly with composition, indicating that inhomogeneity and alloy scattering terms were unimportant compared with the effect of polar scattering. The value of the energy gap was seen to have a minimum at $x = 0.4$ with a value of $E_{oo} = 0.17$ eV. The composition variation was shown to be roughly parabolic and to agree more closely with the optical results than either of the other two studies of these alloys.

Since the publication of the earlier work on $InAs_xSb_{1-x}$ alloys, the author has extended the analysis of the electrical measurements to include considerations of the non-parabolicity and degeneracy since in these alloys, more than in other III - V material, these factors are very significant. In the middle composition regions the energy gap is so small that intrinsic degeneracy can occur very near to room

temperature and non-parabolic effects are enhanced by interactions between the conduction and valence bands. References to studies of electrical properties in other alloy systems are given on table 4.2.1.

TABLE 4.2.1

REVIEW OF ELECTRICAL STUDIES OF III - V ALLOYS

$Ga_xIn_{1-x}Sb$	(57B2) (60W8) (68P1) (67K1) (67K2) (60I1) (61I3) (62I1) (65B1) (68A2)
$Ga_xIn_{1-x}As$	(66H1) (63M5) (59A1) (60A2) (61W7) (69B1)
$InAs_xSb_{1-x}$	(67S2) (67S3) (68C1) (68A1) (66B2) (68K2)
$GaAs_xSb_{1-x}$	(67S1)
$GaAs_{1-x}P_x$	(65T1) (68L1) (68L2) (68C3)
$InAs_{1-x}P_x$	(59E6) (56W2) (59B10) (60U1) (5901) (59W2)
$Al_xIn_{1-x}Sb$	(60A4) (61A2)
$Al_xGa_{1-x}Sb$	(58B6) (59B15) (60M3) (61B19)
$Ga_xIn_{1-x}P$	
$Al_xGa_{1-x}As$	
$Al_xIn_{1-x}As$	
$(GaAs)_x(InP)_{1-x}$	

4.3 Energy Band Models

4.3.1 Parabolic Band Model

The electron density for an energy band, where the zero of energy is taken as the bottom of the band, may be written as

$$n = \int_{o}^{top} g\,(E)\, f_e\,(E)\, dE \qquad [4.1]$$

where g(E) is the density of states in the energy increment between E and E + dE and $f_e(E)$ is the Fermi-Dirac probability that these states will be occupied by electrons.

$$f_e(E) = \{1 + \exp[(E - E_F)/kT)]\}^{-1} \qquad [4.2]$$

If the surfaces of constant energy in $\hbar$-space are spherical then the $\hbar$-volume in the energy increment from E to E + dE will be given by

$$dV_{\hbar} = 4\pi\hbar^2\, d\hbar \qquad [4.3]$$

The total number of non equivalent states in all of $\hbar$-space is $V/8\pi^3$ and so, allowing an electron of either spin to occupy each state, the electron density in the band will be

$$g(E)\, dE = (\hbar^2/\pi^2)\, d\hbar \qquad [4.4]$$

Thus equation [4.1] may be written as

$$n = \frac{1}{\pi^2} \int_0^{top} f_e k^2 \frac{dk}{dE} dE \qquad [4.5]$$

In an isotropic, parabolic energy band the energy is related to k in the following way:

$$E = \frac{h^2 k^2}{8\pi^2 m_e^*} \qquad [4.6]$$

where m_e^* is the density of states effective mass. By changing variables and differentiating [4.6] we get

$$n = \int_0^{top} \frac{4\pi(2m_e^*/h^2)^{3/2} E^{1/2} dE}{1 + \exp[(E - E_F)/kT]} \qquad [4.7]$$

Since there are no occupied states at the top of a band the integral may be extended to infinity and therefore:

$$n = 4\pi\left(\frac{2m_e^*}{h^2}\right)^{3/2} \int_0^{\infty} \frac{E^{1/2} dE}{1 + e^{(E - E_F)/kT}} \qquad [4.8]$$

or

$$n = 4\pi\left(\frac{2m_e^* kT}{h^2}\right)^{3/2} F_{1/2}(E_F/kT) \qquad [4.9]$$

where $F_{1/2}(E_F/kT)$ is the standard Fermi integral

$$F_n(\zeta) = \int_0^{\infty} \frac{x^n dx}{1 + e^{x - \zeta}} \qquad [4.10]$$

Under non-degenerate conditions, i.e. $E > E_F$ [4.9] reduces to the form:

$$n = 4\pi\left(\frac{2m_e^* kT}{h^2}\right)^{3/2} e^{E_F/kT} \Gamma_{3/2}(E/kT) \qquad [4.11]$$

or

$$n = 2\left(\frac{2\pi m_e^* kT}{h^2}\right)^{3/2} e^{E_F/kT} \qquad [4.12]$$

where

$$\Gamma(3/2) = \int_0^\infty e^{-x} x^{1/2} dx = \sqrt{\pi}/2 \qquad [4.13]$$

is the well known Gamma function.

Equation [4.9] may be considered as the definition of the density of states electron effective mass. This is to say, m_e^* has the value which makes the equation valid.

Analagous expressions may be derived in a similar way for electrons in other conduction band minima and also for holes in valence band maxima. The assumptions employed must however, be modified to suit each particular case. Local band minima are found in each of the eight ⟨111⟩ directions but since they are centered at the Brillouin Zone boundaries, only one half of the states in each are associated with non-equivalent states. Thus a multiplicity factor of four must be included for ⟨111⟩ band carrier density equations. In the case of minima found along the ⟨100⟩ directions, the multiplicity factor is three or six, depending on whether or not the minima are at the zone boundary. This is not known as

yet in zincblende materials but a multiplicity of six is usually assumed since this is the case in silicon.

The surfaces of constant energy in these higher minima are not spherical but are ellipsoids of revolution along the k-axes. This means that the effective mass of carriers in these minima are not isotropic but have components related to the different band curvatures in different orientations. For the purpose of this analysis the constant average density of states effective mass has been used for these band minima:

$$m_i^* = (m_t^2 \, m_\ell)^{1/3} \qquad i = 1, 2 \qquad [4.14]$$

These subsidiary band minima may be considered to be parabolic and so, if the surfaces of constant energy are approximated as spheres, the carrier density equations for electrons in the ⟨111⟩ and ⟨100⟩ conduction band minima may be written:

$$n_1 = 4\pi\left(\frac{2m_1^* kT}{h^2}\right)^{3/2} 4F_{1/2}[(E_F - \Delta E_1)/kT] \qquad [4.15]$$

and

$$n_2 = 4\pi\left(\frac{2m_2^* kT}{h^2}\right)^{3/2} 6F_{1/2}[(E_F - \Delta E_2)/kT] \qquad [4.16]$$

where ΔE_1 and ΔE_2 are the energy separations of these minima from the bottom of the (000) conduction band, and m_1^* and m_2^* are the average density of state electron effective masses of each band minima. The subscripts 1 and 2 refer to the ⟨111⟩ and ⟨100⟩ bands respectively throughout this thesis.

The valence bands have maxima only at $k = 0$ but there are three different bands, two of which are degenerate at $k = 0$. These bands are approximated as parabolic in this simple band picture and the surfaces of constant energy are assumed to be spherical. The first assumption is relatively valid for small values of k; but because of the interactions of the light and heavy hole bands, which are degenerate at $k = 0$, the surfaces of constant energy are not spheres but complex fluted shapes. Thus the effective hole masses are composed of several different k-components but are usually considered as isotropic by averaging over all the various components. Under these restrictions, the valence band carrier density equations may be written as:

$$p_{V_2} = 4\pi\left(\frac{2m_{h_2}^{*}\, kT}{h^2}\right)^{3/2} F_{1/2}\left[-(E_F + E_o)/kT\right] \qquad [4.17]$$

and

$$p_{V_1} = 4\pi\left(\frac{2m_{h_1}^{*}\, kT}{h^2}\right)^{3/2} F_{1/2}\left[-(E_F + E_o)/kT\right] \qquad [4.18]$$

where the subscripts h_1 and h_2 designate the heavy and light holes respectively, and E_o is the intrinsic energy gap.

Except where it is otherwise stated the symbol m* with appropriate subscript is the density of states effective mass and is defined by the relations given in equations [4.9] and [4.15-18] for each band. For a more complete discussion of the

various definitions for effective masses which are employed in semiconductor physics the reader is referred to vanTongerloo (69V1).

4.3.2 The Kane Band Model

The assumption which was used in the preceding section, that the energy bands are parabolic is not always valid. The (000) minimum in particular can show quite extreme deviations from parabolicity as $\hbar$ increases from zero. In order to give a band model more closely correlated with reality Kane (57K2) has calculated the E versus $\hbar$ relations for the four most important (0,0,0) extrema for $\hbar$ values near $\hbar = 0$, by considering the effects of spin-orbit interactions between these bands.

Starting with a Schroedinger equation of the form

$$\left[\frac{p^2}{2m} + V + \frac{\hbar}{4m^2c^2}(\nabla V \times p).\sigma\right] \Psi_{\hbar} = E_{\hbar}\Psi_{\hbar} \qquad [4.19]$$

where p is the momentum operator and σ the spin operator and by operating on the Bloch function $\Psi_{\hbar} = u_{\hbar}\, e^{i\hbar.r}$ we find [4.19] may be written in the form

$$(H_o + H_1 + H_2 + H_3)u_{\hbar} = E'_{\hbar}\, u_{\hbar} \qquad [4.20]$$

where $H_o = \frac{p^2}{2m} + V$ is the Hamiltonian of the unperturbed problem

$H_1 = \hbar/m \; k.p$ is the so called $k.p$ interaction which is a spin independent perturbation.

$$H_2 = \frac{\hbar}{4m^2 c^2} (\nabla V \times p).\sigma$$

and

$$H_3 = \frac{\hbar}{4m^2 c^2} (\nabla V \times k).\sigma$$

are the spin dependent perturbations.

and

$$E'_k = E_k - \frac{\hbar^2 k^2}{2m} \; .$$

When the wave functions of the perturbed problem are expanded in terms of those of the unperturbed problem using first order perturbation theory, a set of linear equations may be determined for the expansion coefficients whose secular determinant must vanish. The roots of this secular equation were determined to be

$$E' = 0$$

$$\text{and } E'(E' - E_o)(E' + \Delta_o) - k^2 P^2 (E' + 2/3\Delta_o) = 0 \qquad [4.21]$$

where the zero of energy is taken to be the top of the valence band, and P is the matrix element of the momentum.

The trival solution for the first energy band is

$$E_{V_1} = \frac{-\hbar^2 k^2}{2m_{h_1}^*} \qquad [4.22]$$

which is seen to describe the parabolic heavy hole valence band maximum, where $m_{h_1}^*$ is equal to the free electron mass.

By manipulation of Equation [4.21] and by keeping only to energies near to $\hbar = 0$ we can get these three roots:

$$(E \simeq E_0) \quad E_c = \frac{h^2\hbar^2}{2m_o} + \frac{E_o}{2} + \frac{1}{2}\left[E_o^2 + \frac{4\hbar^2P^2}{3}\left(\frac{3E_o + 2\Delta_o}{E_o + \Delta_o}\right)\right]^{1/2} \qquad [4.23]$$

$$(E \simeq 0) \quad -E_{V_2} = \frac{h^2\hbar^2}{2m_{h_2}} + \frac{E_o}{2} - \frac{1}{2}\left[E_o^2 + \frac{8\hbar^2P^2}{3}\right]^{1/2} \qquad [4.24]$$

and

$$(E \simeq -\Delta_o) \quad -E_{V_3} = \frac{h^2\hbar^2}{2m_{h_3}} - \frac{\Delta_o}{2} - \frac{1}{2}\left[\Delta_o^2 + \frac{2\hbar^2P^2}{3}\,\frac{\Delta_o}{E_o + \Delta_o}\right]^{1/2} \qquad [4.25]$$

These roots can be associated with the conduction band, C, the light hole valence band, V_2, and the split-off valence band, V_3, respectively.

E_o is the intrinsic energy gap and Δ_o is the spin-orbit splitting between the V_2 and V_3 valence bands at $\hbar = 0$.

By differentiating equations [4.23] and [4.24] and applying the definitions of the cyclotron effective masses for electrons and holes

$$\frac{1}{m_{o_c}^*} = \frac{1}{h^2\hbar}\,\frac{dE}{d\hbar} \qquad [4.26]$$

$$\frac{1}{m_{h_{2c}}^*} = \frac{1}{h^2\hbar}\,\frac{dE}{d\hbar}$$

and letting $k = 0$, we obtain the following equations relating the matrix element P to the bottom and top of the band effective masses m_{oo}^* and $m_{h_{2o}}^*$ respectively:

$$P^2 = 3/2\, \hbar^2 \left(\frac{1}{m_{oo}^*} - \frac{1}{m}\right) \frac{E_o(E_o + \Delta_o)}{3E_o + 2\Delta_o} \qquad [4.27]$$

and $$P^2 = 3/4\, \hbar^2 \; E_o \left(\frac{1}{m} - \frac{1}{m_{h_{2o}}^*}\right) \qquad [4.28]$$

Substituting these relations in [4.23] and [4.24] we obtain

$$E_c = \frac{\hbar^2 k^2}{2m} + \frac{E_o}{2}\left[\left\{1 + \frac{2\hbar^2 k^2}{E_o}\left(\frac{1}{m_{oo}^*} - \frac{1}{m}\right)\right\}^{1/2} - 1\right] \qquad [4.29]$$

$$E_{V_2} = \frac{\hbar^2 k^2}{2m} - \frac{E_o}{2}\left[1 + \left\{1 + \frac{2\hbar^2 k^2}{E_o}\left(\frac{1}{m} - \frac{1}{m_{h_{2o}}^*}\right)\right\}^{1/2}\right] \qquad [4.30]$$

The intrinsic energy gap E_o varies with temperature as a result of two processes with approximately equal effect. These are lattice thermal dilatation and lattice thermal vibration, or interaction with the phonon field. The second of these factors has no influence on the band curvature which determines effective masses of the charge carriers and so must be neglected when deriving band equations such as [4.29] and [4.30]. Therefore, according to Ehrenrich (57E2) we must

replace the intrinsic energy gap E_o with an effective mass band gap E_o^* where E_o^* represents the position of the energy gap were lattice dilatation the only process acting to change it.

The carrier concentration in a band with spherical constant energy surfaces has been given by the relation

$$n = \frac{1}{\pi^2} \int_o^\infty f_e \, k^2 \frac{dk}{dE} \, dE \qquad [4.5]$$

By rearranging equations [4.29] and [4.30] so that k is expressed in terms of E and by differentiating to obtain $\frac{dk}{dE}$, retaining all terms up to and including the fourth power in energy and making use of the relation:

$$(kT)^{n+1} F_n(\zeta) = \int_o^\infty f_e \, E^n \, dE \qquad [4.31]$$

we obtain the carrier concentrations for non-parabolic bands:

$$n_c = 4\pi \left(\frac{2m_{oo}^* kT}{h^2}\right)^{3/2} \{F_{1/2}(\zeta) + (\tfrac{5}{2} - 5\gamma)\beta F_{3/2}(\zeta) +$$

$$+ (\tfrac{7}{8} - \tfrac{21}{2}\gamma)\beta^2 F_{5/2}(\zeta) - (\tfrac{1}{4} + \tfrac{7}{2}\gamma)\beta^3 F_{7/2}(\zeta)\} \qquad [4.32]$$

and

$$p_{V_2} = 4\pi \left(\frac{2m_{h_{2o}}^* kT}{h^2}\right)^{3/2} \{F_{1/2}(-\zeta - \xi_o) + (\tfrac{5}{2} - 5\gamma_h)\beta F_{3/2}(-\zeta - \xi_o) +$$

$$+ \left(\frac{7}{8} - \frac{21}{2}\gamma_h\right)\beta^2 \; F_{5/2}(-\zeta - \xi_o) - \left(\frac{1}{4} + \frac{7}{2}\gamma_h\right)\beta \; F_{7/2}(-\zeta - \xi_o)\Big\} \qquad [4.33]$$

where
$$\zeta = E_F/kT$$
$$\xi_o = E_o/kT$$
$$\gamma = m_{oo}^*/m$$
$$\gamma_h = m_{h_{2o}}^*/m$$
$$\beta = kT/E_o^*$$

Equations [4.32] and [4.33] should be compared with [4.9] and [4.18].

Under conditions of non-degeneracy, i. e. $\zeta \ll x$,

$$F_n(\zeta) \to \Gamma(n+1).\, e^{\zeta},$$

and equations [4.32] and [4.33] reduce to the forms

$$n_c = 4\pi\left(\frac{2m_{oo}^* kT}{h^2}\right)^{3/2} e^{\zeta}\left\{\frac{\sqrt{\pi}}{2} + \left(\frac{5}{2} - 5\gamma\right)\frac{3\sqrt{\pi}}{4}\beta + \left(\frac{7}{8} - \frac{21}{2}\gamma\right)\frac{15\sqrt{\pi}}{8}\beta^2 - \left(\frac{1}{4} + \frac{7}{2}\gamma\right)\frac{105}{16}\beta^3\right\} \qquad [4.35]$$

$$p_{V_2} = 4\pi\left(\frac{2m_{h_{2o}}^* kT}{h^2}\right)^{3/2} e^{-(\zeta + \xi)}\left\{\frac{\sqrt{\pi}}{2} + \frac{15\sqrt{\pi}}{4}\left(\frac{1}{2} - \gamma_h\right)\beta + \frac{105\sqrt{\pi}}{16}\left(\frac{1}{4} - 3\gamma_h\right)\beta^2 - \frac{105\sqrt{\pi}}{32}\left(\frac{1}{2} + 7\gamma_h\right)\beta^3\right\} \qquad [4.36]$$

which when $\beta \ll 1$ or $E_o^* \gg kT$ reduce to the form of [4.12]

Since the V_1 valence band can be considered to be parabolic as indicated by equation [4.21], the hole concentration relation for this band as given in section 4.3.1 equation [4.18] will be assumed valid.

Although the Kane model was calculated for application to the bands of InSb alone it has been shown that the model applies equally well to the other III - V zincblende compounds, and in the present work it is assumed that the alloy perturbation terms are sufficiently small that the model is valid for the III - V alloys as well.

4.4 The Hall Effect

4.4.1 Historical Introduction

The Hall effect is one of the oldest phenomena of solid state physics having been discovered in 1879 by E. H. Hall (79H1) who determined that a transverse potential was established in a thin metallic ribbon which was subjected to crossed electric and magnetic fields. The magnitude of this voltage was very small and its sign apparently arbitrary in various metals, and so the effect was an unimportant unexplained curiousity for many years. It was not until some fifty years later that the development of energy band theory and the discovery of semiconductors roused this effect from relative obscurity and made it the powerful tool it has become today.

The Hall voltage is several magnitudes larger in semiconductors than it is in metals. It is proportional to the Lorentz force which depends in turn on the drift velocity of the charge carriers. In a semiconductor carrying a given current the average drift velocity of carriers is much higher than in metals since the carrier density is very much smaller.

The Hall effect was the first experiment to show the effect of conduction by holes in materials where the energy bands were almost filled by electrons. Such metals as iron, cobalt, beryllium, and zinc were found to exhibit hole conduction long before the concept of a hole had been formulated.

4.4.2 Determination of the Hall Coefficient

The equations of motion for electrons in crossed electric and magnetic fields may be written in the form,

$$\dot{v}_x = -\left(\frac{e}{m_e}\right) \mathcal{E}_x - \omega v_y \qquad [4.37]$$

$$\dot{v}_y = -\left(\frac{e}{m_e}\right) \mathcal{E}_y + \omega v_x \qquad [4.38]$$

where $\omega = eB/m_e$. $\omega/2\pi$ is the cyclotron frequency.

Using the complex variables, $Z = v_x + iv_y$ and $z = x + iy$ equations [4.37] and [4.38] may be written in the form

$$\dot{Z} - i\omega Z = -\left(\frac{e}{m_e}\right) (\mathcal{E}_x + i\mathcal{E}_y) \qquad [4.39]$$

The general solution of this equation is

$$Z = Z_o + \frac{e}{m_e\, i\omega} (\mathcal{E}_x + i\mathcal{E}_y)(1 + e^{i\omega t}) \qquad [4.40]$$

where $Z_o = v_{xo} + iv_{yo}$ vanishes when the average over all collision times is taken. This average for equation [4.40] is found as follows

$$\bar{Z} = \bar{v}_x + i\bar{v}_y = \frac{\int_0^\infty Z\, e^{-t/\tau}\, dt}{\int_0^\infty e^{-t/\tau}\, dt} \qquad [4.41]$$

where τ is the relaxation time,

or $$\bar{Z} = \frac{1}{\tau} \frac{e}{m_e i\omega} (\varepsilon_x + i\varepsilon_y)(1 + e^{i\omega t})\ e^{-t/\tau}\, dt \qquad [4.42]$$

$$= -\left(\frac{e}{m_e}\right)(\varepsilon_x + i\varepsilon_y)\frac{\tau}{1 - i\omega\tau} \qquad [4.43]$$

Multiplying top and bottom by $(1 - i\omega\tau)$ and taking the real and imaginary parts, if $J_x = -ne\bar{v}_x$ and $J_y = -ne\bar{v}_y$, we get for these current densities

$$J_x = \frac{ne^2}{m_e}\left\{\frac{\tau\varepsilon_x}{1 + \omega^2\tau^2} - \frac{\omega\tau^2\varepsilon_y}{1 + \omega^2\tau^2}\right\} \qquad [4.44]$$

$$J_y = \frac{ne^2}{m}\left\{\frac{\tau\varepsilon_y}{1 + \omega^2\tau^2} + \frac{\omega\tau^2\varepsilon_x}{1 + \omega^2\tau^2}\right\} \qquad [4.45]$$

Equation [4.44] and [4.45] may be written in the form

$$J_x = A\varepsilon_x - D\varepsilon_y \qquad [4.46]$$

$$J_y = A\varepsilon_y + D\varepsilon_x \qquad [4.47]$$

At equilibrium, the total transverse current is zero, i. e. $J_y = 0$, hence,

$$\mathcal{E}_y = \frac{-D}{A}\,\mathcal{E}_x \qquad [4.48]$$

If this relation is substituted into equation [4.46] we get

$$J_x = \left(A + \frac{D^2}{A}\right)\mathcal{E}_x \qquad [4.49]$$

Since the Hall constant

$$R_H = \mathcal{E}_y / J_x B\,, \qquad [4.50]$$

we have

$$R_H = \frac{-D/B}{A^2 + D^2} \qquad [4.51]$$

If, in the conductor, the currents are made up of contributions from more than one type of carrier, equations [4.46] and [4.47] must include additively all of these contributions, hence

$$J_x = \Sigma A_i \mathcal{E}_x - \Sigma D_i \mathcal{E}_y \qquad [4.52]$$

$$J_y = \Sigma A_i \mathcal{E}_y + \Sigma D_i \mathcal{E}_x \qquad [4.53]$$

In a manner analagous to that described above, we may define the Hall constant as

$$R_H = \frac{-\Sigma D_i/B}{(\Sigma A_i)^2 + (\Sigma D_i)^2} \qquad [4.54]$$

where terms are included for each type of charge carrier, and the D_i take their sign from the sign of the carrier.

In the materials which were the subject of the present work the carriers which contributed to conduction were a) electrons in the (000) conduction band b) electrons in each of the ⟨100⟩ and ⟨111⟩ bands, and c) holes in both the light and heavy hole valence bands.

We will now consider the terms A_i and D_i of equation [4.54] appropriate to each of these bands.

4.4.3 The Hall Factors for Single Valued Bands

The conduction electrons in the (000) band minimum can have very high mobilities in III - V material and hence, unless experiments are carried out in very low magnetic fields, the terms $(\omega\tau)^2$ may not be neglected.

Therefore the terms A and D in equation [4.54] must be evaluated by averaging over all possible energies in the following manner.

$$A = \frac{ne^2}{m_e} \left\langle \frac{\tau}{1 + \omega^2\tau^2} \right\rangle \qquad [4.55]$$

$$D = \frac{ne^2}{m_e} \left\langle \frac{\omega\tau^2}{1 + \omega^2\tau^2} \right\rangle \qquad [4.56]$$

Let us proceed first with equation [4.55]. Averaging over all allowed energies we have

$$\langle C \rangle = \frac{\int_0^\infty C\, E^{3/2} f_e\, dE}{\int_0^\infty E^{3/2} f_e\, dE} \qquad [4.57]$$

which assumes the constant energy surfaces are spherical and the band is parabolic. Hence,

$$A = \frac{ne^2}{m_e} \frac{\int_0^\infty \frac{\tau}{1 + \omega^2\tau^2} E^{3/2} f_e\, dE}{\int_0^\infty E^{3/2} f_e\, dE} \qquad [4.58]$$

Assuming that $\tau = aE^{-s}$ (isotropic scattering and) (parabolic band assumption) [4.59]

for the available energies, we now have

$$A = \frac{ne^2}{m_e} \frac{a \int_0^\infty E^{3/2 - s}(1 + \omega^2 a^2 E^{-2s})^{-1} f_e\, dE}{\int_0^\infty E^{3/2} f_e\, dE} . \qquad [4.60]$$

By letting $x = E/kT$ [4.61]

we may write

$$A = \frac{ne^2 a}{m_e kT^s} \frac{\int_0^\infty x^{3/2 + s} f_e (x^{2s} + a^2\omega^2/kT^{2s})^{-1}\, dx}{\int_0^\infty x^{3/2} f_e\, dx} \qquad [4.62]$$

For polar, optical phonon scattering at elevated temperatures the value of s is-1/2 (53H1). In which case it may be easily shown that

$$\langle \tau \rangle = \frac{a(kT)^{1/2} \; F_2(\zeta)}{F_{3/2}(\zeta)} \qquad [4.63]$$

where

$$F_n(\zeta) = \int_o^\infty \frac{x^n \; dx}{1 + e^{x - \zeta}} \qquad [4.64]$$

is the standard form of the Fermi integral.

Using [4.63], [4.62] may be written in the form

$$A = \frac{ne}{F_2(\zeta)} \; \frac{e\langle \tau \rangle}{m_e} \int_o^\infty \frac{x \; f_e \; dx}{x^{-1} + a^2 \omega^2 \; kT} \qquad [4.65]$$

Letting μ_c, the conductivity mobility for the electrons be defined as

$$\mu_c = \frac{e\langle \tau \rangle}{m_e} \qquad [4.66]$$

we may write

$$A = \frac{ne\mu_c}{F_2(\zeta)} \int_o^\infty \frac{x \; (1 + e^{x - \zeta})^{-1} \; dx}{x^{-1} + \mu_c^2 B^2 [F_{3/2}(\zeta)/F_2(\zeta)]^2} \qquad [4.67]$$

In the limit of complete non-degeneracy, i.e. when $x > \zeta$, the

Fermi integrals reduce to the form of Gamma functions such that

$$F_n(\zeta) = e^{\zeta}\,\Gamma(n+1) \qquad [4.68]$$

where

$$\Gamma(n+1) = \int_o^{\infty} x^n\, e^{-x}\, dx \quad . \qquad [4.69]$$

In this case [4.67] may be written

$$A = ne\mu_c 1/2 \int_o^{\infty} \frac{x\; e^{-x}\; dx}{x^{-1} + (9\pi/64)\mu_c{}^2\, B^2} \qquad [4.70]$$

In the low field limit, i.e. when $\mu B \ll 1$, this may be reduced to the form

$$A = 1/2ne\mu_c\;\; \Gamma(3) = ne\mu_c \qquad [4.71]$$

In order to evaluate [4.56] we must write

$$D = \frac{ne^2}{m_e} \quad \frac{\int_o^{\infty} \frac{\omega\tau^2}{1+\omega^2\tau^2}\; E^{3/2}\; f_e\; dE}{\int_o^{\infty} E^{3/2}\; f_e\; dE} \qquad [4.72]$$

$$= \frac{n\;\; e^3\; a^2 B}{m_e{}^2\;\; kT^{2s}} \quad \frac{1}{F_{3/2}\,(\zeta)} \int_o^{\infty} \frac{x^{3/2}\, f_e\; dx}{x^{2s} + a^2\omega^2/kT^{2s})} \qquad [4.73]$$

Taking $s = -1/2$ and letting $\mu_c = \frac{e\langle\tau\rangle}{m_e}$ we now have

$$D = ne\,\mu_c^2\,B\,\frac{F_{3/2}(\zeta)}{[F_2(\zeta)]^2}\int_o^\infty \frac{x^{3/2}\,f_e\,dx}{x^{-1}+\mu_c^2B^2\,[F_{3/2}(\zeta)/F_2(\zeta)]^2} \qquad [4.74]$$

When $x \gg \zeta$ [4.74] may be written

$$D = ne\,\mu_c^2\,B\,\frac{3\sqrt{\pi}}{16}\int_o^\infty \frac{x^{3/2}\,e^{-x}\,dx}{x+\mu_c^2\,B^2\,\frac{9\pi}{64}}\quad , \qquad [4.75]$$

and when $\mu B \ll 1$,

$$D = \frac{\Gamma(5/2)\,\Gamma(7/2)}{[\Gamma(3)]^2}\,ne\mu_c^2\,B = \frac{45\pi}{128}\,ne\mu_c^2\,B \qquad [4.76]$$

In the above derivations the non-parabolicity of the bands and any energy dependence of the effective mass has been neglected, as these would be of secondary significance.

Considering the holes in the two valence band maxima, the mobilities involved are small enough to allow the low field conditions to be applicable. Boltzmann statistics apply since the Fermi level is normally far from top of the valence band at elevated temperatures. Thus equations [4.69] and [4.75] may be used and we may write

$$A_3,\ A_4 = p_{1,2}\,e\,\mu_{h_{1,2}} \qquad [4.77]$$

$$D_3,\ D_4 = -1.1\ p_{1,2}\ e\ \mu_{h_{1,2}}^2\ B \qquad [4.78]$$

$3 \equiv V_1$ band; $\quad 4 \equiv V_2$ band.

4.4.4 The Hall Factors for Multi-Valued Bands *

The subsidiary conduction bands are characterized by ellipsoidal energy surfaces and low mobilities. Thus the μ^2B^2 or $\omega^2\tau^2$ terms may be neglected but the anisotropicity of the effective mass must be included. The effective mass will have components along each of the $\hat{k}_x$, $\hat{k}_y$, and $\hat{k}_z$ axes. Assuming τ to be isotropic and depending only on E, the equations of motion may now be written:

$$\dot{v}_x = -\frac{e}{m_1}\mathcal{E}_x - \omega_1 v_y \qquad [4.79]$$

$$\dot{v}_y = -\frac{e}{m_2}\mathcal{E}_y + \omega_2 v_x \qquad [4.80]$$

Multiplying [4.79] by $\omega_2^{1/2}$ and [4.80] by $\omega_1^{1/2}$ and defining a complex variable

$$Z = \omega_1^{1/2}\ v_x + i\omega_2^{1/2}\ v_y \qquad [4.81]$$

we obtain

$$\dot{Z} = -e\left(\frac{\omega_2^{1/2}}{m_1}\mathcal{E}_x + i\ \frac{\omega_1^{1/2}}{m_2}\mathcal{E}_y\right) + i\omega_1^{1/2}\omega_2^{1/2}Z \qquad [4.82]$$

* This section is valid only for the case of orthogonal $\hat{k}$- direction minima. A different derivation as found in Smith must be used for ⟨111⟩ bands; however the resulting expressions are exactly the same in both cases.

If $\omega^2 = \omega_1\omega_2$, then the appropriate solution for [4.82] is

$$Z = Z_o - \frac{e}{i\omega}\{\frac{\omega_2^{1/2}}{m_1}\varepsilon_x + i\frac{\omega_1^{1/2}}{m_2}\varepsilon_y\}(1 - e^{i\omega t}) \qquad [4.83]$$

By averaging over all collision times we obtain

$$\bar{Z} = \frac{-\tau e}{1 - i\omega\tau}\{\frac{\omega_2^{1/2}\varepsilon_x}{m_1} + \frac{i\omega_1^{1/2}\varepsilon_y}{m_2}\} \qquad [4.84]$$

Taking the real and imaginary parts we get

$$-e\bar{v}_x = e^2\{\frac{\tau\varepsilon_x}{m_1(1 + \omega^2\tau^2)} - \frac{\omega_1\tau^2\varepsilon_y}{m_2(1 + \omega^2\tau^2)}\}$$

$$-e\bar{v}_y = e^2\{\frac{\tau\varepsilon_y}{m_2(1 + \omega^2\tau^2)} + \frac{\omega_2\tau^2\varepsilon_x}{m_1(1 + \omega^2\tau^2)}\} \qquad [4.85]$$

Neglecting terms in $(\omega\tau)^2$, and carrying out the usual averaging process for τ, summing the contributions from all equivalent ellipsoids, and permuting the masses, m_1, m_2, m_3, we have

$$J_x = -ne\Sigma\bar{v}_x = \frac{ne^2}{3}\{\langle\tau\rangle\varepsilon_x(\frac{1}{m_1} + \frac{1}{m_2} + \frac{1}{m_3}) - eB\langle\tau^2\rangle\varepsilon_y\frac{m_1 + m_2 + m_3}{m_1m_2m_3}\} \qquad [4.86]$$

$$J_y = -ne\,\Sigma\bar{v}_y = \frac{ne^2}{3}\left\{\langle\tau\rangle\varepsilon_y\left(\frac{1}{m_1}+\frac{1}{m_2}+\frac{1}{m_3}\right) + eB\langle\tau^2\rangle\varepsilon_x\frac{m_1+m_2+m_3}{m_1m_2m_3}\right\}$$

[4.87]

If $m_2 = m_3 = m_t$ $m_1 = m_\ell$ and $K = m_\ell/m_t$ [4.88]

$$A_{1,2} = n_{1,2}e^2\,\langle\tau\rangle\,\frac{1}{3}\left(\frac{1}{m_\ell}+\frac{2}{m_t}\right) \qquad [4.89]$$

$$D_{1,2} = n_{1,2}e^3\,\langle\tau^2\rangle B\frac{(m_\ell+2m_t)}{3(m_\ell m_t^2)} \qquad [4.90]$$

Evaluating $\langle\tau^2\rangle$ when $\tau = aE^{+1/2}$ we find

$$\langle\tau^2\rangle = \frac{5a^2\,kT}{2} \qquad [4.91]$$

which may be written,

$$\langle\tau^2\rangle = \frac{45\pi}{128}\langle\tau\rangle^2 \quad , \qquad [4.92]$$

and taking $\mu_c = \dfrac{e\langle\tau\rangle}{m^*}$ [4.93]

where $m^* = (m_\ell m_t^2)^{1/3}$

we get for [4.89] and [4.90]

$$A_{1,2} = n_{1,2} e \mu_{c_{1,2}} \frac{2K + 1}{3K^{2/3}} \qquad [4.94]$$

$$D_{1,2} = 1.1 \; n_{1,2} e \mu_{c_{1,2}}^{2} B \frac{(2 + K)}{3K^{1/3}} \qquad [4.95]$$

Using equations [4.67, 74, 77, 78, 94 and 95], the Hall coefficient may be determined.

$$R_H = \frac{-\Sigma \, r_{D_i} \, n_i e \, \mu_i^{\,2}}{(\Sigma \, r_{A_i} \, n_i e \, \mu_i)^2 + (\Sigma \, r_{D_i} \, n_i e \, \mu_i^{\,2} B)^2} \qquad [4.96]$$

where $$r_{D_o} = \frac{F_{3/2}(\zeta)}{[F_2(\zeta)]^2} \int_o^{\infty} \frac{x^{3/2} \, f_e \, dx}{x^{-1} + \mu_o^{\,2} B^2 [F_{3/2}(\zeta)/F_2(\zeta)]^2}$$

$$r_{D_1} = r_{D_2} = 1.1 \frac{K + 2}{3K^{1/3}}$$

$$r_{D_3} = r_{D_4} = - 1.1$$

$$r_{A_o} = \frac{1}{F_2(\zeta)} \int_o^{\infty} \frac{x \, f_e \, dx}{x^{-1} + \mu_o^{\,2} B^2 [F_{3/2}(\zeta)/F_2(\zeta)]^2}$$

$$r_{A_1} = r_{A_2} = \frac{2K + 1}{3K^{2/3}}$$

$$r_{A_3} = r_{A_4} = 1$$

The integrals in equations [4.67] and [4.73] have been evaluated numerically for several values of μB and several values of $\zeta = E_F/kT$ both in the non-degenerate and degenerate cases and it was shown that the values of r_A were always within 5% of the factor $\left(\frac{1}{1 + \mu^2 B^2}\right)$ and that the r_D were within 5% of $\left(\frac{1.1}{1 + \mu^2 B^2}\right)$ in all cases.

4.4.5 Conductivity

The conductivity of a material is defined by the relation

$$\sigma = J/\mathcal{E} \quad . \qquad [4.97]$$

Where the material exhibits multiband conduction the conductivity can be obtained from [4.52] taking the zero field limit, i. e. $B = 0$, $\omega = 0$. Hence,

$$\sigma = \Sigma A_i \qquad [4.98]$$

or

$$\sigma = \Sigma r_{A_i} n_i e \mu_{ci} \qquad [4.99]$$

Combining [4.50] and [4.97] we may define the Hall mobility as

$$\mu_H = R_H \sigma = \frac{\mathcal{E}_y}{\mathcal{E}_x B} \qquad [4.100]$$

which from [4.48] may be expressed as

$$\mu_H = \frac{-\Sigma D_i}{\Sigma A_i \quad B} \qquad [4.101]$$

4.5 Evaluation of the Hall coefficient and Conductivity

The Hall constant can be calculated in a parallelepipedal specimen from a measurement of the sample size, the strength of the magnetic field and the magnitude of the current flowing in the sample. If the current flows in the X direction and the magnetic field acts along the Z direction, then the Hall voltage V_H can be detected along the transverse Y direction. The magnitude of the Hall voltage enables the Hall constant to be determined by the following expression

$$R_H = \frac{V_H\, t}{I\, B} \quad , \qquad [4.102]$$

where t is the sample thickness in the Z direction. R_H is expressed in MKS units as metres^3 per coulomb. More commonly however, the Hall constant is given in units of cm^3/coulomb.

The conductivity is determined from the measured potential drop along a known length of a material with known constant cross section in which a known current is flowing.

The potential drop V_σ is related to the conductivity by the relation

$$\sigma = \frac{I\, \ell}{V_\sigma\, a}$$

where "ℓ" is the distance between the electrodes and "a" is the area of the cross-section.

The conductivity in MKS units is measured as $(\text{ohm-m})^{-1}$ but is more commonly reported in $(\text{ohm-cm})^{-1}$ or "mhos"/cm.

CHAPTER V

EXPERIMENTATION

5.1 Apparatus

5.1.1 Hall Effect Probes

The sample holder for the high temperature Hall measurements is shown diagrammatically on figure 5.1.1. The sample was mounted on a block of pyrophilite (soapstone) measuring approximately 4.2 x 1.0 x 0.5 cm. The block was fastened at the end of a compound shaft composed of a stainless steel tube $\frac{1}{4}$ inch in diameter and two four-holed alumina conduits. These were held together by a series of stainless steel discs approximately three inches apart along the length of the 30 cm. shaft. A spring-loaded 1/16 inch diameter stainless steel rod was placed inside the stainless steel tube and was fastened to a small stainless steel block A on the top surface of the pyrophilite sample holder. The sample was held by spring action between this block and another similar block B, the two serving as contacts for the sample current.

Voltage electrodes were 0.004 inch platinum wires which were connected to small bolts (D, E, F, G,) on the probe head. The bolts were connected on the bottom side of

FIGURE 5.1.1

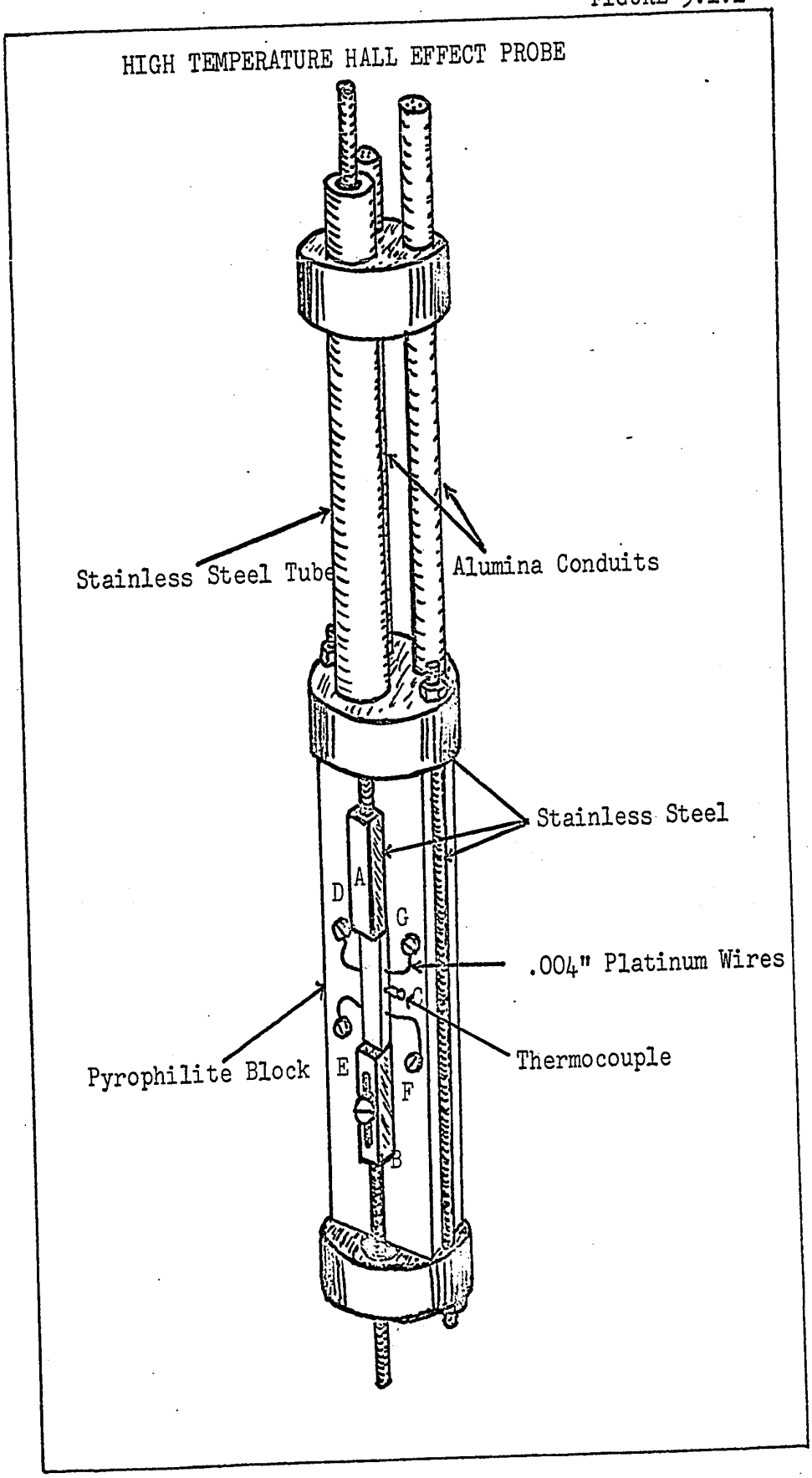
HIGH TEMPERATURE HALL EFFECT PROBE
Stainless Steel Tube
Alumina Conduits
Stainless Steel
.004" Platinum Wires
Thermocouple
Pyrophilite Block
A
B
C
D
E
F
G

the probe to copper leads which were fed through the alumina conduits from the top of the shaft. Other holes in the alumina conduits were used for the current lead to the block B and for the platinum and platinum -13% rhodium thermocouple wires which were joined at point C as shown on figure 5.1.1.

Hall voltages were read across either of the pairs of electrodes at E and F or D and G while resistivity was determined from the voltage drop from D to E or G to F.

At the end of the shaft away from the sample all leads were connected to ceramic feed-throughs which were soldered into a flat brass plate.

The sample holder for low temperature measurements is shown on figure 5.1.2. This probe featured phospor-bronze spring contacts for the voltage contacts and .004" platinum wire electrodes for the current contacts at either end. When the sample was placed in the center of holder, the side contacts were made by tightening the set screws as indicated on figure 5.1.2. When physical contact was made as indicated by a low resistance reading across the transverse electrodes, the junctions were spark-welded to decrease the contact resistance. The current contacts at the ends were spark-welded to the specimen.

FIGURE 5.1.2

LOW TEMPERATURE HALL EFFECT PROBE

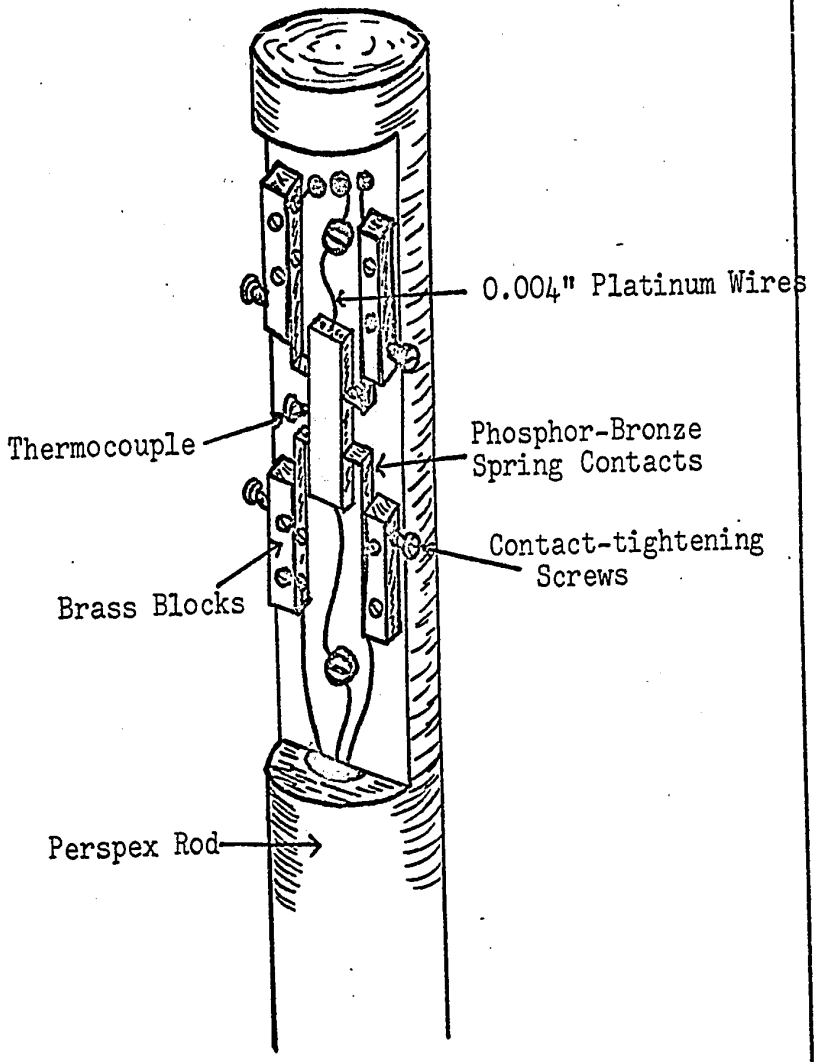

5.1.2 High Temperature Hall Furnace

For high temperature measurements the Hall probe was placed vertically downwards into a mullite refractory tube of 1/2 inch inner diameter. The lower end of this mullite furnace tube was sealed and at the top end a water-cooled flange was fixed to the tube by means of epoxy cement. The water cooling was necessary to protect the epoxy from excessive heat as this would cause deterioration of the seal. The brass plate of the Hall probe and the flange of the furnace met to form a vacuum tight O-ring seal. This arrangement is shown on figure 5.1.3.

The heating element of the furnace was Nichrome resistance wire (1.26 ohm/ft) wound about the mullite tube and sealed in place with 1/8" coat of Kyanex refractory cement. The furnace and cement coating were surrounded by a water jacket which served to protect the magnet pole pieces from excessive heat. The total resistance of the furnace windings was approximately 20 ohms and the temperature could be adjusted from room temperature to a maximum of ~1000^{o}K by means of a 220 volt Variac. The voltage was never allowed to exceed 135 volts giving a maximum current of seven amperes.

When measurements were needed below room temperature the magnet was rolled to a second position where a pyrex dewar replaced the furnace. The dewar could be filled with

FIGURE 5.1.3

HIGH TEMPERATURE HALL EFFECT FURNACE

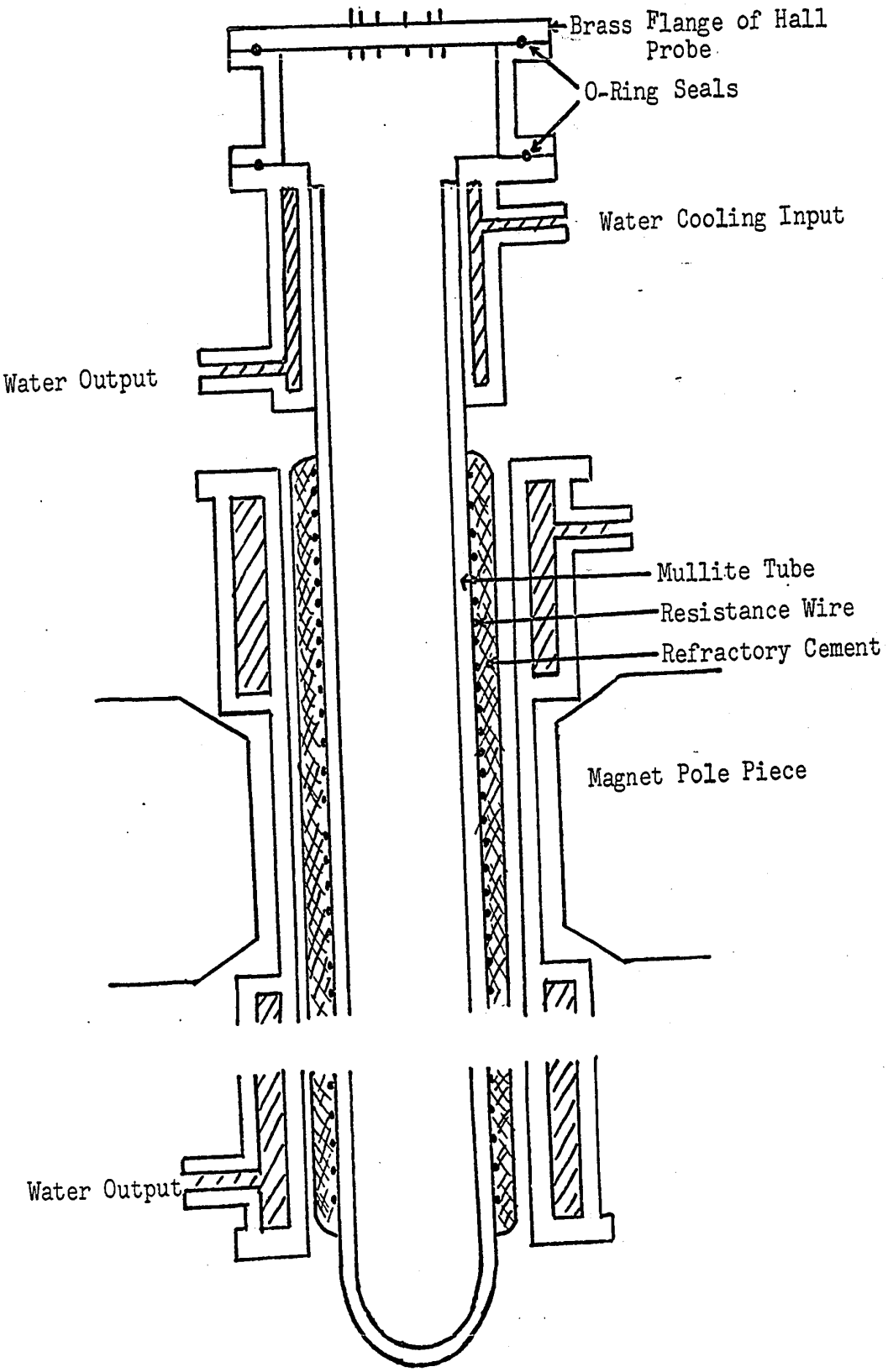

liquid nitrogen and the probe immersed into the liquid or the cold gas above the liquid surface to attain temperatures from ~80°K to room.

5.1.3 Auxillary Equipment

The temperature of the Hall furnace could be increased at a constant low rate. A small electric motor (1/15 rpm) equipped with a gear and pulley drive gradually increased the output of a 2 KVA variac at a rate of ~35 volts per hour. This caused the temperature of the furnace at the sample to rise at the rate of about 200°C per hour or ~3.6°C per minute. The thermocouple output was continuously monitored with a Tinsley potentiometer with a Pye Scalamp null galvanometer. The thermocouple voltage was compared with a similar junction in an ice and water bath.

The furnace could be evacuated to a pressure of less than 10^{-4} mm Hg. as measured on a Pirani gauge. This vacuum was achieved with a water-cooled diffusion pump backed by a rotary pump.

The magnet current was supplied and controlled by a 2 KVA Harvey Wells power supply. The current could be stabilized at any value from zero to ten amperes creating fields in the two inch pole gap up to 8200 gauss accurate to within one percent. The stability of the field was

assisted by the fact that the field began to saturate above 8 amperes. The magnetic field was calibrated for both current directions using a rotating coil flux meter. For the Hall experiments a field of 8000 gauss was used. The appropriate current value could be preset on the power supply and the appropriate field established in the pole gap automatically by means of an internal motor drive in the power supply.

5.2 Electrical Circuitry

5.2.1 Voltage Selection

The heart of the Hall and conductivity measuring circuit was the selector switch as shown in the circuit diagram, figure 5.2.1. The voltage leads from the sample at the probe-head were fed to the selector switch S1, a two bank - 12 point sealed rotary switch with low noise, low resistance silver contacts. One of each of the Hall contacts leads was interrupted to allow a variable voltage to be applied in order to back off any offset potential drop between the Hall contacts. The back-off voltage was supplied from a 1.5 volt dry cell battery V2 with on-off and reversing switches S2 and S3 and two variable programming resistances R1 and R2. R1 was a 100 Ω helipot for fine control and R2 was a 10K one turn pot for coarse adjustments. A back-off voltage was included in the resistivity circuits as well, in order to eliminate thermoelectric power voltages which sometimes arose at high temperatures due to slight temperature gradients along the sample. Again the back-off voltage was supplied by a 1.5 volt dry cell (V3) with a switching arrangement (S4) which allowed measurements to proceed with or without its inclusion in the circuit. The voltage was adjusted by the rheostats R3 and R4 which were coarse and fine controls respectively.

HALL AND CONDUCTIVITY MEASURING CIRCUIT

FIGURE 5.2.1

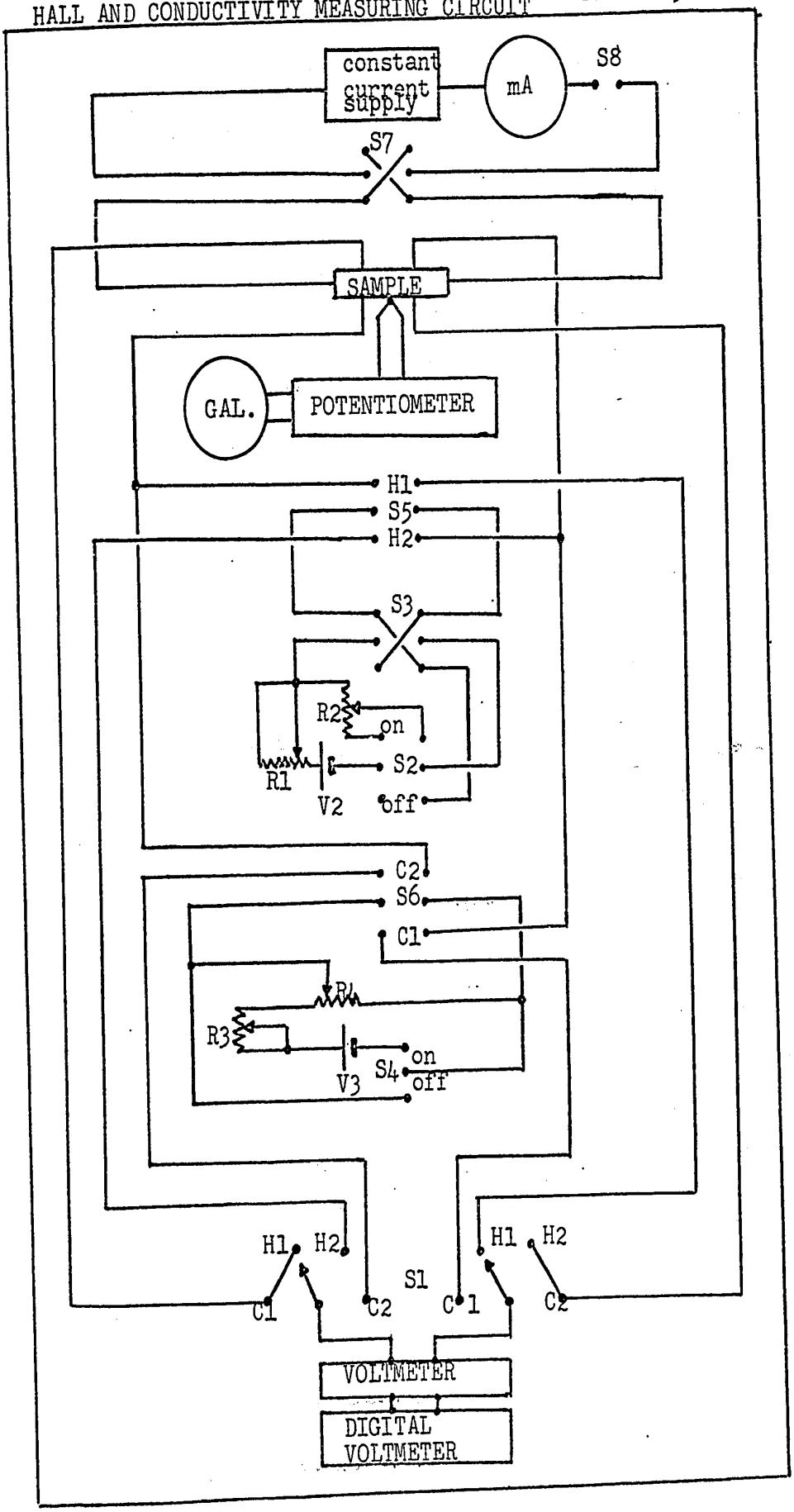

The sample current was generated by a Hewlett-Packard constant current supply, V1. A milliameter and a reversing switch S7 were included in the circuit. The current supply was regulated by external programming resistors R5 and R6 which were respectively a 100 ohm ten turn helipot for fine control and a 10 K ohm ten turn helipot for coarse adjustments. The sample current was normally set at 100 milliamps but when a specimen of high resistivity was measured currents as small as one milliamp could be used. The constant current supply had two ranges, one of 20 volts which had maximum current of 1500 mA and the other of 40 volts with a maximum current of 750 mA. The current stability was dependent on the programming resistors but after allowing sufficient time for warm up the current was constant within 0.2%.

5.2.2 Voltage Detection

The output of the selector switch was conducted on a shielded coaxial cable to a Hewlett-Packard "419A" DC null voltmeter. The impedance of the voltmeter was one meg-ohm or greater on all scales from 3 μV to 1000 volts. Voltages could be detected with an accuracy of one percent of the full scale value. The full scale output from the voltmeter was one volt on all ranges and was fed directly to a Hewlett-Packard four figure digital voltmeter. The resolution of the

digital voltmeter was 0.05%, ± 1 count. The sampling time was 12 milliseconds and the sampling rate could be adjusted manually. Under normal operation the voltmeter was set to a range on which the decimal points and units were changed automatically. When a typical specimen was being measured, the absolute error in the Hall voltage or in the resistivity potential drop was due mainly to the uncertainty in the physical dimensions of the sample (5%) and in the distance between electrodes (10%). These factors, however, were relatively constant with temperature and so did not contribute to the relative or random error in the measurements. The uncertainty in the sample temperature was the main source of random error in the experiments and in the following section the methods used to minimize this effect will be discussed.

5.3 Operational Procedure

5.3.1 Specimen Preparation for Hall Measurements

Samples used in the present Hall and conductivity experiments were cut from cross-sectional slices of ingots. Various slices had thicknesses ranging from 0.5 to 1.0 millimeters. Thinner specimens were required for those ingots which exhibited a rapid composition variation along their lengths, while thicker specimens were sometimes required when the material to be measured proved to be extremely fragile. For most cases, the slice was cut to give a specimen in the form of a parallelepiped roughly 1.0 x 0.5 x 10.0 mm. with dimensional uniformity within 5 % of these values as determined by a micrometer.

All cutting of ingots and slices was done by means of a carborundum rotary saw with the crystal mounted on slabs of "arborite" by means of "glyptal" cement.

5.3.2 Specimen Mounting

When a sample was cut from a cross-sectional slice of an ingot, an adjacent sample was cut from the same slice for use in the X-ray analysis to determine the composition and homogeneity of the slice. When this was done, and if the slice was found to be homogeneous, the parallelepipedal sample was measured with a micrometer and its dimensions noted. The sample was then mounted on the low temperature

probe and the electrodes spark-welded to it in the bridge configuration by discharging a 10 μfd capacitance through the sample from electrode to electrode. After spark-welding the contacts were tested for ohmic behaviour and for low resistivity using an AVO meter. Any contact which was not satisfactory was rewelded.

The relative spacing of the resistivity electrodes was measured with a micrometer and the probe was placed into the pyrex dewar containing liquid N_2. As the nitrogen evaporated and the sample temperature increased, a series of measurements of the Hall voltage and potential drop across the resistivity contacts were taken.

For high temperature measurements the specimen was mounted on the pyrophilite holder between the stainless steel blocks (A and B on figure 5.1.1). The platinum electrodes were placed in a bridge configuration using the intrinsic springiness of the wire to make a light pressure contact. These contacts were then spot-welded by discharging a 10 μfd capacitor through each electrode to either of the end contacts of the sample. When samples of relatively high resistivity were measured small discs of indium were inserted between the specimen and the current contact blocks. After each of the electrodes was so welded, the contacts were tested for ohmic behaviour and for low

resistance with an AVO meter. If there was any detectable rectification then a fresh junction was made.

When all contacts were satisfactory the distance between the side contacts was measured using a micrometer and the probe was carefully lowered into the Hall furnace and bolted into the correct alignment. There may have been an error in the Hall measurements since the specimen may not have been perfectly perpendicular to the field, but the angle did not change during an experiment nor from experiment to experiment as the position of the probe was permanently fixed. Hence, there was little relative error on this account. When the vacuum seal at the top of the furnace was made, the furnace was evacuated and flushed several times with helium gas then filled with helium. A very slight over pressure of helium was maintained by a balloon which was connected to the system. This balloon permitted a relatively free expansion of the gas during heating so that the furnace was not subjected to an increasing positive gas pressure.

5.3.3 Sample Uniformity

The sample current was switched on and allowed to warm up while the furnace was still at room temperature. The Hall back-off voltage was adjusted so that the zero field signal for each set of Hall contacts was minimal.

While the furnace was still cool a study was made of the uniformity of the sample by checking the Hall voltages from both sets of contacts while reversing both the sample current and the magnetic field polarity in turn. As well the resistivity voltage drop was checked for both sets of contacts for both current directions. In none of the samples measured did the signal variation determined in this manner exceed ten percent. Any discrepancy was mainly due to such geometrical factors as variation in the sample thickness or uncertainty in the relative positions of the electrodes as much as from the slight compositional variation within a specimen. If for any reason the non-uniformity exceeded 10% then the sample is not used for the experiment.

5.3.4 Heating Cycle

During a temperature cycle readings were taken with a constant current direction but with magnetic field reversal. Only one set of Hall and resistivity electrodes was used, the other two electrodes being kept in reserve if for any reason a contact was broken during a run. The pattern for reading the voltages was to set the thermocouple potentiometer to a preestablished voltage corresponding to a known temperature. Then, as the galvanometer spot approached the null position, a reading was taken of the resistivity

voltage. The magnet power supply was then switched on and within five seconds would reach its preset value of 8 kilogauss. During these five seconds the selector was rotated to the Hall position and any necessary scale change was made on the voltmeter. When the field had stabilized, the Hall voltage was read, the magnet current reversed and the new Hall voltage recorded. The magnet was then switched off and a setting corresponding to five degrees higher was made on the potentiometer.

The time involved for the furnace to increase in temperature five degrees was approximately 85 seconds and the time involved in reading the Hall voltage in both field directions was less than 10 seconds. Thus the temperature uncertainty for the signal voltages was less than one degree, which was partially compensated for by the fact that the magnet field was reversed in alternate directions from measurement to measurement.

By this continuous heating method, within three hours measurements could be taken at five degree intervals over the temperature range from 300°K to 1000°K, involving up to one hundred and forty sets of values. If a temperature controller were employed and readings were taken only at steady temperatures, any gain in thermal stability would be more than offset the prohibitively long duration of the experiments for the same number of points.

During the one minute of waiting between sets of voltage readings, the thermoelectric power back-off was checked by reversing the sample current and adjusting the voltage difference to zero. As well any necessary corrections to the Hall back-off voltage were made.

When the maximum desired temperature was reached the furnace power was turned down by stages and the Hall and resistivity voltages were checked for any major deviations. For most specimens there were slight variations in the extrinsic carrier concentration but negligible variation in the readings in the intrinsic conduction range.

For measurements below room temperature the same procedure as outlined above was followed except that the temperature increments were ten degrees C. In a normal low temperature run the temperature remained relatively constant at an initial temperature near to that of liquid nitrogen for several minutes. Then the sample began to warm up as the nitrogen in the dewar evaporated. No attempt was made to control the temperature rise in these experiments as their main purpose was merely to check the absolute value of the extrinsic carrier concentration in those specimens which exhibited intrinsic conduction at room temperature.

5.3.5 Tabulation of Observations

The voltage data was recorded on tables prepared in advance with the temperature and thermocouple voltage pre-recorded. Columns were available for the resistivity voltage and the two Hall voltages as they were read from the digital voltmeter. Columns were reserved for a notation of the scale factors since these would change during a temperature run. As well there was a column for the algebraic difference between the two Hall voltages, this being equal to twice the Hall voltage with terms involving the offset potential drop and magnetoresistance voltages eliminated. Finally there were columns for the calculated values of the Hall constant R_H, the resistivity, and the Hall mobility ($R_H\sigma$) as calculated from the voltage data. An example of such a data sheet is shown on Table 5.3.1.

TABLE 5.3.1

EXPERIMENTAL DATA TABULATION

t = 0.107 cm
ω = 0.145 cm

ℓ = 0.325 cm

I = 100 mA
B = 8KG

V_T	V_ρ	V_H +	V_H-	$2V_H$	$R_H(\frac{cc}{C})$	T (°C)	$\rho(\Omega\text{-cm})$	μ_H (cm^2/V.sec)	V_H scale	V_ρ scale
									3×10^{-2}	3×10^{-1}
129	393.3	934.4	980.0	1914.4	-384.79	180	5.62×10^{-1}			10^{-1}
134	104.4	910.8	881.8	1792.6	-360.31	185	4.480	722.0		
138	830.7	825.5	827.0	1652.5	-332.15	190	4.411			
143	830.7	762.7	773.0	1535.7	-308.68	195	3.962			
147	739.1	680.4	717.1	1397.5	280.89	200	3.526	797.		
151	657.3	614.2	655.5	1269.7	255.21	205	3.135			
155	608.8	570.6	628.0	1198.6	240.92	210	2.904			
160	530.5	563.6	498.7	1062.3	213.52	215	2.530			
164	484.2	494.9	486.3	981.2	197.22	220	2.310			
169	404	422.0	417.7	839.7	168.78	225	1.927			
173	121.2	402.2	378.0	780.2	156.92	230	1.735			
178	117.0	372.8	362.0	734.8	147.69	235	1.673			

CHAPTER VI

RESULTS AND ANALYSIS

6.1 Introduction

In this chapter the experimental results of high temperature measurements on three different alloy systems will be presented. These data will be analysed using a standard two band, non-degenerate, parabolic band analysis. It will be shown that while meaningful determinations of energy gaps and their composition dependence may be obtained in this manner over a wide range of alloy compositions, there are certain significant inadequacies inherent in the assumptions required for this work.

In order to eliminate as many as possible of these limitations, an analysis is presented which incorporates such sophistocations as Kane non-parabolic energy bands, Fermi-Dirac statistics, and consideration of the contributions of three conduction and two valence bands. In order to apply such a complex investigation, extensive computer calculations were employed and a general computer program applicable to any semiconducting material with zincblende band structure has been prepared.

The results of this analysis are presented with special

emphasis on the relative energy separations of the conduction band minima and the influence of the higher bands on conduction processes.

6.2 Experimental Results

Measurements of the Hall effect and the conductivity over a wide range of temperatures were made on samples of $Ga_xIn_{1-x}Sb$ alloys obtained from several ingots prepared by the gradient freeze and step freeze methods. All alloys were homogeneous and coarsely polycrystalline. Samples measured covered a wide range of impurity concentrations both p- and n-type. Different ingots were doped with tellurium, cadmium, or left undoped. The ingots which supplied samples for the present work are listed on Table 6.2.1 together with the pertinent data concerning each. Such factors as the method of preparation, mean starting composition, dopant, range of impurity concentration, alloy composition range, and homogeneity are indicated. The various samples used in the Hall experiments are listed on Table 6.2.2. Included in this table are various properties of each sample such as the composition, homogeneity, and lattice parameter, and the room temperature Hall coefficient, resistivity and Hall mobility.

The results of the high temperature measurements of the Hall coefficient for some representative experiments are shown on figures 6.2.1 and 6.2.2. Typical p-type results are presented on figure 6.2.1. The progressive increase of the energy gap with alloy composition is indicated by the increased temperature of the Hall coefficient null position. The variation of the Hall constant of n-type alloys is shown

TABLE 6.2.1

ALLOY INGOT DATA

INGOT	ALLOY	METHOD OF GROWTH	$\overline{X}$ (mole-fraction)	DOPANT	$N_A - N_D$ RANGE (cm^{-3})	COMP. RANGE (mole-fraction)	HOMO-GENEITY
DFA5	GaInSb	G.F.	0.7	Te	$+10^{16}/+10^{17}$	.95 - .75	±.02
DFA6	GaInSb	G.F.	0.5	--	$-10^{16}/-10^{17}$	.87 - .00	±.015
DFA8	GaInSb	G.F.	0.3	--	$-10^{16}/-10^{17}$	.75 - .10	±.01
TFA1	GaInSb	S.F.	0.7	Te	$+10^{17}/-10^{18}$	.80 - .60	±.005
TFA4	GaInSb	S.F.	0.3	--	$+10^{16}/-10^{16}$	.80 - .00	±.005
TFA6	GaInSb	S.F.	0.5	--	$+10^{12}/-10^{16}$	.90 - .00	±.005
TFA7	GaInSb	S.F.	0.7	Te	$+10^{17}/-10^{18}$	.98 - .88	±.005
TFA9	GaInSb	S.F.	0.7	--	$+10^{17}/-10^{18}$	.98 - .75	±.005
TFA11	GaInSb	S.F.	0.5	Cd	$+10^{17}/-10^{17}$	.90 - .00	±.005
TFB3	GaInAs	S.F.	0.3	--	$-10^{16}/-10^{17}$	.70 - .00	±.005
TFB6	GaInSb	S.F.	0.7	--	$-10^{17}/-10^{18}$	.92 - .80	±.01
TZC1	InAsSb	ZR	0.5	--	$-10^{14}/-10^{16}$	.97 - .85 .42 - .00	±.015
TZC3	InAsSb	ZR	0.5	--	$-10^{16}/-10^{17}$	.90 - .00	±.01
TZF1	GaAsSb	ZR	0.3	--	$+10^{17}/+10^{18}$	.92 - .82 .35 - .00	±.015 ±.025
TFC1	InAsSb	S.F.	0.3	--	$-10^{16}/-10^{17}$	.90 - .00	±.015

TABLE 6.2.2

EXPERIMENTAL DATA

SAMPLE	X (mole-fraction)	±ΔX	a_o (Å)	R_H ($\frac{cm^3}{C}$)	ρ (Ω-cm)	μ_H (cm^2/V.sec)
GaSb	1.00		6.092	+54.1	.078	+705
CP0.75	.975	.005	6.105	+104.	.22	+473
CP7.75	.94	.005	6.120	-265.		
CA1	.94	.01	6.12	-24.0		
CA8	.91	.01	6.13	-14.0	.20	-70
CD3	.90	.01	6.13	+84.	.17	+494
CN1.0	.89	.005	6.135	+203.	.32	+635
CA10	.87	.01	6.141	-8.5		
RA30	.85	.01	6.15	-265.		
CN5.1	.85	.005	6.152	-980..		
CF4	.84	.01	6.155	-180.	.15	-1200
TF1.2	.80	.005	6.170	+54.	.10	+540
CN6.6	.795	.005	6.172	+620	1.0	+620
CK1.0	.775	.005	6.179	+570	.48	+1187
RA4.1	.73	.01	6.20	-80.		
CN7.6	.75	.005	6.187	+635	1.18	+538
RB51	.75	.01	6.19	-55		
CK1.6	.73	.005	6.198	+775	1.0	+775
CF6	.69	.01	6.22	-35.	.008	-4380
A2.9	.655	.005	6.228	+35	.074	+473
CK3.2	.60	.005	6.255	-1000	.6	-1660
A3.9	.56	.005	6.270	+64	.114	+561
CK3.8	.545	.005	6.275	-2600	.12	-21630
CK4.2	.50	.005	6.295	-1500	.10	-15000
CN10.1	.45	.005	6.315	-630	.047	-13400
A4.9	.445	.005	6.317	+90	.195	+461
CK5.1	.37	.005	6.340	-1700	.143	-11880
CN11.2	.32	.005	6.360	-490	.020	-24500

TABLE 6.2.2 (cont.)

SAMPLE	X	±ΔX	a_o(Å)	$R_H(\frac{cm^3}{C})$	ρ(Ω-cm.)	$\mu(\frac{cm^2}{Vsec})$
CX13.7	.31	.01	6.365	-17.5		
CK6.0	.30	.005	6.370	-700	.02	-35000
CN12.4	.19	.005	6.413	-405	.0105	-38600
CK9.8	.10	.005	6.448	-400	.0064	-62600
InSb	.00		6.478	-197	.0031	-63500

FIGURE 6.2.1

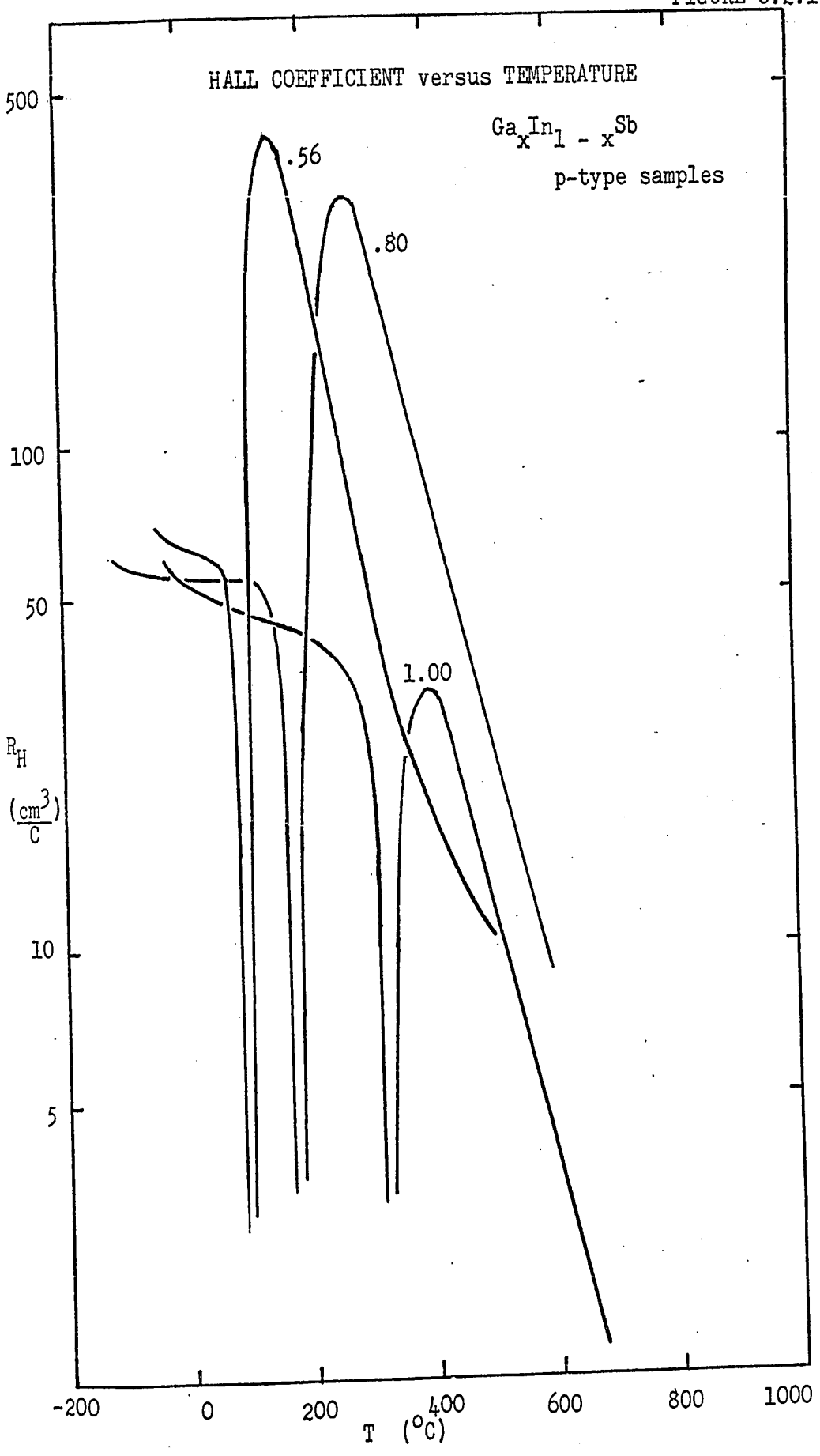
HALL COEFFICIENT versus TEMPERATURE
$Ga_xIn_{1-x}Sb$
p-type samples
.56
.80
1.00
500
100
50
10
5
R_H
$(\frac{cm^3}{C})$
-200
0
200
400
600
800
1000
T (°C)

HALL COEFFICIENT versus TEMPERATURE FIGURE 6.2.2

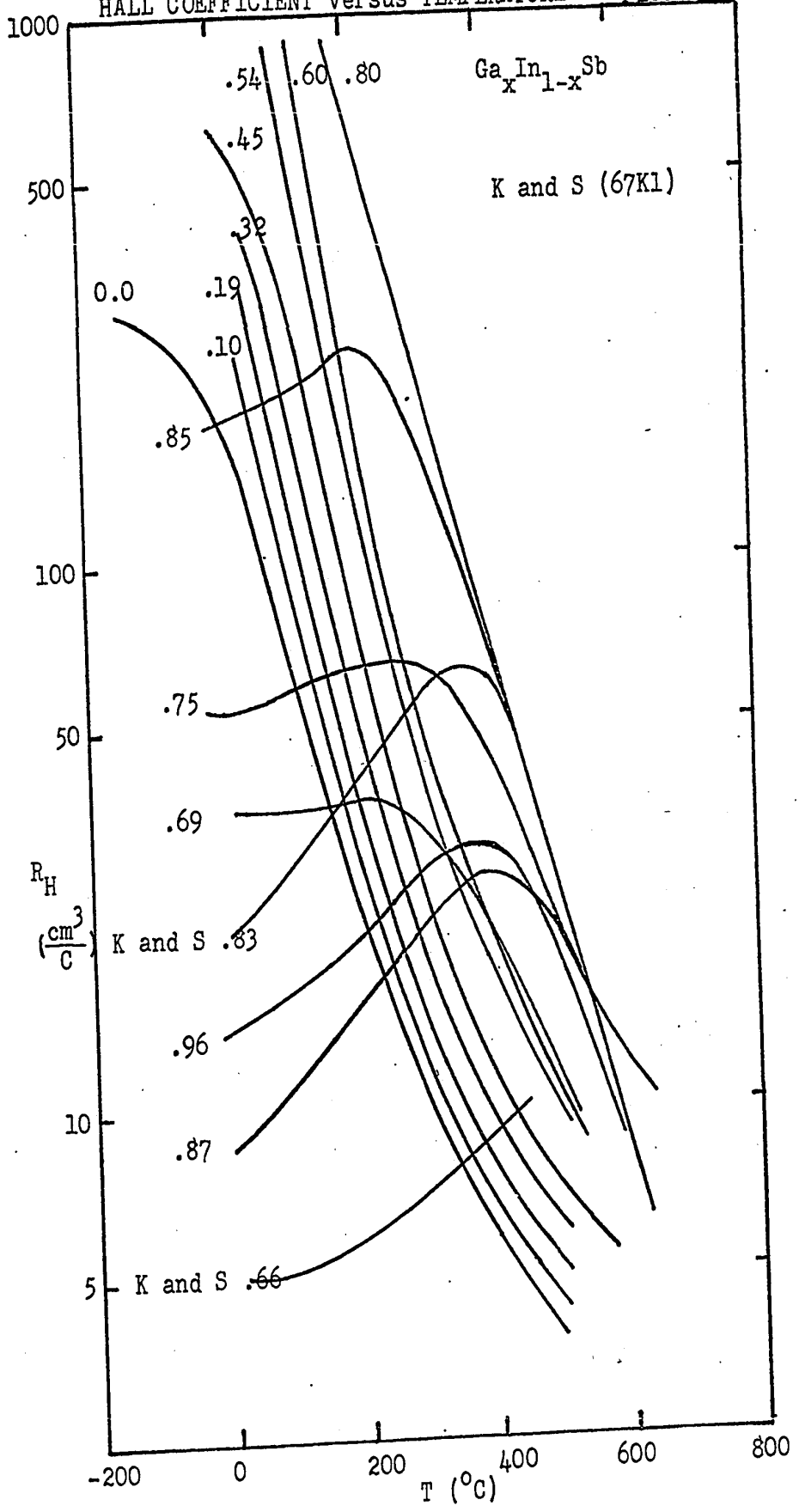

on figure 6.2.2. In each case the Hall constant is seen to vary roughly exponentially at high temperatures. In specimens with high GaSb concentrations, the effect of a subsidiary band is in evidence where the Hall constant is seen to rise with increasing temperature. This effect is enhanced in the more heavily doped material as the probability of occupation of the higher band states is increased.

The variation of the resistivity as a function of temperature for several typical specimens is shown on figure 6.2.3. In each of these curves the experimental points are not shown since the scatter among the points is neglible on this scale and the density of points (20 per $100^{o}C$) is too high to conveniently display.

Samples used in the high temperature measurements of the electrical properties of the $Ga_xIn_{1-x}As$ alloy system were obtained from polycrystalline ingots prepared by the step-freeze method. One ingot with a mean starting composition of 30 mol % GaAs yielded samples of all compositions in the range $0.66 > x > 0.0$. Another ingot with a 50 mol % starting composition supplied samples for compositions in the range $0.9 > x > 0.66$. All specimens were n-type with impurity carrier concentrations ranging from $3 \times 10^{16} cm^{-3}$ to $2 \times 10^{17} cm^{-3}$.

Pertinent room temperature data for all of the samples measured are listed on Table 6.2.3. The results of the high temperature Hall effect measurements are shown on figure 6.2.4.

RESISTIVITY versus TEMPERATURE FIGURE 6.2.3

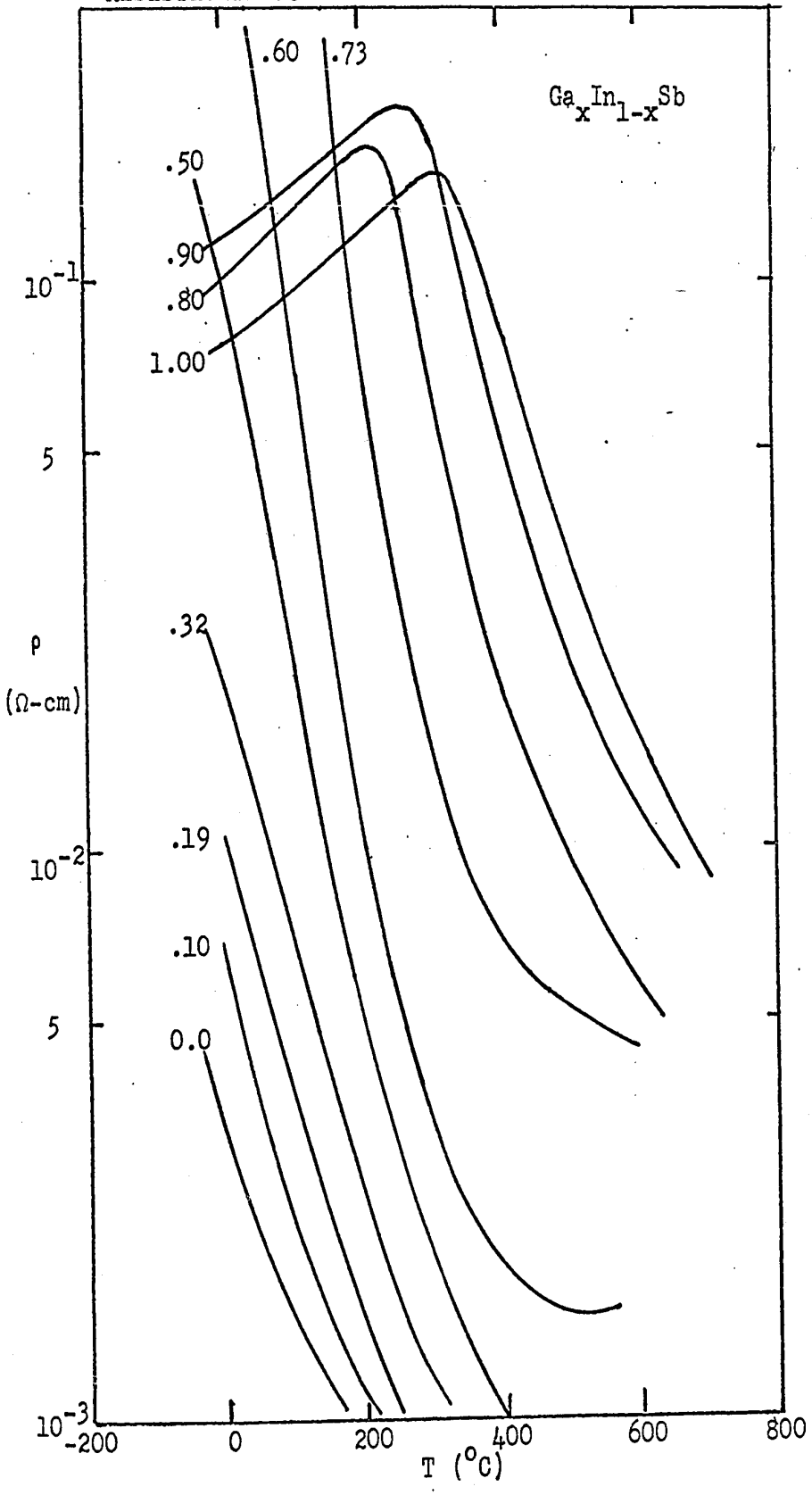

TABLE 6.2.3

EXPERIMENTAL DATA

$Ga_xIn_{1-x}As$ ALLOYS

SAMPLE	x (mole-fraction)	±Δx	a_o(Å)	R_H (cm^3/Coul.)	ρ (Ω-cm.)	μ_H (cm^2/V.sec)	E_{oo} (eV)	T_θ (^oK)
GaAs	1.0	--	5.66	-290	.209	-1385.	(1.52)	--
CY 7.2	.83	.010	5.728	-60	.35	-171.5	(1.20)	--
CT 0.4	.665	.005	5.791	-135.	.030	-4200.	.975	850
CT 1.05	.600	.005	5.818	-110.	.018	-611.0	.945	790
CT 1.8	.490	.005	5.860	-114.	.0185	-61.70	.842	755
CT 2.8	.370	.005	5.904	-78.	.0094	-83.00	.721	670
CT 3.7	.290	.005	5.940	-71.	.0074	-9600.	.657	620
CT 5.4	.200	.005	5.976	-74.	.0063	-11750.	.584	545
CT 7.4	.100	.005	6.015	-51.	.0039	-13100.	.493	534
CT 9.5	.050	.005	6.022	-43.	--	--	.456	--
InAs	.00	--	6.056	-220.	.015	-17000.	.448	--
InAs	.00	--	6.056	-23.	.0016	-13000.	.448	512

HALL COEFFICIENT versus TEMPERATURE Figure 6.2.4

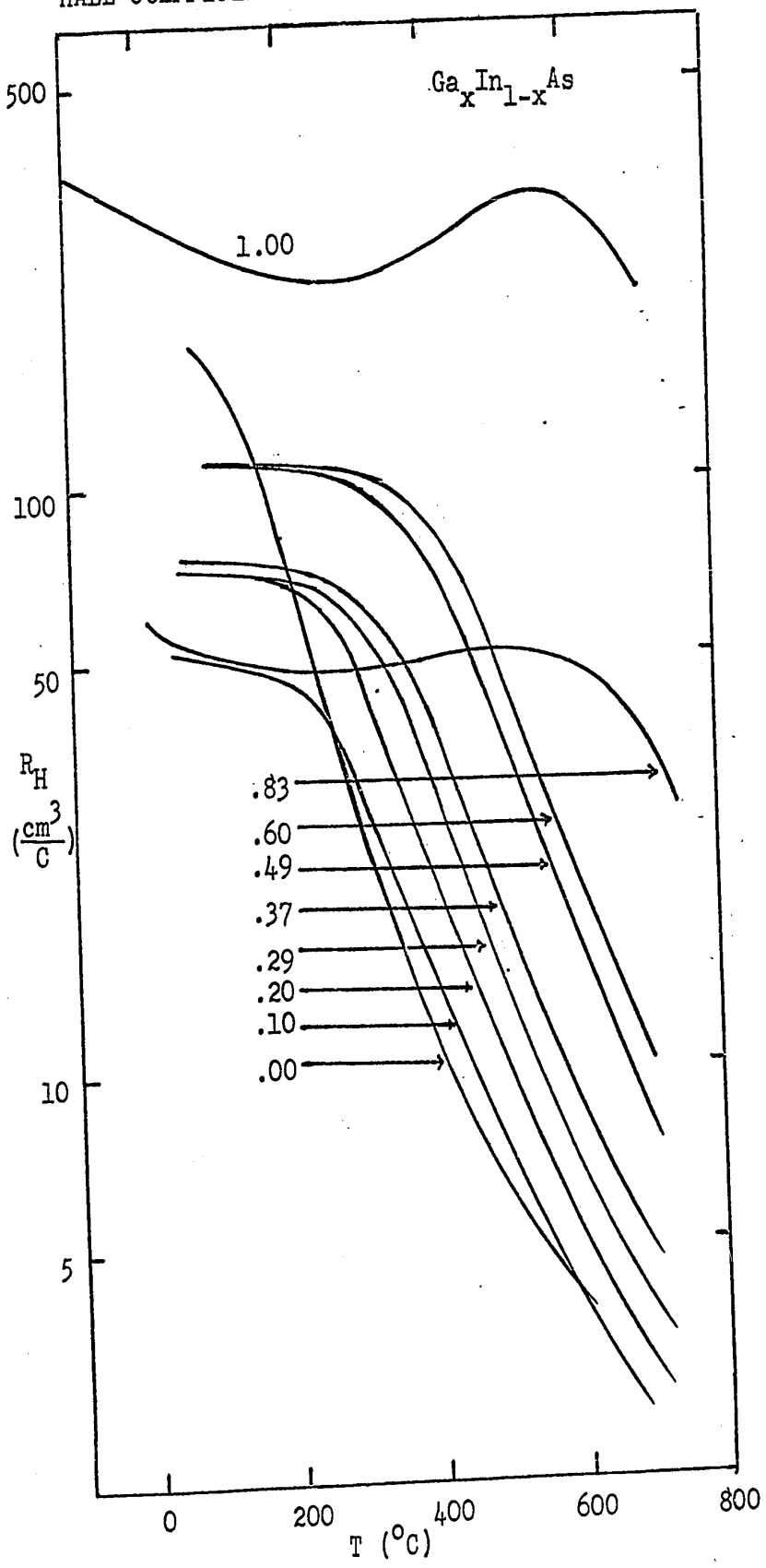

It can be seen that the measured samples from ingot SF.B.3 had roughly equivalent carrier concentrations. There is no higher band contribution evident in the greater part of the alloy range, and none is expected, as the ⟨111⟩ and ⟨100⟩ bands are more than 0.5 eV above the (000) band minimum except in the very GaAs rich alloys. These alloys feature a contribution from the ⟨100⟩ band which in GaAs is thought to be ~ 0.36 eV above the gap. The effect of this band can be seen in the samples with $x > 0.8$. At very high temperatures, all specimens are seen to exhibit an exponential variation of the Hall constant. The changing temperature at which this rapid increase in intrinsically excited carriers begins, indicates the increase in the energy gap as the alloy composition changes from InAs at $x = 0$ to GaAs at $x = 1.0$. The temperature variation of the resistivity for several specimens is presented on figure 6.2.5. Similar observations concerning the wide variation of the energy gap across the alloy range can be made from these data.

Electrical experiments over a wide temperature range were performed on $InAs_x Sb_{1-x}$ samples obtained from step-frozen and from zone-recrystallized ingots. All specimens were n-type and polycrystalline with carrier concentrations in the range from 4.1×10^{15} cm^{-3} to 1.3×10^{17} cm^{-3}. The homogeneity of samples in the middle composition range within ± 0.015 in x while at all other compositions the homo-

RESISTIVITY versus TEMPERATURE FIGURE 6.2.5

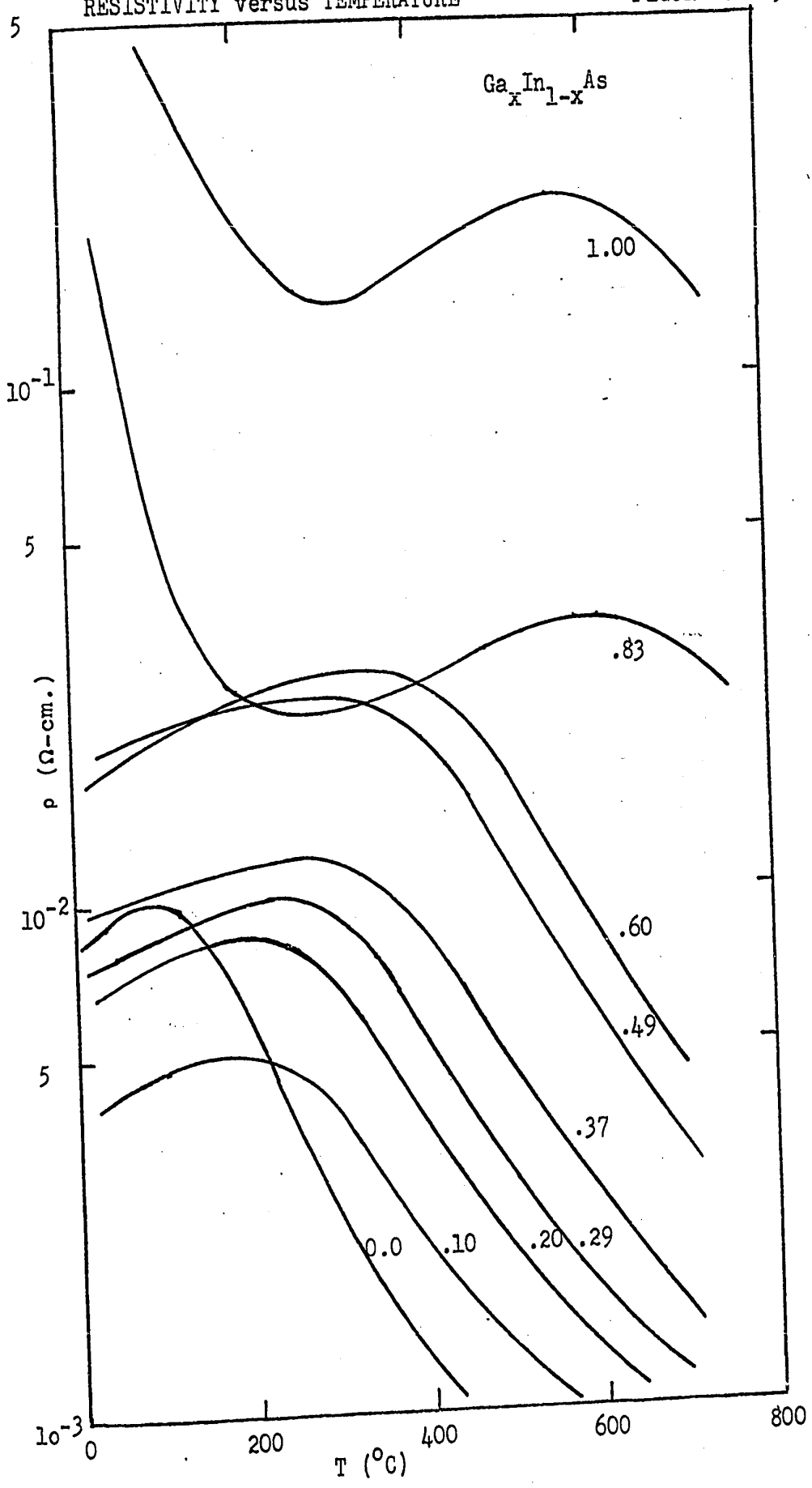

geneity was considerably better than this. In the middle composition region of an ingot the rate of change of composition with ingot length was quite rapid and this was the largest factor in limiting the homogeneity of samples.

Data pertinent to each of the measured samples such as the composition, lattice parameter, homogeneity, and room temperature electrical observations are listed for reference on Table 6.2.4.

Specimens in the middle composition region were found to exhibit intrinsic conduction at temperatures as low as 50°C. This indicates an extremely low intrinsic energy gap for these compositions. This feature is shown on figure 6.2.6 which gives the temperature variation of the Hall constant for some typical specimens. At no composition is any deviation from the temperature dependence expected for a single conduction minimum observed. In these alloys, with the given impurity concentrations, the occupation density of electrons in any subsidiary bands is apparently negligible. From the temperature position of the onset of intrinsic conduction it seems that the energy gap goes through a minimum in the middle composition range.

The results obtained for the resistivity as a function of the temperature for some of these alloys are shown on figure 6.2.7. The variation of the energy gap with composition is evident from these curves as it is on figure 6.2.6.

TABLE 6.2.4

EXPERIMENTAL DATA

$InAs_xSb_{1-x}$ Alloys

SAMPLE	X (mole-fraction)	±ΔX	a_o (Å)	$-R_H(\frac{cm^3}{C})$	ρ(Ω-cm)	μ_H (cm^2/V.sec)	E_{oo} (eV)	T_θ (°K)
InSb	0.0		6.478	240	.0030	-45000	.242	233
CG97	.03	.005	6.475	550	.014	-42000	.224	
CE8.15	.09	.005	6.455	450	>.05	-50000	.210	
CE4.0	.15	.005	6.417	2876	.45	-38000	.201	
CE7.4	.15	.005	6.433	400	>.40	-38000	.192	
CE4.3	.17	.005	6.420	>65002	>.50	-46000	.174	250
CE4.6	.19	.005	6.415	>4000	>.20	-42000	.184	255
CE5.0	.255	.01	6.897	450	.55	-40000	.177	
CV4.1	.265	.01	6.380	600	.0033	-50000	.176	240
CE6.0	.35	.01	6.353			-30000	.177	
CV3.6	.38	.01	6.240	455	.0019	-32000	.165	250
CE6.2	.41	.01	6.335	160	.0027	-29000	.165	
CV3.35	.535	.01	6.268	122	.0050	-30000	.175	264
CV3.05	.685	.01	6.162	90	.0027	-22500	.203	342
CV2.6	.765	.01	6.143	67	.0042	-15000	.248	392
CV2.45	.79	.01	6.123	77	.0035	-20000	.277	350
CG5.0	.84	.01	6.105	56	.0030	-18700	.321	

TABLE 6.2.4

CE3.0	.88	.005	6.097	27	.0016	-16000	.361	
CG3.0	.905	.005	6.080	55	.0037	-14500	.368	
CE2.0	.905	.005	6.073	62	.098	-6400	.418	
CE1.0	.955	.005	6.069	170	.013	-14000	.422	
InAs	1.0		6.056	220	.015	-17000	.448	
InAs	1.0		6.056	23	.0016	-13000		512

HALL COEFFICIENT versus TEMPERATURE FIGURE 6.2.6

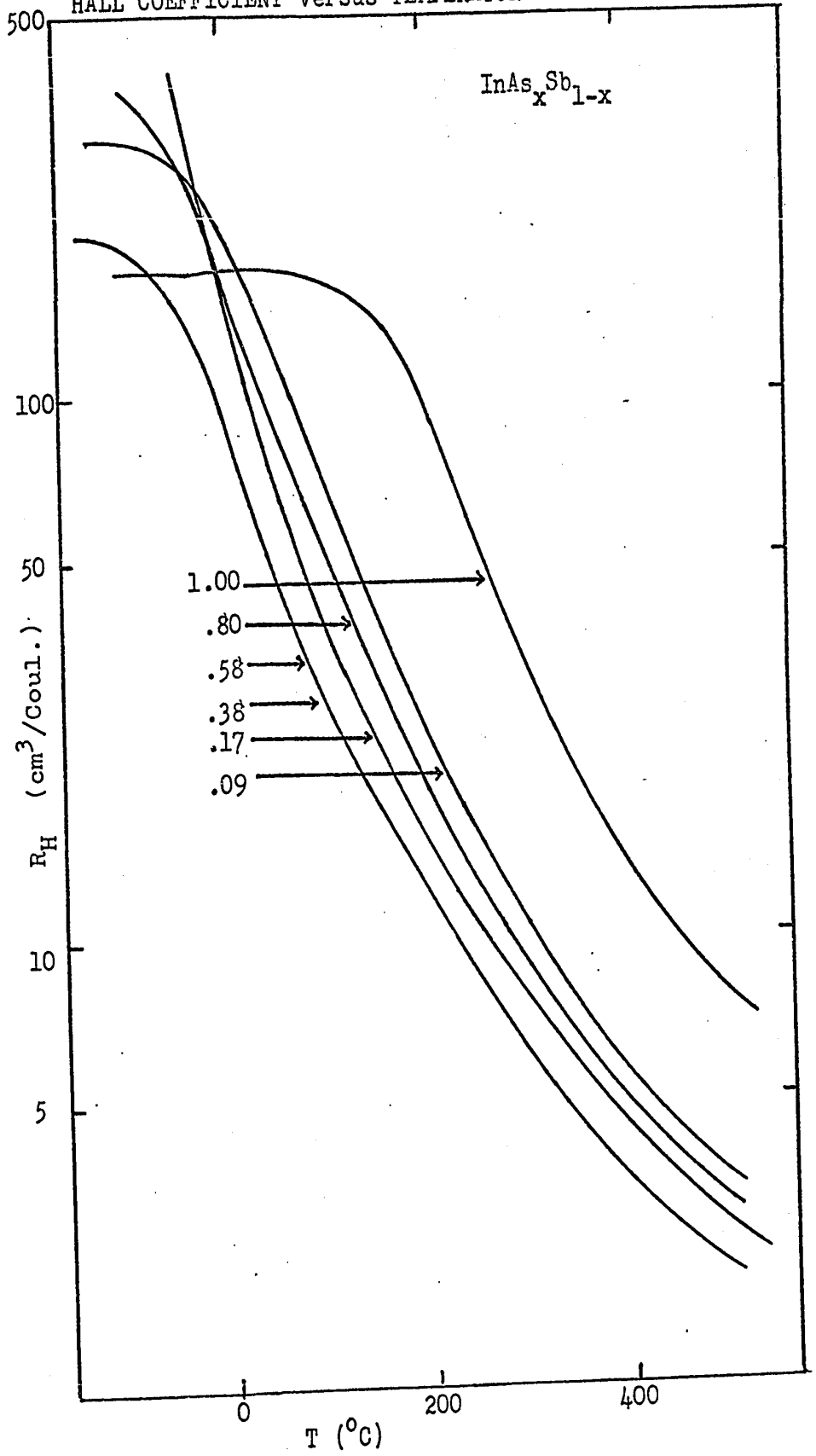

RESISTIVITY versus TEMPERATURE FIGURE 6.2.7

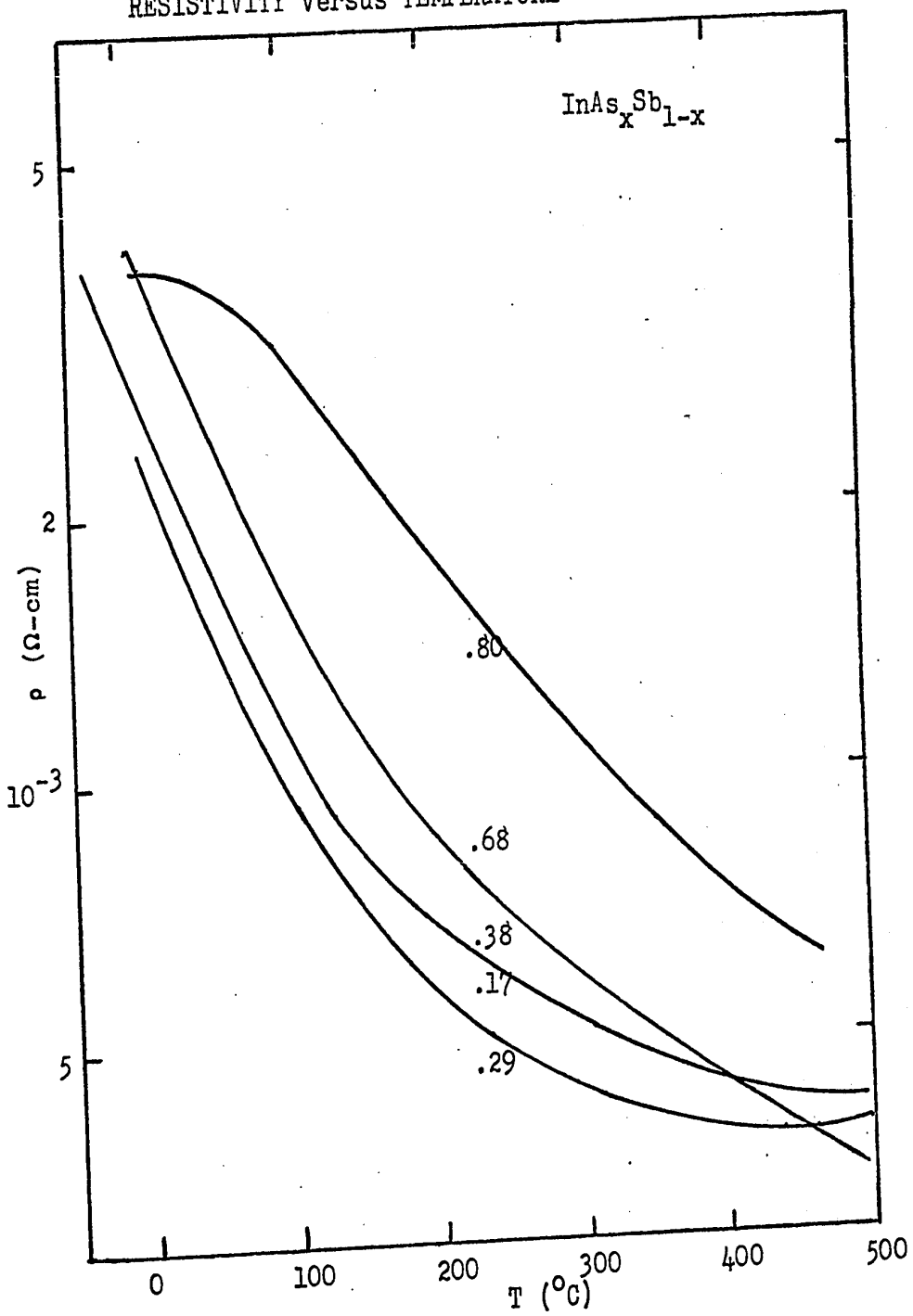

A limited number of samples from the $GaAs_xSb_{1-x}$ alloy system were obtained from an ingot prepared by zone-recrystallization. There was some inhomogeneity at all alloy compositions. Samples which were measured are listed on Table 6.2.5 together with all pertinent data concerning each. All samples were GaSb rich and were p-type, presumably for the reasons that the compound GaSb is p-type; i. e. gallium atoms on antimony sites. The results of the experiments are shown in figures 6.2.8 and 6.2.9. Samples had very high impurity concentration and were probably heavily compensated as indicated by very low values of the Hall mobility.

It is noteworthy that in almost all of the alloy systems investigated there was no apparent variation in the Hall constant attributable to progressive ionization of donor impurities. This would seem to indicate that the donor levels are either very near to the conduction band minimum or above it.

In contrast to the situation observed in n-type samples, in p-type material the activation of acceptor impurities is demonstrated by the fall in the magnitude of the Hall constant with increasing temperatures in the extrinsic conduction region. The magnitude of this variation and the temperature at which it is observed indicate that these are deep levels, approximately 0.06 eV above the valence band.

Using proper analysis, a great wealth of information concerning important band parameters of the alloys can be obtained from the many experimental observations taken. In the following sections of this chapter the methods used together with the results attained will be presented.

TABLE 6.2.5

EXPERIMENTAL DATA

$GaAs_xSb_{1-x}$

SAMPLE	X (Mole-Fraction)	$\pm\Delta X$	a_o(Å)
CS 7.9	.067	.010	6.06
CS 11.8	.13	.015	6.03
CS 4.8	.23	.010	5.99

$R_H(cm^3/C.)$	$\rho(\Omega\text{-cm})$	$\mu_H(cm^2/V.sec)$	E_{oo}(ev)
+67	.165	406	.75
+8.2	.020	410	.95
+96.	.45	213	.614

HALL COEFFICIENT versus TEMPERATURE FIGURE 6.2.8

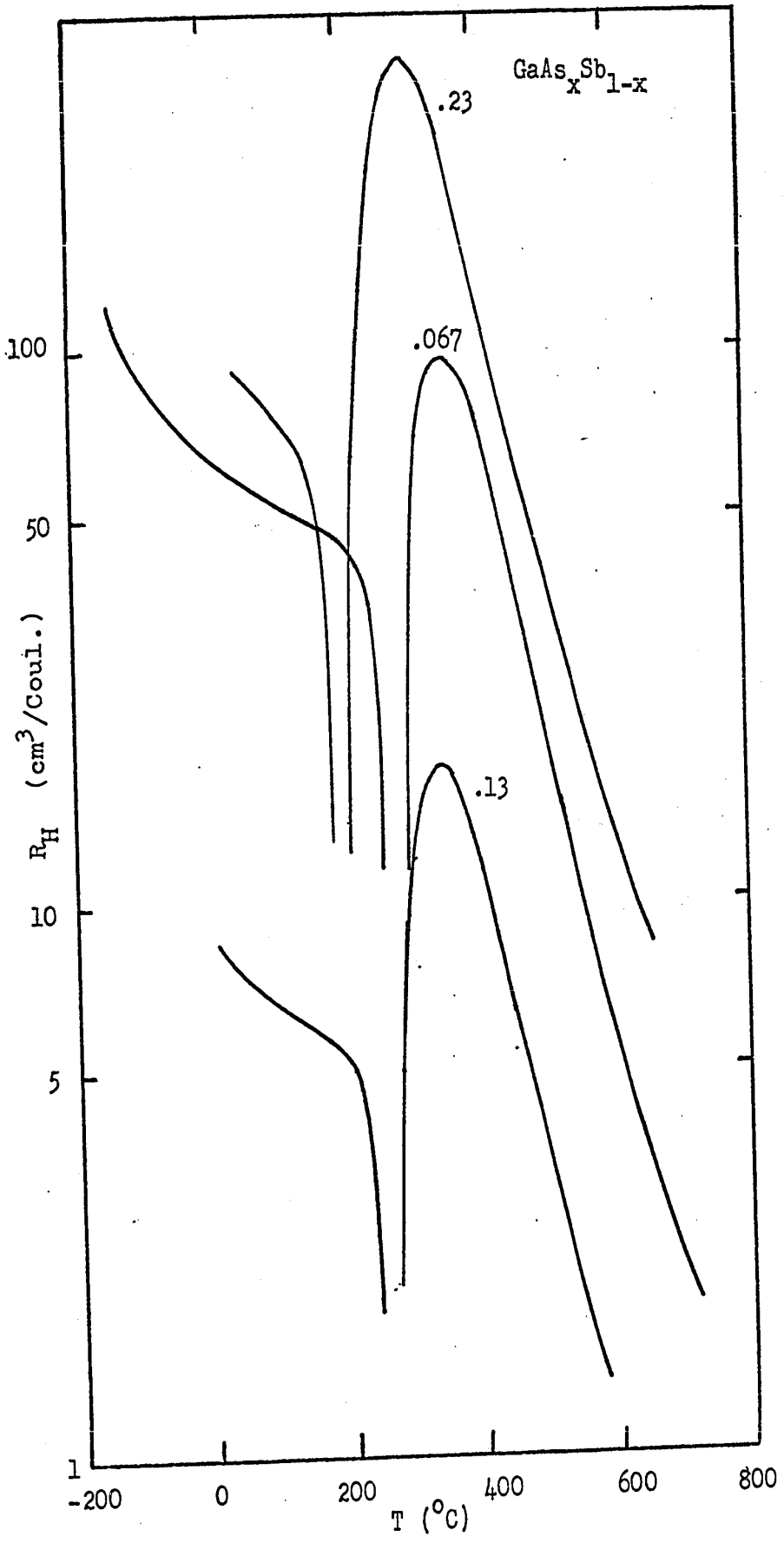

RESISTIVITY versus TEMPERATURE FIGURE 6.2.9

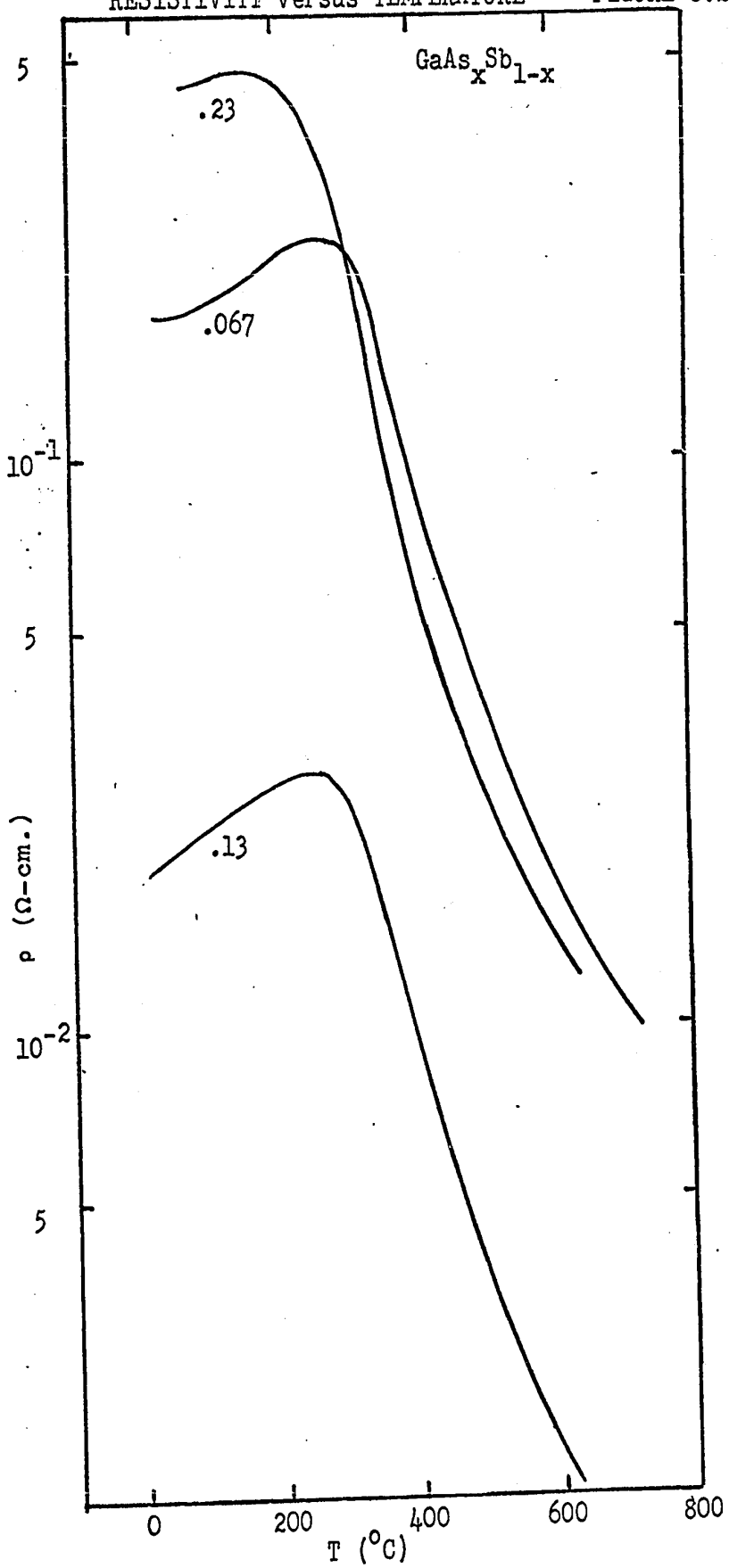

6.3 Two-Band Analysis

Assuming that at the temperatures where intrinsic effects dominate, all conduction depends on carriers in only two bands, the Hall coefficient may be written as follows:

$$R_H = \frac{r}{e} \frac{p - nb^2}{(p + nb)^2} \qquad [6.1]$$

for n electrons and p holes.

The factor b is the electron to hole mobility ratio and r is a parameter which depends upon the predominant scattering mechanism in the crystal. In equation [6.1] it is assumed that the electrons and holes are scattered in a similar manner. For most III - V materials, r can be taken as approximately 1.1 at temperatures above room provided the concentration of impurity is not too large. This value assumes that the predominant scattering mechanism is polar scattering. Typically, the factor b is assumed to be independent of temperature, however in n-type material, provided $b \gg 1$ the exact value of b is quite unimportant in the evaluation of equation [6.1]. In p-type material featuring two-band conduction, the mobility ratio b may be obtained from the Hall coefficient versus temperature data by using the well known relation

$$-R_{max} = \frac{r(b - 1)^2}{4\, eZb}, \qquad [6.2]$$

where R_{max} is the largest value of the Hall coefficient after its sign changes from positive to negative with increasing temperature. Equation [6.2] is valid only when [6.1] is the correct form for the Hall coefficient. Equation [6.2] assumes that all the carriers are found in only one conduction and one valance band and that Z can be obtained validly according to

$$Z = \frac{r}{R_{H_o} e} \qquad [6.3]$$

where R_{H_o} is the low temperature Hall constant, provided all of the impurities states are ionized. The hole concentration p is related to the electron concentration n and the impurity concentration Z by the equation

$$p = n \pm Z \qquad [6.4]$$

where the sign of Z depends on the sign of the residual impurity concentration $(N_A - N_D)$.

From [6.1] and [6.4] it can be shown that

$$n = \frac{1}{2}\left(\frac{1 - b}{1 + b}\right)\frac{r}{eR_H} - \frac{Z}{(1 + b)} + \frac{1}{(1 + b)}\left[\left\{\frac{r(b - 1)}{2eR_H}\right\}^2 + \frac{rZb}{eR_H}\right]^{\frac{1}{2}} \qquad [6.5]$$

Using elementary band theory, assuming non-degeneracy,

parabolic bands and spherical energy surfaces, the carrier density in the conduction and valence bands may be given according to [4.72], whence

$$n = 2\left[\frac{2\pi kT}{h^2}\right]^{3/2} m_e^{3/2} e^{E_F/kT} \qquad [6.6]$$

$$p = 2\left[\frac{2\pi kT}{h^2}\right]^{3/2} m_h^{3/2} e^{-(E_F + E_o)/kT} \qquad [6.7]$$

where E_o is the intrinsic energy gap.

Combining [6.6] and [6.7] we obtain:

$$np = 4\left[\frac{2\pi kT}{h^2}\right]^{3} (m_e m_h)^{3/2} e^{-\left(\frac{E_{oo} + \beta T}{kT}\right)} \qquad [6.8]$$

where

$$E_o = E_{oo} + \beta T \qquad [6.9]$$

m_e, m_h, and β are assumed to be constants independent of the temperature.

By plotting values of $\log \left(\frac{np}{T^3}\right)$ obtained from [6.4] and [6.5] against $1/T$, a straight line should be obtained, the slope of which is $-E_{oo}/k$ where E_{oo} is the value for the energy gap extrapolated linearly to absolute zero. If however, any of the assumptions in the analysis are invalid, it is to be expected that the resulting plots of $\log (np/T^3)$ versus $1/T$ will not be straight lines.

The resistivity of a specimen featuring two band conduction is given by

$$\frac{1}{\rho} = \sigma = e(n\mu_e + p\mu_h) \qquad [6.10]$$

which combined with [6.4] gives

$$\frac{1}{\mu_e} = \rho e[n(1 - \frac{1}{b}) + \frac{Z}{b}] \qquad [6.11]$$

When $b >> 1$ it can be seen that the dominant contribution to mobility is from the conduction band electrons alone and $\mu_e \simeq (ne\rho)^{-1}$.

Using [6.11], values of μ_e as a function of temperature can be calculated from the Hall and resistivity data, provided once again that the assumptions of two band conduction are valid.

6.4 Results of Two Band Analysis

6.4.1 $Ga_xIn_{1-x}Sb$ Results

The results for some typical $Ga_xIn_{1-x}Sb$ specimens of a plot of log (np/T^3) against inverse temperature are shown in figure 6.4.1. It can be seen that for n-type specimens which have composition values within $0.0 < x < 0.65$, the lines are straight over a large temperature range. For higher values of x however, the lines do not remain straight but curve pronouncedly upwards as the temperature increases. It is a well substantiated fact that the compound GaSb possesses a band structure which features a set of subsidiary conduction band minima in the ⟨111⟩ direction in $\vec{k}$ space. These minima are variously reported to be 0.078 eV (69V1), 0.082 eV (66H2) above the (000) conduction band minimum and hence can contribute substantially to conduction band processes even at relatively low temperatures. Indeed, as Woolley (66W1) has shown, even the conduction band minima in the ⟨100⟩ $\vec{k}$-directions can be occupied by substantial numbers of electrons at elevated temperatures. Hence the assumption of the analysis that there are carriers in only two bands is not valid in GaSb nor is it valid in GaSb rich alloys.

In p-type material there is a further inconsistancy inherent in the application of the two band analysis in that the presence of the V_2 valence band is neglected. Since holes

FIGURE 6.4.1

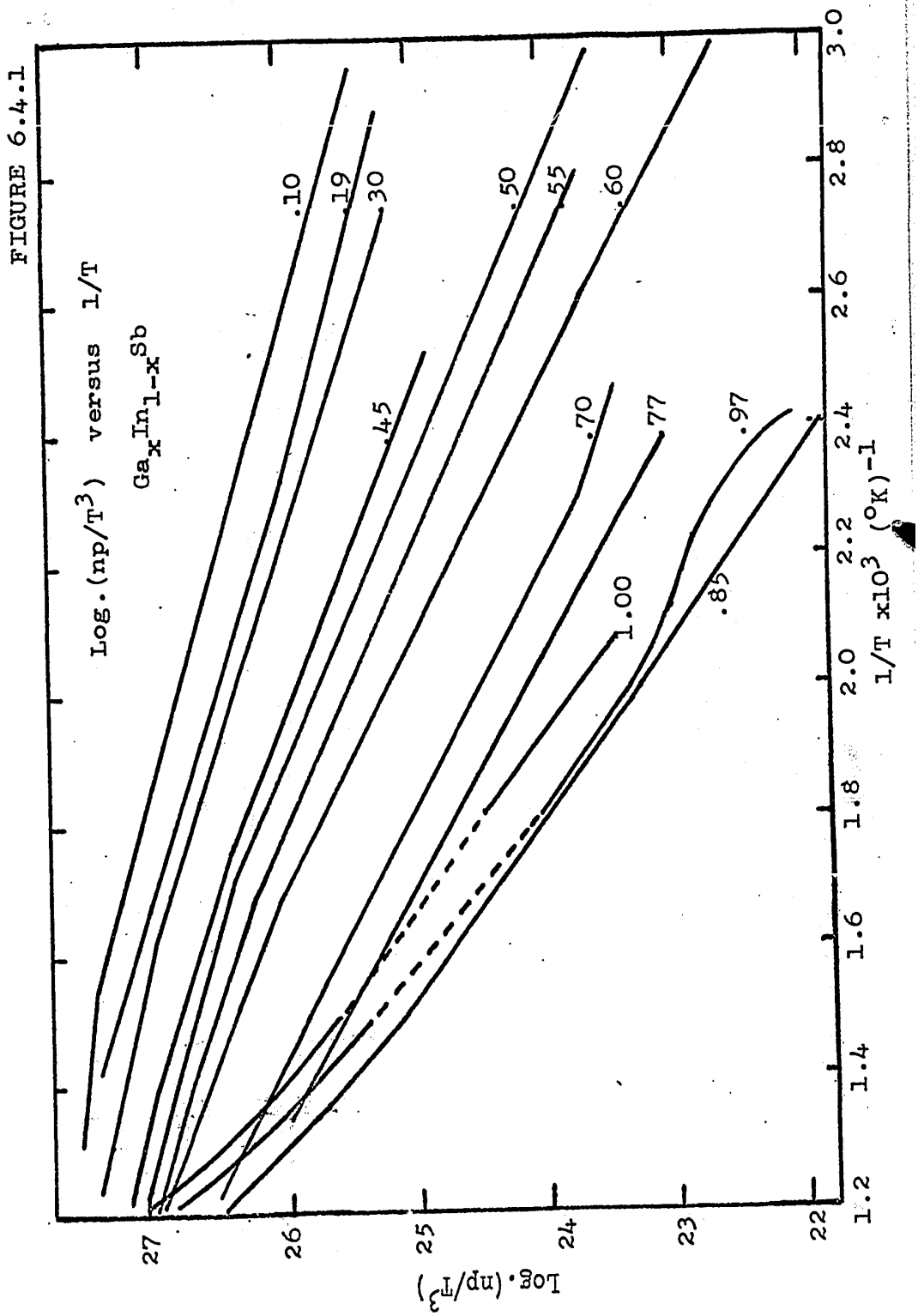
FIGURE 6.4.1
Log.(np/T³) versus 1/T
$Ga_xIn_{1-x}Sb$
.10
.19
.30
.45
.50
.55
.60
.70
.77
.97
1.00
.85
Log.(np/T³)
1/T x10³ (°K)⁻¹
27
26
25
24
23
22
1.2
1.4
1.6
1.8
2.0
2.2
2.4
2.6
2.8
3.0

from acceptor states may be excited into this light hole band as well, the measured value of Z from equation [6.3] can be very erroneous. As Beer has pointed out, (63B18) neglect of the contribution of the holes in the V_2 band can result in calculated acceptor densities which are much too large in p-type InSb. This error would be propogated through equation [6.4] into the product np of equation [6.5], which would tend to raise the low temperature part of the plots of np/T^3 versus $1/T$, where the contribution of Z is significant, (see figure 6.4.1), and cause values of E_{oo} to be determined which are too low. This is presumably why Woolley and Gillet obtained low values for their low temperature determinations of E_{oo} in p-type GaSb rich alloys (see figure 6.4.2).

Samples which are very rich in InSb also show a deviation from linearity at high temperatures as indicated in figure 6.4.1. It is well known that in InSb, the combination of small energy gap and low effective mass result in electron degeneracy at relatively low temperatures even in pure materials; and as well, the Kane band analysis indicates as strong deviation from parabolicity at energies above the bottom of the band. Thus in alloys rich in InSb it is not unexpected that non-degenerate analysis will not apply exactly, in particular at high temperatures.

By taking the straight line portion of the lines of figure 6.4.1 for n-type material, values of E_{oo} have been calculated and these values are presented on figure 6.4.2. It can be seen that the energy gap has a monotonic, approximately parabolic dependence on composition which agrees well with previously determined optical values (60W9).

Using equation [6.11] on data from samples of all compositions, values for the electron mobility have been determined and these values are shown as functions of temperature on figure 6.4.3. The temperature variation of the electron mobility for n-type samples shows that for temperatures near to room there is a significant contribution of scattering by impurities. This is demonstrated by the rise in mobility with increasing temperature. Above 150°C however, samples in the range $0.0 < x < 0.7$ exhibited the exponential temperature dependence for electron mobility which is characteristic of polar scattering (64M4) (64Z1).

The mobility variation with temperature for GaSb rich alloy compositions was of a more complicated form. The rate of decrease of mobility increased rapidly with increasing temperature as the thermal distribution placed more and more electrons into the low mobility ⟨111⟩ and ⟨100⟩ bands.

Accurate evaluation of the mobility of electrons in the (000) minimum is not possible unless some method for determing the relative carrier concentration in the higher

EXTRAPOLATED ENERGY GAP versus COMPOSITION FIGURE 6.4.2

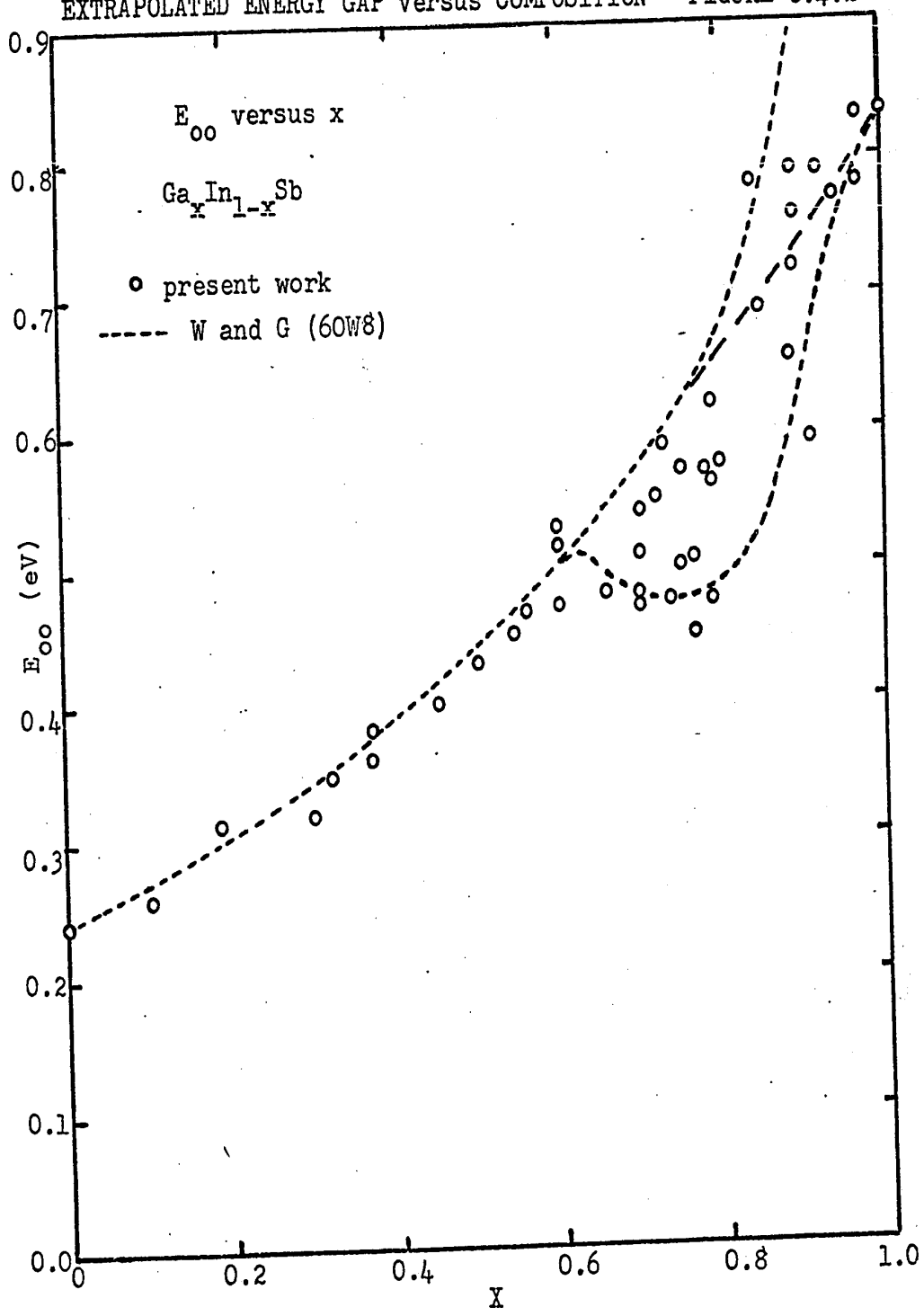

FIGURE 6.4.3

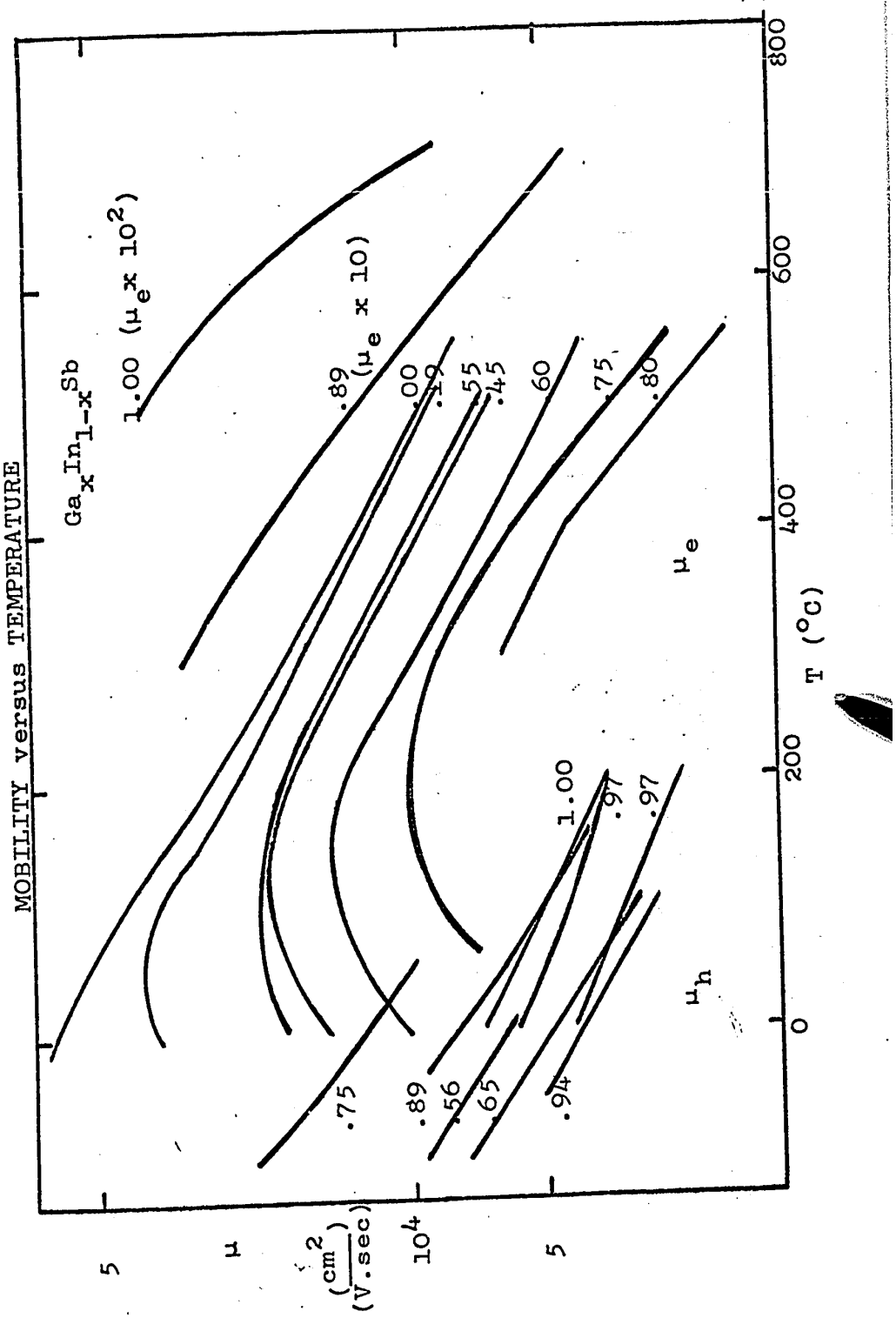
MOBILITY versus TEMPERATURE
$Ga_xIn_{1-x}Sb$
1.00 (μ_e x 10^2)
.89 (μ_e x 10)
.00
.19
.55
.45
60
75
.80
1.00
.97
.97
.75
.89
.56
.65
.94
μ_e
μ_h
μ $\left(\frac{cm^2}{V.sec}\right)$
10^4
5
5
0
200
400
600
800
T (°C)

bands is found.

By extrapolating the mobility values from the polar scattering region to room temperature it is possible to show the variation of room temperature mobility as a function of composition, without impurity effects. This variation is presented on figure 6.4.4 where it is seen to be roughly linear.

Values of the hole mobility can be obtained from p-type materials, where such material is available. Results of these samples are presented on figures 6.4.3 and 6.4.4 as functions of temperature and composition respectively.

The range upon which the hole mobility has been calculated is limited to those temperatures below the onset of intrinsic conduction, that is to say, where $p > nb^2$. Since the analysis assumes the holes are all in one band the resulting mobility is a combined hole mobility, μ_{hc}, where

$$\mu_{hc} = \frac{p_1 + b_h^2 \, p_2}{p_1 + b_h p_2} \, \mu_{h_1} \qquad [6.12]$$

$$b_h = \frac{\mu_{h_2}}{\mu_{h_1}}$$

MOBILITY versus COMPOSITION FIGURE 6.4.4

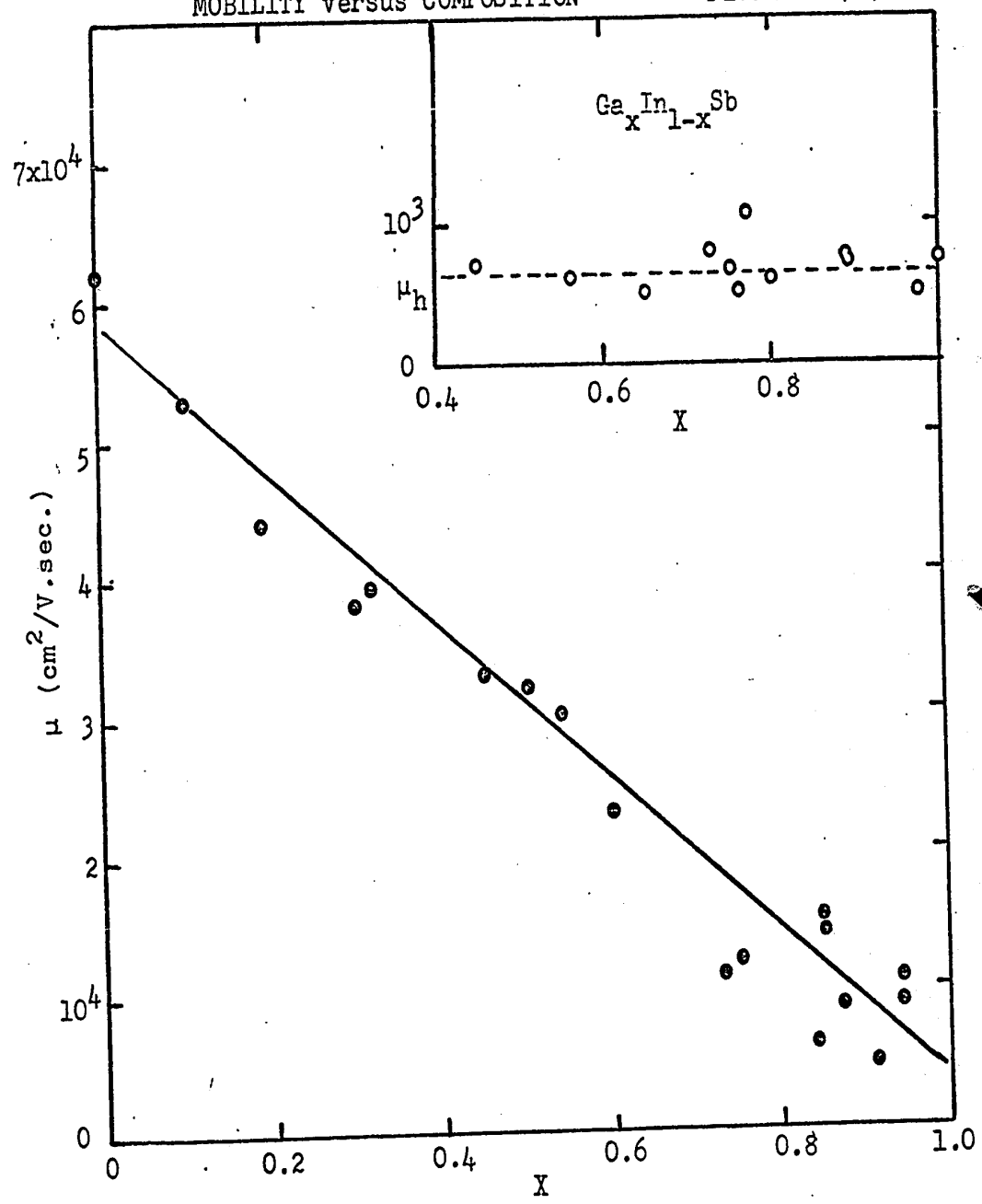

6.4.2 $Ga_xIn_{1-x}As$ Results

Application of the two band analysis to the high temperature Hall measurements on the $Ga_xIn_{1-x}As$ alloys has given the curves plotted on figure 6.4.5. It is seen that alloys in the composition range $0.0 < x < 0.66$ exhibit a straight line behaviour over a wide temperature range. Using these lines, values for the extrapolated absolute zero band gap E_{oo} have been determined and the results are shown in figure 6.4.6. The energy gap values are shown to vary smoothly with composition and to agree well with E_g values from the absorption measurements of Woolley, Thomas and Thompson (68W1).

It is difficult to apply the two band analysis to samples rich in GaAs since because of the large energy gaps of these materials, the number of intrinsic carriers is very small compared with the impurity concentrations until very high temperatures, and hence there is a very large uncertainty in the product np. A further complicating factor is the presence of subsidiary conduction band minima in the $\langle 100 \rangle$ &-directions which can be significant in alloys of high GaAs concentration and at high temperatures. The existence of such minima has been reported previously as a result of pressure experiments (61P6), from high temperature Hall effect, (68I1), (60A15), (58G15), and I-R absorption (59S6), and have been variously reported to be 0.25 eV (59S6), 0.38 eV (60A15),

FIGURE 6.4.5

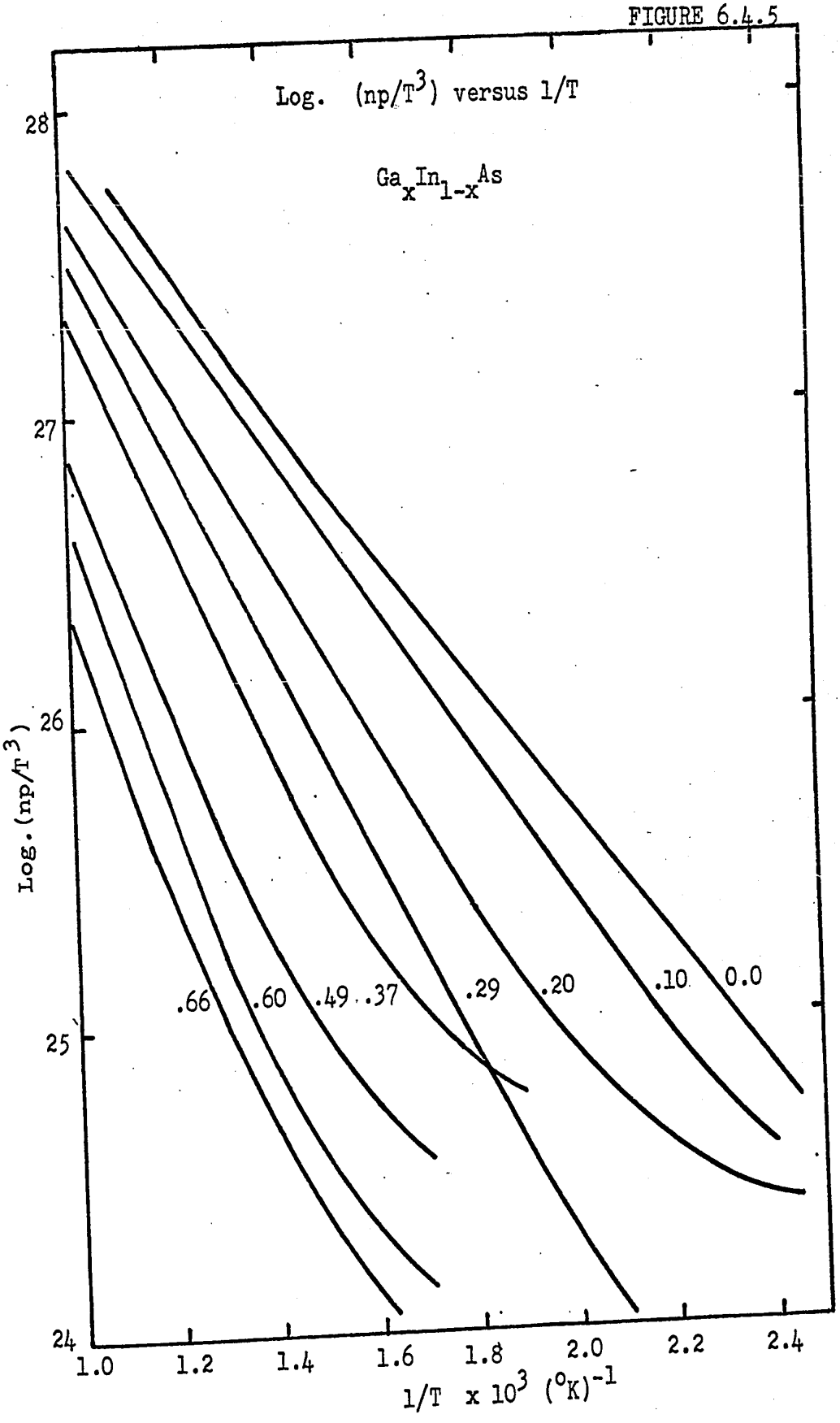
Log. (np/T³) versus 1/T
Ga$_x$In$_{1-x}$As
Log.(np/T³)
28
27
26
25
24
.66
.60
.49
.37
.29
.20
.10
0.0
1.0
1.2
1.4
1.6
1.8
2.0
2.2
2.4
1/T x 10³ (°K)⁻¹

FIGURE 6.4.6

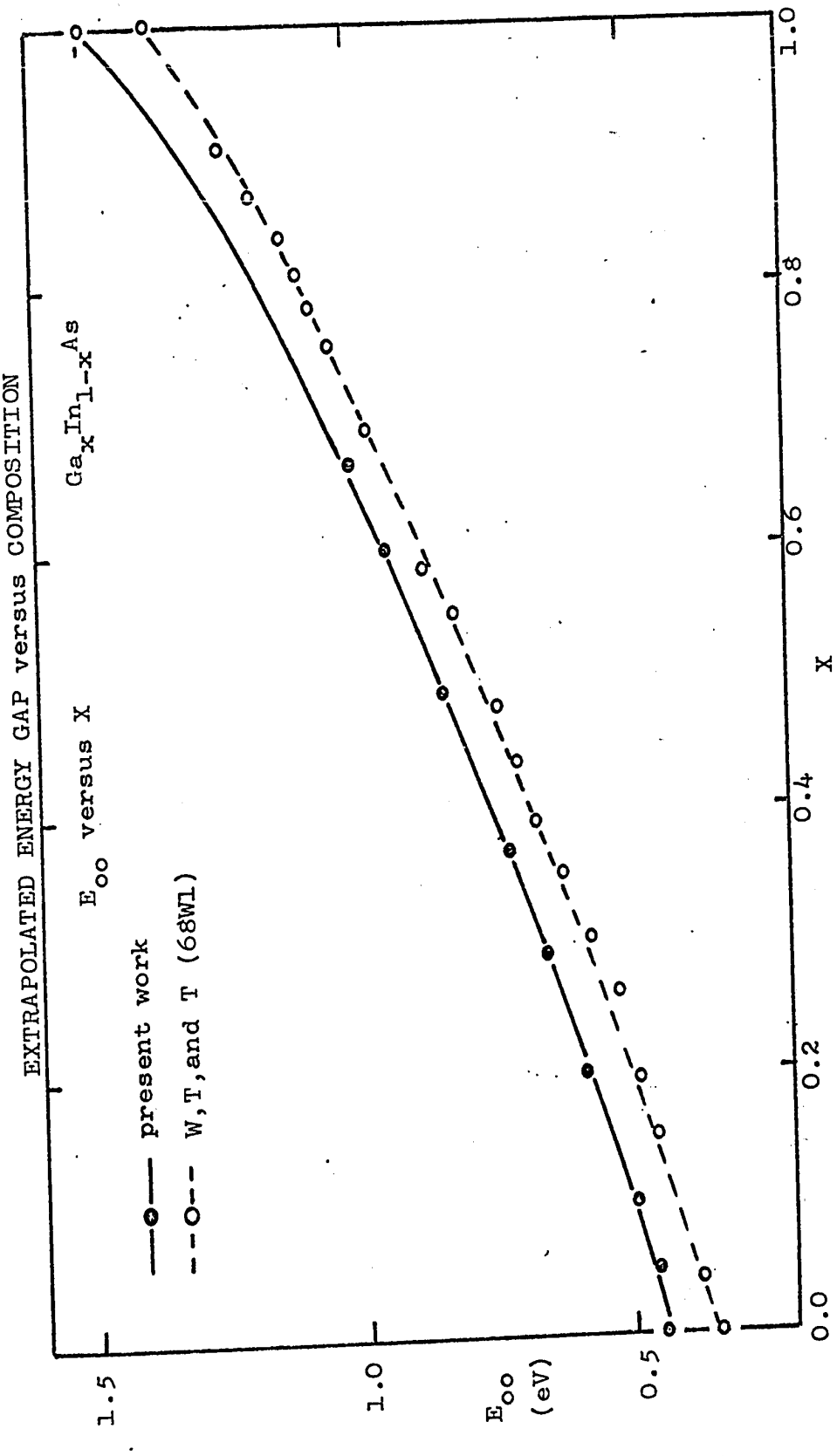
EXTRAPOLATED ENERGY GAP versus COMPOSITION
$Ga_xIn_{1-x}As$
E_{oo} versus X
present work
W,T,and T (68WL)
E_{oo} (eV)
1.5
1.0
0.5
0.0
0.2
0.4
0.6
0.8
1.0
X

0.36 eV (60E3), 0.35eV (61P6), above the (000) conduction band minimum in GaAs.

On figure 6.4.5. it is seen that in the InAs rich samples there is a deviation from straight line behaviour at very high temperatures presumeably because of the effects of non-parabolicity in these materials.

On figure 6.4.7 are shown the results of the electron mobilities calculated from eq. [6.11] for the $Ga_xIn_{1-x}As$ alloys as a function of temperature. The mobility is seen to obey an empirical law of the form

$$\mu_e(T) = \mu_e(0)\ e^{-T/T_\theta} \qquad [6.13]$$

where the values of T_θ vary smoothly with x as shown on figure 6.4.8. An exponential variation has been reported previously for polar-type scattering (64Z1). Polar scattering has been shown to be the predominant mechanism in the III - V compounds (64M4) and in III - V alloys (68A1), (69A1).

Figure 6.4.9 displays the variation of the room temperature mobility with composition x. As in the case of $Ga_xIn_{1-x}Sb$ alloys the mobility is seen to vary linearly with composition for samples with roughly equal impurity concentrations, and so in these materials it appears that alloy scattering is a relatively unimportant mechanism compared with polar scattering.

MOBILITY versus TEMPERATURE FIGURE 6.4.7

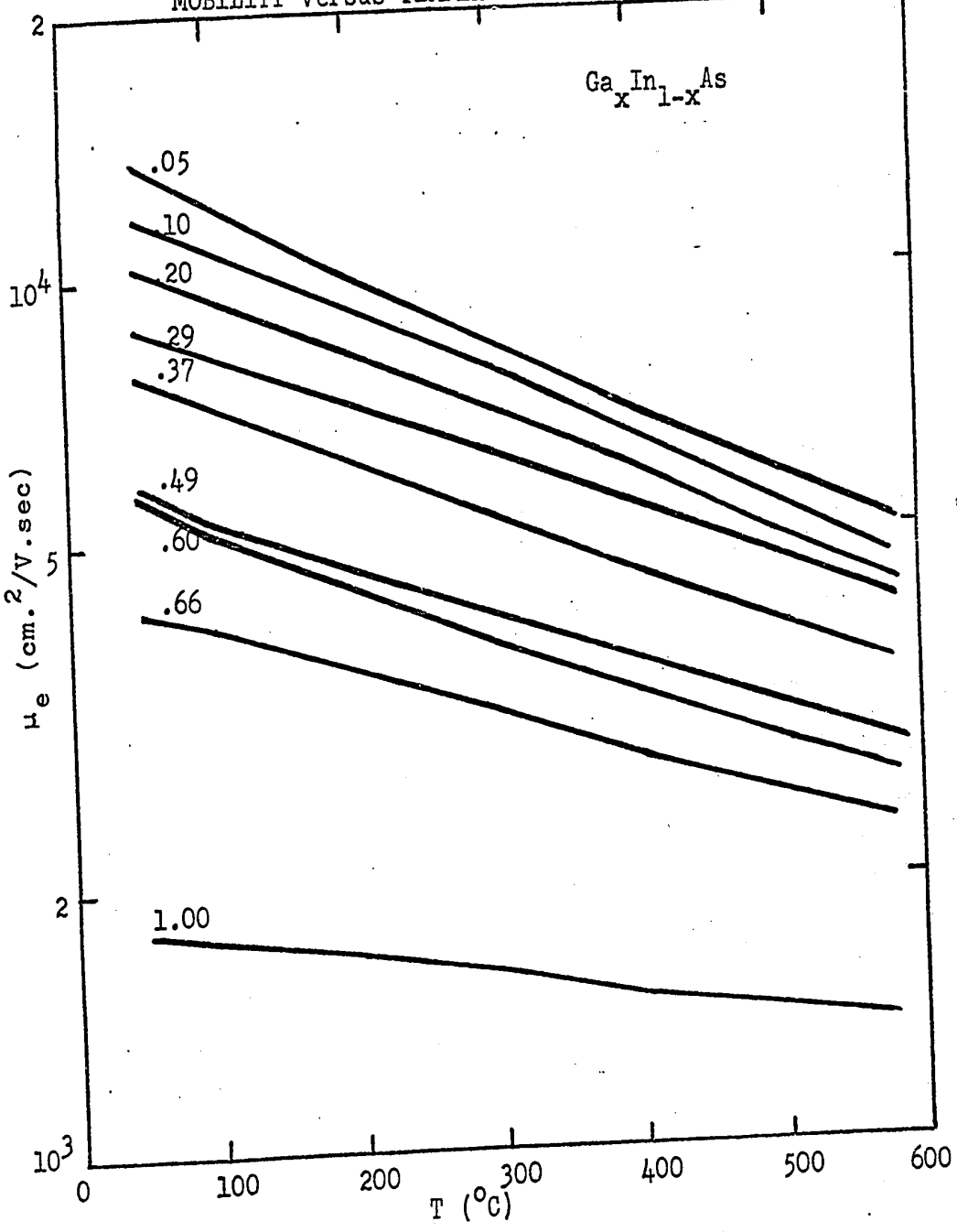

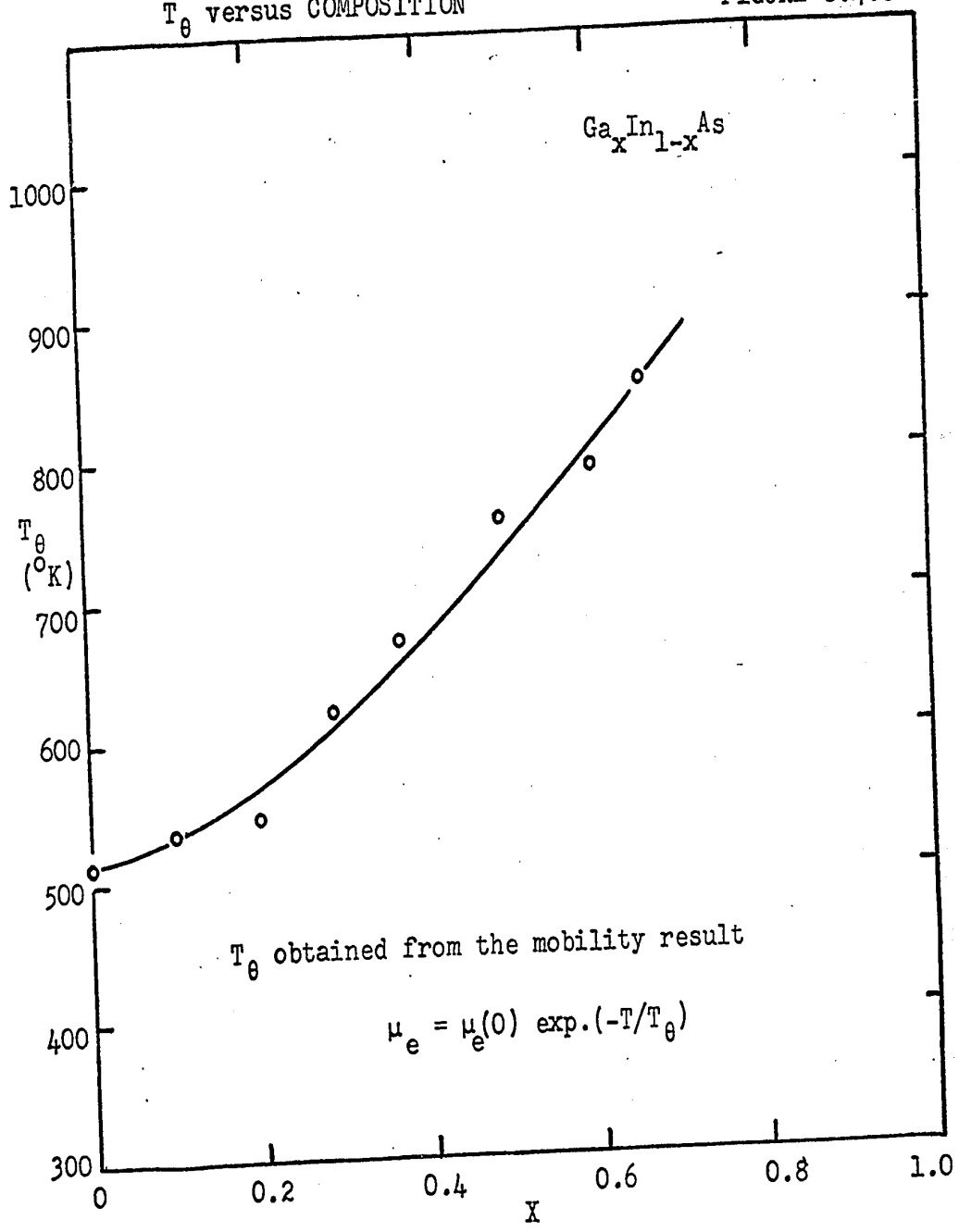
T_θ versus COMPOSITION
$Ga_xIn_{1-x}As$
1000
900
800
T_θ (^oK)
700
600
500
400
300
0
0.2
0.4
0.6
0.8
1.0
X
T_θ obtained from the mobility result
$\mu_e = \mu_e(0)\ exp.(-T/T_\theta)$

FIGURE 6.4.8

MOBILITY versus COMPOSITION FIGURE 6.4.9

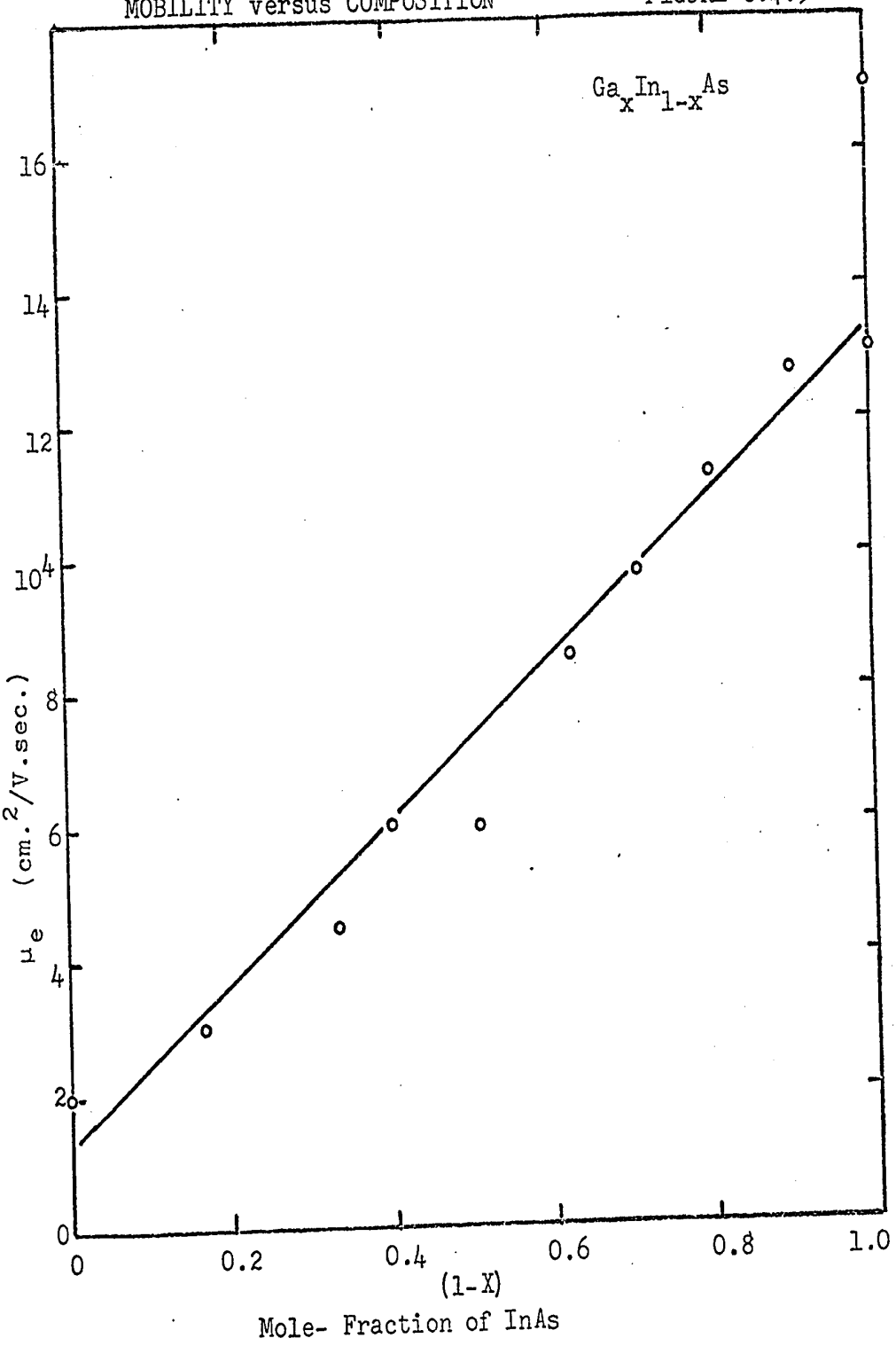

6.4.3 In As_xSb_{1-x} Results

Values of log (np/T^3) as functions of inverse temperature for various $InAs_xSb_{1-x}$ alloy samples are shown on figure 6.4.10. It is seen that, although the lines are straight over most of the temperature range, there are deviations from linearity at high temperatures. This effect is attributed to factors of degeneracy and non-parabolicity. At such temperatures, the energy gaps E_o of these alloys are small and $E_o \sim kT$, so that the assumption of non-degenerate behaviour is not valid. Since, according to the Kane band analysis, the contribution of the valence bands to non-parabolicity of the conduction band is inversely proportional to the energy gap, non-parabolic effects in these alloys will be substantial. Realizing then, that a non-degenerate, parabolic analysis is only roughly appropriate, values of E_{oo} have been calculated and are presented on figure 6.4.11 as a function of x. The values of E_{oo} from this analysis are compared with the previous optical data (64W2) both for room temperature energy gap, E_g, and its extrapolation to 0^oK, E_{go}. The values of E_{go} obtained previously were limited to small regions at either end of the composition range because of problems of preparation. The differences between the E_{oo} and E_{go} values could be due to any of several factors besides those mentioned above. The E_{go} values could be high because of

LOG. (np/T^3) versus COMPOSITION FIGURE 6.4.10

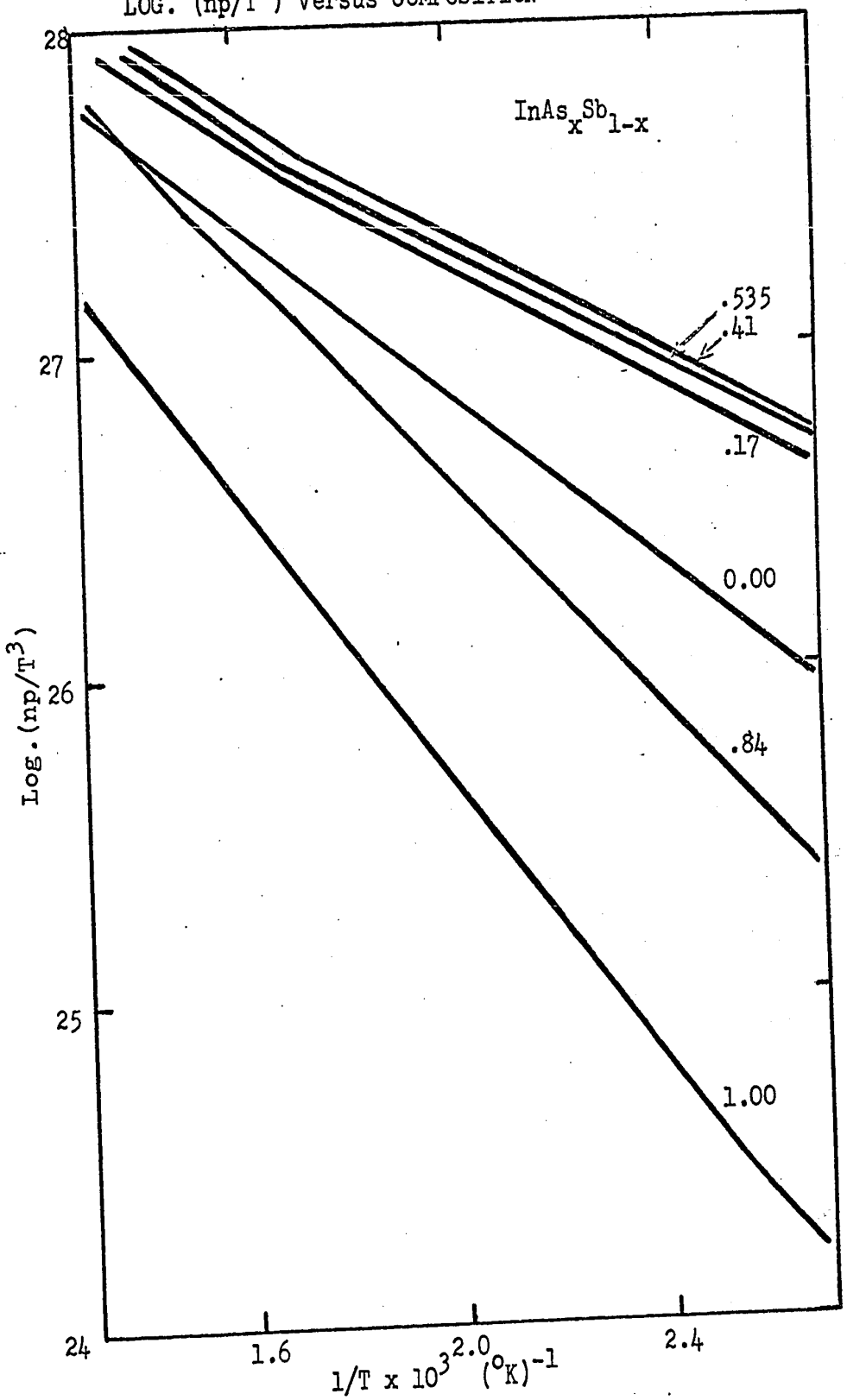

EXTRAPOLATED ENERGY GAP versus COMPOSITION FIGURE 6.4.11

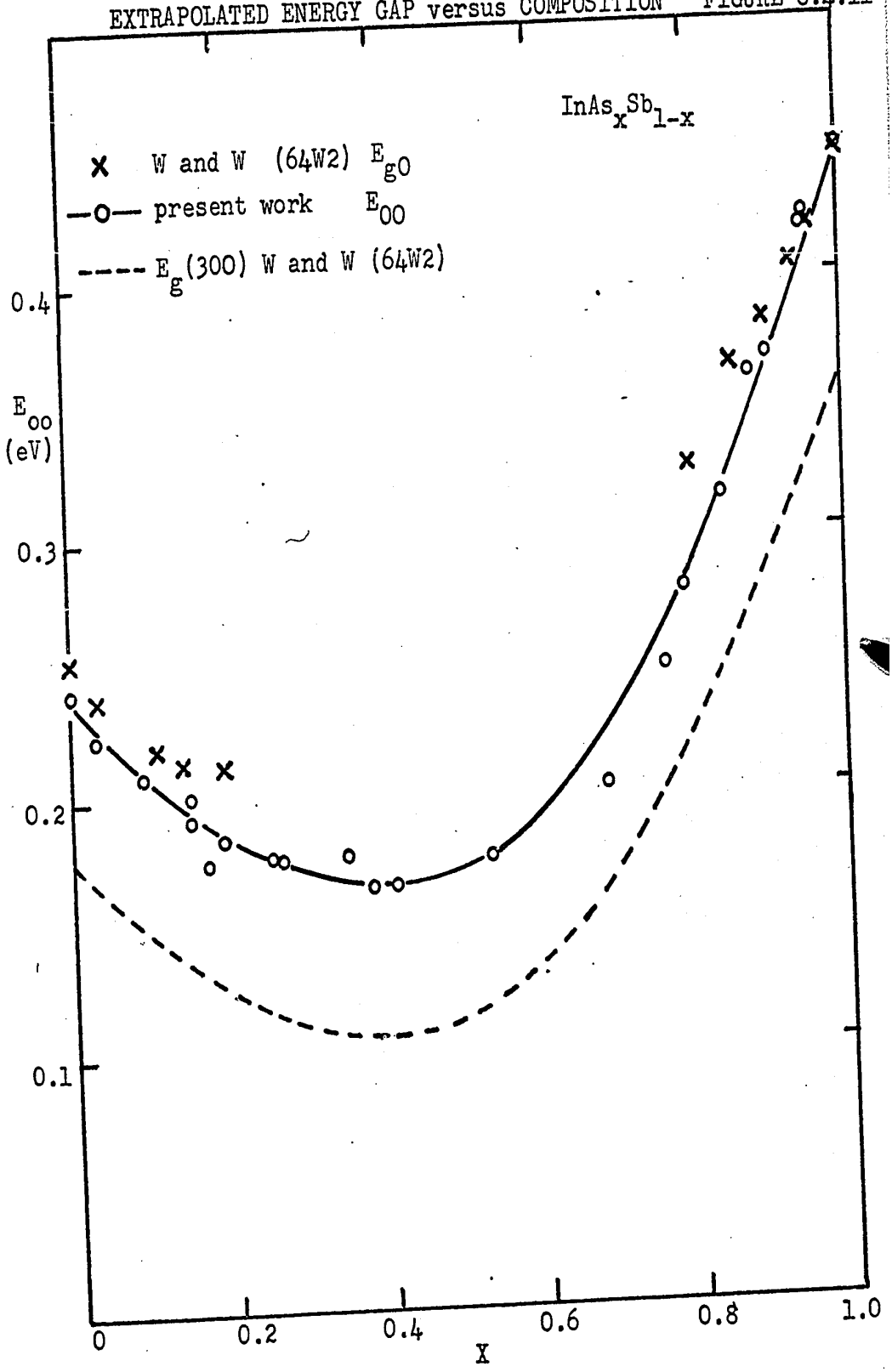

a) inhomogeneity in the earlier material, b) the presence of a Burstein shift, or c) an incorrect selection of the position of the absorption edge corresponding to the band gap.

Values of room temperature mobility, μ_e, were obtained for all specimens. The alloys all had carrier concentration in the range 10^{16} - 10^{17} cm^{-3} and so mobility values were determined for specimens with these carrier concentrations. Thus a graph of μ_e versus x for samples of roughly equal impurity was plotted and this is shown in figure 6.4.12. It is seen that within the limits of experimental error the room temperature electron mobility varies linearly with composition.

The variation of μ_e with temperature for some typical specimens is shown on figure 6.4.13. As in the case of $Ga_xIn_{1-x}As$ alloys the mobility temperature dependence was found to obey the empirical relation given in equation [6.13]. The variation of the empirical parameter T_θ with composition is given in figure 6.4.14.

6.4.4 $GaAs_xSb_{1-x}$ Results

The alloy samples used in this study were all GaSb rich and were within the composition range $0.0 < x < 0.23$. As in GaSb the conduction processes in these alloys features multi-band behaviour and hence the plots of log (np/T^3) against $1/T$

MOBILITY versus COMPOSITION FIGURE, 6.4.12

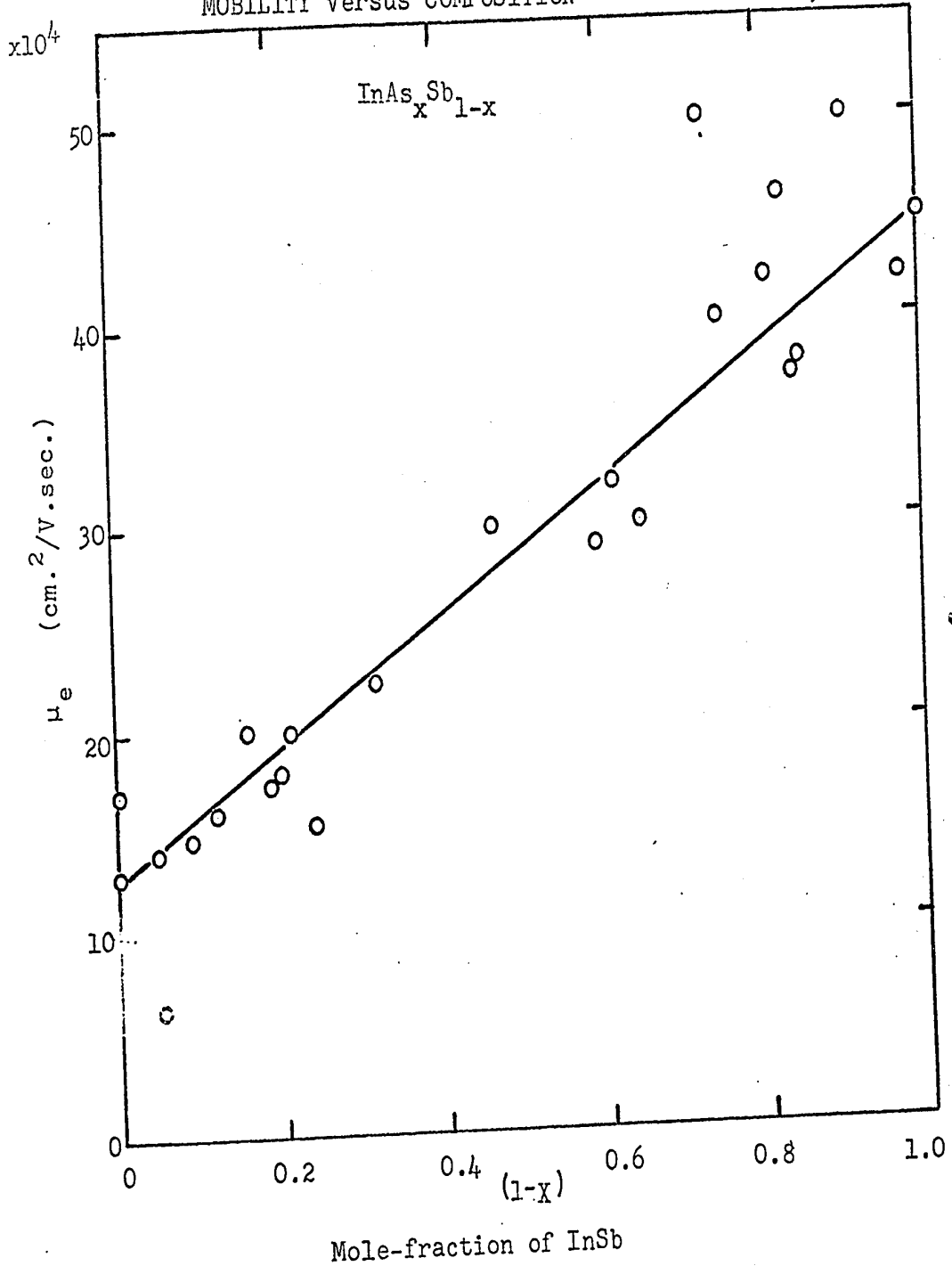

MOBILITY versus TEMPERATURE

FIGURE 6.4.13 -

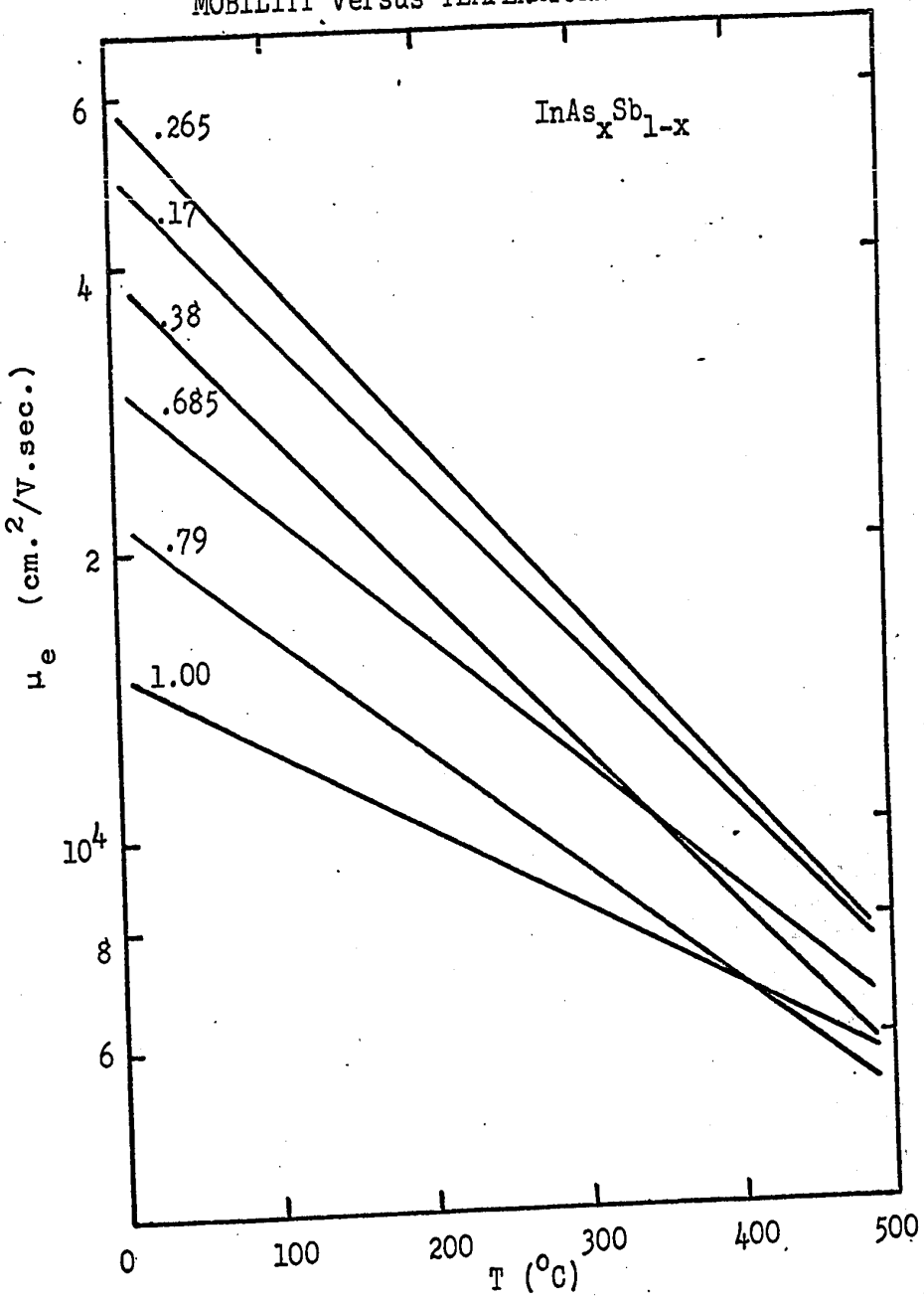

FIGURE 6.4.14

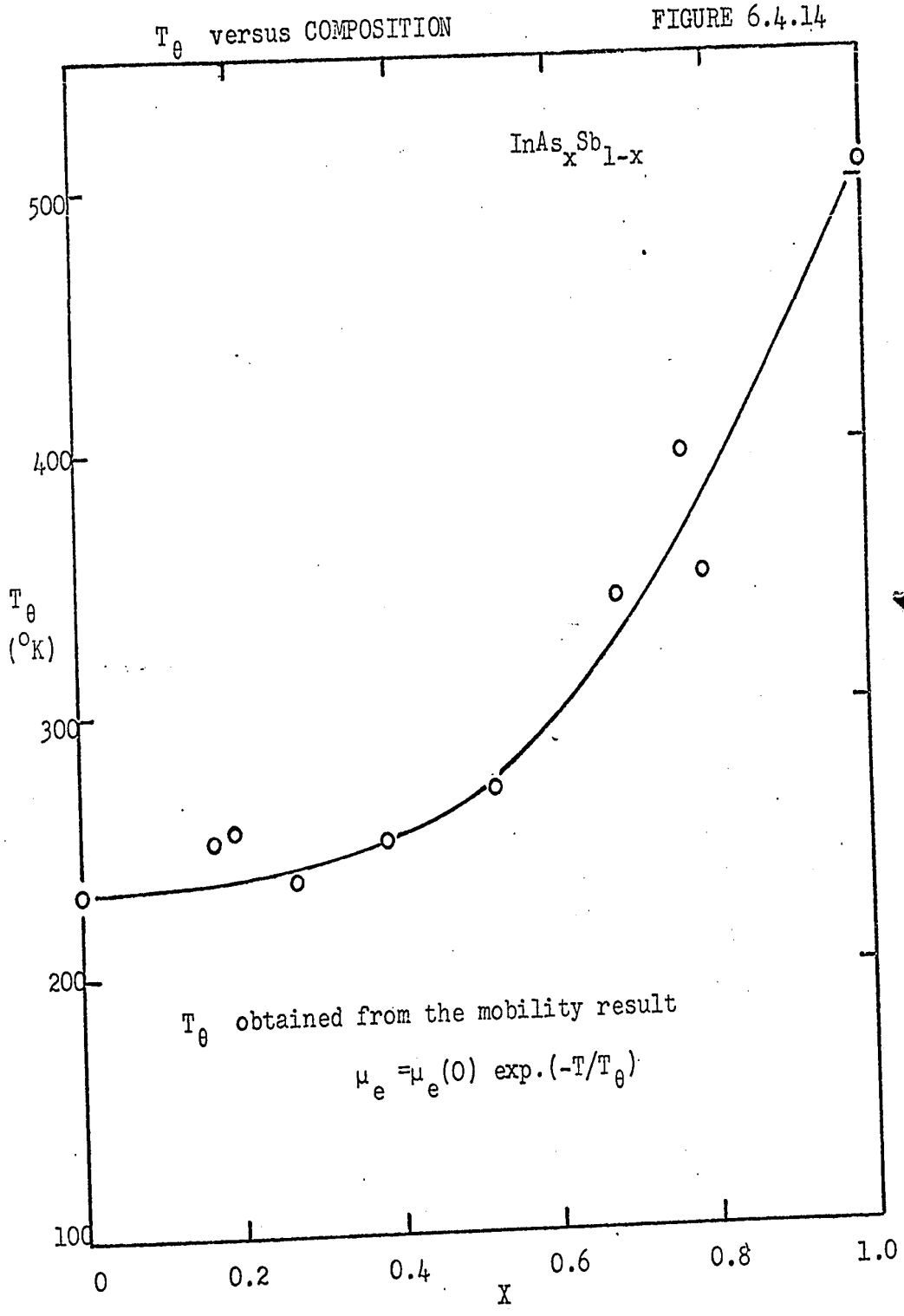
T_θ versus COMPOSITION
$InAs_xSb_{1-x}$
500
400
300
200
100
T_θ (^oK)
0
0.2
0.4
0.6
0.8
1.0
X
T_θ obtained from the mobility result
$\mu_e = \mu_e(0) \exp.(-T/T_\theta)$

did not yield straight lines. The study of these materials was also hampered by the fact that they had high impurity concentrations and did not show intrinsic behaviour until very high temperatures. On figure 6.4.15 the variation of log (np/T^3) versus 1/T is presented for the three alloy samples measured.

Although meaningful values of E_{oo} could not be obtained from figure 6.4.15, it was observed that the energy gap appears to fall as the concentration of GaAs increases. This would lead to a minimum in the energy gap at some alloy composition.

FIGURE 6.4.15

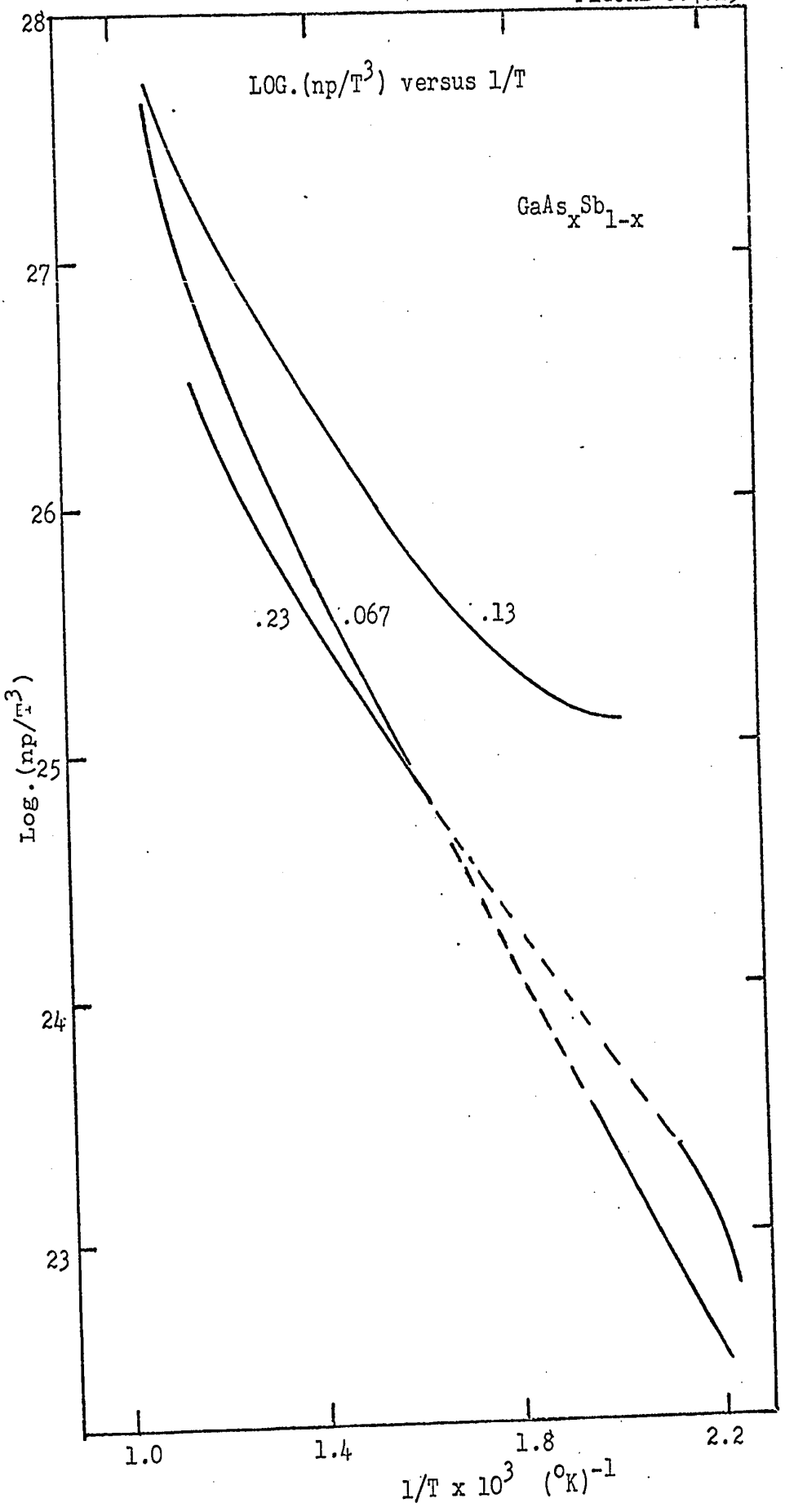
LOG.(np/T³) versus 1/T
GaAsxSb1-x
.23
.067
.13
Log.(np/nᵢ³)
28
27
26
25
24
23
1.0
1.4
1.8
2.2
1/T x 10³ (°K)⁻¹

6.5 Multiband Analysis

6.5.1 Introduction

Noting the limitations of the preceding analysis it was felt that meaningful determinations of the energy band gaps in multiband, degenerate, and non-parabolic materials might be obtained through the use of a more exact model. The basis of this analysis is the Kane band model as was outlined in Chapter IV.

By considering the carrier concentrations in both the light and heavy hole valence bands, as well as in all available conduction band minima and applying the resulting carrier densities to a general Hall equation of the form of equation [4.59], it is possible to calculate the variation of the Hall constant with temperature and to compare it with the experimental results. In the same way, using the resistivity equation of the form given in equation [4.62]; it is possible to evaluate the resistivity which results from the combination of the various band contributions, each with its characteristic mobility. These values of resistivity are also compared with the experimental results. By a judicious adjustment of the associated parameters, good agreement between the theory and experiment can be realised, and thus the values of certain unknown quantities can be obtained. The parameters of particular interest from this analysis are the energy gaps and various band separation as functions of both temperature and

alloy composition.

It might be well to mention here that such an approach has never been tried before in either compound or alloy semiconductors. The usual technique for studying the effects of higher band contribution is to work on degenerate material with impurity concentrations so great that simplified statistics can be used, and the contributions of the valence bands may be ignored. The present method may be applied to any material whether non-degenerate, quasidegenerate or completely degenerate, whether there is strong non-parabolicity or not. As well, it may be extended to include any number of significant bands.

6.5.2 Evaluation of Carrier Concentrations

The concentration of electrons in the (000) conduction band can be evaluated using equation [4.32] as derived in Chapter IV.

$$n_o = 4\pi\left(\frac{2m_{oo}^* kT}{h^2}\right)^{3/2} \{F_{1/2}(\zeta) + (\tfrac{5}{2} - 5\gamma)\beta F_{3/2}(\zeta)$$

$$+ (\tfrac{7}{8} - \tfrac{21}{2}\gamma)\beta^2 F_{5/2}(\zeta) - (\tfrac{1}{4} + \tfrac{7}{2}\gamma)\beta^3 F_{7/2}(\zeta)\} \qquad [4.32]$$

where

$$\gamma = \frac{m_{oo}^*}{m}$$

$$\zeta = E_F/kT$$

$$\beta = \frac{kT}{E_o^*}$$

$$F_n(\zeta) = \int_0^\infty \frac{x^n\, dx}{1 + e^{x - \zeta}}$$

In the calculations of the electron concentration at various temperatures, the following thermal variation relations were employed:

$$\frac{m_{oo}^*(T)}{m} = \frac{m_{oo}^*(0)}{m}\,\frac{E_o^*}{E_{oo}} \qquad \text{(Ehrenreich (57E2)}$$

[6.14]

$$E_o^*(T) = E_{oo} - \frac{E_{oo} - E_o}{n} \qquad 2 < n < 3 \text{ (ibid)} \qquad [6.15]$$

$$E_o(T) = E_{oo} + \frac{\beta T^2}{\alpha + T} \qquad \text{(Varshni (67V1))} \qquad [6.16]$$

In these relations E_o^* represents the effective mass band gap which changes more slowly with temperature than the intrinsic energy gap, E_o, for the reasons outlined in section 4.3. In equation [6.14] the bottom of the band effective mass is seen to decrease slowly with increasing temperature as the band curvature is changed by the dilation of the lattice. This results from the fact that, as the intrinsic energy gap closes with temperature, the curvature of the band increases. If the gap were to close completely the effective mass would still be finite since the temperature dependence of E_o^* is only roughly half of that of E_o.

The temperature variation of the intrinsic energy gap is usually assumed to be a linear function at high temperatures but Varshni (67V1) has shown that the energy gap at all temperatures can be obtained from a relation of the form given in [6.16] where the factor α has dimensions of temperature and can be equated roughly to the Debye temperature.

It can be seen that equation [6.16] approaches linearity at temperature $T > \alpha$.

Evaluation of the carrier concentration in the higher conduction bands is carried out using equations [4.15] and [4.16] from section 4.3

$$n_1 = 4\pi \left(\frac{2m_1^* kT}{h^2}\right)^{3/2} 4 F_{1/2}(\zeta - \delta_1) \qquad [4.15]$$

$$n_2 = 4\pi \left(\frac{2m_2^* kT}{h^2}\right)^{3/2} 6 F_{1/2}(\zeta - \delta_2) \qquad [4.16]$$

where the subscripts 1, and 2 represent the ⟨111⟩ and ⟨100⟩ bands respectively. The density of states effective masses m_1^* and m_2^* are taken to be constant scalars which are related to the longitudinal and transverse components of the effective mass by

$$m_i^* = (m_{\ell i}\, m_{ti}^{\,2})^{1/3} \qquad [4.93]$$

The factors δ_i represent the energy separations between the (000) band minimum and the higher bands and these separations are assumed to vary linearly with temperature.

Hence $\delta_i = \Delta E_i / kT$

and $$\Delta E_i = \Delta E_{io} + \beta_i T \qquad [6.17]$$

where the β_i are usually negative quantities.

The carrier concentrations in the valence bands are determined using equations[4.18] and [4.33] of section 4.3. In this analysis it is assumed that the large values of Δ_o preclude the presence of significant numbers of holes in the V_3 band and so this contribution is neglected.

$$P_{V_1} = 4\pi\left(\frac{2m_{h_1}^* kT}{h^2}\right)^{3/2} F_{1/2}(-\zeta - \xi_o) \qquad [4.18]$$

$$P_{V_2} = 4\pi\left(\frac{2m_{h_{2o}}^* kT}{h^2}\right)^{3/2} \{F_{1/2}(-\zeta - \xi_o) + \text{higher terms}\} \qquad [4.33]$$

where the higher terms are similar to those found in equation [4.32].

The "top of the band" effective hole mass, $m_{h_{2o}}^*$, in the V_2 band has a similar temperature variation to that of the (000) bottom of the band effective electron mass, i.e.

$$\frac{m_{h_{2o}}^*(T)}{m} = \frac{m_{h_{2o}}^*(0)}{m} \frac{E_o^*}{E_{oo}} \qquad [6.18]$$

The density of states hole mass in equation [4.18], $m_{h_1}^*$, is taken to be a constant scalar for the purposes of this analysis.

Since the V_1 band has a much larger density of states, it contains almost all of the total hole concentration. Quantitatively in III - V materials, the V_2 band contains from two to four percent only of the holes and is frequently neglected in analysis of electrical phenomena. This is a grave omission when considering galvanomagnetic effects since, because of the much smaller effective masses of the V_2 holes, their mobility can be considerably larger than those in the V_1 band. In the Hall effect, the carrier concentration is modified by terms involving the square of the mobility and hence, the light V_2 hole contribution can be very significant.

Let us now consider the contributions of impurity states to the conduction and valence bands. If there are N_D donor levels and N_A acceptor levels per unit volume in the crystal, then the residual impurity concentration which may contribute to conduction is given by $N_A - N_D$, the remaining levels being ionized by compensation. Let us assume for the present analysis that all donors are found at only one energy level ϵ_d below the conduction band and that the acceptors are all found at energy ϵ_a above the valance band. The relations giving the number of unionized donors and acceptors in each of these levels can be expressed as

$$n_d = N_D \left[1 + \frac{1}{2}\exp\left(-\zeta - \frac{\epsilon_d}{kT}\right)\right]^{-1} \qquad [6.19]$$

and

$$n_a = N_A \left[1 + \frac{1}{2}\exp\left(\zeta + \xi_o - \frac{\epsilon_a}{kT}\right)\right]^{-1} \qquad [6.20]$$

all ionized carriers from the residual impurity states will be found in either the conduction or valence bands.

Clearly each of the equations enumerating the concentrations of carriers in each band cannot be evaluated unless the position of the Fermi level, upon which each expression is seen to depend, is known. The equation expressing the condition for electrical neutrality, and which determines the position of the Fermi level is now given by

$$n_o + n_1 + n_2 - N_D + n_d = p_1 + p_2 - N_A + n_a \qquad [6.21]$$

Using each of the concentration equations, [6.21] may be expressed in terms of E_F and solved by an iterative procedure using tables of the Fermi functions especially prepared for this analysis.

The resulting carrier concentrations for each band are then combined with the appropriate Hall scattering factors from section 4.4 and the appropriate mobilities as determined according to subsection 6.5.3, then substituted into the definition of the Hall constant as given in equation [4.96]

$$R_H = \frac{-\Sigma r_{Di}\, n_i\, e\, \mu_i^2}{(\Sigma r_{Ai}\, n_i\, e\, \mu_i)^2 + (\Sigma r_{Di}\, n_i\, e\, \mu_i^2 B)^2} \qquad [4.96]$$

6.5.3 Evaluation of Mobilities

The values for the various charge carrier mobilities are obtained by fitting test values into the relation for the conductivity as given by

$$\sigma = \Sigma r_{Ai}\, n_i\, e\, \mu_i \qquad B = 0 \qquad [4.99]$$

together with the values of carrier concentrations, and by adjusting all necessary parameters until the calculated values of the resistivity and the Hall constant are simultaneously satisfied.

The relation governing the temperature variation of the various electron mobilities assumes that the predominant scattering mechanism is polar scattering. In this case we may write

$$\mu(T) = \mu(0)\, T^{1/2}\, (e^{\theta/T} - 1). \qquad [6.22]$$

(Ehrenreich (60E3))

This is a relation combining polar and impurity scattering, where the θ term is a lattice phonon temperature approximately equal to the Debye temperature.

The hole mobilities are assumed to have a power law temperature dependence of the form

$$\mu_h(T) = \mu_h(0)\ T^{-p}. \qquad [6.23]$$

A value of $p \simeq 1.5$ would indicate that polar scattering is predominant for holes, but previous work on p-type samples of InSb has yielded values of $p = 2.55$. In the case of p-type germanium, Beer(63B18) has suggested that the inter- and intraband interactions of the holes in the two degenerate valence bands are the most important scattering mechanisms, but germanium is not a polar material. The exact combination of processes is not at all known, and for the purposes of this analysis the value of p has been adjusted to fit the experimental data for each p-type alloy sample.

All of the expressions needed for this analysis have been collected on figure 6.5.1 for more convenient reference. The computer program which was prepared to carry out the complex iterative solution of the carrier concentration equations, and the evaluation of the Hall coefficient and the resistivity, is listed in Appendix I.

6.5.4 Discussion of Band Parameters

It is immediately evident from a glance at the equations on figure 6.5.1 that this analysis requires quantitative values

FIGURE 6.5.1

RELEVANT EQUATIONS FOR MULTIBAND ANALYSIS

I $$n_o = 4\pi\left(\frac{2m_{oo}^* kT}{h^2}\right)^{3/2} \{F_{1/2}(\zeta) + \text{non parabolic terms}\}$$

II $$n_1 = 4\pi\left(\frac{2m_1^* kT}{h^2}\right)^{3/2} 4F_{1/2}(\zeta - \delta_1)$$

III $$n_2 = 4\pi\left(\frac{2m_2^* kT}{h^2}\right)^{3/2} 6F_{1/2}(\zeta - \delta_2)$$

IV $$p_1 = 4\pi\left(\frac{2m_{h_1}^* kT}{h^2}\right)^{3/2} F_{1/2}(-\zeta - \xi_o)$$

V $$p_2 = 4\pi\left(\frac{2m_{h_{2o}}^* kT}{h^2}\right)^{3/2} \{F_{1/2}(-\zeta - \xi_o) + \text{non parabolic terms}\}$$

VI $$n_d = N_D[1 + 1/2\exp(-\zeta - \varepsilon_d/kT)]^{-1}$$

VII $$n_a = N_A[1 + 1/2\exp(\zeta + \xi_o - \varepsilon_a/kT)]^{-1}$$

VIII $$n_o + n_1 + n_2 - N_D + n_d = p_1 + p_2 - N_A + n_a$$

IX $$\mu_i(T) = \mu_i(0)T^{1/2}(e^{\theta_i/T} - 1)$$

X $$\mu_{h_i}(T) = \mu_{h_i}(0)\, T^{-p_i}$$

XI $$R_H = \frac{+ \Sigma r_{D_i} p_i e\mu_{h_i}^2 - \Sigma r_{D_i} n_i e\mu_i^2}{[\Sigma r_{A_i} n_i e\mu_i + \Sigma r_{A_i} p_i e\mu_{h_i}]^2 + [\Sigma r_{D_i} n_i e\mu_i^2 B - \Sigma r_{D_i} p_i e\mu_{h_i}^2 B]^2}$$

XII $$\rho = [\Sigma r_{A_i} n_i e\mu_i + \Sigma r_{A_i} p_i e\mu_{h_i}]^{-1} \qquad B = 0$$

for several parameters in order to allow evaluation. The requisite factors have been listed for convenience on figure 6.5.2. In this subsection the significance of each of these parameters will be discussed, and it will be shown that the analysis is not sensitive to variations in many of them.

Of the parameters which are significant, in some cases their importance is restricted to limited temperature or alloy composition ranges; in other cases values for the parameters have been made available by independent investigations. By far the most important factors governing the behaviour of the Hall constant and the resistivity with temperature are the energy separations of the bands and their respective temperature dependence. It was to evaluate these factors that the present analysis was instigated.

Of the parameter values obtained from other investigations, the most notable are the accurate determinations of the bottom of the band electron effective masses for the $Ga_xIn_{1-x}Sb$ alloy system, evaluated by Aubin et. al. (69A1), and for the $InAs_xSb_{1-x}$ alloy system, evaluated by Aubin (68A1) and by vanTongerloo (68V1). The effective mass values for the $Ga_xIn_{1-x}As$ system have been calculated, using a semiempirical method, by Woolley and Thompson (64W4). These sets of values which have been taken directly into present work are presented on figure 6.5.3.

FIGURE 6.5.2

m_{oo}*:	Bottom of the (000) band electron effective mass
m_1*:	Density of states electron mass for ⟨111⟩ band
m_2*:	Density of states electron mass for ⟨100⟩ band
m_{h_1}*:	Density of states heavy hole mass for V_1 band
$m_{h_{2o}}$*:	Top of the V_2 band hole effective mass
E_{oo}:	Intrinsic energy gap at absolute zero
β_o:	Temperature coefficient of E_o
ΔE_{1o}:	(000) to ⟨111⟩ band separation at 0^oK
β_1:	Temperature coefficient of ΔE_1
ΔE_{2o}:	(000) to ⟨100⟩ band separation at 0^oK
β_2:	Temperature coefficient of ΔE_2
N_D:	Density of donor levels.
N_A:	Density of acceptor levels.
ε_d:	Activation energy of donor levels.
ε_a:	Activation energy of acceptor levels.
$\mu_{h_1}(300)$:	Heavy hole mobility at room temperature
$\mu_o(300)$:	(000) electron mobility at room temperature
p:	Power of temperature dependence for $\mu_h \propto T^{-p}$

BOTTOM OF THE BAND ELECTRON EFFECTIVE MASS

FIGURE 6.5.3

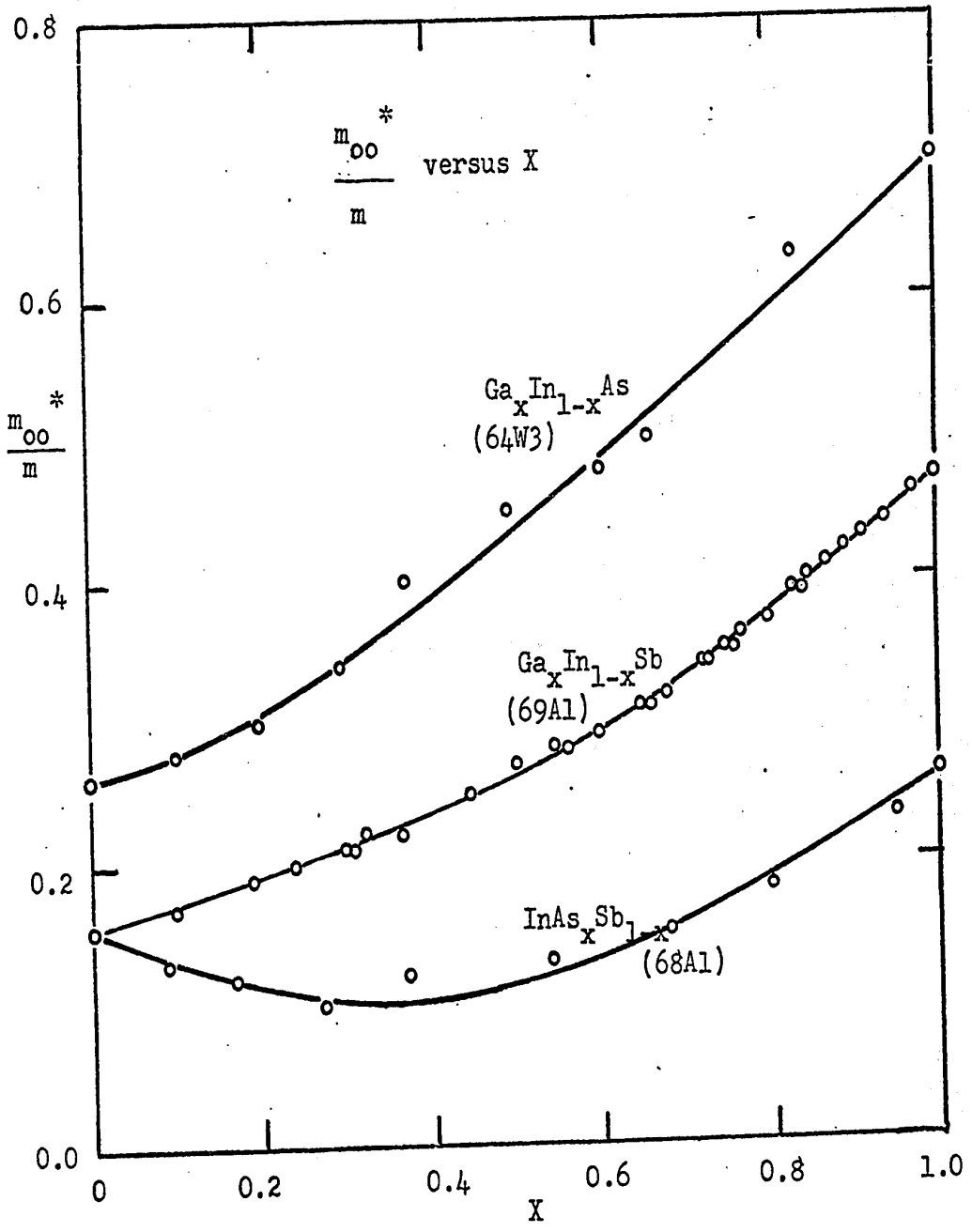

Effective mass values for the holes were obtained from published work on the III - V compounds by Cardona (63C3) and linear interpolations were assumed valid for the alloy materials. A value of the density of states effective mass for the ⟨111⟩ conduction in GaSb has been determined by vanTongerloo (69V1). This value of $m_1^*/m = 0.226$ has been used in the present analysis and has been assumed to be a slowly varying function with alloy composition. Since the ⟨111⟩ band is significant only in alloys rich in GaSb this is a reasonably valid assumption.

The density of states electron effective mass for the ⟨100⟩ band has been taken from measurements on silicon. In this material, where the ⟨100⟩ band is the lowest, the measured effective mass is 1.2 m. Since the multiplicity of this band is thought to be six-fold this gives the value of $m_2^*/m = 0.36$ which was used for all alloy compositions as this was not found to be a significant parameter.

The residual impurity concentration is usually determined from measurements of the Hall constant at temperatures low enough that intrinsically activated carriers are negligible but high enough that all available impurity states are ionized. From this measured extrinsic Hall coefficient which is characterized by a constant value with temperature, one can calculate the concentration of impurity carriers from

$$n = (N_A - N_D) = \frac{r}{R_{Hext}\, e} . \qquad [6.24]$$

This method is acceptable when the residual impurity states are donors, contributing electrons to a single conduction band. However, when the subsidiary conduction bands are sufficiently close that they may contain a sizeable proportion of the extrinsic electrons, a two conduction band analysis must be employed and equation [6.24] is not valid.

In the case when the residual impurity states are acceptors, these states are ionized by electrons from both the V_1 and V_2 valance bands. Although it can easily be calculated that the light hole valence band contributes only a small percentage of the total ionizing electrons; it is not permissable to neglect the contribution of the light holes in the Hall effect, as is so frequently done, since the concentration of these holes is modified by a term involving the square of their mobility in the Hall relations. Neglecting the effect of this band in extrinsic p-type material can lead to estimations of the acceptor density which are in error by factors of up to 80%, (Beer 63B18). Propogation of this error can cause faulty conclusions to be drawn in calculations of many band parameters.

In order to arrive at meaningful values for the impurity concentration, the effect of each contributing band has been

included and the impurity density treated as an adjustable parameter until close agreement was reached between the calculated and experimental Hall coefficient values in the extrinsic temperature region.

It can be shown that for various scattering mechanisms the resulting carrier mobility exhibits a characteristic dependence on the density of states effective mass. In polar materials this dependence can be expressed as

$$\mu \propto m^{-3/2} \quad . \qquad \text{(Ehrenrich(60E3))} \quad [6.25]$$

Hence, the mobility of electrons in the subsidiary bands of the III - V alloys can be found by

$$\mu_i = \mu_o (m_{do}^*/m_i^*)^{3/2} \qquad i = 1, 2 \qquad [6.26]$$

where m_{do}^* is the density of states electron effective mass of the (000) band and μ_o is the mobility of the (000) electrons.

In the valence bands the scattering processes are not well defined and so for the purposes of the present analysis the relative light to heavy hole mobility has been assumed to be inversely proportional to the density of states effective hole masses. This at first glance would seem to be an arbitrary criterion, however, measurements of the relative hole mobilities in InSb have indicated that this relation is approximately correct (Beer) (Blatt (68B1)). In germanium and silicon,

arguments based on interband scattering indicate that the relaxation times for both the heavy and light holes are determined by the very much higher density of heavy hole states and that because of this the mobilities are inversely proportional to the effective masses. These are not polar materials however, as are III - V compounds, and the accurate hole scattering arrangement in the alloys of interest are to date not understood.

The room temperature values of the mobility of various carriers were obtained by adjusting the values for the (000) electron mobility and the heavy hole mobility until good agreement was reached between the calculated and experimental values of the Hall constant and the resistivity.

In III - V crystals featuring a direct band gap the electron mobility is very much greater than that of the holes. As a result of this, in n-type material the actual value of the hole mobility is quite unimportant and provided $\mu_e > \mu_h$ any value of μ_h will serve. Obviously in these cases no conclusion can be drawn regarding the values of the hole mobility from n-type samples alone.

In p-type material the values of the hole mobilities are important parameters in the extrinsic temperature range. As a p-type crystal nears the temperature at which the sign of the Hall constant reverses, the ratio of the electron to hole

mobility becomes an extremely critical parameter. This ratio determines the maximum value to which the Hall constant rises after its sign changes to negative. The larger the ratio μ_e/μ_h, the higher the Hall maximum relative to the positive extrinsic level.

By adjusting both the heavy hole mobility and the (000) electron mobility so that the calculated resistivity in the p-type and n-type temperature regions fit the experiment, while the calculated Hall curves also fit their experimental values in the transition region, we can arrive at reasonably accurate values for the various mobilities. Values obtained for hole mobilities from p-type samples are then used in the analysis of n-type material assuming that the electron to hole mobility ratio is a linear function with composition.

The remaining parameters of the analysis, which are by far the most significant, are the relative energy positions of the bands and their thermal variation. Obviously, the Hall constant and the resistivity are inherently dependent on the number of carriers in the bands which are in turn functions primarily of the temperature and the energy gap.

The characteristic shoulder in the variation of the Hall constant and the resistivity with temperature is the result of sufficient thermal energy becoming available to allow significant numbers of electrons and holes to be excited between valence and conduction band states, and hence to contribute to conduction.

When the numbers of such electrons and holes are significant, the material is said to be in the intrinsic condition, i.e. $n_i = p_i \geq |N_D - N_A|$. The temperature at which the transition from the extrinsic to the intrinsic condition occurs depends both on the intrinsic energy gap and on the density of the impurity states. If the latter of these factors is known from calculations based on extrinsic Hall measurements, then the intrinsic energy gap may be obtained. Since preliminary values of the gap have already been obtained by means of the two band analysis presented in sections 6.3 and 6.4, it remains a slight refinement in two band nondegenerate, n-type material to adjust the value of E_{oo} in the multiband analysis until the experimental and calculated Hall curves exhibit the onset of intrinsic behaviour at the same temperatures.

In material where there are degenerate effects such as in the very low energy gap $InAs_xSb_{1-x}$ alloys, or when the subsidiary conduction bands contain significant numbers of electrons as in the GaSb rich and GaAs rich alloys; the multiband analysis will allow determinations of the intrinsic energy gap which were otherwise only roughly approximate.

In material featuring significant multiband conduction, the Hall constant curves have a characteristic temperature variation in the extrinsic region. As the thermal energy of the crystal is increased, the total number of conduction electrons being roughly fixed at $N_D - N_A$ these electrons will redis-

tribute themselves according to the Fermi statistics into the various available bands. The ⟨111⟩ conduction band is characterized by a relatively high density of states compared with the (000) band and this difference is further assisted by the multiplicity of the higher band minima. Because of this, as sufficient thermal energy is supplied, a substantial number of electrons can be removed from (000) states and placed into ⟨111⟩ states. When this happens, the total number of occupied states remains unchanged but the mobility of the electrons in the higher states is so reduced that they seem to disappear. As a result, the Hall coefficient is seen to increase with increasing temperature. The magnitude of this rise is related to the number of electrons which make the transition, which is in turn related to the energy separation of the ⟨111⟩ and (000) bands.

By adjusting this energy separation in the analysis until the predicted rise in the Hall constant matches that in the Hall experiments we can arrive at the correct value.

The temperature at which changes are noted in the Hall constant, the rates of variations of the Hall constant with temperature in various characteristic temperature regions, and the absolute magnitude of the Hall constant, are the features through which the effects of the various energy parameters can be studied. After observing the changes in the calculated curves, with several adjustments of the various parameters, one is able to develop a "feel" for the significance of each

factor and thus proceed to the final close agreement between the resulting calculated curves and the experiments.

Throughout the analysis of the many alloy samples whose electrical properties were measured, an over-riding criterion was applied that all fundamental parameters determined for each sample must fit into a monotonic variation with alloy composition. The application of this criterion together with the wealth of measurements on material of all compositions has increased the reliability of the values which have been determined.

The parameter values resulting from the application of the multiband analysis on samples from the $Ga_xIn_{1-x}Sb$, $Ga_xIn_{1-x}As$ and $InAs_xSb_{1-x}$ alloy systems are presented in the next section.

6.6 Results of Multiband Analysis

6.6.1 $Ga_xIn_{1-x}Sb$ Results

Calculated Hall constant and resistivity curves were fitted to experimental measurements of no fewer than thirty-four samples of $Ga_xIn_{1-x}Sb$ alloys. The values of the important band parameters needed to accomplish this correspondence are listed on table 6.6.1.

The variations of the relative energy band positions at room temperature with alloy composition are shown on figure 6.6.1. In this figure the energy values are shown relative to the top of the valence band. The sensitivity of the analysis to the positions of the higher bands decreased as the alloy composition varied from GaSb to InSb. Because of this fact the reliability of the energy position of these bands exhibits a corresponding gradual deterioration. Certain samples measured had high donor impurity densities. In these the higher band effects were more noticeable, and hence more accurately determined. The samples in which the higher bands contributed significantly are indicated by circles, closed circles representing n-type material, open circles representing p-type. Questionable values are indicated by error bars where the outside limits of the bars represent the energy variation within which the calculated curves were essentially unaltered. The energy gap variation with alloy composition at absolute

zero is shown on figure 6.6.2. It can be seen that the energy separation between the ⟨111⟩ and (000) bands in GaSb has been found to be 0.078 eV at $0^{o}K$. This value is in excellent agreement with that determined by vanTongerloo (68V1) but is somewhat larger than the value given by Kudman and Seidel (67K2). See also (61C2), (61B7) and (59S15).

It has been suggested by Paul (68K3) that in GaSb the position of the ⟨100⟩ minima will be found ~ 0.315 eV above the (000) band at room temperature. This agrees reasonably well with the findings of the present work where

$$(E_{\langle 100\rangle} - E_{(000)})_{300^{o}K} \simeq 0.26 \text{ eV}.$$

In InSb the ⟨111⟩ band has been variously reported to be between 0.3 and 0.55 eV above the fundamental gap at absolute zero. (Filipchenko, (66F1), Aubin (68A2)).

This extended range would seem to include the extrapolated value of the ⟨111⟩ band energy from the present calculations in the alloys.

Experimental curves from Kudman and Seidel (67K2) for heavily doped alloys of this system at x = 0.83 and x = 0.66 were compared with calculated curves from the present analysis and it was found that the energy separation values were lower than the values quoted by the above workers. These specimens are indicated on figure 6.6.2.

ENERGY BANDS versus COMPOSITION FIGURE 6.6.1

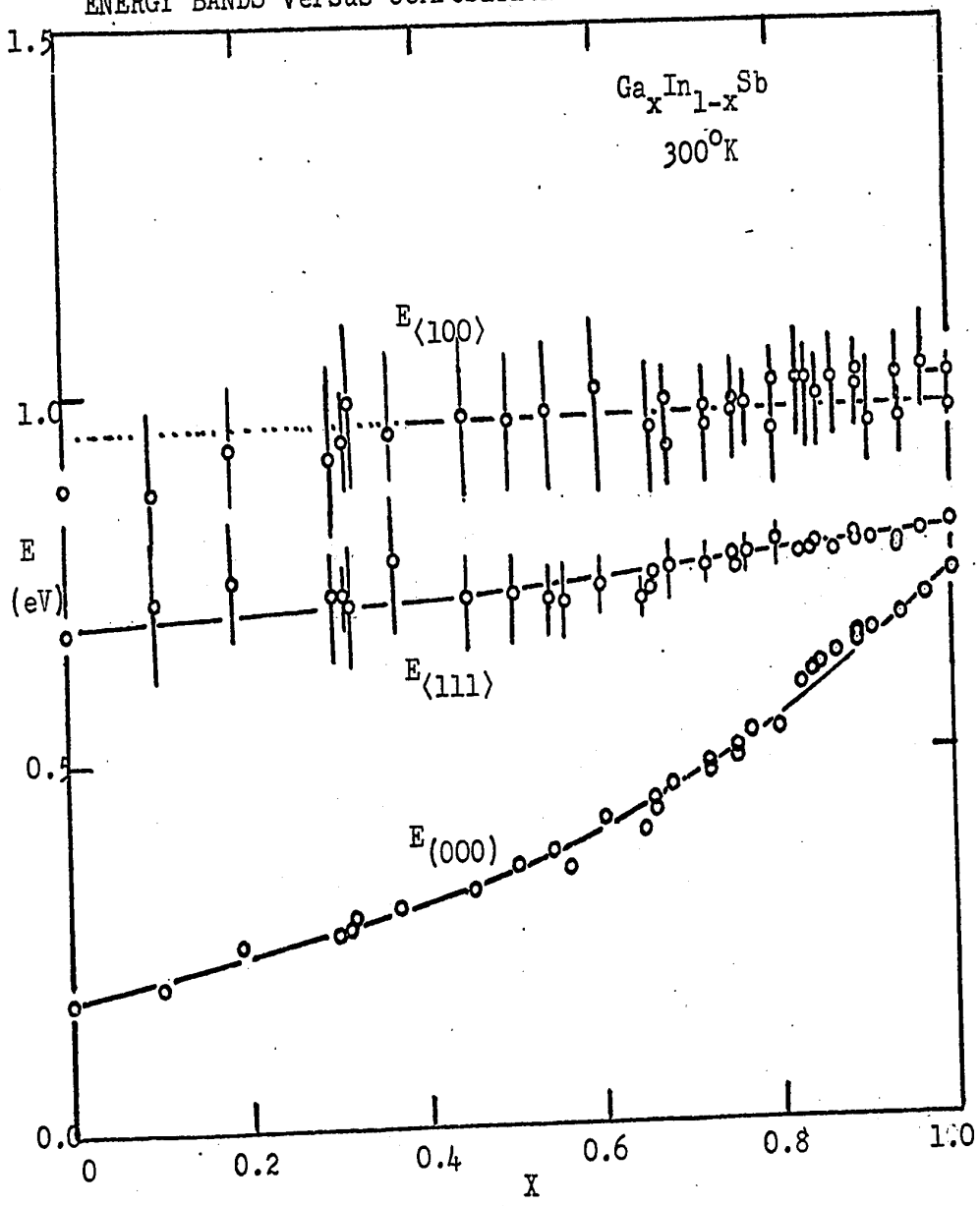

ENERGY BANDS versus COMPOSITION FIGURE 6.6.2

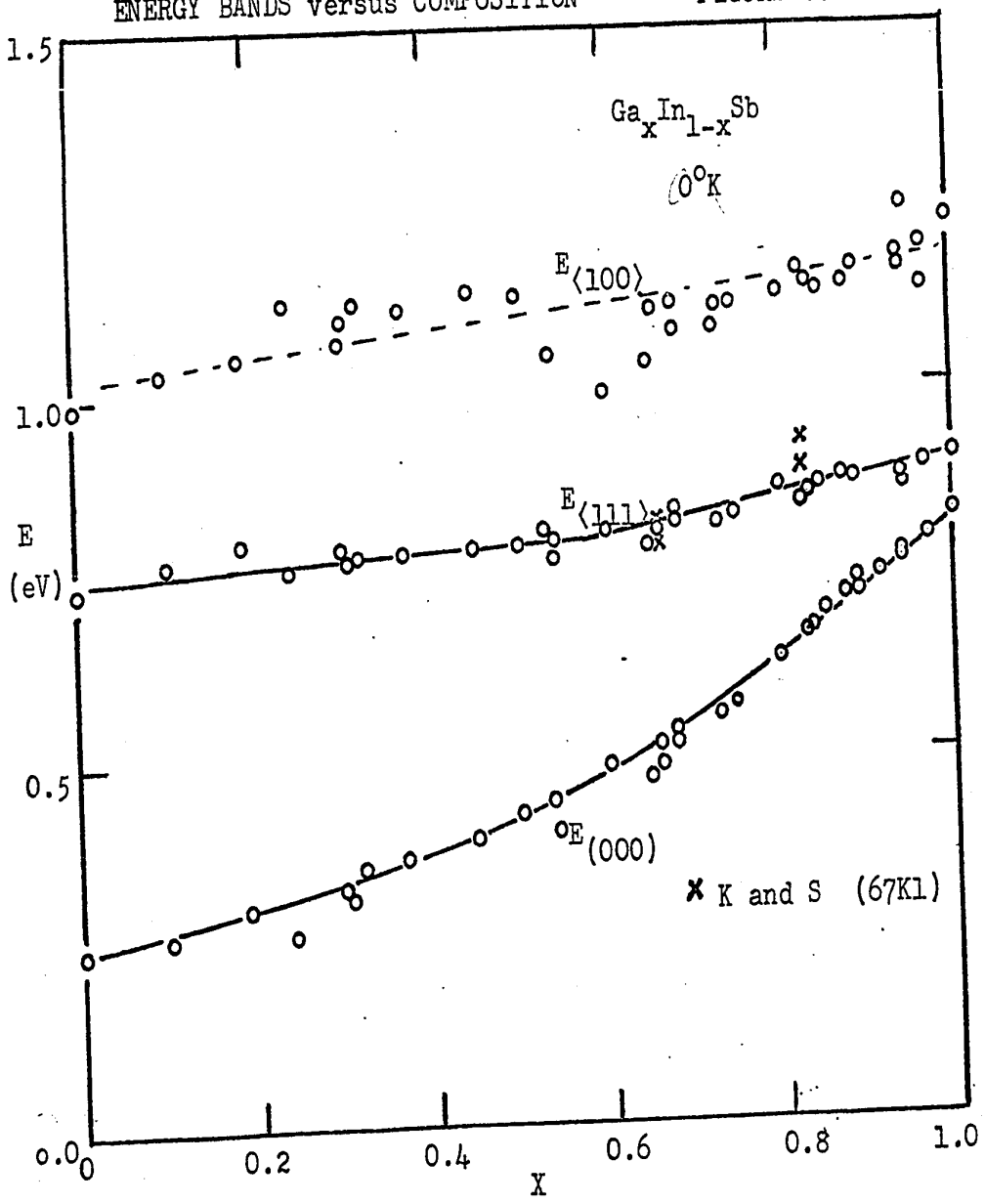

The values determined for the coefficients of the temperature dependence of the intrinsic energy gap are listed on table 6.6.1. The variation of these parameters with alloy composition is shown on figure 6.6.3. It can be seen that this variation is similar in form to that reported by Woolley and Evans (60W7) from optical absorption measurements.

It was found that acceptor states in GaSb rich alloys were characterized by an ionization energy near to $\epsilon_a = 0.06$ eV but as the alloy composition varied towards InSb, the ionization energy for acceptors was seen to decrease. In contrast to the p-type results, the ionization in n-type samples was found to be negative, that is the donor states appeared to be situated above the minimum of the (000) energy gap.

This observation would seem to corroborate the work of Bate (62B2) and Paul (68K3) who have indicated that for such impurities as selenium and tellurium the donor states are associated not with the (000) band but with the higher conduction band minima.

The calculated variation of the room temperature mobilities with composition for the carriers in various bands are shown in figure 6.6.4. Electron mobilities are indicated by closed circles when the values were determined from n-type samples and by open circles where the values were derived from

TABLE 6.6.1

$Ga_xIn_{1-x}Sb$ BAND PARAMETERS

SAMPLE	X (mole-fraction)	Z x 10^{-16} (cm^{-3})	m_{h1}*/m	m_{oo}*/m m_{h2o}*/m	m_1*/m	m_2*/m	E_{oo} (eV)	ΔE_{1o} (eV)	ΔE_{2o} (eV)
GaSb	1.0	+44.	.500	.047	.226	.36	.825	.078	.325
CP 0.75	.975	+25.	.505	.046	.22	.36	.79	.10	.44
CA 1	.94	-46.	.500	.044	.22	.38	.765	.105	.422
CA 8	.91	-105.	.504	.043	.22	.38	.74	.135	.40
CD 3	.89	+30.	.50	.042	.22	.38	.738	.130	.423
CN 1.0	.89	+10.	.50	.042	.22	.38	.72	.15	.453
CA 10	.87	-105.	.50	.041	.21	.38	.71	.165	.435
CN 5.1	.85	-0.6	.473	.040	.22	.36	.695	.170	.430
CF 4	.84	-4.2	.484	.04	.22	.38	.665	.19	.48
TF 1.2	.80	+38.	.48	.037	.22	.38	.63	.23	.50
CK 1.0	.77	+3.5	.445	.036	.22	.38	.60	.25	.52
RB 5.1	.75	-11.3	.458	.035	.23	.38	.565	.26	.54
CK 1.6	.73	+2.6	.461	.034	.22	.38	.56	.27	.55
RA 4.1	.73	-12.6	.461	.034	.22	.38	.562	.27	.53
CF 6	.68	-18.0	.448	.032	.24	.36	.52	.31	.60
A 2.9	.65	+64.	.432	.031	.22	.38	.465	.32	.58
CK 3.2	.60	-.034	.43	.029	.24	.38	.485	.32	.50

TABLE 6.6.1

A 3.9	.56	+34.	.436	.028	.20	.38	.40	.37	.62
CK 3.8	.54	-0.18	.438	.028	.25	.38	.44	.36	.65
CK 4.2	.50	-0.50	.425	.027	.25	.38	.42	.37	.71
CN 4.5	.45	-1.0	.423	.025	.26	.38	.385	.40	.75
CK 3.7	.37	-1.05	.415	.022	.27	.38	.363	.42	.752
CN 11.2	.32	-1.15	.402	.021	.227	.38	.35	.43	.78
CX 13.7	.31	-33.	.403	.021	.227	.38	.31	.46	.75
CK 6.0	.30	-0.70	.415	.021	.27	.38	.320	.47	.76
CN 12.4	.19	-1.35	.401	.019	.28	.38	.30	.50	.76
CK 9.8	.10	-0.88	.415	.017	.20	.38	.26	.51	.76
InSb	.00	-2.06	.400	.0155	.20	.40	.24	.50	.75

TABLE 6.6.1

SAMPLE	θ_D (^oK)	β_o (x 10^4 ev / ^oK)	β_1	β_2	μ_o (300) (cm^2/ V.sec)	μ_h (300) (cm^2/V.sec)	p	ε_d (eV)	ε_a (eV)
GaSb	265	-6.3	-0.32	-2.5	5500	190	1.35		.045
CPO.75	264	-6.2	-0.32	-3.0	5900	120	1.18		.07
CA1	262	-6.0	-0.3	-3.0	5000	70		-.05	
CA8	260	-5.8	-0.35	-3.0	4325	67		-.07	
CD3	260	-5.8	-0.26	-2.5	10200	199	1.40		0.0
CN1.0	260	-5.5	-0.28	-3.5	15400	193	1.34		.06
CA10	260	-5.6	-0.28	-3.0	6743	85		-.16	
CN5.1	255	-5.4	-0.25	-2.5	13810	183		-.17	
CF4	254	-5.35	-0.25	-2.5	6554	81		-.03	
TF1.2	250	-5.3	-0.25	-2.5	14760	158	1.30		0.0
CK1.0	250	-5.2	-0.25	-2.5	15000	145	1.502		0.065
RB5.1	248	-5.1	-0.24	-2.5	11855	113		-.23	
CK1.6	246	-5.2	-0.26	-2.5	23066	209	1.50		0.065
RA4.1	246	-5.2	-0.25	-2.5	11521	115		-.02	
CF6	243	-5.0	-0.20	-2.5	10620	92		-.35	
A12.9	241	-4.8	-0.22	-2.5	15450	129	1.24		.010
CK3.2	238	-4.9	-0.22	-1.8	23200	230		-.04	
A3.9	235	-3.8	-0.21	-4.0	15400	154	1.51		.00
CK3.8	232	-4.7	-0.20	-2.5	29550	230		-0.02	
CK4.2	232	-4.4	-0.20	-4.0	31730	230		0.0	

TABLE 6.6.1

CN4.5	228	-4.3	-0.20	-4.0	32800	230	-0.05
CK3.7	225	-4.3	-0.20	-4.0	20170	138	-0.04
CN11.2	218	-4.0	-0.20	-3.0	38185	230	-.05
CX13.7	220	-3.9	-0.20	-3.0	25255	150	-.38
CK6.0	220	-4.0	-0.20	-4.0	38200	230	-0.02
CN12.4	212	-3.7	-0.20	-3.0	44457	230	-0.04
CK9.8	208	-3.8	-0.20	-3.0	52260	230	-0.02
InSb	202	-3.8	-0.0	-2.0	63070	230	-.44

FIGURE 6.6.3

TEMPERATURE COEFFICIENT OF THE ENERGY GAP versus COMPOSITION

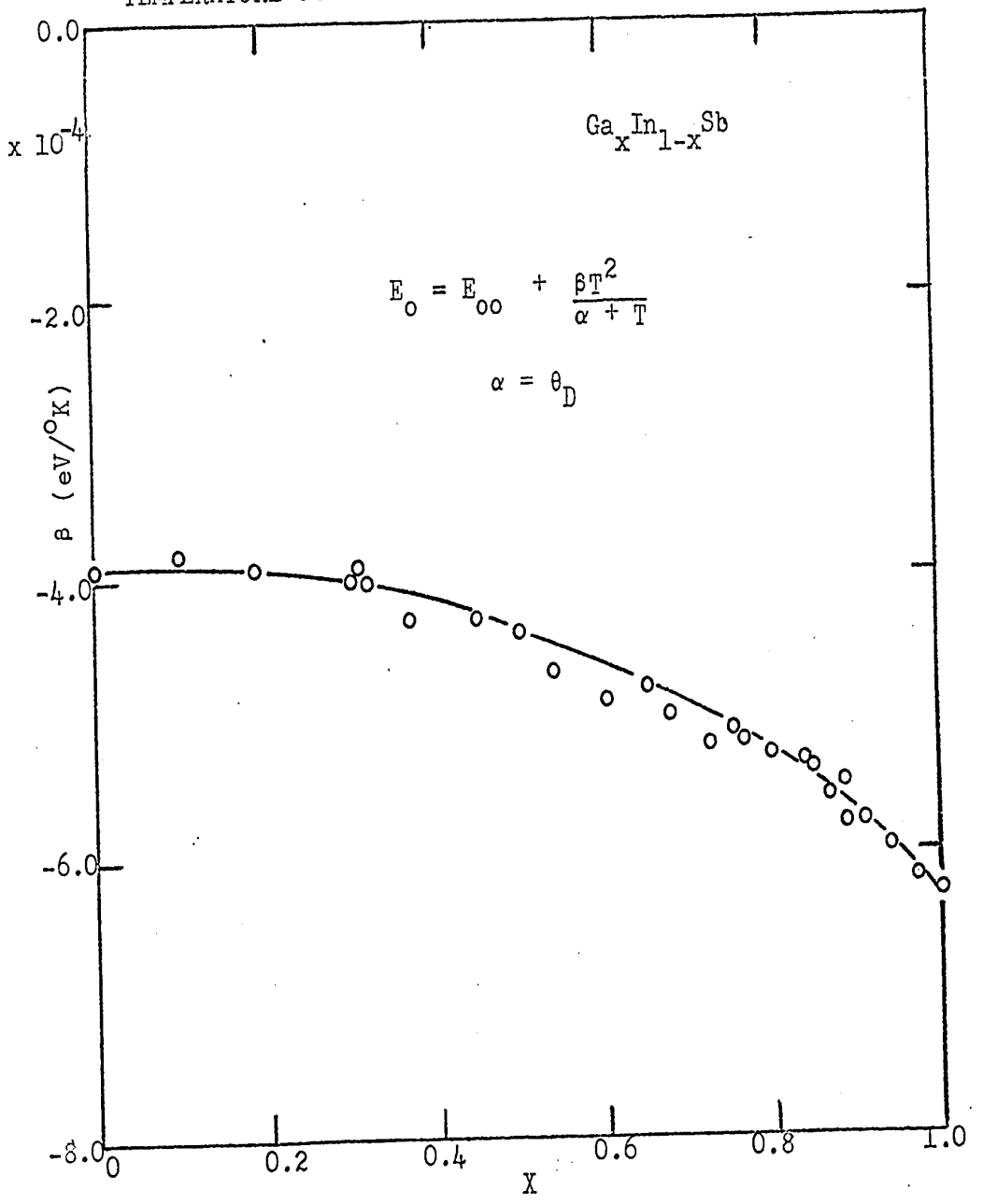

MOBILITY versus COMPOSITION FIGURE 6.6.4

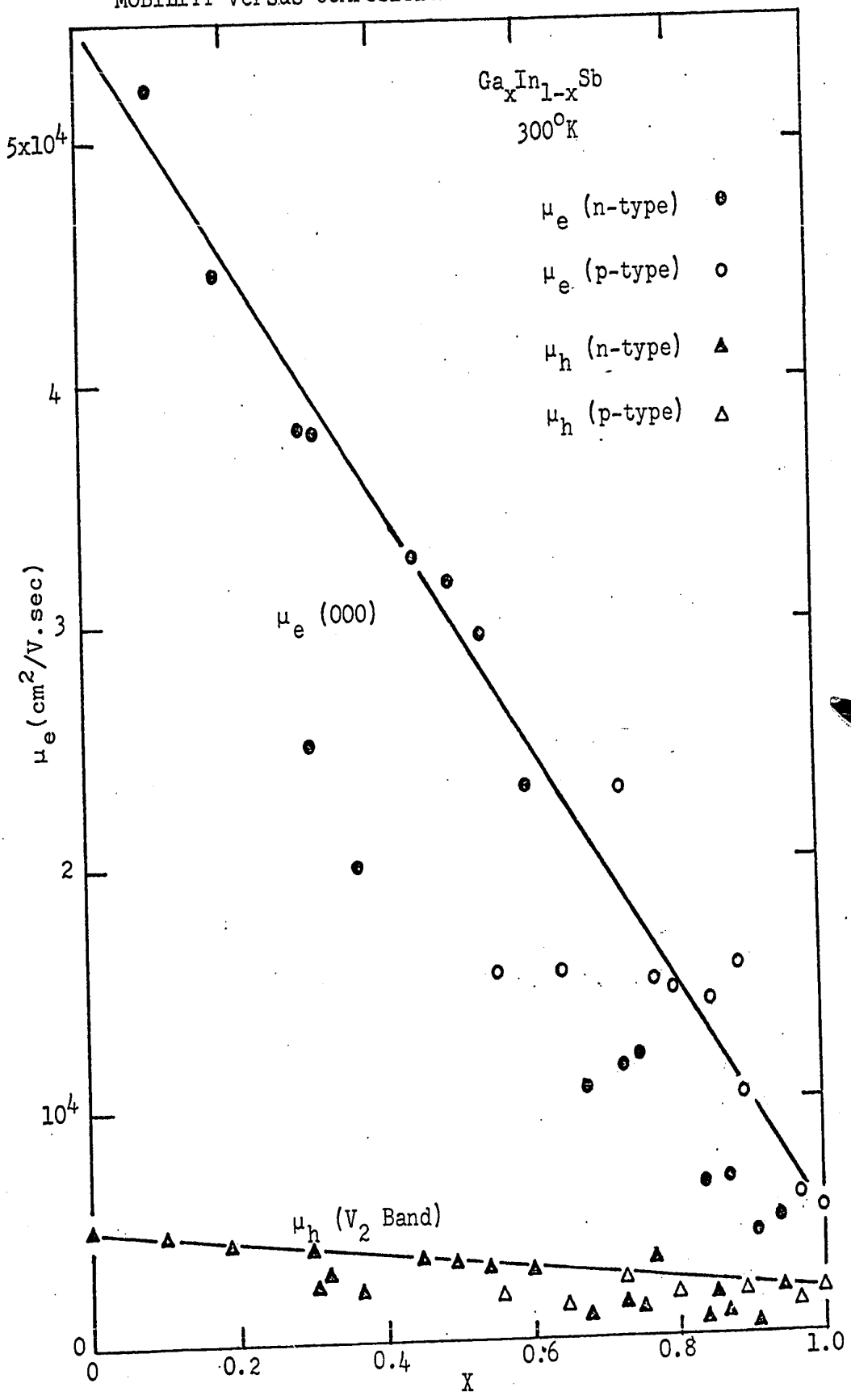

p-type material. The values of the hole mobilities in the light and heavy hole bands are represented by open triangles for p-type material and filled triangles for n-type samples.

The position of the combined mobility indicates which band has the most effective conduction at room temperature. The temperature dependence of the mobility of these alloys is very complex because of the contribution of charge carriers in several band minima. The temperature dependence of the mobility for each type of carrier for a p-type samples with x = 0.73 is shown on figure 6.6.5. For comparison the resultant Hall mobility ($R_H \sigma$) is shown as well. The transitions from p to n-type behaviour is characterized in the resultant mobility and the effect of the upper conduction bands on the mobility is clearly demonstrated at higher temperatures.

6.6.2 $Ga_xIn_{1-x}As$ Results

The various parameter values which were determined from the multiband analysis of this alloy system are given on table 6.6.2. The composition variation of the intrinsic energy gap at absolute zero and at room temperature is shown on figure 6.6.6. The contribution of the ⟨100⟩ conduction band

MOBILITY versus TEMPERATURE FIGURE 6.6.5

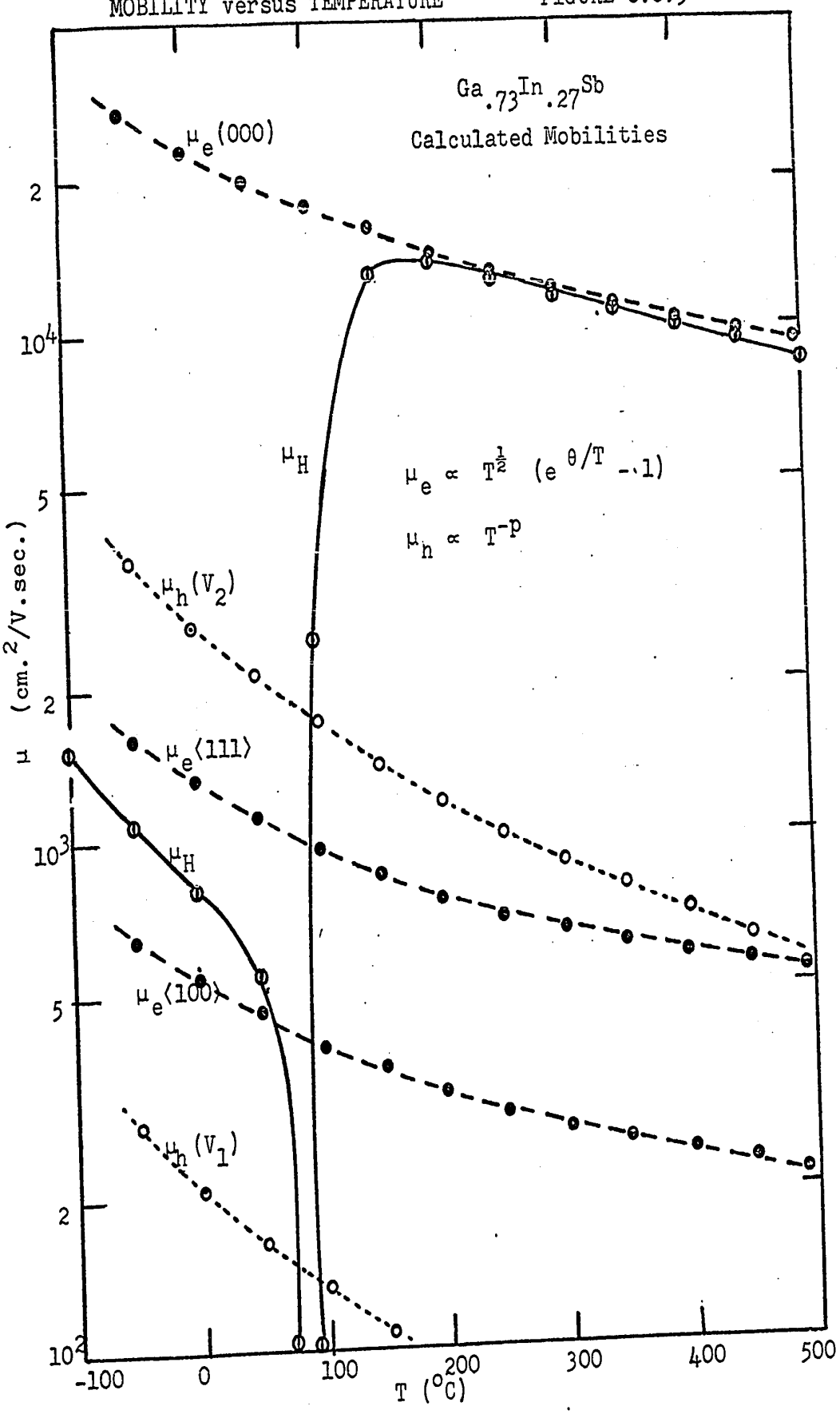

TABLE 6.6.2

$Ga_xIn_{1-x}As$ BAND PARAMETERS

SAMPLE	x (mole-fraction)	Z ($\times 10^{-16}$ cm^{-3})	$m_{h_1}^*/m$	m_{oo}^*/m $m_{h_2}^*/m$	$E_{\theta\theta}$ (eV)	θ (^oK)	β_o ($\times 10^{-4}$ eV/^oK)	$\mu_o(300)$ (cm^3/V.sec)	ε_d (eV)	ΔE_{2o} (eV)
GaAs	1.0	3.53	.68	.07	1.52	345	-6.2	3363	.04	~.37
CY 7.2	.83	17.2	.63	.063	1.20	330	-6.3	4224	-.02	~.44
CT 0.4	.66	5.5	.585	.05	.95	315	-6.1	6627	-.02	---
CT 1.05	.60	6.9	.575	.048	.88	310	-6.0	7743	-.02	---
CT 1.8	.49	7.35	.54	.045	.81	300	-5.9	9058	-.01	---
CT 2.8	.37	12.1	.51	.040	.685	293	-5.7	10452	-.01	---
CT 3.7	.29	12.5	.485	.034	.620	285	-5.6	12622	-.024	---
CT 5.4	.20	13.1	.46	.030	.55	279	-5.5	13327	-.020	---
CT 7.4	.10	21.1	.44	.028	.485	270	-5.4	14492	-.025	---
InAs	0.0	3.32	.41	.026	.426	264	-5.0	27052	-.06	.70(ΔE_{1o})

ENERGY GAP VERSUS COMPOSITION FIGURE 6.6.6

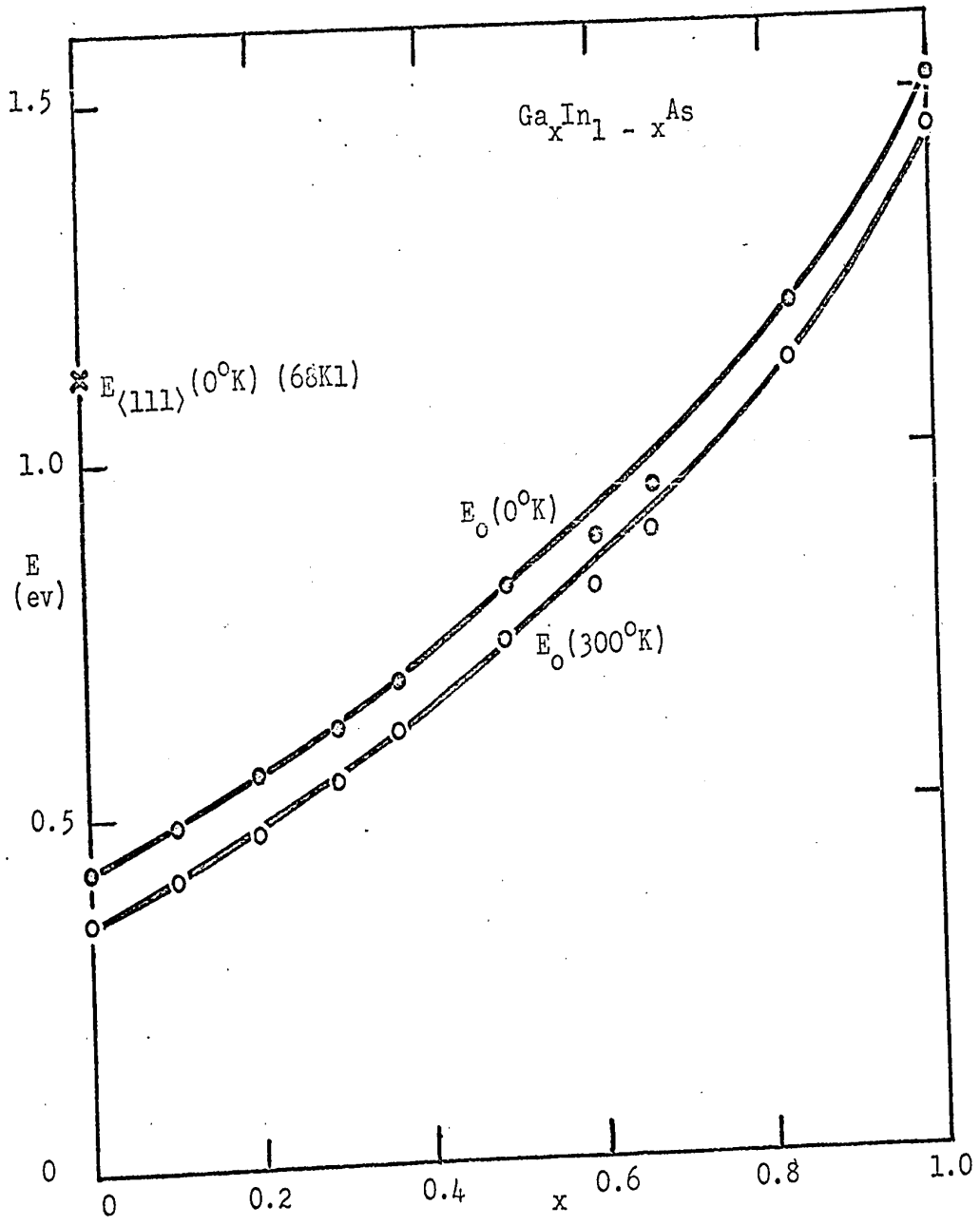

was significant only in the very GaAs rich alloys and the values determined for its position were at best approximate. These are shown on table 6.6.2 and as well the position of the ⟨111⟩ band in InAs as determined by Kwan (68K1) is shown.

The intrinsic energy gap values determined from the present analysis are in good agreement with the best optically determined values (68W1) and the position of the ⟨100⟩ band at ~ 0.38 eV above the (000) band is in approximate agreement with earlier determinations.

The values of the temperature dependence of E_o in this system are presented as a function of composition on figure 6.6.7. It is seen that the composition dependence of this factor is roughly linear.

The electron mobility of $Ga_xIn_{1-x}As$ alloys was found to fit quite well to the temperature dependence predicted for polar scattering. The mobility as a function of temperature from experiments, and calculated by the relation

$$\mu(T) = \mu(0)\, T^{1/2} \left[e^{\theta/T} - 1\right] ,$$

where θ was chosen to be close to the Debye temperature, is shown on figure 6.6.8 for a few alloy specimens.

6.6.3 $InAs_xSb_{1-x}$ Results

Although the effects of higher conduction band minima are negligible in these alloys, it was necessary to apply the

TEMPERATURE COEFFICIENT OF E_o VERSUS COMPOSITION FIGURE 6.6.7

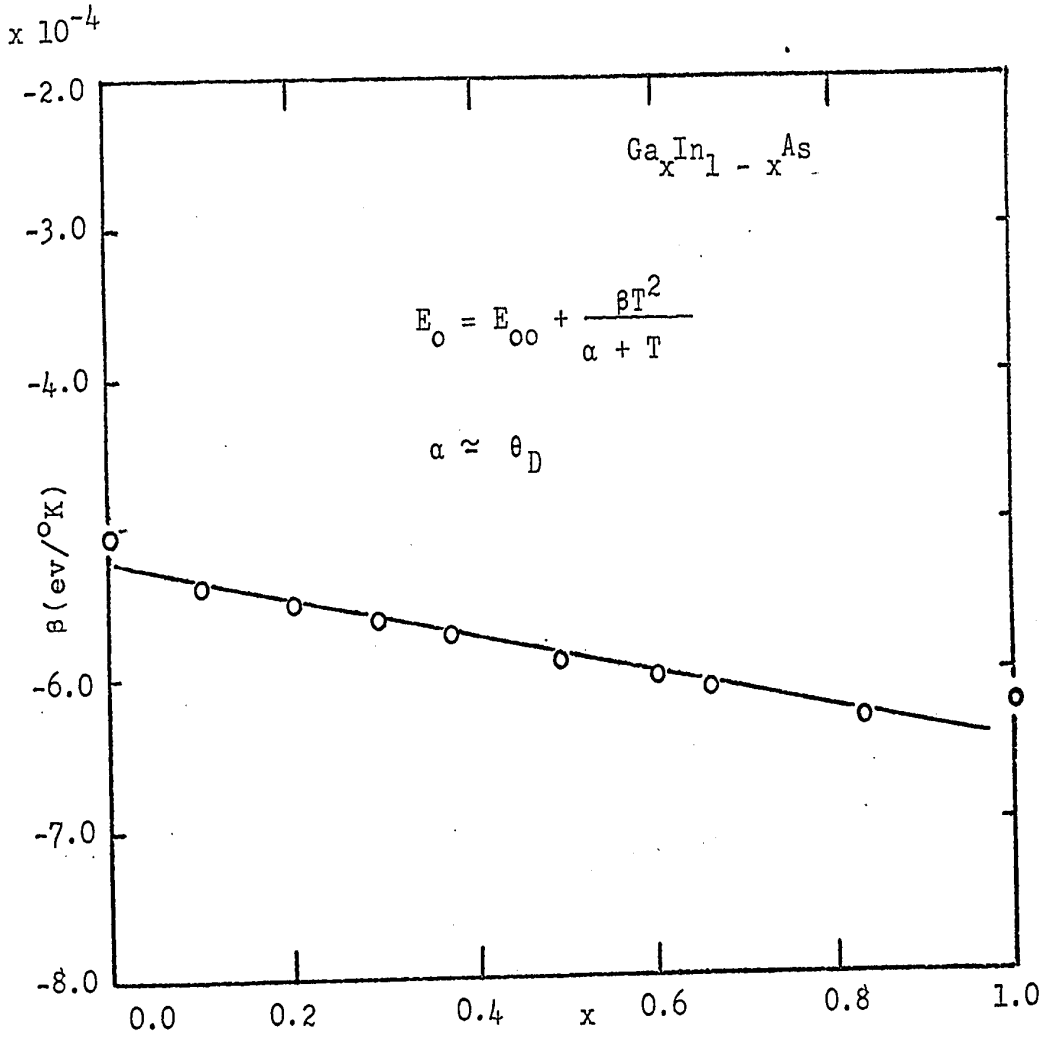

CALCULATED AND EXPERIMENTAL
MOBILITY VERSUS TEMPERATURE

FIGURE 6.6.8

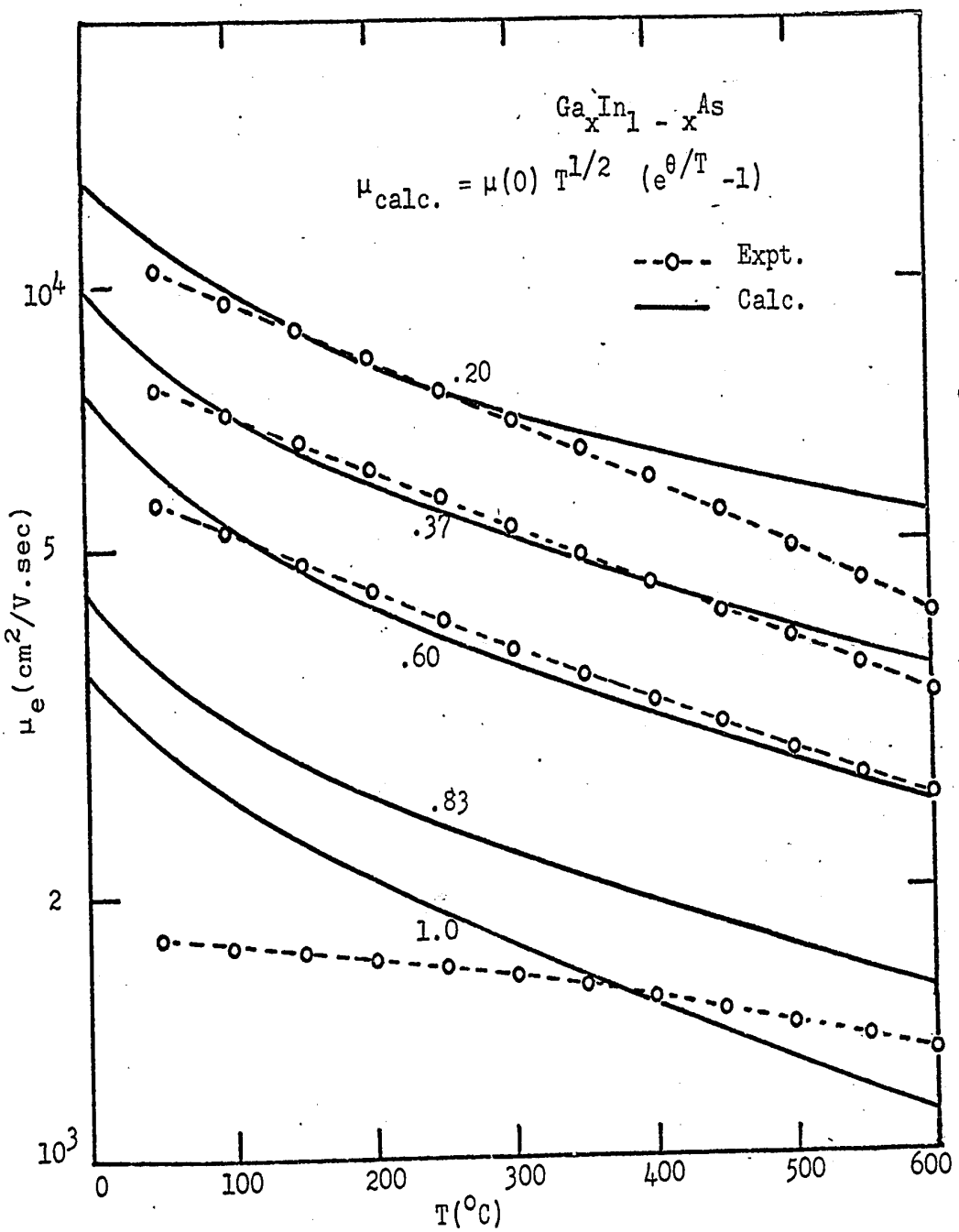

multiband analysis in order to accomodate the conditions of non-parabolicity of the bands and degeneracy of carriers in the conduction band which result from the very small energy gap involved. The parameter values used in and determined by the analysis are given on Table 6.6,3.

The values of the absolute zero and room temperature energy gaps determined are shown as functions of composition on figure 6.6.9. The values of the temperature dependence parameter β are shown on figure 6.6.10.

Since the alloys do not exhibit multiband conduction, the mobility obtained by the two band analysis is valid for the (000) electrons (see figure 6.4.12).

The temperature dependence of mobility predicted by polar scattering alone is not in complete agreement with the observed experimental results. On figure 6.6.11, the polar dependence

$$\mu \propto (e^{\theta/T} - 1) \quad T^{1/2}$$

is compared with the experiments. The deviations are presumably due to the effect of electron-hole scattering which can be shown to be very significant in these alloys (69V2) at high temperatures.

TABLE 6.6.3

$InAs_xSb_{1-x}$ BAND PARAMETERS

SAMPLE	X (mole-fraction)	$-Z \times 10^{-16}$ (cm^{-3})	$m_{h_1}^*/m$	$m_{h_2}^*/m$	m_{oo}^*/m	E_{oo} (eV)	θ_D (^oK)	$\beta_o \times 10^4$ (eV/^oK)	$\mu_o(300)$ (cm^2/V.sec)	ε_d (eV)
InAs	1.0	3.3	.41	.026		.426	264	-5.1	27050	-.06
CE 1.0	.95	3.94	.40	.023		.41	260	-4.6	15155	-.05
CE 3.0	.88	13.3	.39	.020		.32	240	-4.5	14100	-.05
CV 2.45	.80	12.7	.38	.018		.26	220	-4.4	21637	-.05
CV 3.05	.68	6.35	.40	.015		.19	211	-4.0	29806	-.20
CV 3.35	.54	5.14	.40	.013		.17	195	-3.7	39131	-.15
CV 3.6	.37	6.2	.41	.012		.162	185	-3.6	42688	-.03
CV 4.1	.27	1.7	.40	.010		.160	185	-3.6	56743	-.05
CE 4.3	.17	0.41	.38	.012		.176	190	-3.7	60141	-.03
CE 8.15	.09	1.39	.40	.013		.195	195	-3.7	--	-.05
InSb	.00	2.06	.40	.0155		.24	202	-3.8	63070	-.44

ENERGY VERSUS COMPOSITION

FIGURE 6.6.9

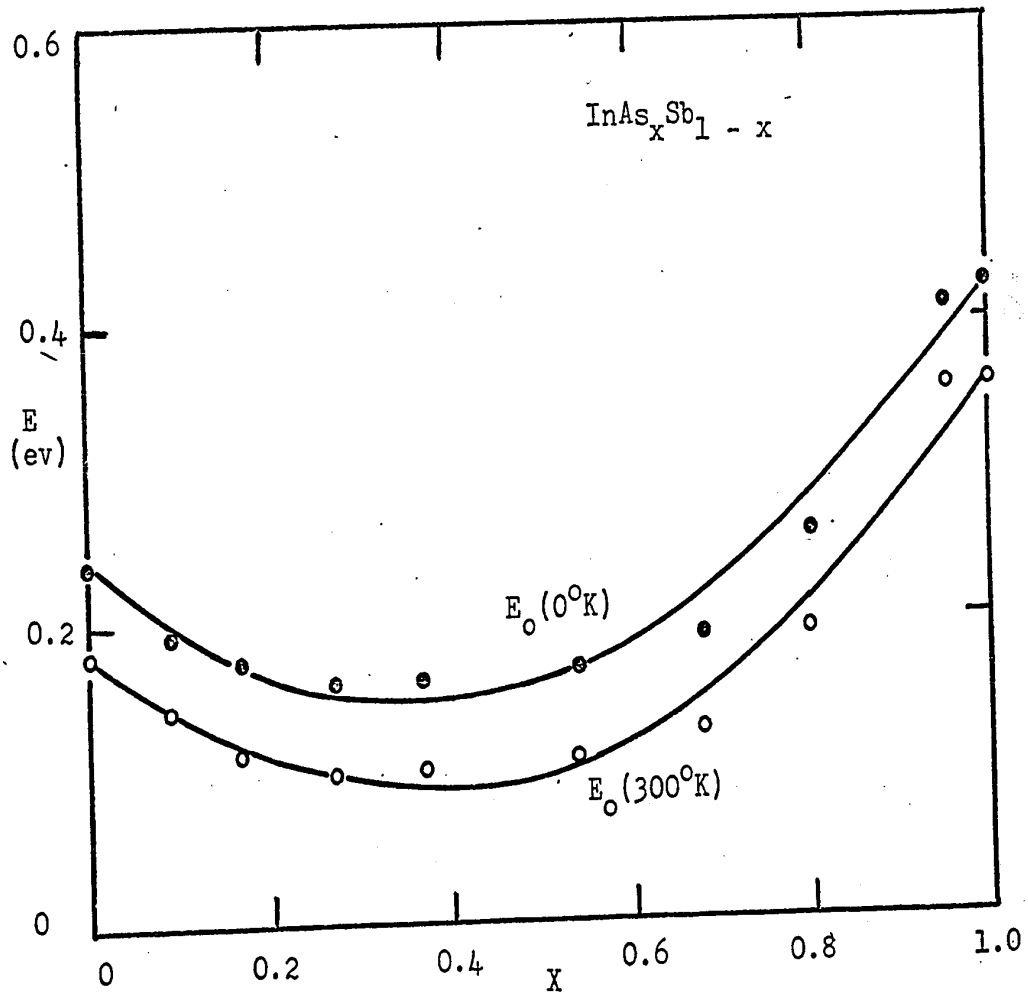

TEMPERATURE COEFFICIENT OF E_o VERSUS COMPOSITION

FIGURE 6.6.10

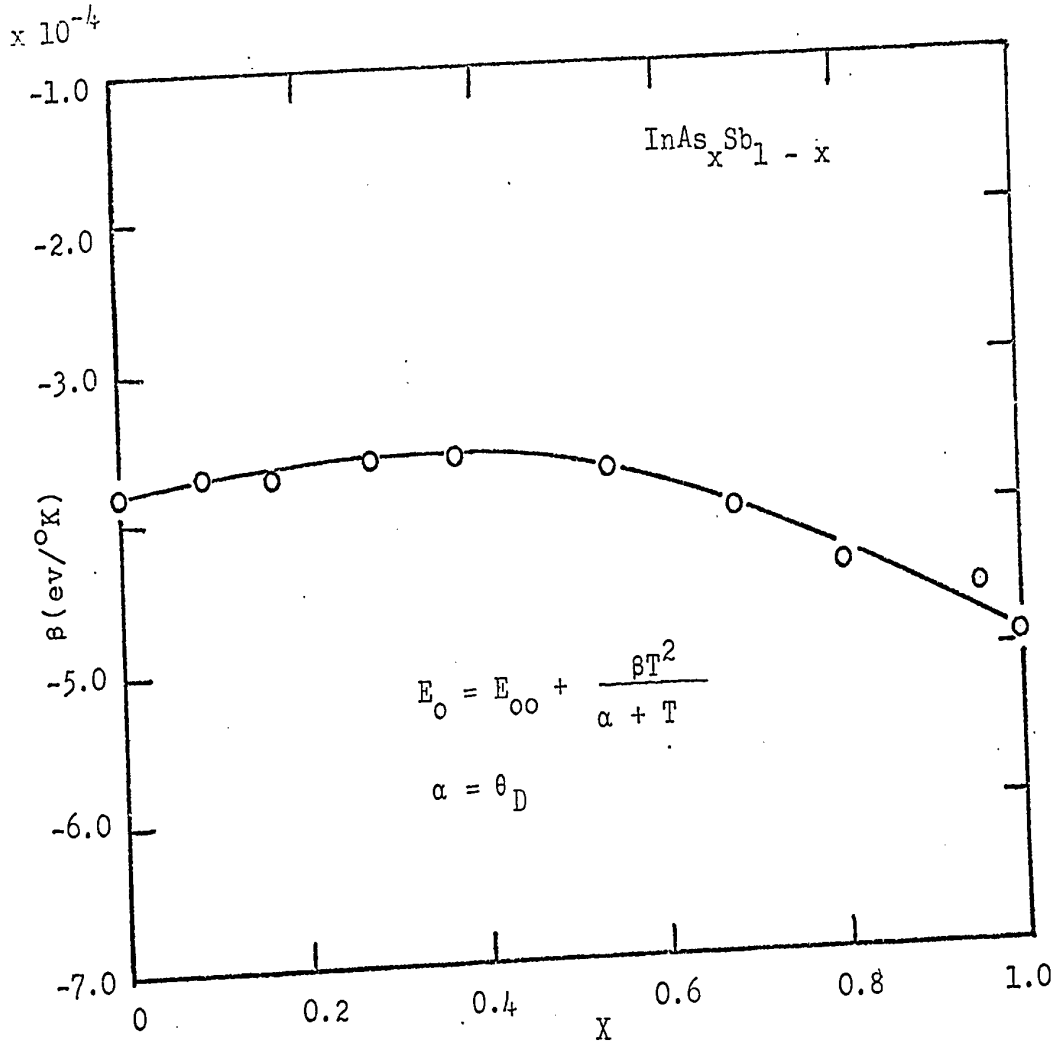

CALCULATED AND EXPERIMENTAL
MOBILITY VERSUS TEMPERATURE

FIGURE 6.6.11

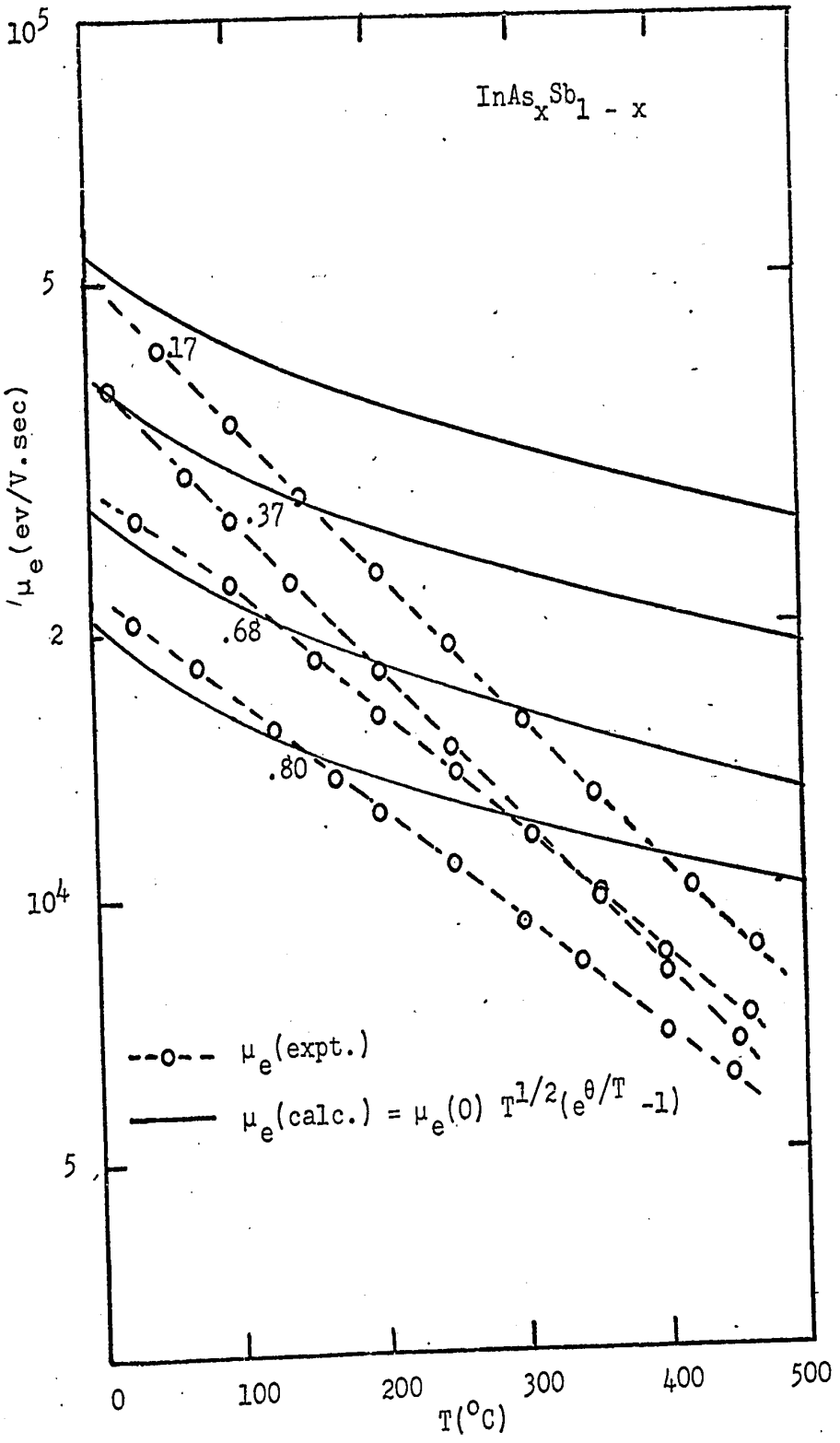

6.7 Discussion of Results

$InAs_xSb_{1-x}$ alloys are the only III - V materials known where the temperature dependence and the small magnitude of the energy gap allow the intrinsic energy gap to close completely at temperature below the melting point of the material. In the middle composition region this occurrance takes place at temperatures as low as 350°C, according to the calculated temperature variation of the gap. What happens to the various bands after they cross at $k = 0$ is not known. The Hall and resistivity experiments indicated that there is no significant change in the properties of the material as the band gap closes, but the Kane type analysis becomes invalid as the non-parabolic terms in equation [4.32] begin to dominate, and the calculated Hall coefficient values begin to increase with increasing temperature.

On figure 6.7.1 the experimental and calculated Hall coefficients are contrasted to show the effect of this phenomenon.

As a result of the very small electron effective masses in these alloys, and because the energy gap is small as well, the Fermi level is several kT above the bottom of the (000) band at elevated temperatures. The position of the Fermi level and of the conduction band relative to the top of the valence band is shown on figure 6.7.2 as functions of temperature. The approximate values of E_o^* and of the corresponding kT's are shown

HALL COEFFICIENT VERSUS TEMPERATURE FIGURE 6.7.1

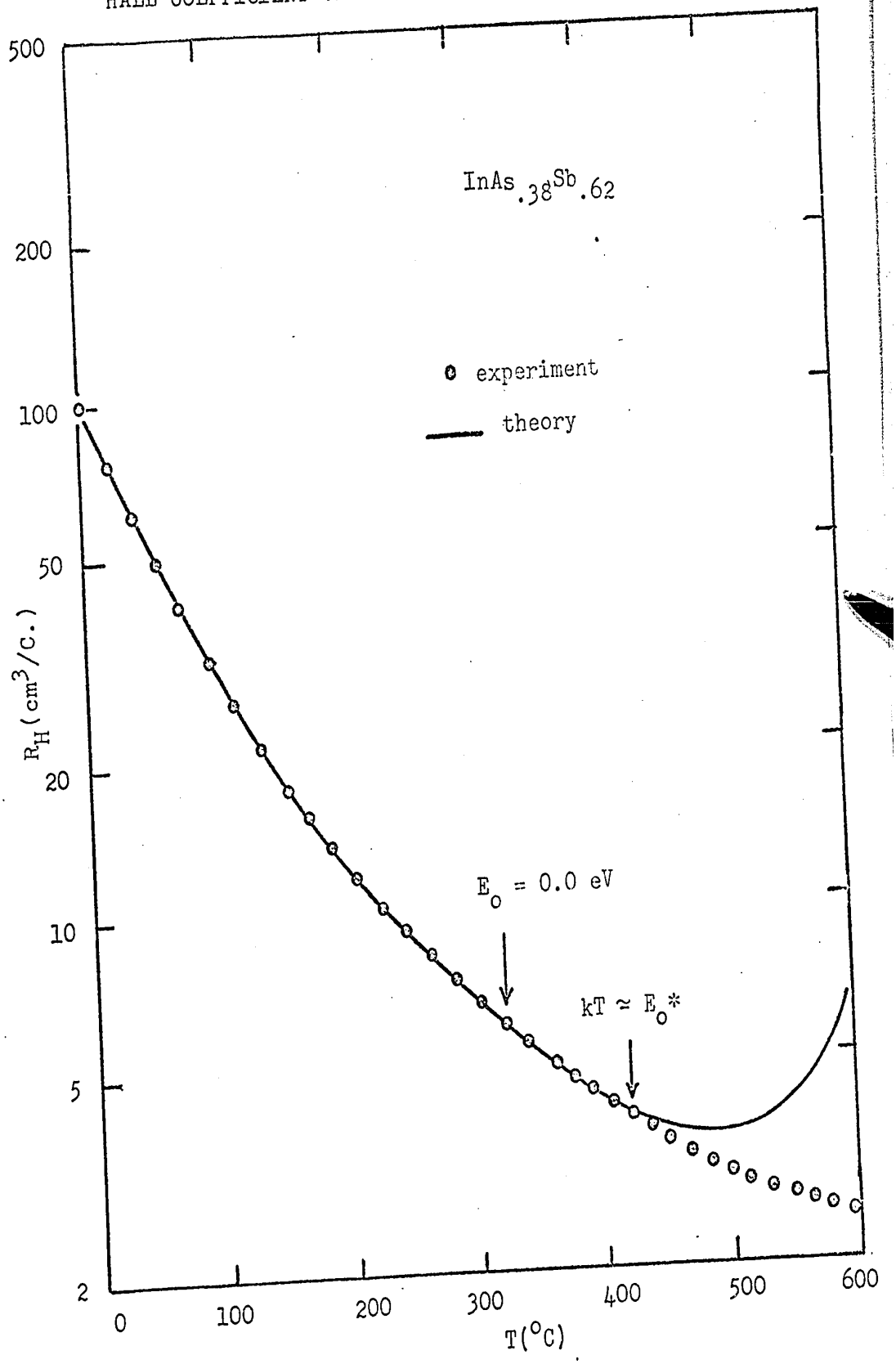

as well. It can be seen by comparing figures 6.7.1 and 6.7.2 that the calculated R_H values begin to deviate from the experimental values only when the ratio $kT/E_o^* > 1$. In this range the Kane type carrier concentration relations are no longer valid.

Some useful information can be obtained from the multi-band analysis in the course of its application. Since, in order to obtain values for the Hall constant at various temperatures, it is necessary to evaluate the carrier concentrations in each band; the variations of these carrier concentrations have been obtained for each specimen. Figure 6.7.3 shows the temperature dependence of the various carrier concentrations in a typical p-type alloy specimen where the subsidiary band contributions are significant. From this figure it is easy to see where the contributions of the various bands begin to become significant in turn. The Hall coefficient variation is plotted on the same figure in order to show the correlated effects of the carrier variations on the Hall effect.

Another interesting "spin-off" from the multiband analysis is the temperature dependence of the density of states effective electron mass. This variation is shown on figure 6.7.4 for a few samples of $Ga_xIn_{1-x}Sb$ alloys where the effect of non-parabolicity is known to be great. The density of states effective mass values were obtained by substituting the carrier concentrations values from the Kane type band calculation of

FIGURE 6.7.2

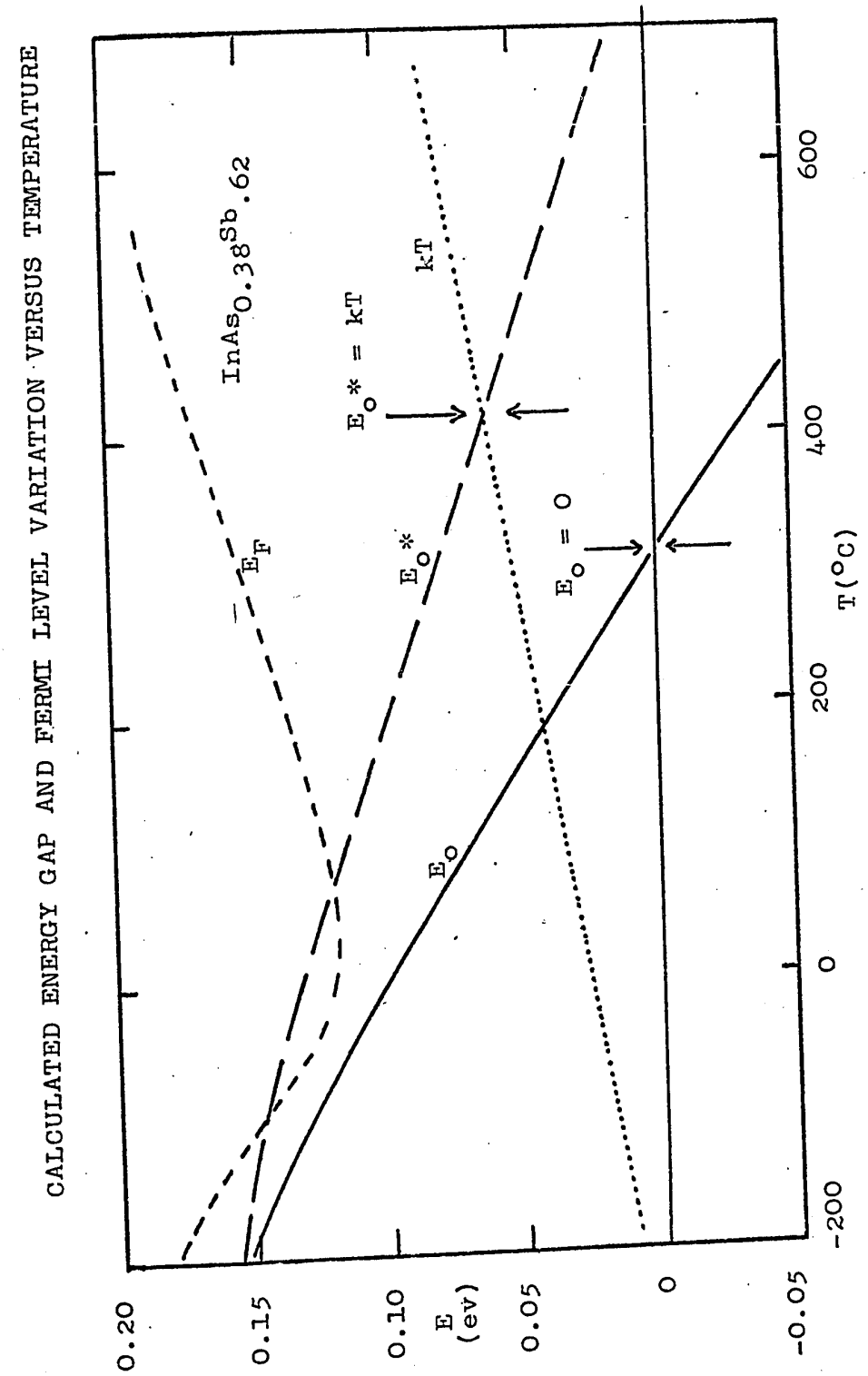
CALCULATED ENERGY GAP AND FERMI LEVEL VARIATION VERSUS TEMPERATURE
InAs0.38Sb.62
E = kT
kT
E*
E = 0
E
E
(ev)
T(°C)
0.20
0.15
0.10
0.05
0
-0.05
-200
0
200
400
600

FIGURE 6.7.3

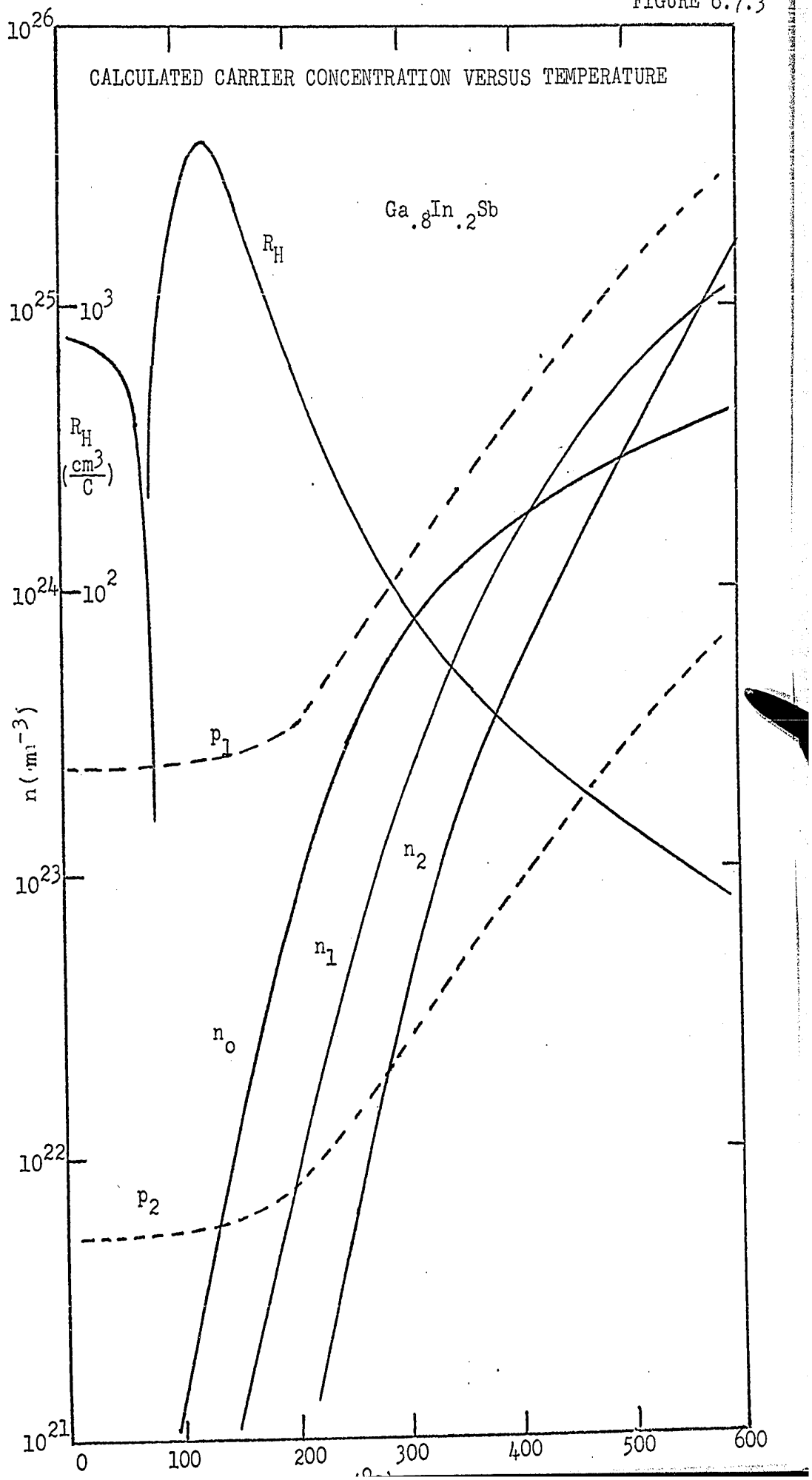
CALCULATED CARRIER CONCENTRATION VERSUS TEMPERATURE
Ga .8In .2Sb
10^{26}
10^{25}
10^{24}
10^{23}
10^{22}
10^{21}
10^3
10^2
R_H
R_H ($\frac{cm^3}{C}$)
$n(m^{-3})$
p_1
p_2
n_o
n_1
n_2
0
100
200
300
400
500
600

DENSITY OF STATES EFFECTIVE MASS
VERSUS TEMPERATURE

FIGURE 6.7.4

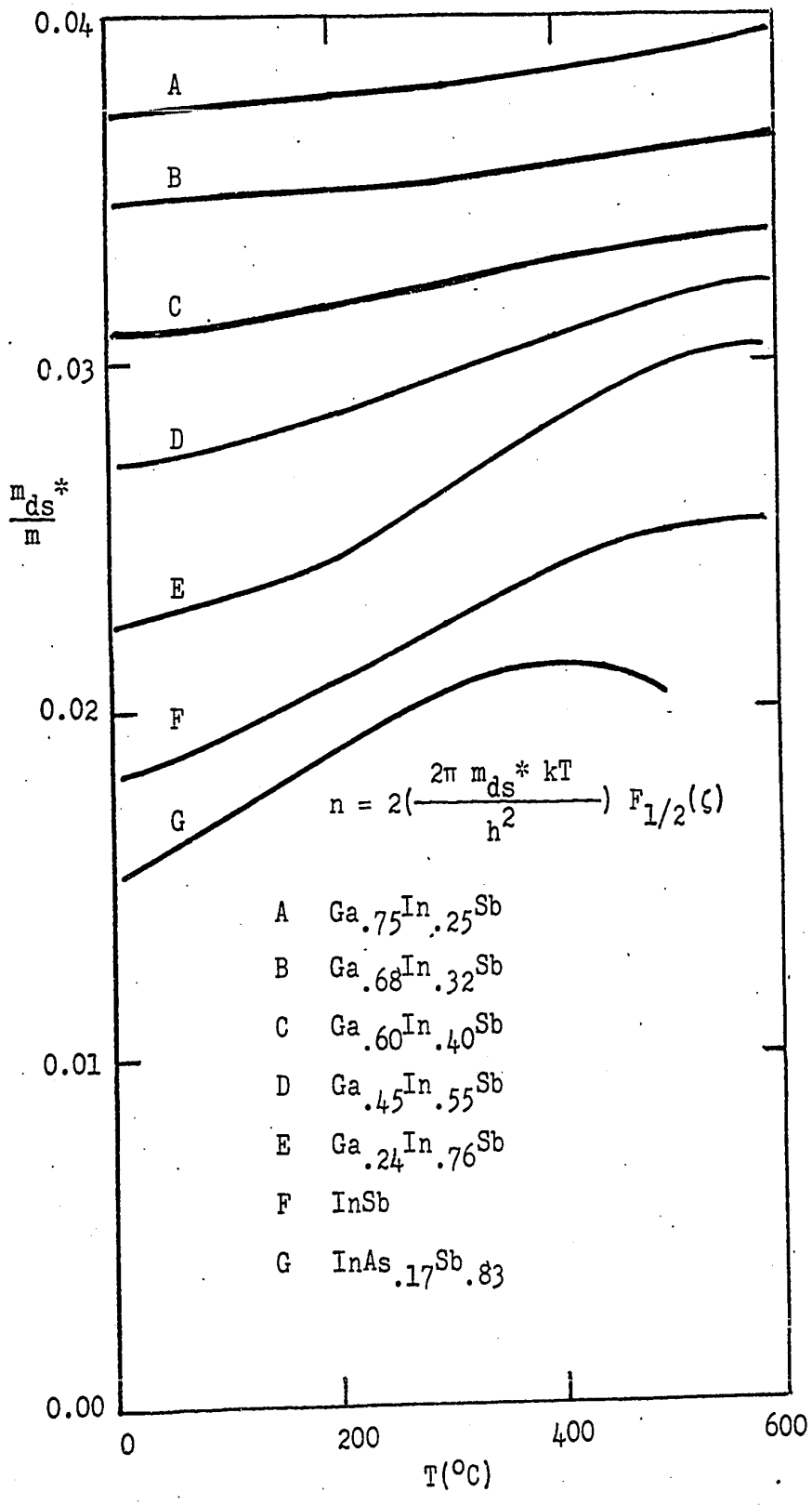

of equation [4.32] into a parabolic band carrier density equation of the form of equation [4.9] using the values of the Fermi level determined from the multiband analysis. The effect mass parameter in equation [4.9] was then determined by the satisfaction of the equation. It can be seen on figure 6.7.4 that the density of states effective mass can change drastically with temperature because of the effect of non-parabolicity.

CHAPTER VII

CONCLUSIONS

7.1 Alloy Preparation

Homogeneous alloy material over the complete composition range has been prepared for three III - V alloy systems: $Ga_xIn_{1-x}Sb$, $Ga_xIn_{1-x}As$ and $InAs_xSb_{1-x}$. Various methods of preparation have been investigated and it has been shown that the step freeze method is the most efficient, practical, and successful growth technique for the above mentioned systems. Some investigations into other more difficult alloy systems have indicated that slow zone recrystallization would be the only practical method for attaining homogeneous material.

7.2 Electrical Measurement

The Hall effect and the resistivity over a very wide temperature range were measured in samples from each of the alloy systems prepared. These measurements were carried out at temperature intervals of five degrees from 300°K to 1000°K where possible.

The results of these measurements were used in a standard two band analysis and values of E_{oo}, the intrinsic energy gap extrapolated to 0°K, and μ_e, the electron mobility were determined as functions of composition. It was shown in all three alloy systems that the energy gap exhibits a parabolic dependence with composition while the mobility varies roughly linearly across an alloy range.

7.3 Multiband Analysis

Because the materials investigated were not accurately described in the assumption of the two band analysis, a procedure enabling considerations of such factors as multiplicity of bands, non-parabolicity of bands and electron degeneracy was developed. This multiband analysis was applied to each of the three alloy systems and as a result values of the positions of subsidiary energy bands were obtained where such bands were significant. As well, the temperature dependence of the intrinsic energy gap and of the subsidiary bands was determined.

7.4 Future Work and Suggestions

Construction of a narrow zone zone-recrystallization furnace has been started in these laboratories for the purpose of preparing alloy material of the systems $GaAs_xSb_{1-x}$ and $InAs_xSb_{1-x}$. For the former system this should produce homogeneous material in the middle composition region for the first time, for the latter systems it is hoped that this method will increase the availability of material in the middle composition range.

Studies will soon commence on the effect of hydrostatic pressure on the electrical properties of the III - V alloys. This work will allow the positions of the higher conduction bands to be determined in an independent manner and will thus correlate with the high temperature results.

The method of the multiband analysis will be used to determine the energy band separation between the (000) and higher conduction bands in the $GaAs_{1-x}P_x$ alloy system. Measurements of the electrical properties will be carried out on the apparatus described in chapter V. There is considerable interest in this system since it features energy gaps large enough to permit luminescence in the visible wavelength spectrum. It is in these materials too that the phenomenon of Gunn effect oscillations is observed. For these effects, it is important to determine the various band parameters involved.

These can be determined using the methods of analysis described herein.

Using data from the present work, Varshni (69V2) has compared the mobility as functions of temperature and alloy composition from theoretical calculations with the experimental results. In this work, which will soon be published, Varshni has shown that the electron mobility of alloys of the $Ga_xIn_{1-x}As$ system is dominated by polar scattering mechanisms which alone are sufficient to predict the magnitude of thermal variation of the mobility. In the $InAs_xSb_{1-x}$ alloys he has shown that electron-hole scattering is of almost equal importance with polar scattering in determinig the electron mobility. In neither case was any significant contribution attributable to alloy scattering noted.

The multiband analysis may be modified to treat the electrical results of the alloys of the $Pb_{1-x}Sn_xTe$ and $Pb_{1-x}Sn_xSe$ systems which are being obtained at the present time in these laboratories. These alloys feature conduction in two separated valence bands and one conduction band.

Another interesting study which suggested by the present work is an investigation into the behaviour of semiconducting material when the intrinsic energy gap is reduced to zero at higher temperatures.

```
FORTRAN IV G LEVEL 1, MOD 3          MAIN          DATE = 69087          09/44/09

C
C
C
C
C     FIVE BAND CALCULATIONS
C     ALL BANDS ,  DEGENERATE STATISTICS
C     (000) BAND :  NON-PARABOLIC      V2 BAND :   NON-PARABOLIC
      DIMENSION ETA(300),F(300),F32(300),F52(300),F72(300)
0001  READ(1,8)(ETA(I),F(I),F32(I),F52(I),F72(I), I=1,235)
0002
0003 8 FORMAT(F10.4,4E14.7)
0004  READ(1,1) NDECKS
0005 1 FORMAT(I5)
C
C     DATA & DEFINITIONS
C
0006  AK=8.6168E-05
0007  DEG=2.*3.14159**(-0.5)
0008  H=4.1356E-15
0009  E=1.602E-19
0010  C=2.9979E+10
0011  DO 7  J=1,NDECKS
0012  TK=73.1600
0013  READ(1,4)NA,ME,EX,PA,ENA,EDO,EA,THE,PMU,POWE,PAWN
0014 4 FORMAT(2A3,F5.3,2E11.3,2F6.3,2F6.1,F6.3,F6.0)
0015  WRITE(3,82)     PA,ENA,EDO,EA,THE,PMU,POWE,PAWN
0016 82 FORMAT(1H1,2E12.4,2F10.3,2F10.2,F10.3,F10.3)
0017  READ(1,2 )PM,AME,AM1,AM2,E00,E10,E20,BE0,BE1,BE2,B0
0018  WRITE(3,2)PM,AME,AM1,AM2,E00,E10,E20,BE0,BE1,BE2,B0
0019 2 FORMAT(7F5.3,3E9.2,F6.1)
0020  WRITE(3,3) NA,ME
0021 3 FORMAT(//1X,2A3/)
0022  WRITE(3,84) EX
0023 84 FORMAT(1X,F4.2,'  NO        N1        N2        PHEAVY
     1     PLIGHT      RH        T      RHO      EF       EG     MN*DS  MP*
     2DS       MU       B0'//)
C
C     PRELIMINARY CALCULATIONS
C
0024  DO 6 K=1,18
0025  TK=TK+50.0
0026  TC=TK-273.16
0027  AKT=AK*TK
0028  EG=    (E00+BE0*TK*TK/(TK+THE))
```

```
C
C
C
C
0029            EGSTAR=E00-(E00-EG)/3.
0030            IF(EG.LT.-0.1) GO TO 7
0031            IF(EGSTAR.LT.0.0) GO TO 7
0032            AM0=AMF*EGSTAR/E00
0033            AMP=AM0
0034            POWN=THF+PAWN
0035            POWG=(EXP(POWN/TK)-1.0)/(EXP(POWN/300.0)-1.0)
0036          200 B0=B0*(TK/300.0)**POWE*POWG*(TK/300.0)**0.5
0037          201 B1=(AM0/AM1)**(3./2.)*B0
0038            B2=(AM0/AM2)**(3./2.)*B0
0039            E1=E10+BE1*TK
0040            E2=E20+BE2*TK
0041            EF=-EG
0042            AA=2.*3.14159*5.11*10.**5*AK/(H*C)**2
0043            L=1
0044         1010 N=1
0045            M=1
C
C       (100) CONDUCTION BAND
C
0046            IF(((EF-E2)/AKT).LT.-170.0) GO TO 4000
0047            IF((EF-E2)/AKT+9.8) 10,10,3102
0048              10 AN2=-6.*(AA*TK*AM2)**1.5*EXP((EF-E2)/(  AKT))*2.0
0049            GO TO 4401
0050          3102 DO 3500 I=1,235,10
0051            IF((EF-E2)/AKT-ETA(I)) 3330,3301,3500
0052          3500 CONTINUE
0053          3330 DO 30 IA=1,10,1
0054            IF((EF-E2)/AKT-ETA(I-IA)) 30,9301,40
0055            30 CONTINUE
0056          9301 I=I-IA
0057          3301 FERMO=F(I)
0058            70 M=1
0059            72 GO TO 3103
0060            40 I=I-IA
0061          3300 UM=(F(I-1)-F(I))/(ETA(I-1)-ETA(I))
0062            73 M=1
0063            75 FERMO=F(I)+UM*((EF-E2)/AKT-ETA(I))
0064          3103 AN2=-DEG*6.*(AA*TK*AM2)**1.5*FERMO*2.0
```

```
C
C
C
C
0065            GO TO 4401
0066       4000 AN2=0.0
C
C       (111) CONDUCTION BAND
C
0067       4401 IF(((EF-E1)/AKT).LT.-170.0) GO TO 4402
0068       3111 IF((EF-E1)/(AK*TK)+9.80) 2001,2001,2002
0069       2001 AN1=-8.*(AA*TK*AM1)**1.5*EXP((EF-E1)/(2*AKT))*EXP((EF-E1)/(2*AKT))
0070            GO TO 4403
0071       2002 DO 1500 I=M,235,10
0072            IF((EF-E1)/AKT-ETA(I)) 1330,1301,1500
0073       1500 CONTINUE
0074       1330 DO 32 IA=1,10,1
0075            IF((EF-E1)/AKT-ETA(I-IA)) 32,8301,41
0076         32 CONTINUE
0077       8301 I=I-IA
0078       1301 FERME=F(I)
0079            IF(I-10) 76,76,77
0080         77 N=I-10
0081            GO TO 78
0082         76 N=1
0083         78 GO TO 9
0084         41 I=I-IA
0085       1300 EM=(F(I-1)-F(I))/(ETA(I-1)-ETA(I))
0086            IF(I-10) 79,79,80
0087         80 N=I-10
0088            GO TO 81
0089         79 N=1
0090         81 FERME=F(I)+EM*((EF-E1)/(AK*TK)-ETA(I))
0091          9 AN1=-8.*DEG*(AA*TK*AM1)**1.5*FERME
0092            GO TO 4403
0093       4402 AN1=0.0
C
C       (000) CONDUCTION BAND
C
0094       4403 IF((EF/AKT).LT.-170.0) GO TO 4404
0095         19 IF(EF/(AK*TK)+9.80) 2011,2011,2012
0096       2011 FERMI=EXP(EF/AKT)/DEG
0097            F32S=1.33*EXP(EF/AKT)/DEG
```

```
                C
                C
                C
                C
0098                  F52S=3.33*EXP(EF/AKT)/DEG
0099                  F72S=11.633*EXP(EF/AKT)/DEG
0100                  GO TO 2999
0101             2012 DO 500 I=N,235,10
0102                  IF(EF/AKT-ETA(I)) 330,301,500
0103              500 CONTINUE
0104              330 DO 34 IA=1,10,1
0105                  IF(EF/AKT-ETA(I-IA)) 34,901,42
0106               34 CONTINUE
0107              901 I=I-IA
0108              301 FERMI=F(I)
0109                  GO TO 29
0110               42 I=I-IA
0111              300 AM=(F(I-1)-F(I))/(ETA(I-1)-ETA(I))
0112                  FERMI=F(I)+AM*(EF/(AK*TK)-ETA(I))
0113               29 DETAS=EF/AKT-ETA(I)
0114                  DELETA=ETA(I-1)-ETA(I)
0115                  AM32=(F32(I-1)-F32(I))/DELETA
0116                  AM52=(F52(I-1)-F52(I))/DELETA
0117                  AM72=(F72(I-1)-F72(I))/DELETA
0118                  F32S=F32(I)+AM32*DETAS
0119                  F52S=F52(I)+AM52*DETAS
0120                  F72S=F72(I)+AM72*DETAS
0121             2999 BETA=AKT/EGSTAR
0122                  DELFER=BETA*(2.5-5.*AMO)*F32S+BETA*BETA*(7./8.-10.5*AMO)*F52S
                     1-(.25+3.5*AMO)*BETA**3*F72S
0123                  ANO=-2.*DEG*(AA*TK*AMO)**1.5*(FERMI+DELFER)
0124                  AMD=AMO*(1.+DELFER/FERMI)**(0.66667)
0125                  GO TO 4407
0126             4404 ANO=0.0
                C
                C     VALENCE BAND
                C
0127             4407 IF(-(EF+EG)/AKT.LT.-170.0) GO TO 6666
0128                  BETA=AKT/EGSTAR
0129                  IF(-(EF+EG)/AKT+9.8) 3001,3001,3000
0130             3001 PCAL =  2.*(AA*TK*PM )**1.5*EXP(-(EF+EG)/(AK*TK))
0131                  FERMA=EXP(-(EF+EG)/AKT)/DEG
0132                  F32S=1.33*EXP(-(EF+EG)/AKT)/DEG
```

```
C
C
C
C
0133          F52S=3.33*EXP(-(EF+EG)/AKT)/DEG
0134          F72S=11.633*EXP(-(EF+EG)/AKT)/DEG
0135          DELFER=BETA*(2.5-5.*AMP)*F32S+BETA*BETA*(7./8.-10.5*AMP)*F52S
             1-(.25+3.5*AMP)*BETA**3*F72S
0136          PNPAR=2*DEG*(AA*TK*AMP)**1.5*(FERMA+DELFER)
0137          GO TO 3005
0138    3000  DO 3004 I=1,235,10
0139          IF(-(EF+EG)/AKT-ETA(I)) 3032,3003,3004
0140    3004  CONTINUE
0141    3032  DO 36 IA=1,10,1
0142          IF(-(EF+EG)/AKT-ETA(I-IA)) 36,9003,43
0143      36  CONTINUE
0144    9003  I=I-IA
0145    3003  FERMA=F(I)
0146          GO TO 3006
0147      43  I=I-IA
0148    3002  DM=(F(I-1)-F(I))/(ETA(I-1)-ETA(I))
0149          FERMA=F(I)+DM*(-(EF+EG)/AKT-ETA(I))
0150    3006  PCAL =DEG*2.*(AA*TK*PM )**1.5*FERMA
0151          DETAS=(-(EF+EG)/AKT)-ETA(I)
0152          DELETA=ETA(I-1)-ETA(I)
0153          AM32=(F32(I-1)-F32(I))/DELETA
0154          AM52=(F52(I-1)-F52(I))/DELETA
0155          AM72=(F72(I-1)-F72(I))/DELETA
0156          F32S=F32(I)+AM32*DETAS
0157          F52S=F52(I)+AM52*DETAS
0158          F72S=F72(I)+AM72*DETAS
0159          DELFER=BETA*(2.5-5.*AMP)*F32S+BETA*BETA*(7./8.-10.5*AMP)*F52S
             1-(.25+3.5*AMP)*BETA**3*F72S
0160          PNPAR=2*DEG*(AA*TK*AMP)**1.5*(FERMA+DELFER)
0161          GO TO 3005
0162    6666  PCAL=0.0
0163          PNPAR=0.0
0164    3005  SUM=AN0+AN1+AN2
0165          PCALC=PCAL +PNPAR
0166          PMDS=AMP*(1+DELFER/FERMA)**(0.666667)
0167          BH=PM/PMDS
C
C       EXTRINSIC CARRIER ACTIVATION
```

```
                C
                C
                C
                C
                C
0168             6667 ED=EDO
0169                  IF((-(ED+EF)/AKT).GT.+170.0) GO TO 4405
0170                  ENDL=ENA/(1.0+0.5*EXP(-(ED+EF)/AKT))
0171                  GO TO 4406
0172             4405 ENDL=0.0
0173             4406 PAL1=PA/2./(1.0+0.5*EXP((EF+EG-EA)/AKT))
0174                  PAL2=PA/2./(1.0+0.5*EXP((EF+EG-0.5*EA)/AKT))
0175                  PAL=PAL1+PAL2
0176                  X=PA-PAL+ENA-ENDL
0177                  IF(X) 90,90,91
                C
                C     FINDING THE FERMI LEVEL FOR P-TYPE
                C
0178               91 P=X-SUM
0179                  GO TO (4007,4008,4009),L
0180             4007 IF(PCALC-P)4011,4001,4006
0181             4006 EF=EF+.01
                C     FINDING THE FERMI LEVEL FOR N-TYPE
0182                  GO TO 1010
0183             4011 L=2
0184             4008 IF(P-PCALC) 4100,4001,4110
0185             4110 EF=EF-.001
0186                  GO TO 1010
0187             4100 L=3
0188             4009 IF(PCALC-P) 4001,4001,4220
0189             4220 EF=EF+.0001
0190                  GO TO 1010
                C
                C
0191               90 YN=X-PCALC
0192                  GO TO (5007,5008,5009),L
0193             5007 IF(YN-SUM)5006,4001,5011
0194             5006 EF=EF+.01
0195                  GO TO 1010
0196             5011 L=2
0197             5008 IF(SUM-YN)5110,4001,5100
0198             5110 EF=EF-.001
0199                  GO TO 1010
```

```
                C
                C
                C
                C
0200             5100 L=3
0201             5009 IF(YN-SUM)5220,4001,4001
0202             5220 EF=EF+.0001
0203                  GO TO 1010
0204             4001 IF(PCALC-1.)4002,4003,4003
0205             4002 PCALC=1.0
0206             4003 IF(SUM+1.)4004,4004,4005
0207             4005 SUM=-1.0000
                C
                C       THE HALL EQUATIONS
                C
0208             4004 RSCAT=1.1
0209                  IF(X.GT.9.9E+17) RSCAT=1.53
0210                  RHP=1.0
0211                  IF(EF.LT.4.0) GO TO 4116
0212                  RSCAT=1.0
0213                  RHP=1.53
0214             4116 CONTINUE
0215                  EF=EG+EF
0216                  E1=EG+E1
0217                  E2=EG+E2
0218                  PMU1=PMU*(TK/300.0)**(-POWE)
0219                  AMU0=B0*PMU1
0220                  AMU1=B1*PMU1
0221                  AMU2=B2*PMU1
0222                  PMU2=BH*PMU1
0223             3334 IF(TC.EQ.0C.) GO TO 707
0224                  GO TO 4447
0225              707 WRITE(3,717)B0,B1,B2,BH,AMU0,AMU1,AMU2,PMU1,PMU2,E1,E2,POWN
0226              717 FORMAT(/5X,4F10.2,5F11.1,3F10.3/)
0227             4447 AN0=AN0*10.**6
0228                  AN1=AN1*10.**6
0229                  AN2=AN2*10.**6
0230                  PCAL=PCAL*10.**6
0231                  PNPAR=PNPAR*10.**6
0232                  AMU0=AMU0*10.**(-4)
0233                  AMU1=AMU1*10.**(-4)
0234                  AMU2=AMU2*10.**(-4)
0235                  PMU1=PMU1*10.**(-4)
```

```
C
C
C
C
0236            PMU2=PMU2*10.**(-4)
0237            AA=AN0*E*AMU0/(1.+AMU0**2*0.64)
0238            AB=AN1*E*AMU1/(1.+AMU1**2*0.64)*7.0/10.0**(2./3.)
0239            AC=AN2*E*AMU2/(1.+AMU2**2*0.64)*7.0/10.0**(2./3.)
0240            AD=PCAL*E*PMU1/(1.+PMU1**2*0.64)
0241            AE=PNPAR*E*PMU2/(1.+PMU2**2*0.64)
0242            SUMA=AA+AB+AC+AD+AE
0243            DA=AN0*E*AMU0**2*0.8/(1.+AMU0**2*0.64)
0244            DB=AN1*E*AMU1**2*0.8/(1.+AMU1**2*0.64)*RHP*4.0/10.0**(1./3.)
0245            DC=AN2*E*AMU2**2*0.8/(1.+AMU2**2*0.64)*RHP*4.0/10.0**(1./3.)
0246            DD=PCAL *E*PMU1**2*0.8/(1.+PMU1**2*0.64)*RHP
0247            DE=PNPAR*E*PMU2**2*0.8/(1.+PMU2**2*0.64)*RHP
0248            SUMD=-RSCAT*(DA+DB+DC+DE+DD)
0249            RHM=(-SUMD/.8)/(SUMA**2+SUMD**2)
0250            RH =RHM*1.0E+06
0251            RHO=100.0/(E*(AN0*AMU0+AN1*AMU1+AN2*AMU2+PCAL*PMU1+PNPAR*PMU2))
0252            EXMU=RH /RHO
0253       4440 WRITE(3,5)AN0,AN1,AN2,PCAL,PNPAR,RH,TC,RHO,FF,EG,AMD,PMDS,EXMU,BO
0254          5 FORMAT(5E12.4,2F8.2,F8.5,4F8.4,F10.2,F6.0)
0255          6 CONTINUE
0256          7 CONTINUE
0257            RETURN
0258            END
```

References

1879

H1 Hall, E. H.: Amer. J. Math, 2 287

1928

B1 Bloch, F.; Zeit, Phys., 52 555

S1 Sommerfeld, A.; Zeit, Phys., 47 1

1930

B1 Brillouin, L.; J. Phys. Radium, 1, 377

1931

N1 Nordheim, L.; Ann. Phys. (Leipzig) 9, 641

W1 Wilson, A. H.; Proc. Roy. Soc. A 133 458

W2 Wilson, A. H.; Proc. Roy. Soc. A 134 277

1938

M1 Muto, T.; Sci. Papers, Inst. Phys. Chem. Research (Toyko) 34, 377

1939

S1 Stohr, H. and Klemm, W.; Z. Anorg. Allgem. Chem. 241, 304

1951

H1 Henry, N. E. M., Lipson, H. and Wooster, W. A. ; "Interpretation of X-Ray Diffraction Photographs", Macmillan and Company, London, (1951).

1952

H1 Hume-Rothey, W., Christian, J. W., Pearson, W. B.; "Metallurgical Equilibrium Diagrams", The Institute of Physics, London, (1952).

W1 Welker, H.; Z. Naturforsch, 7a, 744

1953

H1 Howarth, D. J., and Sondheimer, E. H.; Proc. Phys. Soc. (London), Ser. A, 219 53

S1 Shih and Peretti; J. Am. Chem. Soc. 75 608

1954

J1 Johnson, E. R., and Christian, S. M.; Phys.Rev. 95 560

M1 Madelung, O, and Weiss, H.; Z. Naturf. 9a 527

1955

D2 Dresselhaus, G., Kip, A. F., and Kittel, C.; Phys. Rev., 100, 618

F2 Folberth, O. G.; Z. Naturf. 10a, 502

G2 Goryunova, N. A., and Federova, N. N.; Zhur. Tech. Fiz. 25, 1339

G4 Glicksman, M.; Phys. Rev., 100, 1146

K4 Koster, W. B., and Thomas, B.; Z. Metall, 46, 295

P2 Parmenter, R. H.; Phys. Rev., 97 3, 587

P3 Parmenter, R. H.; Phys. Rev., 99 6, 1759

S2 Stern, H, and Talley, R. M.: Phys. Rev. 100, 1638

1956

K7 Kittel, C.; "Introduction to Solid State Physics", 2nd edition, J. Wiley and Sons (1956) Chapter 1

P5 Parmenter, R. H.; Phys. Rev. 104, 1, 22

W2 Weiss, H.; Z. Naturforsch, 11a, 430

W6 Woolley, J. C., Smith, B. A., and Lees, D. G.: Proc. Phys. Soc., 69B, 1339

1957

A3 Antell, G. R., Chasmar, R. D., Champness, C. H., and Cohen, E.; Proc. Rugby. Conf. Phys. Soc., London, p. 99

B2 Blakemore, J. S.; Can. J. Phys. 35, 91

D4 Dekker, A.; "Solid State Physics" Prentice Hall Inc. (1957) Chapter 1

E2 Ehrenreich, H.; J. Phys. Chem. Solids. 2, 131

K2 Kane, E. O.; J. Phys. Chem. Solids, 1, 249

K6 Kolm,C., Kulin, S. A., and Averbach, B. L.; Phys. Rev. 108, 965

W3 Woolley, J. C., and Smith B. A.; Proc. Phys. Soc. 70B, 153

1958

B6 Burdiyan, I. I., and Borshchovskii, A. S.; Sov. Phys. Tech. Phys., 3, 2451

B7 Braunstein, R., Moore, A. R., and Herman, F.; Phys. Rev., 109, 695

1956

K7 Kittel, C.; "Introduction to Solid State Physics", 2nd edition, J. Wiley and Sons (1956) Chapter 1

P5 Parmenter, R. H.; Phys. Rev. 104, 1, 22

W2 Weiss, H.; Z. Naturforsch, 11a, 430

W6 Woolley, J. C., Smith, B. A., and Lees, D. G.: Proc. Phys. Soc., 69B, 1339

1957

A3 Antell, G. R., Chasmar, R. D., Champness, C. H., and Cohen, E.; Proc. Rugby. Conf. Phys. Soc., London, p. 99

B2 Blakemore, J. S.; Can. J. Phys. 35, 91

D4 Dekker, A.; "Solid State Physics" Prentice Hall Inc. (1957) Chapter 1

E2 Ehrenreich, H.; J. Phys. Chem. Solids. 2, 131

K2 Kane, E. O.; J. Phys. Chem. Solids, 1, 249

K6 Kolm, C., Kulin, S. A., and Averbach, B. L.; Phys. Rev. 108, 965

W3 Woolley, J. C., and Smith B. A.; Proc. Phys. Soc. 70B, 153

1958

B6 Burdiyan, I. I., and Borshchovskii, A. S.; Sov. Phys. Tech. Phys., 3, 2451

B7 Braunstein, R., Moore, A. R., and Herman, F.; Phys. Rev., 109, 695

B10 Bowers, R., Bauerle, J. E., Cornish, A. J.;
J. Appl. Phys. 30, 1050

F4 Folberth, O. G.; Z. Naturforsch, 13a, 856

G10 Goryunova, N. A., and Burdiyan, I. I.;
Dok. Akad. Nauk, SSSR., 120, 1031

G14 Goryunova, N. A., and Gorskhov, .; Z. Neorg, Khim.,
3, 668

G15 Gray, P. V., and Ehrenreich, H.; Bull. Am. Phys. Soc.,
II, 3, 225

H1 Herman, F.; Reviews of Modern Physics, 30, 102

K4 Koster, W., and Ulrich, W.; Z. Metall. 49, 365

P5 Paul, W.; J. Phys. Chem. Solids., 6, 6

S7 Steele, M. C., and Rosi, F. D.; J. Appl. Phys.,
29, 1517

W9 Woolley, J. C., and Smith, B. A.; Proc. Phys. Soc.
72, 214

W10 Woolley, J. C., and Smith, B. A.; Proc. Phys. Soc.
72, 867

1959

A1 Abrahams, M., Braunstein, R., and Rosi, F. D.;
J. Phys. Chem. Solids, 10 204

B10 Bower, R., Banerle, J. E., and Cornish, A. J.;
J. Appl. Phys. 30, 1050

B15 Burdiyan, I. I., and Kolomiets, S. I.;
Fiz. Tv. Tela, 1, 1165 Sov. Phys. Sol. Stat. 1, 1967 (1960)

E5 Ehrenreich, H.; J. Phys. Chem. Solids. 9, 129

E6 Ehrenreich, H.; J. Phys. Chem. Solids, 12, 97

I1 Ivanov-Omskii, V. I., and Kolomiets, B. T.;
Dok. Akad. Nauk., SSSR., 127, 135

I2 Ivanov-Omskii, V. I., and Kolomiets, B. T.;
Fiz. Tv. Tela, 1, 913

I3 Ivanov-Omskii, V. I., and Kolomiets, B. T.;
Fiz. Tv. Tela, 1, 568

O1 Oswald, F.; Z. Naturf. 14a, 374

S6 Spitzer, W. G., and Whelan, J. M.; Phys. Rev. 114, 59

S14 Smith, R. A.; "Semiconductors" Cambridge 1959

S15 Sagar, A.; 1959 Westinghouse Research Report 6-40602-3R1

W2 Weiss, H.; Ann. Phys. 4, 121

W7 Woolley, J. C., Evans, J. A. and Gillett, C. M.;
Proc. Phys. Soc. 74, 244

W8 Woolley, J. C., Lees, D. G.; J. Less Common Metals 1, 3

1960

A2 Abrahams, M. S., Braunstein, R., and Rosi, F. D.;
Met. Soc. Conf. Vol. 5

A4 Ageev, Ya., and Nasledov, D. N.; Fiz. Tv. Tela, 2 826
Sov. Phys. Solid State 2, 758

A15 Aukerman, L. W., and Willardson, R. K.; J. Appl. Phys.,
31, 439

B2 Baranov, B. V., and Goryunova, N. A.; Fiz Tv. Tela, 2 284
Sov. Phys. Solid State 2, 262 (1961)

B12 Busch, G., and Vogt, O.; Helv, Phys. Acta. 33, 437

E3 Ehrenreich, H.; Phys. Rev. 120, 1951

H9 Hilsum, C.; Proc. Phys. Soc. 76, 3, 414

I1 Ivanov-Omskii, V. I., and Kolomiets B. T.;
Sov. Phys. Solid State, 2, 363

M3 Miller, J. F., Goering, H. L., and Himes, R. C.;
Electrochem. Soc. 107, 527

S1 Sagar, A.; Phys. Rev., 117, 93

U1 Ure, R. W., Bowers, R., and Miller, R. C.;
Met. Soc. Conf. Vol. 5 "Properties of Elementary and
Compound Semiconductors" p. 245

W7 Woolley, J. C., Gillet, C. M., and Evans J. A.;
J. Phys. Chem. Solids, 16, 138

W8 Woolley, J. C. and Gillett, C. M.; J. Phys. Chem. Solids,
17, 1/2, 34

1961

A2 Ageev, Ya., Emelyanenko, O. V., and Nasledov, D. N.;
Fiz. Tv. Tela, 3, 194

B7 Becker, W. M., Ramdas, A. K., and Fan, H. Y.;
J. Appl. Phys., 32 2094

B19 Burdiyan, I. I., Rosneritsa, Ya. A., and Stepanov, G. I.;
Fiz. Tv. Tela, 3, 1879

B12 Busch, G., and Vogt, O.; Helv, Phys. Acta. 33, 437

E3 Ehrenreich, H.; Phys. Rev. 120, 1951

H9 Hilsum, C.; Proc. Phys. Soc. 76, 3, 414

I1 Ivanov-Omskii, V. I., and Kolomiets B. T.;
Sov. Phys. Solid State, 2, 363

M3 Miller, J. F., Goering, H. L., and Himes, R. C.;
Electrochem. Soc. 107, 527

S1 Sagar, A.; Phys. Rev., 117, 93

U1 Ure, R. W., Bowers, R., and Miller, R. C.;
Met. Soc. Conf. Vol. 5 "Properties of Elementary and
Compound Semiconductors" p. 245

W7 Woolley, J. C., Gillet, C. M., and Evans J. A.;
J. Phys. Chem. Solids, 16, 138

W8 Woolley, J. C. and Gillett, C. M.; J. Phys. Chem. Solids,
17, 1/2, 34

1961

A2 Ageev, Ya., Emelyanenko, O. V., and Nasledov, D. N.;
Fiz. Tv. Tela, 3, 194

B7 Becker, W. M., Ramdas, A. K., and Fan, H. Y.;
J. Appl. Phys., 32 2094

B19 Burdiyan, I. I., Rosneritsa, Ya. A., and Stepanov, G. I.;
Fiz. Tv. Tela, 3, 1879

C2 Cardona, M.; J. Phys. Chem. Solids, 17 356

E1 Ehrenreich, H.; J. Appl. Phys. 32, 10, 2155

G23 Goryunova, N. A., and Tahktareva, N. K.; Izv. Akad. Nauk. Mold., SSSR, 10 88

I3 Ivanov-Omskii, V. I., and Kolomiets, B. T.; Sov. Phys. Sol. Stat. 3, 2581

P6 Paul, W.; J. Appl. Phys., 32, 2082

S16 Strauss, A. J.; Phys. Rev., 121, 1087

S20 Stambaugh, E. P., Miller, J. F., and Himes, R. C.; "Growth of Refractory III - V Compounds and Alloys from Solutions", in "Metallurgy of Elemental and Compounds Semiconductors" R. O. Grubel, editor, Interscience, New York, (1961)

T1 Tauc, J., and Abraham, A.; Proc. Int. Conf. Phys. Semicond. Prague, 1960 p. 375

T2 Tauc, J., and Abraham, A.; J. Phys. Chem. Solids, 20, 190

W5 Woolley, J. C.; Proc. Int. Conf. Phys. Semicond., Prague, 1960 p. 966.

W7 Woolley, J. C., Gillet, C. M., and Evans, J. A.; Proc. Phys. Soc., 77, 700

W8 Woolley, J. C., and Evans, J. A.; Proc. Phys. Soc., 78, 354

1962

A7 Ageev, Ya., Emelyanenkov, O. V., and Nasledov, D. N.; Sov. Phys. Solid State, 3, 141

B2 Bate, R. T.; J. Appl. Phys., 33, 1, 26

I1 Ivanov-Omskii, V. I., and Kolomiets, B. T.; Sov. Phys. Solid State, 4, 216

P11 Pizzarello, F. A.; J. Electrochem. Soc. 109, 226

S12 Stone, L. E.; J. Appl. Phys. 33, 2795

T5 Trumbore, F. A., Freeland, P. E., and Mills, A. D.; J. Electrochem. Soc., 109, 7, 645

W7 Woolley, J. C.; Chap. 1 "Preparation of III - V Compounds" Willardson and Goerring, editors, Reinholt, 1962

W8 Weinstein, M. et al.; AFCRL Report No. 62-503, June 14, 1962

1963

C3 Cardona, M.; J. Phys. Chem. Solids, 24, 1543

B18 Beer, A. C.; "Galvanomagnetic Effects in Semiconductors" supp. 4 to "Solid State Physics", Academic Press, N.Y. 1963

M5 Melngailus, I., Strauss, A. J., and Rediker, R. H.; Proc. IEEE., 51, 8, 1154

N9 Nelson, H.; RCA Review, 24, 603

S9 Sirota, N. N., and Makovetskaya , .; Report of the Acad. of Sci. of BSSR., 7, 4, 230

V4 van Hook, H. J., and Lenker, E. S.; Trans. Met. Soc., AIME, 227, 220

1964

A2 Alexander, F. B., et al.; Appl. Phys. Letters, 4, 113

C2 Chalmers, B.; "Principles of Solidification". J. Wiley and Sons, Inc., New York, (1964) Chap. 5

D2 Dismukes, J., et al.; J. Appl. Phys., 35, 2899

F2 Fulton, J. A., Fitcher, D. B., and Fenner, G. E.; Appl. Phys. Letters, 4, 9

F5 Finch, W. F., and Mehal, E. W.; J. Electrochem. Soc. 111, 7, 814

H7 Hull, E. M.; J. Electrochem. Soc. 111, 11, 1295

K6 Kittel, C.; "Introduction to Solid State Physics", 3rd edition, J. Wiley and Soncs, Inc., (1964)

M4 Madelung, O.; "Physics of the III - V Compounds"; J. Wiley and Sons, Inc., (1964)

M5 Müller, E. K., and Richards, J. L.; J. Appl. Phys., 35, 1233

P3 Potter, R. F., and Stierwalt, D.L.; Proc. Int. Conf. Phys. Semicond., Paris, (1964), p. 1111

P4 Potter, R. F., and Kretschmar, G. G.;
J. I. R. Phys., 4, 57

S8 Sirrine, R.; J. Electrochem. Soc., 111, 750

W1 Woolley, J. C., and Mal'tsev, Ya. V.;
Sov. Phys. Solid State, 5, 10, 2144

W2 Woolley, J. C., and Warner, J.; Can. J. Phys., 42, 1879

W4 Woolley, J. C., and Thompson, A. G.;
Can. J. Phys., 42, 2030

Z1 Ziman, J. M.; "Principles of the Theory of Solids"
Cambridge, 1964

1965

B1 Baukin, I. S., Ivanov-Omskii, V. I., and Kolomiets, B. T.;
Sov. Phys. Solid State, 1, 1019

B2 Baxter, R. D., Bate, R. T., and Reid, F. J.;
J. Phys. Chem. Solids, 26, 41

D1 Dismukes, J., Ekstrom, L.; Trans, Met. Soc. AIME, 223

G2 Gottlieb, G. E.; J. Electrochem. Soc., 112, 2, 192

K1 Kradinova, L. V.; "Sov. Phys. in New Sci. Mat".,
New York Consultants Bureau

M1 Minden, H. T.; J. Electrochem. Soc., 112, 3, 300

O1 Otsaka, E. et al.; J. Phys. Soc., Japan, 20, 727

R1 Rubenstein, M.; J. Electrochem. Soc. 112, 426

S1 Straumanis, M. E., and Kim, C. D.;
J. Electrochem. Soc., 112, 1, 112

T1 Tietjen, J. T., and Weisberg, L. R.; Appl. Phys. Letters, 7, 10, 261

W2 Woolley, J. C.; J. Electrochem. Soc., 112, 4

1966

B1 Bolvanovich, E. I.; Izvest. Akad. Nauk. SSSR. Neorg. Mat. 2, 11, 2080

B2 Basov, N. G., Dudenkov, A. V., Krasil'nikov, A. I., Nikitin, V. V., and Fedoseev, K. P.; Sov. Phys. Solid State, 8, 4, 847

B5 Black, J. F., and Ku, S. M.; J. Electrochem. Soc., 113, 3, 249

C1 Conrad, R. W., Jones, C. E., and Williams, E. W.; J. Electrochem. Soc. 113, 3, 287

C2 Coderre, W. M., and Woolley, J. C.; Physics in Canada, 22, 56

F1 Filipchenko, A. S., Molodian, I. P., Nasledov, D. N., Siderov, V. G., and Emelyanenko, O. V.; Phys. Status Solidi, 14, K195

H1 Hockings, E. F., Kudman, I., Seidel, T. E., Schmelz, C. M., and Steigmeier, E. F.; J. Appl. Phys., 37, 7, 2879

H2 Harland, B., and Woolley, J. C.; Can. J. Phys., 44, 2715

J1 Jones, C. E.; Appl. Spect. 20, 3, 161

T1 Tietjen, J. J., and Amick, J.A.; J. Electrochem. Soc., 113, 724

W1 Woolley, J. C.; Can. J. Phys., 44, 2709

1967

C1 Conrad. R. W., Hoyt, P. L. and Martin, D. D.; J. Electrochem. Soc. 114, 2, 164

I1 Iglitsyn, M. I., Kistova, E. M., Maslov, V. N., and Yarova, E. S.; Fiz. Tekh. Polup., 1, 1, 74

K1 Kudman, I., and Seidel, T. E.; J. Appl. Phys., 38, 11, 4379

K2 Kudman, I., and Ekstrom L., and Seidel, T. E.; J. Appl. Phys., 38, 12, 4641

R1 Rupprecht, T., Woodall, J. M., and Pettit, G. D.; Appl. Phys. Letters, 11, 381

S1 Sahm, R. R., and Pruss, T. U.; Trans. Met. Soc., AIME., 239, 1523

S2 Sirota, N. N., and Bolvanovich, E. I.; Dok. Akad. Nauk., BSSR., 11, 6, 503

S3 Sirota, N. N., and Bolvanovich, E. I.; Dok. Akad. Nauk, BSSR., 11, 7, 593

T1 Thompson, A. G., and Woolley, J. C.; Can. J. Phys., 45, 255

V1 Varshni, Y. P.; Physica, 34, 149

1968

A1 Aubin, M. J., and Woolley, J. C.; Can. J. Phys., 46, 1191

A2 Averous, M., Bougnot, G., and Calas, J.; Phys. Stat. Sol., 29, 807

B1 Blatt, F. J.; "Physics of Electronic Conduction in Solids", McGraw-Hill, (1968)

C1 Coderre, W. M., and Woolley, J. C.; Can. J. Phys., 46, 1207

C3 Crawford, M. G., Stillman, G. E., Rossi, J. A., and Holonyak, N.; Phys. Rev., 168, 3, 867

I1 Ikona, H., and Wang, S. S.; J. Phys. Soc. Japan, 25, 1739

J1 Jean-Louis, A. M., and Bernard, M.; Proc. Int. Conf. Phys. Semicond., Moscow, 1968

J2 Jensen, D. E., Stein, W. W., and Mooney, J. B.; Delivered at Montreal Meeting of Electrochem. Soc., 1968

K1 Kwan, C. C. Y., and Woolley, J. C.; Can. J. Phys., 46, 1669

K2 Kudman, I., and Ekstrom, L.; J. Appl. Phys., 39, 7, 3385

K3 Kosicki, B. B., Jayaraman, A., and Paul, W.; Phys. Rev., 172, 3, 764

L1 Lees, J.; Solid State Comm., 6, 1, 11

L2 Liang, C., Piller, H., and Steirwalt, D.; Appl. Phys. Letters, 12, 2, 49

P1 Pistoulet, B., Robert, J. L., and Barjon, D.; Proc. Int. Conf. Physics. Semicond., Moscow, 1968

S1 Skomyakov, G. P., Tsidel'kovskii, I. M., Chukina, T. P., and Kakoshkin, Ya.; Fiz. Tv. Tela, 9, 9, 2625

V1 vanTongerloo, E. H., and Woolley, J. C.;
Can. J. Phys., 46, 1199

V2 Vishnubhatla, S. S., and Woolley, J. C.,
Can. J. Phys., 46, 1769

W1 Woolley, J. C., Thomas, M. B., and Thompson, A. G.;
Can. J. Phys., 46, 157

W3 Winkler, J. H., Olsen, H. M., and Wagner, J. W.;
Montreal Meeting, Electrochem. Soc., 1968.

1969

A1 Aubin, M. J., vanTongerloo, E. H., Thomas, M. B., and
Woolley, J. C., Can. J. Phys., 47, (to be published)

A2 Aubin, M. J.: Ph.D. Thesis, 1969 Ottawa

B1 Babaev, R. M., Tikhonova, V. I., Khlystovskaya, M. D.
and Dmitrieva N. E.; Sov. Phys. Semicond., 2, 8, 1022

V1 vanTongerloo, E. H., and Woolley, J. C.;
Can. J. Phys., 47, 241

V2 Varshni, Y. P.; (not yet published)

V3 vanTongerloo, E. H.; Ph.D. Thesis, 1969 Ottawa

Curriculum Vitae

NAME: William Michael Coderre

BORN: Kingston, Ontario, Canada, April 11, 1942.

EDUCATED:

Primary: Notre Dame de la Presentation, Ottawa
High School Entrance, 1955

Secondary: St. Patrick's College High School, Ottawa
Senior Matriculation, 1960

University: 1) St. Patrick's College
course: Physics
degree: B.Sc. (Pass) 1963

2) University of Ottawa
course: Physics
degree: B.Sc. (Hons.) 1964

Transfer from M.Sc. Status to Ph.D. Status
University of Ottawa, April, 1966.